A STUDY OF THE SURFACE FILMS FORMED BY ORGANIC CORROSION INHIBITORS ON COPPER

by

Tooraj Hashemi, MSc, DIC

A Thesis submitted for the Degree of

DOCTOR OF PHILOSOPHY, UNIVERSITY OF LONDON

Department of Chemical Engineering and Chemical Technology
Imperial College, London.

May 1978

ACKNOWLEDGEMENTS

The author greatly appreciates advice and encouragement kindly given by Dr D. Chadwick. He also wishes to thank members of Nuclear Technology section of Chemical Engineering Department, in particular Professor G.N. Walton, Dr P.G. Clay and Mr B. Bennett. The author's sincere thanks to his colleagues, Mr S. Bean and A. Christie for many useful discussions. Finally, the author wishes to thank both Miss T. Richardson and Miss S. Box for typing the manuscript.

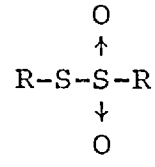
Tooraj Hashemi
May 1978

ABSTRACT

This thesis describes a study of the surface films formed by organic corrosion inhibitors on copper and copper based alloys. This study was carried out using Electron Spectroscopy (ESCA) technique together with infrared spectroscopy and electrochemical polarization measurements. A series of organic inhibitors were used in this study, however, two of them namely benzotriazole (BTA) and 2-mercaptobenzothiazole (MBT) received more attention because of their wide usage in industry.

This work shows that the films formed on the copper surface resulting from interaction between copper and inhibitor are always a copper(I) complex. However this complex undergoes oxidation on exposure to air resulting in degradation of the protective film. The suggested mechanism for the film formation is a dissolution-precipitation mechanism.

In the case of 2-mercaptobenzothiazole (MBT) it was found that Cu(I)-MBT complexes on exposure to air undergo a dimerization-oxidation by formation of a bond through -S-S- groups and elimination of Cu from the molecule. The dimerized molecule was found to be oxidized on exposure to air in its turn. ESCA investigation showed that the final oxidized compound has a formula of



Infrared spectroscopy of Cu-inhibitor complexes showed that in all cases, the hydrogen of N-H group is replaced by copper. Finally, electrochemical measurements showed that among six different organic inhibitors, benzotriazole is the most effective one. Benzothiophene on the other hand, proved to be the worst.

C O N T E N T S

		Page
Acknowledgements		
Abstract		
CHAPTER ONE		1
Introduction		1
1.1	Corrosion	1
1.2	Cost of Corrosion	1
1.3	Corrosion Prevention and Control	3
1.4	Organic Corrosion Inhibitors	4
1.5	Present Study	6
CHAPTER TWO		9
2.1	Introduction	9
2.2	Corrosion of Metals in Gaseous Media	9
2.3	Corrosion of Metals in Aqueous Media	11
	2.3.1 Metal Dissolution	11
	2.3.2 Mixed-Potential Theory of Corrosion	15
	2.3.3 The Active-Passive Transition	18
2.4	Atmospheric Corrosion	19
2.5	Corrosion Prevention and Control	20
	2.5.1 Organic Inhibitors	22
CHAPTER THREE		27
Experimental Methods of Studying Corrosion Inhibition Processes		
3.1	Electrochemical Methods	28
	3.1.1 Experimental Techniques	30

		Page
3.2	Infrared Spectroscopy	36
	3.2.1 Multiple Reflection Techniques	38
CHAPTER FOUR		42
4.1	Electron Spectroscopy for Chemical Analysis (ESCA)	42
4.2	X-ray Photoelectron Spectroscopy (XPS)	44
4.3	Instrumentation	46
4.4	Surface Sensitivity	52
4.5	The Chemical Shift	53
4.6	Shake-up	58
4.7	The Auger Process	60
4.8	Calibration	63
4.9	Application to ESCA	64
	4.9.1 ESCA Study of Copper Compounds	65
	4.9.2 Structure Determination of Organic Compounds using ESCA	71
	4.9.3 ESCA as an Analytical Test	79
	4.9.4 Limitations and Problems	80
CHAPTER FIVE		82
A Review of Previous Work in Inhibition of Copper Corrosion		
5.1	Copper Corrosion	82
5.2	Corrosion Inhibition of Copper	84
5.3	Corrosion Inhibition of Copper and its Alloys by Benzotriazole	86
	5.3.1 Practical Studies	86
	5.3.2 Fundamental Studies	89
5.4	Corrosion Inhibition of Copper and its Alloys by 2-Mercaptobenzothiazole	100
5.5	Electrochemical Polarization of Copper in Brine Solutions	103

Page

5.5.1 Cathodic and Anodic Behaviour of Copper in NaCl solution 103

5.5.2 Electrochemical Polarization Behaviour of Copper in the Presence of Organic Inhibitors 105

CHAPTER SIX 110

Study of Film formation by Benzotriazole on Copper and its Alloys

6.1 Structure of the Films 111

6.1.1 Oxidation State of Copper in the Films 111

6.1.2 ESCA Investigation of Cu-BTA Complexes 125

6.1.3 I.R. Reflectance Spectroscopy of Surface Films and Complexes 129

6.1.4 Structure of Cu(I)-BTA Complexes 133

6.1.5 Depth Profle of the Surface Films 144

6.2 Mechanism of Cu-BTA Film Formation 149

6.2.1 The Role of Cu_2O in Film Formation 150

6.2.2 The Mechanism of Film Formation 164

6.3 Films Formed by BTA on Copper-Nickel Alloys 173

6.3.1 Characterization of Cu/Ni alloys substrate 173

6.3.2 Interaction of BTA with Cu/Ni Alloy 176

6.3.3 Mechanism of Film Formation 183

6.4 Films Formed on Brass 184

6.4.1 Mechanism of Film Formation 192

6.5 Films Formed From Non-Aqueous Media 193

6.6 Summary 166

		Page
CHAPTER SEVEN		196
Study of the Films Formed by 2-Mercapto-benzothiazole on Copper and its Alloys		
7.1	Structure of the Films	197
	7.1.1 Oxidation State of Copper in Surface Film	197
	7.1.2 Stoichiometry of Cu-MBT Surface Films	199
	7.1.3 Binding Energies of Surface Films	201
	7.1.4 Air Oxidation of Cu-MBT Surface Films	202
	7.1.5 Oxidation of Chemically Prepared Cu-MBT Complexes	204
	7.1.6 I.R. Reflectance Spectroscopy of the Cu-MBT Films	207
	7.1.7 Structure of Cu-MBT Complex	214
	7.1.8 O 1s XPS spectra Cu-MBT Complex Films	225
	7.1.9 Depth Profile of the Surface Films	227
7.2	Mechanism of the Film Formation	230
7.3	Films Formed on Copper-based Alloys	238
7.4	Films Formed From Non-Aqueous Media	243
7.5	Summary	243
CHAPTER EIGHT		245
Electrochemical Polarization of Copper in the Presence of Organic Inhibitors		
8.1	Cathodic and Anodic Polarization of Copper in Brine Solutions	245
	8.1.1 Cathodic Polarization of Copper using Linear Potential Sweep	246
	8.1.2 Anodic Polarization of Copper	250
	8.1.3 Time Dependence of the Processes	255

		Page
8.1.4	Effect of Chloride Ion Concentration	257
8.1.5	Effect of Temperature	259
8.1.6	Effect of CuCl Concentration	262
8.1.7	Effect of Stirring	262
8.2	Polarization Behaviour of Copper in the Presence of Inhibitors	264
8.2.1	Polarization of Copper in the Presence of Benzotriazole	267
8.2.2	Polarization of Copper in the Presence of Benzimidazole	270
8.2.3	Polarization of Copper in the Presence of Other Inhibitors	272
8.3	Summary	275
APPENDICES		276
REFERENCES		292

CHAPTER ONE

INTRODUCTION

1.1 Corrosion

Corrosion may be defined as the destructive attack on a metal by chemical or electrochemical reaction with its environment. This excludes mechanical processes which destroy the value of a metallic article by grinding it away as metallic dust. Such purely mechanical damage, in the absence of chemical change, is called erosion. However, some of the most dangerous types of corrosion results from processes that are partly chemical and partly mechanical, for example, stress corrosion. The occurrence of corrosion and its prevention are important engineering problems. Although corrosion is an old problem, its importance has become greater in recent times, because of the increased use of metals in modern society and the wide range of conditions in modern processes.

1.2 Cost of Corrosion

An accurate estimate of the cost of corrosion and also the amount of metal lost through corrosion is impossible, but rough calculations have been made. In the United Kingdom, a Department of Trade and Industry (D.T.I.) Report in 1971 (1) estimated the annual cost of corrosion to be £1,365 m. This represented approximately 3.5% of G.N.P. in 1969. The report considered that over £300 m. per annum could have been saved if existing knowledge and techniques were properly applied. This was about 20% of the estimated total annual cost of corrosion in the U.K. A similar situation exists in the United States. In 1949 the annual cost of corrosion was estimated at £2,359 m. by

Uhlig (2), and in 1966 Leichtenstein (3) estimated it to be £4,350 m. Uhlig (2) suggested that a saving of up to 20% of the actual loss should be possible. The colossal expenditures on all kinds of protective measures, such as paint or lacquer coatings, metallic coatings, production of more corrosion-resistance alloys, and so on, may largely be counted as corrosion costs. The total cost of corrosion should also include the cost of overhauling or rebuilding of corroded equipment, decreased quality of production, compilation of technology, and higher dimensional allowances in structural design to compensate for subsequent corrosion damage. Finally, concerning the importance of corrosion as a cause of accidents, from a survey of major fires and explosions in the chemical industry which were reported in the safety literature, Chadwick and co-worker (4) concluded that approximately 10% of accidents could be attributed to corrosion.

In an estimate of the amount of metal lost through corrosion made by Tomashov (5) from available data in Russia, it was concluded that about one-third of the total output of metal is eliminated from technical consumption because of corrosion. It may be assumed that about two-thirds of corroded metal is recovered by the re-melting of scrap. Hence roughly about 10% of metal is completely lost through the destructive action of corrosion. In 1965 it was expected that about 6-7 million tons of steel would be lost through corrosion in Russia.

Based on the current world production of iron and steel of about 200 million tons per year, we may expect a yearly loss of 20 million tons as a result of corrosion. However, damage caused by corrosion can be of much more

intrinsic value than the actual cost of the metal lost. In 1925 Speller (6) estimated that the tonnage of iron and steel products, such as roofing, wire, tubes and pipes, oil well equipment and many other structures, renewed because of inadequate protection against corrosion, amounted annually by about 2% of the total tonnage of such products in use.

It can be seen from the above mentioned figures that corrosion plays a considerable part in national economies and its prevention is therefore a subject of the greatest importance.

1.3 Corrosion Prevention and Control

The simplest way to prevent reaction between a metal and its environment would be to use a non-corrosive metal (e.g. gold) or a non-corrosive environment (preferably a vacuum). Such methods are not practical in most cases. The methods commonly used to prevent or control corrosion of metals come under the following headings:-

i) modification of the environment

ii) modification of the properties of the metal

iii) protective coatings

iv) cathodic and anodic protection

v) non-metallic materials

In both i) and ii) stable, relatively impermeable barriers are often formed by a corrosion reaction between a metal and its environment. In iii), the properties of barriers deliberately placed between the metal and the environment are responsible for protection. Therefore, in these three classes, metal is frequently prevented from corroding by being isolated from its environment.

Cathodic protection is perhaps the most important of all approaches to corrosion control. Anodic protection although a promising technique, has only been applied in special cases.

Aqueous corrosion can be diminished by the removal of corrosion stimulators or alternatively by addition of inhibitors. De-aeration removes oxygen (the corrosion stimulator), and attack is virtually halted. De-aeration can be achieved either physically, or chemically by the addition of a variety of chemical agents such as sulphites or hydrazine.

The alternative method of decreasing attack in solutions is the use of corrosion inhibitors. In general any phase constituent whose presence is not essential to the occurrence of an electrochemical process, but leads to a retardation of this process may be called an inhibitor. If the inhibition is exercised through a modification of the metal surface this might imply adsorption, the formation of 'surface compounds', or a reaction between the metallic material and the inhibitor with separation of the corrosion products at the metal/electrolyte interface.

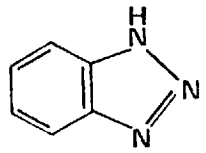
Further details about the corrosion prevention and control as well as the mechanism of corrosion inhibition will be discussed in Chapter 3 .

1.4 Organic Corrosion Inhibitors

Most organic inhibitors function by forming an adsorbed layer on the metal surface, probably no more than a monolayer in thickness, which essentially blocks discharge of H^+ and dissolution of metal ions.

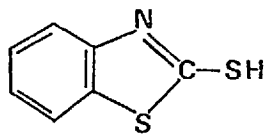
Some inhibitors block the cathodic reaction (hydrogen evolution or oxygen reduction) more than the anodic reaction, or vice versa; but adsorption appears to be general over the surface rather than at specific anodic or cathodic sites, and both reactions tend to be retarded. Compounds serving as inhibitors require, by and large, a favourable polar group or groups by which the molecule can attach itself to the metal surface. These include the organic N, amine, S, and OH groups. The size, orientation, shape, and electric charge of the molecule play a part in the effectiveness of inhibition.

In recent years, investigations have shown that a system of tarnish or corrosion control for copper, brass and bronze can be built around the organic compound, 1, 2, 3, benzotriazole and a number of its related compounds. It has the following structural formula,



and has found some application in various conditions to inhibit the corrosion of copper and copper based alloys.

Among many other heterocyclic compounds suggested as corrosion inhibitors for copper such as benzimidazole and its mercapto derivative, indazole, tolutriazole, benzothiazole and its mercapto compound 2-mercapto bezothiazole (MBT) which has the following structure and its sodium salt are of great importance.



MBT, known commonly as Captax, was first made in 1887 and now has come to be one of the important agents in accelerating vulcanization. Its use as corrosion inhibitor

for copper and copper-based alloys has been recommended. It has also found application in cooling water systems especially for engines, added in small amounts to the mixture of glycol/water.

1.5 Present Study

Because of the great importance of copper corrosion inhibition by organic compounds in general, and benzotriazole in particular, much effort has been devoted to the study of this system for almost two decades. The fundamental studies complement more practical studies of the inhibition properties of BTA and other organic inhibitors in real environments. The aim of fundamental studies is to elucidate the mechanism of inhibition and thus to improve upon the existing inhibitors by modifying them or to find new more effective inhibitors. In other words, the most important problem to be solved, is to find a correlation between the inhibition characteristics of compounds and their molecular structure. This necessitates a vast systematic investigation of organic compounds and their inhibition properties. Obviously, such an investigation is not practical for many reasons; one of them being the tremendous number of organic compounds in use. A more logical approach is to study the mechanism by which existing organic inhibitors operate. If this problem is solved, the range of compounds to be studied will fall into a much narrower range, thus enabling a more realistic investigation.

Fundamental studies on the Cu/inhibitor system, which started in the early 1960s, have brought about

many new facts concerning the system. Different workers have used different techniques to investigate the problem. These techniques have included weight loss measurements, electrochemical methods, infra-red spectroscopy, ellipsometry, etc. However, up to now there has been no satisfactory model proposed for the inhibition mechanism which covers and explains all of the facts observed by different workers.

In view of this, the present study was started in order to elucidate the structure of the surface films and their mechanism of formation both on copper and copper-based alloys. To achieve this, extensive use has been made of a relatively new technique for the first time, namely X-ray photo-electron spectroscopy (XPS or ESCA). This technique has been shown to be a very powerful method in surface studies (7), and it proved to be most useful and informative concerning the mechanism of corrosion inhibition. ESCA is a U.H.V. technique and certain problems are associated with this method, which at first seemed to limit the use of the technique, but proved to be soluble to a large extent. In addition to ESCA, other methods such as infra-red reflectance spectroscopy and electrochemical measurements were used where appropriate.

In this study, particular attention has been given to the reaction mechanism of copper with the inhibitor. Since inhibition is exercised through the formation of a surface film, a great deal of research is devoted to the determination of the nature and the structure of this protective film. Corrosion inhibition of copper-based alloys such as copper-nickel alloys with different compositions as well as brass, have received particular

attention, because these alloys are widely used in industry.

There are many related compounds which are already used or recommended as effective inhibitors for copper such as benzthiazole and its mercapto derivative, benzimidazole and its mercapto derivative, etc. and so a study was carried out to investigate their properties in comparison with BTA.

Finally, because of the lack of a thorough electrochemical study of Cu/inhibitor system in the presence and absence of the inhibitors, the method of linear potential sweep was used for 6 different inhibitors.

The structure of this report is as follows: Chapter 2 deals with the theoretical aspect of corrosion and corrosion prevention. Chapter 3 describes infra-red reflectance spectroscopy and electrochemical methods and Chapter 4 is devoted to the theory and instrumentation of ESCA because of its importance in this study. Chapter 5, is a review of previous works and Chapter 6,7 and 8 presents the results and discussion.
Raw data such as binding energies, materials, specifications and so on appear in Appendices (A-D).

CHAPTER TWO

THEORY OF CORROSION AND CORROSION PREVENTION

2.1 Introduction

With the exception of some noble metals which may occur in the elemental state, metals are usually found in nature as compounds, the principal compounds being oxides and sulphides. Since nearly all reactions of the type

metal → metal compound

take place with a decrease in free energy, the reverse process, (i.e. extraction), requires a supply of energy. Corrosion is essentially the reverse of the extraction process, and thus in general, corrosion processes are associated with a spontaneous decrease in free energy.

2.2 Corrosion of Metals in Gaseous Media

The reaction of a metal with air or pure oxygen to form an oxide on the metal surface constitutes an important branch of corrosion particularly at elevated temperature. The oxidation of metals is a chemical reaction which can be represented by the equation:

$$X\,M + Y/_2\ O_2 \rightarrow M_XO_Y$$

The oxygen atoms gain electrons to become oxygen ions and a stable oxide results, which adheres to the metal surface. Metals possessing more than one valency state, e.g. copper, can form complex layers of oxide, containing oxides of several compositions.

As oxide is formed on the metal surface, it presents a barrier through which the reactant must diffuse if the oxide film is to continue growing. The rate of reaction

may be governed by (a) the rate of transport of reactant through the oxide, or (b) the rate of oxygen supply to the outer oxide surface, or (c) the rate at which the oxygen and metal react to give oxide. If the rate of diffusion of the reactants through the oxide film is the slow step in the oxidation process, the oxidation rate will decrease as the thickness of the film increases. This is the case in practice.

Frequently metal oxides are defective because either cations or anions are missing in the crystal, forming vacancies. In some oxides there is an excess of metal cations which occupy interstitial sites in the lattice. The diffusion of ions through the lattice is via these defects, that is via either the vacant sites or the interstitial sites. Cuprous oxide, Cu_2O, the most commonly encountered oxide on copper is cation deficient, and thus, vacant sites exist within the lattice. As electrical neutrality of the oxide must be maintained, each missing cuprous ion must be compensated by a cupric ion (or positive holes). The more defective the oxide the greater will be the corrosion rate, because of easier ionic diffusion and therefore increased ionic conductivity. The rate of ionic migration increases with temperature leading to an increase in the corrosion rate.

Oxidation of alloys is more complex since several oxides may be formed. With some alloys, it is possible to choose conditions in which only the less noble component of the alloy is oxidized. If this oxide is highly protective, the alloy will have good corrosion resistance. The process of "selective oxidation" has been applied to copper/aluminium and copper/nickel alloys. It also forms the basis

for heat resistance alloys such as Fe-Al, since the Al forms Al_2O_3 on the alloy surface.

2.3 Corrosion of Metals in Aqueous Environments

Corrosion processes in aqueous solution are more complex than those of metal oxidation, but again metal compounds are formed with a decrease in the free energy of the system. The mechanism of corrosion in aqueous media is almost exclusively of an electrochemical nature. Damage from electrochemical corrosion may take many forms. There may be uniform destruction of the material or the corrosion may be highly localized, as in pitting. It may be accelerated by interaction with mechanical stress or attack may be concentrated at areas adjacent to a second more noble metal (galvanic attack) or at points where the oxygen supply is limited (differential aeration).

2.3.1 Metal dissolution

Consider a metal immersed in an aqueous solution of its ions. The metal consists of an atomic lattice of positive metal ions with an electron "cloud" in the space between the ions which bind the lattice together. The liquid consists of water molecules with a small number of hydroxyl ions and hydrated hydrogen ions and hydrated metal ions. All these species of ions and molecules have random movement and there is a definite possibility that the electrons and metal ions will pass into solution and that the water molecules, hydrogen ions, hydroxyl ions and metal ions will enter the metal lattice. The entry of hydrogen ions (or atoms) into the metal lattice, happens in certain cases and may give rise to the phenomenon of hydrogen embrittlement. The entry of metal

ions into solution is important in all cases of immersed corrosion. For the situation under consideration, that is a metal in a solution of its own ions, the important reactions are the metal dissolution (or anodic) reaction:

$$M \rightarrow M^{z+}_{aq} + ze \qquad (2.1)$$

and the reverse (or cathodic) reaction, that is electron transfer from the electrode to a metal ion in solution:

$$M^{z+}_{aq} + ze \rightarrow M \qquad (2.2)$$

For the latter reaction (2.2) when there is no potential difference at the interface, the reaction velocity will be given by:

$$V_- = k_- C_i \qquad (2.3)$$

where k_- is a chemical rate constant and C_i is the concentration of metal ions in solution. When a potential difference V exists, the reaction velocity becomes:

$$V_- = k_- C_i \exp(-\beta VF/RT) \qquad (2.4)$$

where β is the symmetry factor and F is the Faraday. An exactly similar equation can be written for the anodic reaction:

$$V_+ = k_+ C_M \qquad (2.5)$$

However in this case C_M is a constant related to the active sites on the metal surface. [illegible] Under a potential difference V, we have:

$$V_+ = k_+ C_M \exp[(1-\beta) VF/RT] \qquad (2.6)$$

If n moles of electrons are transferred for one complete reaction (n equals z in this simple case) then the current

is given by

$$i = n\ F\ V_{react.} \qquad (2.7)$$

Thus

$$i_- = n\ F\ k_-\ C_i\ \exp\ (-\beta\ VF/RT) \qquad (2.8)$$

$$i_+ = n\ F\ k_+ C_n \exp\ [(1-\beta)\ VF/RT] \qquad (2.9)$$

We define the over potential as the difference between the actual electrode potential difference, V, and the equilibrium potential V_e:

$$\eta = V - V_e \qquad (2.10)$$

Substituted $V = \eta + V_e$ into equations (2.8) and (2.9) they become:

$$i_- = n\ F\ C_i\ k_-\ \exp\ (-\beta\ F\ V_e/RT)\ \exp\ (-\beta\ F\ \eta/RT) \qquad (2.11)$$

$$i_+ = n\ F\ k_+ C_n \exp\ [(1-\beta)\ F\ V_e/RT]\ \exp\ [(1-\beta)\ F\ \eta/RT] \qquad (2.12)$$

All the terms in front of that containing the overpotential η also represent a current density but this is the current density at the equilibrium potential, V_e, when the forward and backward rates are exactly equal i.e. $i_+ = i_- = i_o$

$$i_o = n\ F\ k_+ C_n \exp\ [(1-\beta)\ F\ V_e/RT] = n\ F\ C_i\ k_-\ \exp\ (-\beta\ F\ V_e/RT) \qquad (2.13)$$

i_o is known as the exchange current density and is an important parameter in electrochemical processes. Equations (2.11) and (2.12) can thus be written in a simple form as below:

$$i_- = i_o \exp\ (-\beta\ F\ \eta\ /\ RT) \qquad (2.14)$$

$$i_+ = i_o \exp\ [(1-\beta)\ F\ \eta\ /\ RT] \qquad (2.15)$$

since the net anodic current density is

$$i = i_+ - i_o \qquad (2.16)$$

$$i = i_o \{\exp[(1-\beta)\ F\ \eta\ /\ RT] - \exp(-\beta\ F\ \eta\ /\ RT)\} \qquad (2.17)$$

This is the Butler-Volmer equation relating the net current density of the electrochemical reaction to the overpotential. For large positive η, equation (2.17) reduces to a simpler equation:

$$i = i_o \exp\ [(1-\beta)\ F\ \eta\ /\ RT] \qquad (2.18)$$

The same argument is valid for large negative η when the first exponential term becomes negligible. A similar equation is obtained:

$$i = -i_o \exp\ (-\beta\ F\ \eta\ /\ RT) \qquad (2.19)$$

The meaning of these two equations is very simple. For overpotentials greater than about 50 mV, the effect of the reaction going in a direction opposite to the main one for the sign of the overpotential concerned is negligible. It is only when η is less than about 0.05 V from the equilibrium potential, that the opposite process effects the net current significantly when the complete Butler-Volmer equation should be used.

Taking logarithms of both sides of equation (2.18) or (2.19) we obtain:

$$\text{Ln}\ i = \text{Ln}\ i_o + \frac{(1-\beta)\ F\ \eta}{RT} \qquad (2.20)$$

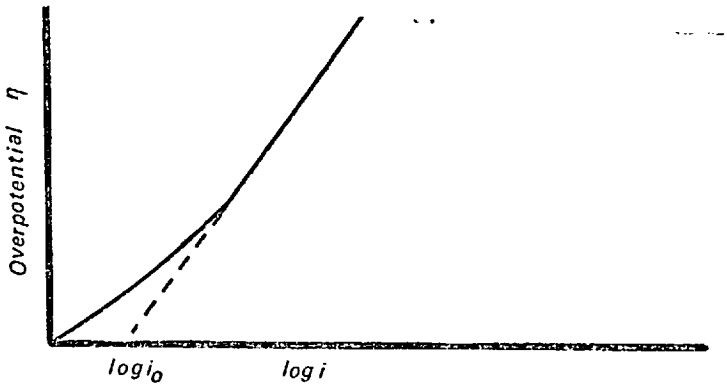
solving explicitly for η,

$$\eta = \frac{RT}{(1-\beta)\ F} \text{ Ln } i_o + \frac{RT}{(1-\beta)\ F} \text{ Ln } i \qquad (2.21)$$

Since in equation (2.21) only η and i are variables for a given system , the equation can be written as:

$$\eta = a + b \text{ Ln } i \qquad (2.22)$$

which is a linear relationship known as the Tafel equation. The relationship between η and Log i is shown below.



The exchange current density is an important parameter in corrosion process because a large i_o is associated with a large $i_{corr.}$ and a small i_o results in a small $i_{corr.}$

Many factors affect the value of the exchange current. Among these, the most important are the nature of the metal surface, concentration of ions in solution, temperature and adsorbed ions or molecules at the interface. The effect of pressure on exchange current is not very clear and various views have been expressed in the literature. However, the effect of pressure can be neglected for conditions around atmospheric pressure.

2.3.2 Mixed-potential theory of corrosion

The mixed potential theory of corrosion consists of two simple hypotheses:

1. Any electrochemical reaction can be divided into two or more partial oxidation and reduction reactions.
2. There can be no net accumulation of electrical charge

during an electrochemical reaction.

The utilization of the mixed-potential theory can be best demonstrated by considering mixed electrodes. A mixed electrode is an electrode or metal sample which is in contact with two or more oxidation-reduction systems. To illustrate let us consider the case of zinc immersed in hydrochloric acid. Under these conditions the zinc is rapidly corroded by the hydrochloric acid, and the electrochemical reactions occurring can be represented as in Figure (2.1). If we consider zinc in equilibrium with its ions, it would be represented by a reversible potential corresponding to the Zn/Zn^{++} electrode reaction, and a corresponding exchange current density. Likewise, if we consider the hydrogen-electrode reaction occurring on a zinc surface under equilibrium conditions, then this particular equilibrium state would be presented by the reversible potential of the hydrogen electrode and the corresponding exchange current density for this reaction on a zinc metal surface. However, if a piece of zinc is inserted in hydrochloric acid containing some zinc ions, the electrode cannot remain at either of these two reversible potentials but must lie at some other potential. Zinc, since it is metallic is an excellent conductor, and its entire surface must be at a constant potential. This potential is achieved when the second hypothesis of mixed-potential theory is satisfied; that is, the total rate of oxidation must equal the total rate of reduction. The only point in this system (Figure 2.1) where the total rates of oxidation and reduction are equal is at the intersection represented by a "mixed" or a corrosion potential E_{corr}. At this point, the rate of metal dissolution is equal

to the rate of hydrogen ~~euulion~~ evolution expressed in the terms of current. The current corresponding to this point is usually called corrosion current $i_{corr.}$, since it represents the rate of zinc dissolution. If the β values and exchange current densities for this system are known it is possible to predict the corrosion rate of zinc in hydrochloric acid from electrochemical data. For the purpose of comparison, a current density of 1 μ A/cm^2 roughly corresponds to a corrosion rate of 1 mpy for most metals. The exact relationship between dissolution current density and corrosion rate can be calculated utilizing Faraday's Law.

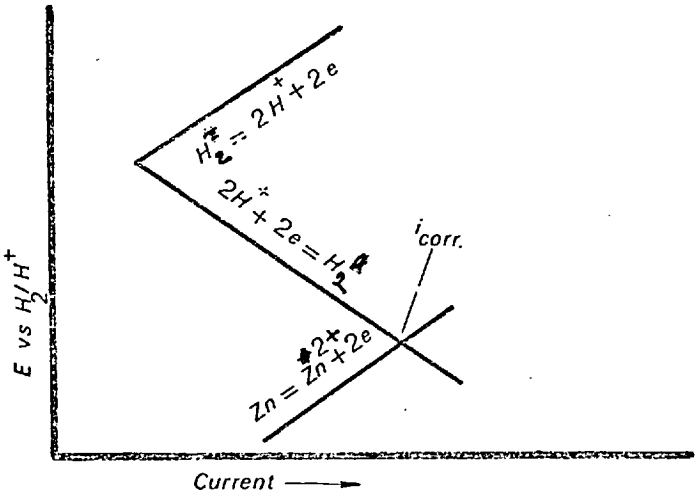


Figure (2.1) Electrode Kinetic Behaviour of Pure Zinc in Acid Solution

The above example was concerned with a system under activation polarization. The same principle can be applied to systems where one or more of the reduction processes are under diffusion control. Such an example is shown in Figure (2.2) which represents the corrosion of a metal M in a weak acid solution where the reduction process is under diffusion control. In this example, the metal M follows the typical anodic dissolution reaction under activation control. Initially, the reduction rate

of hydrogen ions is under activation control; at higher reduction current it is controlled by concentration or diffusional polarization. The corrosion rate of this system is equal to $i_{corr.}$ or i_L, and, as before, is determined by the intersection between the total reduction rate and total oxidation rate.

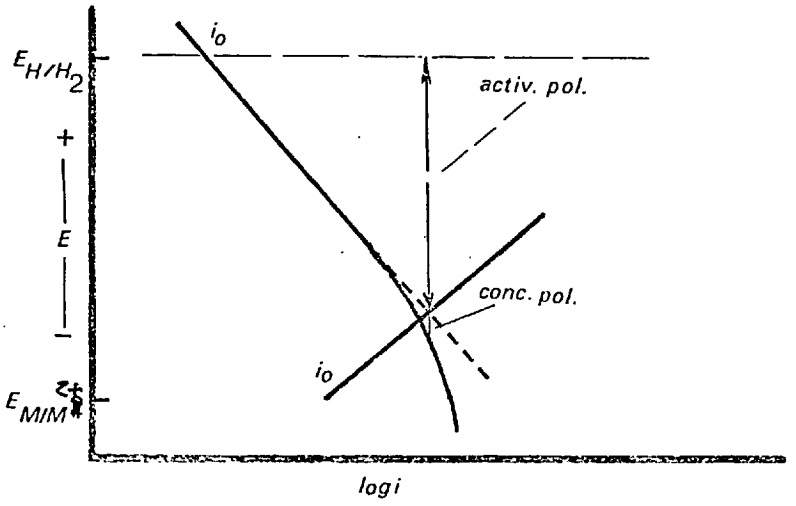


Figure (2.2) Combined Polarization Curve - Activation and Concentration Polarization

Other common cathodic processes besides hydrogen reduction is oxygen reduction which is the cathodic reaction for those electrodes of metals above the H_2/H^+ equilibrium, i.e. copper. The successive steps in this reaction are (a) diffusion of oxygen molecules to the metal surface followed by (b) O_2 adsorption. The overall reaction is according to equation (2.23).

$$O_{2\,(ads)} + 2H_2O + 4e = 4OH^- \qquad (2.23)$$

2.3.3 The active-passive transition

When the potential of a metal is raised above its reversible value E_M, the current density increases exponentially. However, when the potential exceeds that corresponding to equilibrium between the metal and one of its oxides (E_{M/M_xO_y}), we should expect the appropriate oxide or hydroxide to form on the metal surface. It is

because such a film frequently tends to confer protection and slow down dissolution to aquo-ions that a metal in this condition is said to be passive. In the neighbourhood of this region, the current passes through a maximum value, the so-called critical passivating current density i_{crit} and then falls off sharply. The potential at which the minimum current density is reached is termed the Flade potential E_F and corresponds to the onset of full passivity. The dotted line in Figure (2.3) corresponds to the phenomenon of transpassivity where the oxide film can partially re-dissolve as hydrolysed ions above $E_{M/M_{hyd}}$.

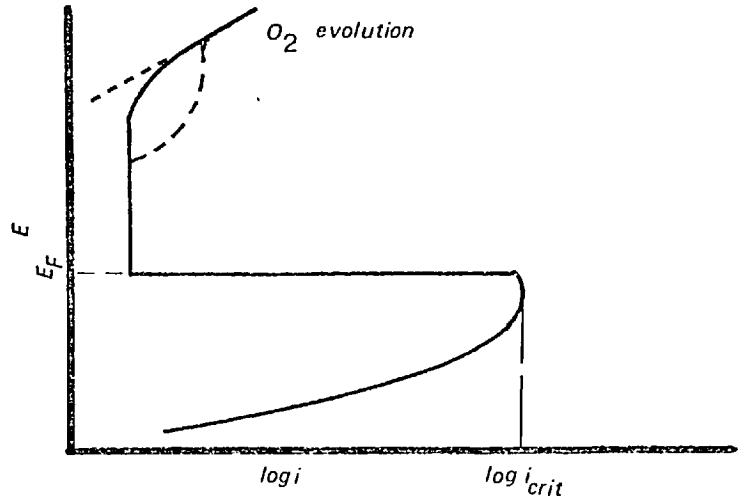


Figure (2.3) Passivation of Metal by Anodic Polarization

2.4 Atmospheric Corrosion

Atmospheric corrosion, principally rusting, is probably the most commonly encountered form of corrosion. If the temperature of a metal surface is below the dew point, a thin layer of moisture will form and corrosion of the metal will occur at places where the air-formed oxide film is thin, in much the same fashion as that described for corrosion in aqueous media. However, there will be an important difference, namely that, in the atmosphere, an abundant supply of oxygen to the cathodic

areas is available. The presence of sulphur dioxide in air is the main accelerator of atmospheric corrosion of metals.

2.5 Corrosion Prevention and Control

Since the requirement for spontaneous electrochemical corrosion are the existance of an efficient electron sink in electrical contact with the metal concerned and a suitable solvating cage for the metal ion, it follows from this that we may prevent and control corrosion in a number of ways.

a) Alloying

Alloying is concerned with the improvement of resistance to corrosion. This involves altering the structure of metal by solid solution in such a way as to bring it into the passive region and so offers a "built-in" kinetic method. An example is the effect of nickel addition to copper.

b) Cathodic protection

By means of an externally applied electric ~~current~~ potential, it is possible to reduce corrosion rate virtually to zero, and a metal surface can be maintained in a corrosive media without deterioration for an indefinite time. Cathodic protection can be applied in practice to protect metals such as steel, copper, lead and brass against corrosion in all soils and almost all aqueous media.

c) Poisons

Group V metals (or metalloids) such as phosphorus antimony and arsenic in the form As_2O_3 can inhibit cathodic reactions, such as hydrogen evolution. It has been supposed that the arsenious ion AsO^+ is sufficiently

surface active to adsorb at the normal points at which pairs of hydrogen atoms can unite.

There are hazards attending this method of corrosion prevention. Besides that of possible poisoning of human operatives, there is also danger of hydrogen embrittlement due to high population of uncombined hydrogen atoms on the surface of the metal.

d) Anodic protection

Some metals (e.g. iron and stainless-steels) can be protected effectively by external polarization, shifting their potentials into the passive region. In practice, this technique has so far been confined to metals and alloys which exhibit base Flade potentials and low i_{crit} values (see section 2.3.4), such as 18 Cr - 8 Ni steels. Anodic protection has found application in handling sulphuric acid, but the method is applicable to other acids and alkalies and some salt solutions providing the critical passivating current is small.

e) Metal coatings

Apart from chemical conversion coatings, where the metal is protected by its own oxide, phosphate, chromate and so on, the most common coatingsused are plastic (polymer) sheet; glass (enamel); pitch (bitumen); grease or oils; paint and metal. The first three owe nothing to additional inhibitors and might be thought to act simply by excluding water and oxygen. Many greases and oils are similarly free from inhibitors although they may contain deliberate "de-watering" additions. Although paints are usually highly complex, their basic purpose is again to provide a high resistance barrier at the metal surface.

Metals are coated with metals in order to improve the corrosion life of the underlayer metal.

f) Corrosion inhibitors

Inhibitors which form a barrier isolating the metal fall fairly clearly into two main categories. Those which promote passivity by causing the corrosion current to exceed the passivating current density and those which encourage the formation of some corrosion products often as an impervious macroscopic layer. Typical examples of first type are oxidizing anions such as nitrite NO_2^- and chromate CrO_4^{2-}. Since they operate by producing a passivating oxide film primarily at those parts of the surface where metal cations are formed (i.e. at the anodes), they are classed as anodic inhibitors.

Specifying cathodic inhibitors inhibit the cathodic regions (i.e. most of the surface) whilst not greatly influencing the active anodic sites. An example of this type of inhibitor are polyphosphates, such as "Calgon". Organic inhibitors also mainly fall into this category. However some organic inhibitors inhibit the corrosion processes both in cathodic and anodic region.

2.5.1 Organic inhibitors

The inhibiting action exercised by organic compounds on the dissolution of metallic material is normally attributed to interaction between the inhibitor and the metal surface resulting in adsorption. The type of interaction involved may be characterized by an examination of the adsorption kinetics, the heat of adsorption, or the reversibility and specificity of the bond established. The type of interaction which occurs between a solution species and a metal surface in contact

with the solution covers a continuum between the limits of no interaction at all and interaction to the extent of compound formation. Nevertheless, it is common practice to place each system into one of two categories and label it either physical adsorption or chemisorption.

When the adsorption process is considered primarily in relation to corrosion inhibition, it seems logical to assume that there exists an optimum type of adsorption bond. Certainly it is true that bonds lying too near the extreme of no interaction at all will have little or no influence on the electrochemical cell which make up the corrosion process. At the other extreme, formation of a true chemical bond between the metal and the solution species will, if anything, actually accelerate the loss of metal. Some evidence for existance of this optimum bond type is found in some observations that good inhibitors can become corrosion accelerators with only small changes in condition of temperature, concentration, etc.

The principal properties which make up the character of the bond between surface and inhibitor are:-

1. Type of electronic interaction - For physical adsorption this consists of either Van der Waals or electrostatic forces, while for chemisorption an actual charge transfer or charge sharing takes place between the solution species and some lattice unit (ion, atom or lattice defect).

2. Reversibility - Physically adsorbed species are readily removed by simply removing the species from solution, while removal of chemisorbed species requires more drastic treatment.

3. Kinetics of bond formation - Physical adsorption occurs rapidly provided it is not limited by transport to the surface or by orientation of complex molecules. It is also relatively temperature independent, though it will quite often exhibit an activation energy about 10 kcal. Chemisorption, on the other hand, is frequently a slow process with a larger temperature coefficient (higher activation energy).

4. Energetics of bond formation - Processes accompanied by a relatively large heat of adsorption are characteristic of chemisorption; lower heats of adsorption are characteristic of physical adsorption.

5. Specificity - Chemisorption processes, since they require charge transfer or charge sharing, are specific in the same sense that bond formation in chemical reactions is specific, i.e. a given species may chemisorb on one metal, but be completely indifferent to another. Physical adsorption is non-specific in this sense.

One mechanism by which adsorbed meterial interferes with the corrosion process is certainly that of pure physical barrier, whereby the inhibitor may cause a straightforward interference with transport of the corrosive agent; the principal effect is on the $H^+ \rightarrow H_2$ reaction since most inhibitors are nitrogen-containing cationic compounds, which are assumed to be ~~asorbed~~ adsorbed preferentially on cathodic area. This barrier film theory requires only a bond of some type between metal and inhibitor; the characteristics of the bond are of secondary importance.

However, it is clear that many effects cannot be explained by the barrier theory alone, and that

in most cases of really effective inhibition, the reduction of metal reactivity which is based upon a change in the nature of the solid surface, predominates. Since a reduction in metal reactivity cannot be accounted for by purely physical adsorption, it is proposed that the major portion of inhibitor action is due to chemisorbed species, and that because of the nature of chemisorption bonds, molecular structure of inhibitor molecules should have a marked effect on inhibitor efficiency.

If it is true that the best inhibitors require chemisorption and a lowering of metal reactivity, it should be possible to correlate certain measurable properties of inhibition and adsorption with known chemical properties associated with the various molecular structure. Most organic inhibitors are compounds with at least one polar functional group containing atoms of nitrogen, sulphur, oxygen, and in some cases, selenium and phosphorus. In general, the polar functional group is regarded as the reaction centre for the establishment of the chemisorption process.

The electron density in the functional group acquires particular importance in aromatic or heterocyclic inhibitors whose electronic structure may be affected by the introduction of substituents in different positions in the rings. The availability of electron pairs for the formation of chemisorption bonds can thus be altered by regular and systematic variation of the molecular structure.

Besides the structural parameters of inhibiting substances, the importance of the magnitude and sign

of the surface charge of the metal for the establishment of the adsorption bonds is clear. The effect exercised by organic inhibitors on the electrode reactions must be connected with the modifications induced in the structure of the electrochemical double layer because of their adsorption.

Among other characteristics of the metal which may exhibit some influence on the inhibition processes must be mentioned purity, the surface treatment and the cold working of metal.

CHAPTER THREE

EXPERIMENTAL METHODS OF STUDYING CORROSION INHIBITION PROCESSES

The conventional methods that are generally used for corrosion studies, can also be used for the study of the corrosion inhibition. Among various methods, corrosion rate measurements, electrochemical methods, radiochemical methods, IR and UV spectroscopy, ellipsometry and more recently photoelectron and Auger spectroscopy have found applications.

The corrosion rate can be expressed as variation in the weight per unit surface and per unit time or as penetration of the corrosive process into the metallic material in unit time. The expressions are valid if we refer to generalized and uniform corrosion processes, but they have a smaller practical significance in the case of localized attack phenomena. In the latter case one obtains an idea of the corrosion rate from the maximum depth of attack that can be deduced by various physical methods or by microscopic observations. The amount of metallic material dissolved can also be determined by estimating spectrophotometrically the metal that has passed into solution. Although these methods are useful in studying the effect of inhibitors upon the corrosion rate, they have little significance in fundamental studies of the mechanisms of corrosion inhibition.

Radiochemical methods with labled inhibitors make it possible to extend the knowledge of inhibition phenomena, permitting trace detection of substances adsorbed even under conditions of extreme dilution and provides an objective

method of evaluating the amount of inhibitor adsorbed. The advantages of radiochemical measurements become particularly obvious when it is shown to be possible to carry out adsorption determination without having to remove the metal sample from the conditions of equilibrium achieved in the environment under study. Because of the very specialised nature of radiochemical methods, and the need for special and expensive equipment for irradiation and detection, these methods have not found a large practical application.

ESCA which has found more applications in corrosion science (8), has been found to be an informative technique in corrosion inhibition studies and because of its extensive use in the present work, it is described in a separate chapter (Chapter 4).

3.1 Electrochemical Methods

Electrochemical methods used to determine corrosion rates are based on mixed potential theory. These methods are Tafel extrapolation, and linear polarization techniques. The Tafel extrapolation technique uses data obtained from cathodic or anodic polarization measurements. A schematic diagram for conducting a polarization measurement which has been used for the present study is shown in Figure (3.1). The metal sample is termed the working electrode and the current is supplied to it by means of an auxiliary electrode composed of some inert material such as platinum. Current is recorded in a logarithmic scale and potential is recorded on the other axis of an x-y plotter. The reference electrode is typically a saturated calomel electrode.

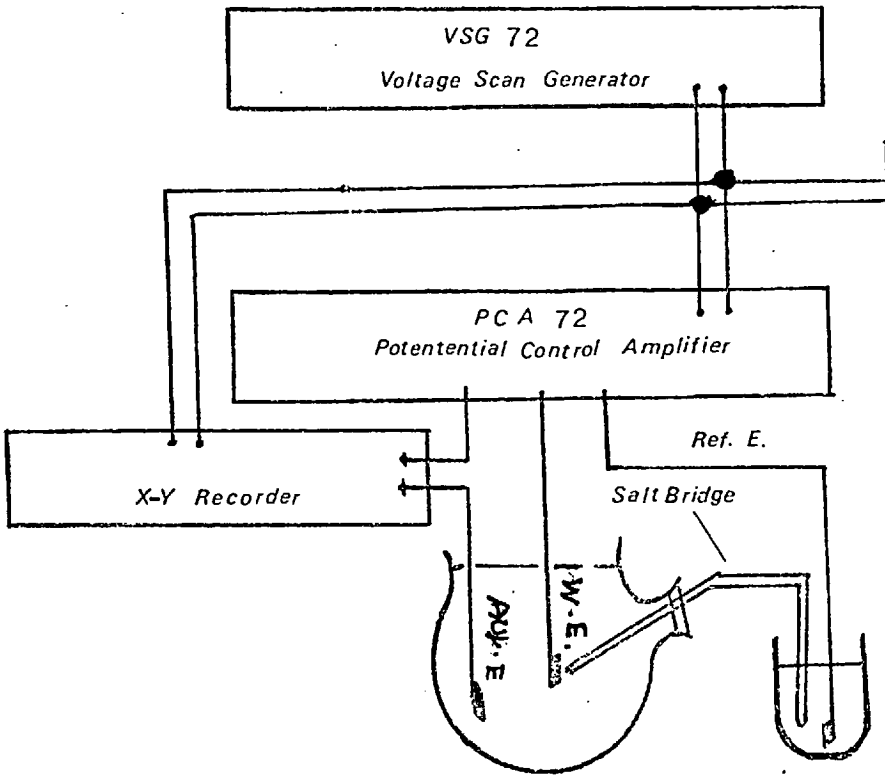


Figure (3.1)

The curve obtained in this fashion is non-linear at low current, but at higher current it becomes linear. Applied cathodic current is equal to the difference between the current corresponding to the reduction process and that corresponding to the oxidation or dissolution process. It is obvious that at relatively high applied cathodic current densities, the applied current begins to approach total actual cathodic current, since the corresponding total anodic current becomes negligible. In actual practice, an applied polarization curve becomes linear on a semi-logarithmic plot at approximately 50 mV more active than the corrosion potential. This region of linearity is referred to as the Tafel region. To determine the corrosion rate from a polarization curve, the Tafel region is extrapolated to the corrosion potential. At the corrosion potential, the rate of cathodic reaction e.g. hydrogen evolution or O_2 reduction is equal to the rate of the metal dissolution, and this point corresponds to the corrosion rate of the system expressed in terms of

current. Under ideal conditions, the accuracy of the Tafel extrapolation method is equal to or greater than conventional weight-loss methods described earlier. With this technique it is possible to measure extremely low corrosion rates, and it can be used to monitor the corrosion rate of a system.

Although this technique can be performed rapidly with high accuracy, there are numerous restrictions which must be met before this method can be used successfully. To ensure reasonable accuracy, the Tafel region must be extended over a current range of at least one order of magnitude. In many systems this cannot be achieved because of interference from concentration polarization and other extraneous effects. Further, the method can only be applied to systems containing one reduction process, since the Tafel region is usually distorted if more than one reduction process occurs. In summary, the Tafel method is very useful and can be used in certain circumstances to rapidly measure corrosion rates. However, the inability of this method to determine the surface film chemistry, limits its usefulness in studying corrosion inhibition mechanisms unless it is used together with another method such as ESCA or I.R. reflectance spectroscopy.

3.1.1 Experimental techniques

All cell-electrode arrangements can be divided into two groups. The first group includes the two electrode arrangement and the second, the three electrode arrangement. Every cell must have an anode and a cathode and each one may be the working electrode. The potential of the working electrode is measured or controlled, hence the need for a

reference electrode. In the two electrode arrangements the reference electrode also serves as a counter electrode. This arrangement is suitable only for cases where the current passed through the cell is very small, so small that the reference-counter electrode can be regarded as ideally non-polarizable (i.e. of constant potential). Since the potential of the reference electrode is constant, any change of cell potential may be regarded as a change in the potential of the working electrode.

The auxiliary electrode must be made of a material that will not react with the solvent or any component of the solution over as wide a potential range as possible.

The potential of reference electrode should be constant, established quickly and not vary much if a few microamperes are passed through the electrode. In other words, the electrode should have a minimal resistance. This resistance should be independent of the direction of current flow and should be constant. This implies that the current-potential curve for a reference electrode should look like that in Figure (3.2a) and not the one in Figure (3.2b).

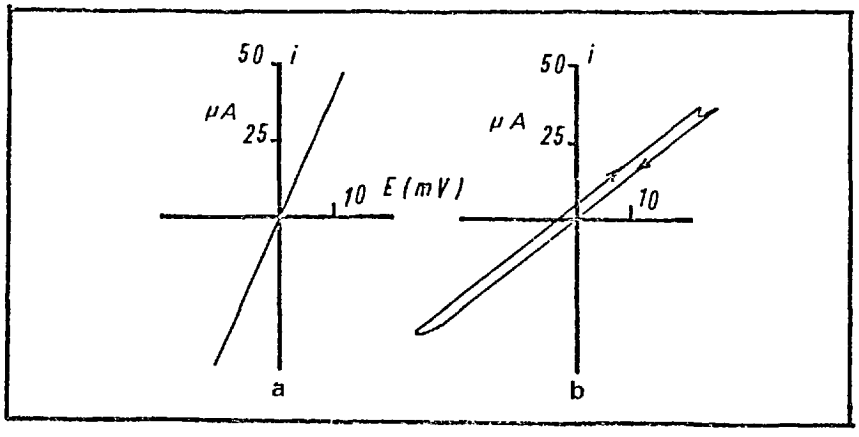


Figure (3.2) Current-potential Curves for Reference Electrodes: a) good, b) bad

Potential of saturated calomel electrode with electrode symbol $Hg/Hg_2Cl_2/KCl$ (sat.) is 0.2412 against the standard hydrogen electrode at 25°C. The electrode reaction given by equation (3.1).

$$2Hg + 2Cl^- = Hg_2Cl_2 + 2e \qquad (3.1)$$

The electronic equipment used in the study of electrode processes may vary considerably in degree of sophistication and in price. However it can conveniently be described by referring to the simple polarographic circuit for three electrode arrangement which is given in Figure (3.3).

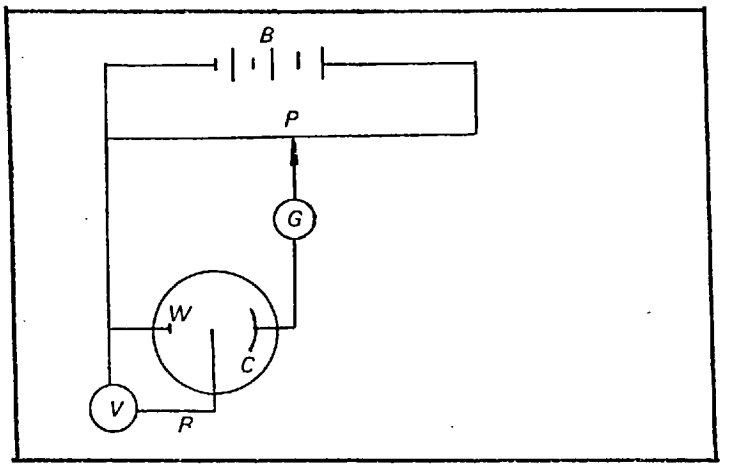


Figure (3.3) Schematic Presentation of a Polarographic Three Electrode Arrangement Circuit

This basic circuit is made up of a variable voltage source, a cell and a current measuring instrument. The voltage of the source is applied across the anode and cathode and the working electrode potential is measured between the latter and a reference electrode using a suitable instrument.

The simple variable voltage source is a battery connected across a potentiometer and adjusted manually. The batteries can be replaced by a mains operated rectifier and the hand-operated potentiometer may be replaced by a

synchronous motor to drive the potentiometer and so provide a linear change of voltage with time.

The simplest current measuring instrument is the galvanometer, but its sensitivity is limited to small currents, the current cannot be conveniently recorded and its operation is slow. If the galvanometer is replaced by a current measuring resistor, the potential drop across the latter is proportional to the current passed. Thus the current measuring problem converted to a voltage measuring problem. Here, potentiometric recorders are very useful when the rate of change of voltage is much lower than the response time of the recorder. For faster changes oscilloscopes are used.

In order to record current voltage curves directly, one may use x-y plotters, where one voltage drop (across the standard resistor) is fed to the y axis and the other (between the working and reference electrodes) is fed to the x-axis. Since large currents are not supposed to pass through the reference electrode, the measuring instrument, i.e. recorder or oscilloscope, must have a high input impedance.

Often, when using three electrode arrangement, one is interested in controlling the rate of change of potential difference not between the cathode and the anode, but between the working and reference electrodes. In other words, one wants to adjust the potential difference between the latter two electrodes to a desired value and apply the voltage between the anode and cathode as needed. This can be done automatically using the instrument known as a potentiostat. In the present study, a Wenking Potential Control Amplifier model PCA72M was

used whose block diagram is shown in Figure (3.4).

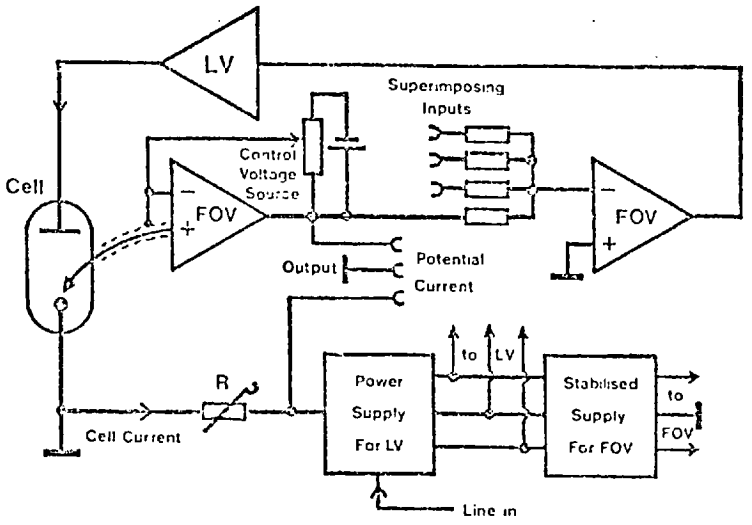


Figure (3.4) Block Diagram PCA 72M

This consists of two operational amplifier (FOV) and one output power amplifier (LV) and a power supply. The potential picked up by the reference electrode capillary system at the surface of the working electrode controls the non-inverting (+) input of the buffer amplifier FOV. This operational amplifier has an output voltage equal to the reference electrode potential vis the grounded working electrode less the voltage suppressed by the control voltage source. The buffer amplifier has a very fast response so that input and output voltage correspond to each other within a short period less than 1 μsec. The output of the buffer amplifier controls the inverting (-) input of the following operational amplifier FOV. This input is kept at virtual ground potential by feedback across LV and the electrochemical cell. The power supply for the output amplifier LV is floating vis ground. The cell

current closes via the variable resistor R. A voltage drop vis ground is proportional to the current is existing at the current output terminals. The voltage drop proportional to current can feed back one of the superimposing inputs. This results in a positive feedback, as it is applied for IR-drop compensation. The R compensated in the cell is equal to the ranging resistor R.

The complete polarization cell used in this study, together with its salt bridge and reference electrode, is shown in Figure (3.5). The cell is a modified, multi-necked, one litre round bottom flask. The multiple necks are used to introduce electrodes, gas inlet tube, thermometer, and other accessories. The Luggin probe (salt bridge) enters the cell through a clamped, ball and socket joint. This arrangement which is recommended by Greene (9) permits the flexibility necessary to align the Luggin probe adjacent to the working electrode. Working electrodes were constructed to have only one flat surface exposed and faced to the Luggin probe. For details of the working electrodes construction see Appendix A.

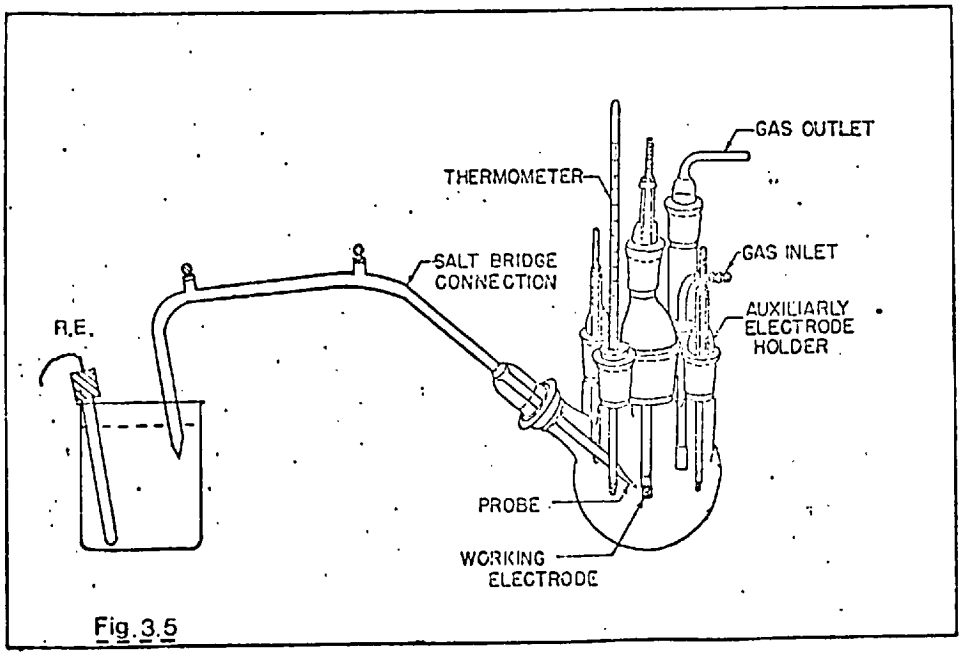


Fig.3.5

3.2 Infra-red Spectroscopy

Infra-red spectroscopy has been of the greatest value in the structural determination of molecules. Its application to the study of surface chemistry has provided one of the most direct means of observing the interactions and perturbations that occur at the surface during adsorption and of determining the structure of adsorbed species.

Infra-red spectra originate in the transitions between discrete vibrational - rotational energy levels of molecules. If radiation of a particular frequency corresponds to the energy difference between the ground and the first vibrational level of a molecule, energy will be absorbed provided the transition is allowed. Hence an absorption band will be observed at the appropriate frequency. Change of rotation state may occur simultaneously with a vibrational transition. This gives rise to the familiar shape of gas-phase vibrational spectra with two or three branches associated with each band indicating the vibrational - rotational transition. Provided the spectral resolution is sufficiently high, the individual rotational lines in the vibration - rotation spectrum may be resolved.

In the liquid phase, the rotational freedom of the molecule is lost and free rotation is replaced by liberational motion within the cage of the solvent molecules. This leads to disappearance of the rotational fine structure and its replacement by a single curve corresponding to the vibrational transition. The suppression of the rotational structure is brought about by the collisions incurred during the restricted rotation in the liquid.

The vibration associated with a molecule, in general, may be described as bond stretching, bond bending, or deformation and torsional vibrational modes. The frequencies of various types of vibrations are determined by the mechanical motion of the molecule and depend on the force constants of the bonds between atoms and the masses of the vibrating atoms. The intensities of the infra-red absorptions are determined by electrical factors such as dipole moments and polarizability.

It has been found that certain structural groups of atoms give rise to vibrational bands in the same region of the infra-red spectrum irrespective of the complexity of the molecule in which the group is situated. In such cases it can be assumed that a particular vibration is essentially localized in that structural group, although for a fundamental vibrational mode every atom in the molecule undergoes periodic displacement, in phase with the same frequency, but the displacements of atoms not in the functional group have small amplitudes. Minor variations of the characteristic group vibrational frequencies arise as a result of local differences in molecular environment, either because of intra-molecular interaction between groups in the molecule, or inter-molecular interaction with the surroundings (e.g. solvent effects). Such frequency changes may be used to investigate the interaction between a group and its environment.

To date, the application of infra-red spectroscopy in surface studies has been confined to rather limited spectral regions and not all absorption bands belonging to a surface molecule have been recorded. This is due to

strong absorption of infra-red radiation by the solid substrate to which the molecules are bound. As a consequence, the assignment of structures has been made on the basis of similarity between relatively few bands in the spectrum of the surface species and those of molecules in bulk liquid or solid phases. The question at once arises as to the validity of this comparison of the spectra of molecules in unsymmetrical surface environment with those in more uniform surroundings. In a review of this subject, Eishens and Pliskin (10) have suggested that such comparisons have produced results which are self-consistent for a wide variety of adsorption systems. At the present stage in the application of the infra-red technique to surface phenomena, a considerable body of evidence has been obtained wherein good correlation exists between the spectra observed and anticipated surface structure.

3.2.1 Multiple-reflection techniques

An important approach to obtaining spectra from adsorbed molecules on metal surfaces is to use a multi-reflection technique. Francis and Ellison (11) first carried out such measurements using a small number of oblique reflections, to obtain spectra from fatty acid layers on metal surfaces. The source and sample optical arrangement is illustrated in Figure (3.6).

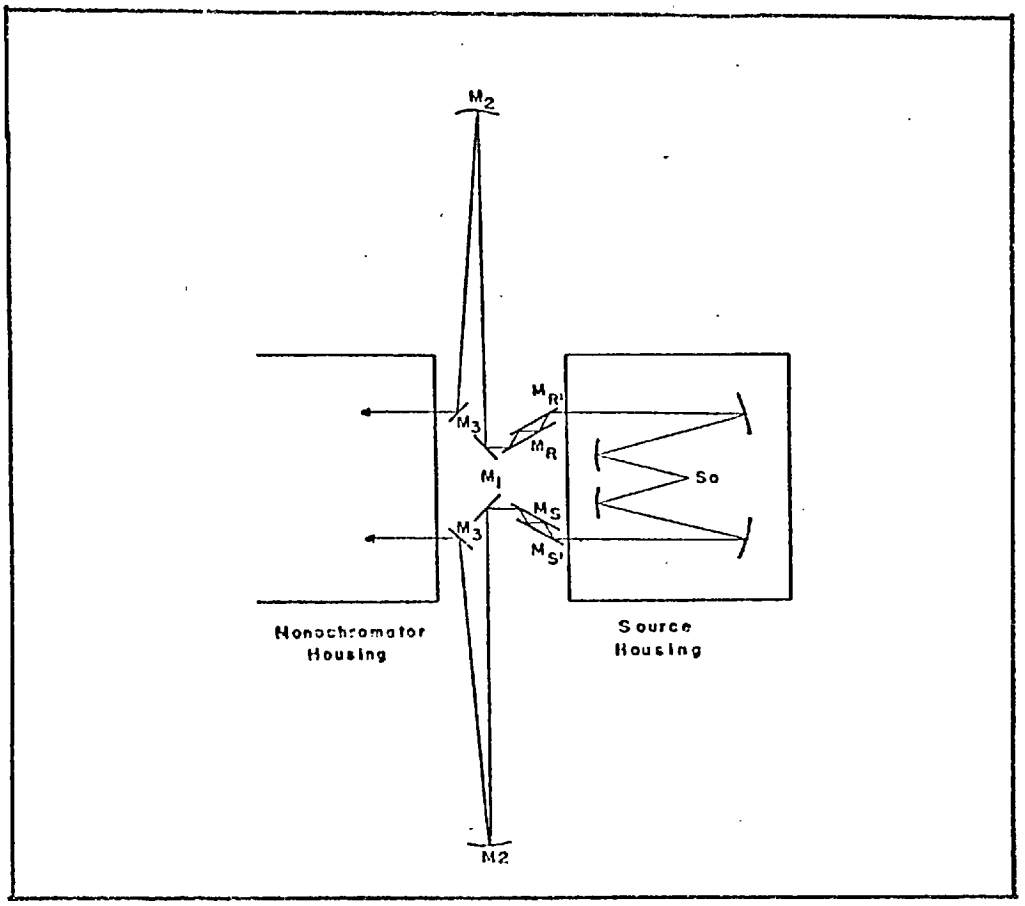


Figure (3.6) Optical Arrangement of Multi-Reflection Unit (Francis and Ellison)

The two beams are focused between the front beam mirror, M_S and M_S', and the back beam mirrors, M_R and M_R'. The sample film whose absorption spectrum is desired is deposited on one of the sets of mirrors M_R and M_R' or M_S and M_S'. The other set is cleaned and serves as reference mirrors. A convenient arrangement used in most of the work consists of mirrors 2 in. long by 1½ in. high separated $\frac{1}{8}$ in. and set to the angle of incidence is 72°. With this arrangement the beam is reflected twice from each mirror, giving a total of four reflections from each pair of sample and reference mirrors. In this arrangement, it is virtually impossible to obtain more than two reflections per mirror.

A modified system by J. Leja et al (12) allowed them to obtain a larger number of reflections. Schematic drawing of sample mirrors used by J. Leja and others

is illustrated in Figure (3.7).

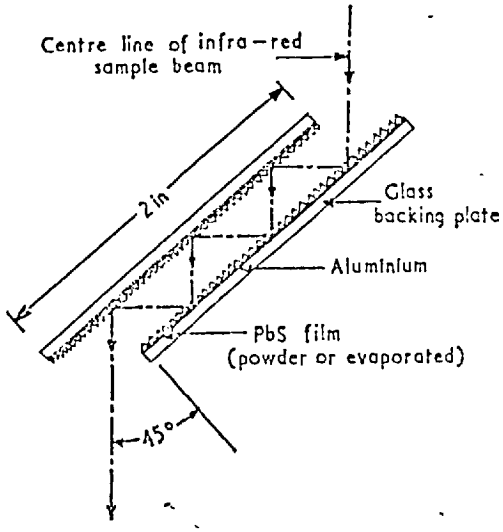


Figure 3.7:

In the modern units, such as the specac multi-reflection A.T.R. 1000, which has been used in this work, a total of 25 reflections is obtainable. The unit is designed for use with internal reflection crystal. This unit permits radiation to be incident on the associated crystal at any angle between 30° and 60°. Radiation is concentrated and collected from the crystal by four surface aluminized mirrors which produce very little energy loss. In the present work, instead of a crystal prism, an air gap between the two parallel reflecting samples was used. Using this technique, the incident angle on the sample could be changed and the gap between the samples is variable, so the number of reflectance could be controlled. Figure (3.8) shows the optical arrangement of this unit.

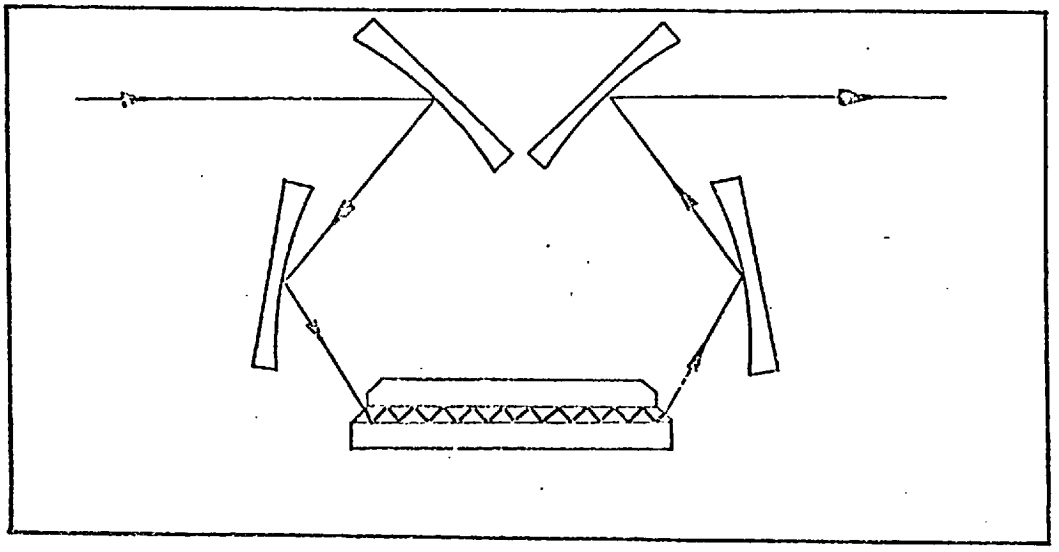


Figure (3.8) Optical Arrangement of Specac ATR 1000

An identical unit was placed in the reference beam to maintain the optical balance.

CHAPTER FOUR

ELECTRON SPECTROSCOPY FOR CHEMICAL ANALYSIS (ESCA)

In the current work, the ability to study the formation of films on metal surfaces is crucial. In recent years, powerful new physical techniques have been developed which are critical in studying surfaces of material. In characterizing a material, perhaps the most important special area of interest, is the surface. A surface, by definition, is an interface - a marked discontinuity from one material to another. Examples of the new techniques for surface studies include X-ray photoelectron spectroscopy (XPS), Auger electron spectroscopy (AES) and low energy electron diffraction (LEED). A way of looking at current techniques used in surface characterization is shown in Figure (4.1). The modes of excitation and emission can best be categorized in terms of photons ($h\nu$), electrons (e^-) and ions. Photons include all wavelengths of electro-magnetic radiation, but for these techniques are restricted to the X-ray and ultra-violet region.

Excitation/ Emission	hν	e^-	Ions
hν	X-RF	EMP	IEX SCANIIR
e^-	ESCA PES AES	SEM AES EM	SEM
Ions			IMMA SIMS ISS RUTHERFORD

AES Auger electron spectroscopy

EM Electron microscopy

EMP Electron microprobe

ESCA Electron spectroscopy for chemical analysis

IEX Ion excited X-ray fluorescence and ion impact radiation

IMMA Ion microcrobe mass analyser

ISS Ion scattering spectroscopy

PES Photoelectron spectroscopy

RUTHERFORD Rutherford scattering

SCANIIR Surface composition by analysis of neutral and ion impact radiation

SEM Secondary electron microscopy

SIMS Secondary ion mass spectroscopy

X-RF X-ray fluorescence

Figure (4.1) Summary of Techniques for Surface Analysis

Excitation and detection system used in surface analysis is shown in Figure (4.2).

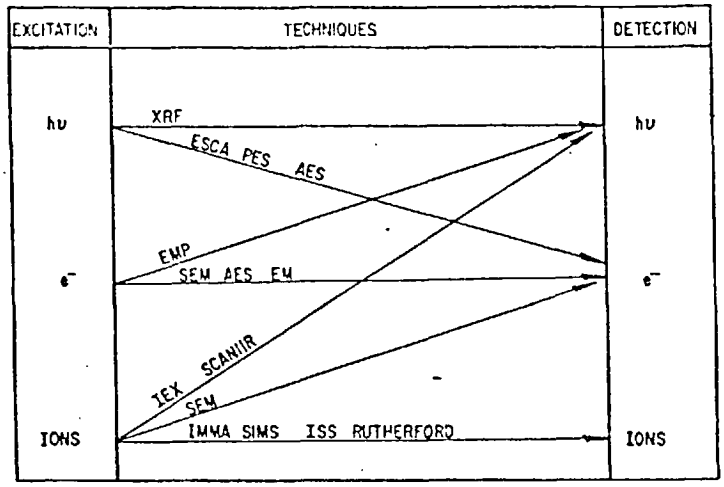


Figure (4.2) Excitation and Detection Systems used in Surface Analysis

For more detail see references (13) and (14) in which these techniques are described in detail.

4.2 X-ray Photoelectron Spectroscopy (XPS or ESCA)

When a solid sample of the material under investigation is exposed to X-ray radiation of an accurately known energy, the photo-electrons freed by the photoelectric process will have a kinetic energy given by

$$E_{kin,C} = h\nu - E_b - \phi_C = E_F - \phi_C \qquad (4.1)$$

where $h\nu$ is the photon energy and E_b is the atomic electron binding energy. The quantity ϕ_C, known as the work function of the sample, is the amount of energy required to raise an electron from the Fermi level edge to just outside the sample bulk, where it has zero kinetic energy. Figure (4.3) shows the relations among the quantities involved. When the electron leaves the vicinity of the converter, the zero energy level

position (at a work function of energy above the Fermi level) will change slightly to refer to that for the spectrometer material. During the time that the energy analysis takes place, its kinetic energy is

$$E_{kin,sp} = E_F - \phi_{sp} \qquad (4.2)$$

which is the measured value. Since the binding energy of an atomic electron in solid converter is defined as the energy necessary to raise it to the Fermi level, its value can be obtained from the photoelectron energy by

$$E_B = h\nu - E_F = h\nu - E_{kin,sp} - \phi_{sp} \qquad (4.3)$$

in which ϕ_{sp} indicates the spectrometer work functions, i.e. the total energy required to remove an electron from the Fermi level to a position outside the material bulk, its final kinetic energy being zero.

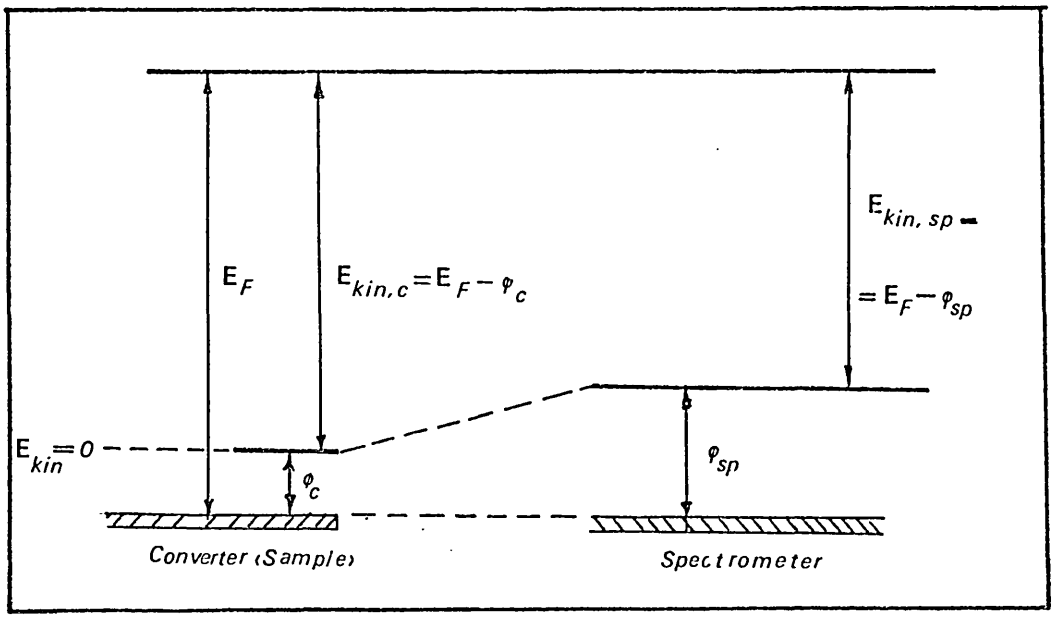


Figure (4.3)

Since a given atom's electrons occupy distinct orbitals of characteristic energy, when photoelectrons are emitted they do so at well defined kinetic energies.

Also, as different elements have different sets of binding energies for various orbitals, energy analysis of the emitted photoelectrons allows the identification of individual elements. Figure (4.4) shows a typical XPS full spectrum for polished copper. The ability to uniquely differentiate between elements was partly responsible for the method being named Electron Spectroscopy for Chemical Analysis (ESCA), and has led to its widespread application for this purpose, especially to solids. Gas phase and liquid phase studies can also be carried out, though they do not concern us here.

4.3 Instrumentation

Essentially, an electron spectrometer works in the following manner. An excitation beam (electrons, ions, X-ray, etc.) irradiates a target sample; the ejected electrons enter the spectrometer and are separated according to their kinetic energies, they then strike a detector and are counted and data are stored in a suitable manner. Figure 4.5. is a schematic drawing of an electron spectrometer divided into its essential components.

Since all results in this work were obtained using a Vacuum Generator ESCA 3 ultra-high vacuum (UHV) photoelectron spectrometer, all diagrams and devices explained are referred to this instrument.

The excitation source is a Mg/Al double anode X-ray gun. This consists of a water-cooled anode coated on one side with magnesium and on the other with aluminium. Close to each coating lies a filament which thermoionically emits electrons which are then

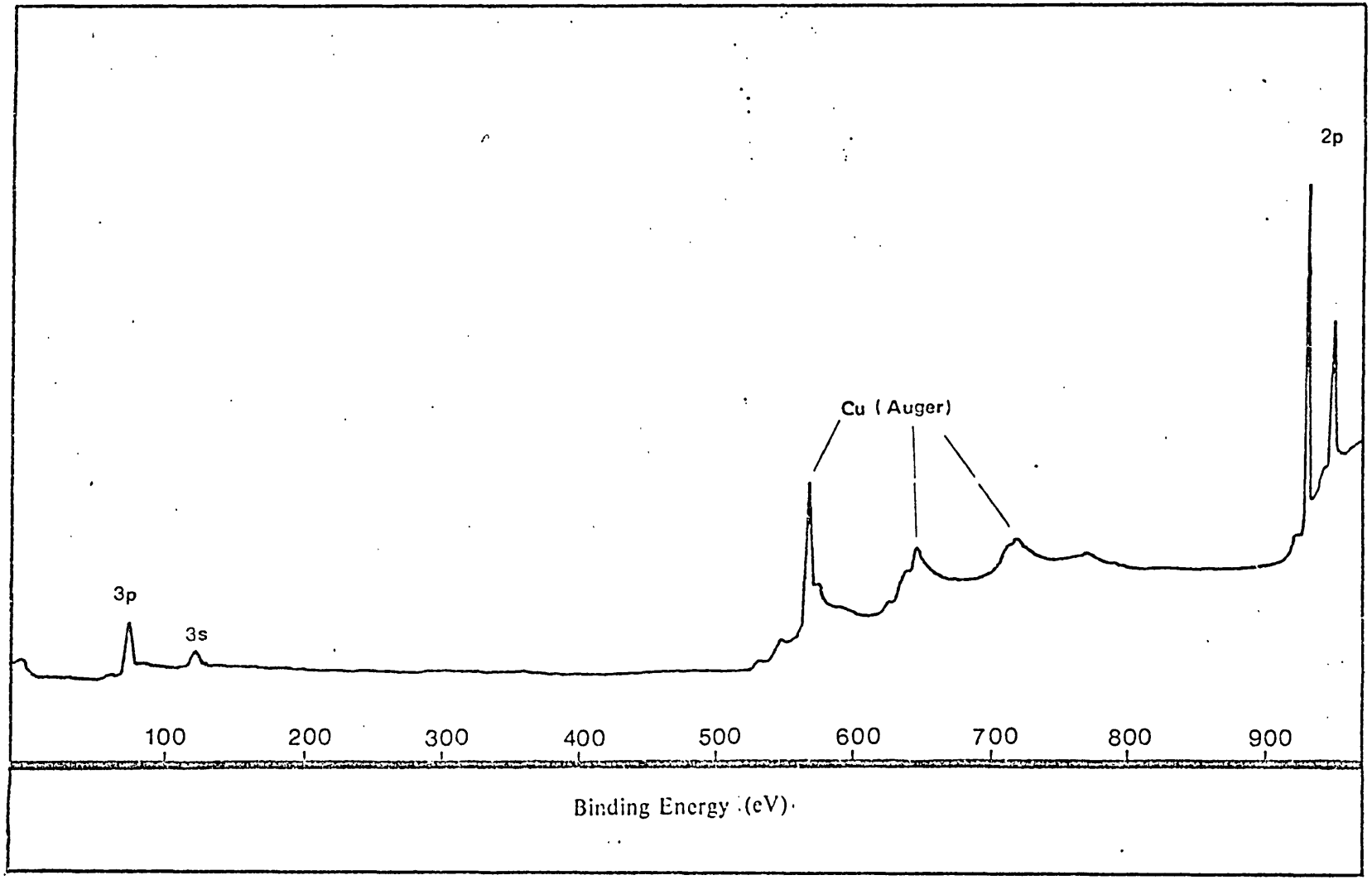


Figure 4.4: X-ray photoelectron full spectrum of a polished and argon ion etched copper sample.

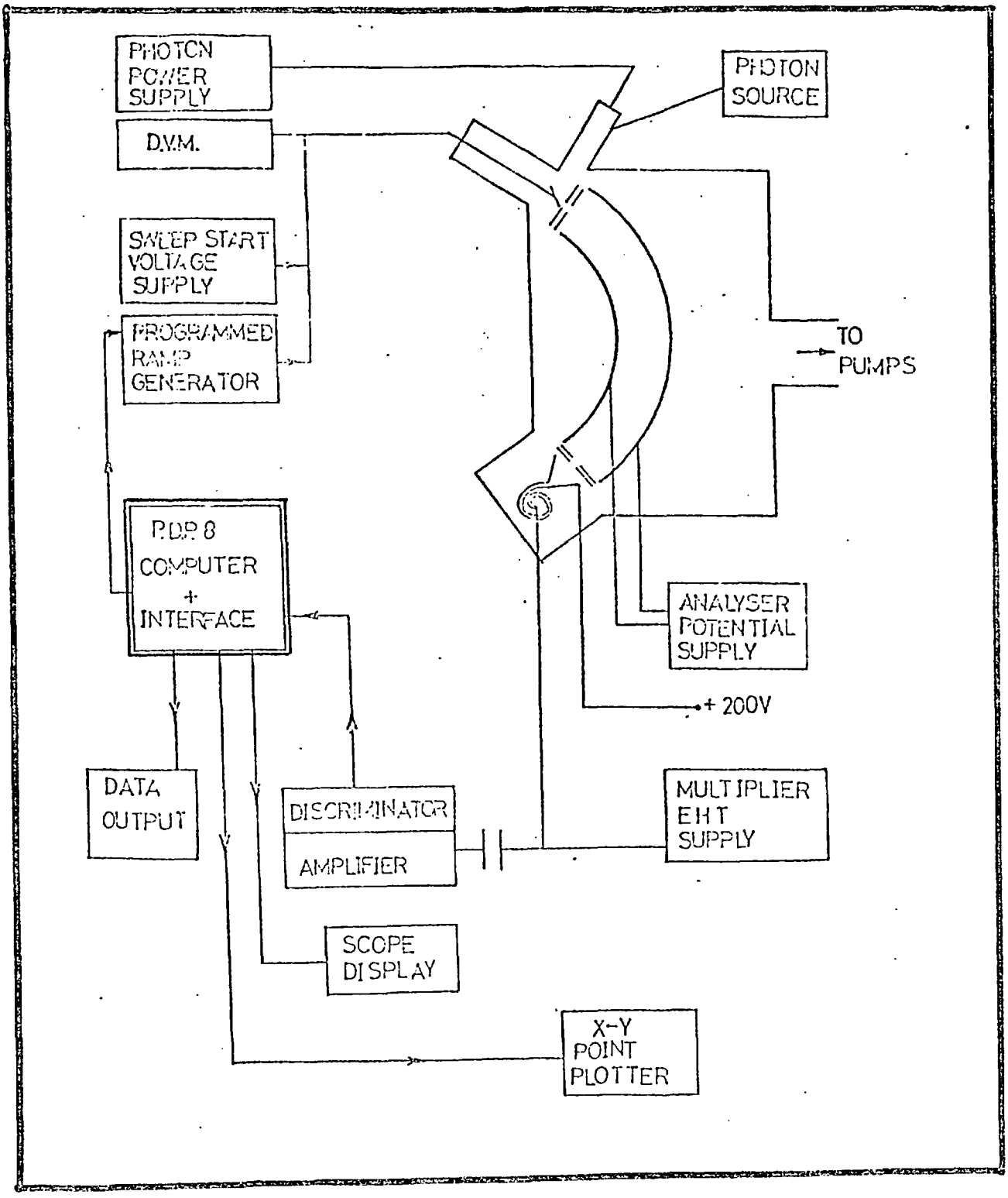


Figure 4.5: Schematic arrangement of the Basic ESCA.

accelerated to the anode, exciting Mg or Al Kα radiation of 1253.6 and 1486.6 eV energy and 0.7 and 0.9 eV band width respectively. An aluminium window isolates the X-ray gun from the analyser chamber. This prevents stray electrons from entering the analyser, lowers the background X-ray level, and keeps the pressure in the analyser chamber as low as possible.

The precision of the final energy measurement is dependent upon using the most narrowly defined source of exiting radiation available. Since the line width of X-ray emission is proportional to atomic number, the lightest elements with well-defined intense radiation are the most desirable sources. Figure (4.6) shows the theoretical and experimental width of the atomic levels.

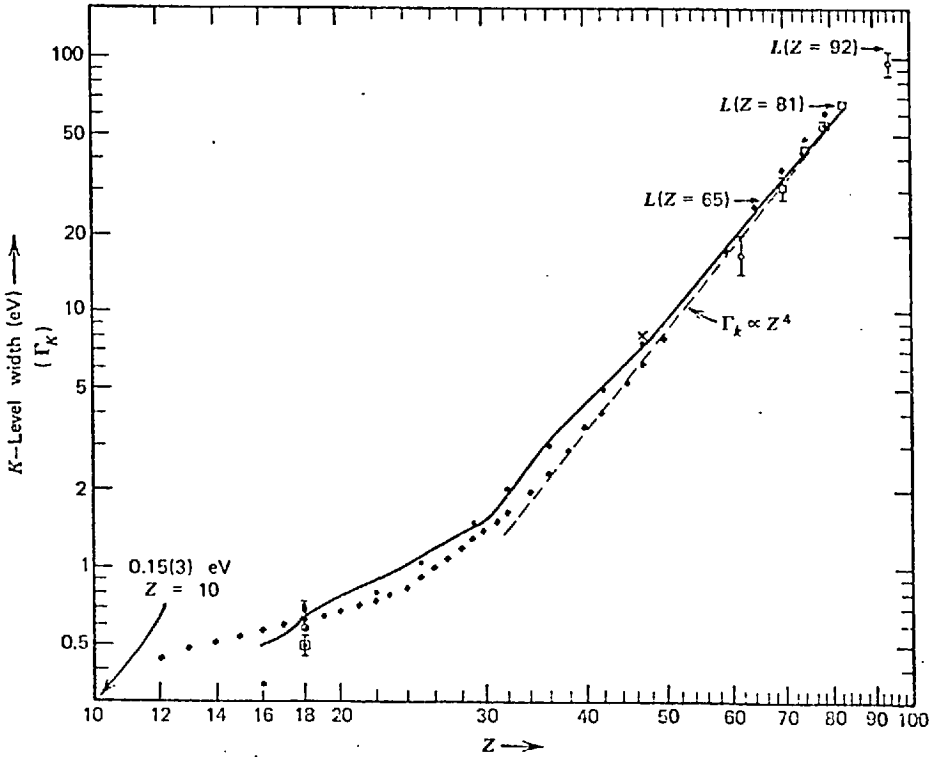


Figure (4.6) Theoretical and Experimental Widths of the Atomic Levels (15)

Although Cu and Cr were used historically, the targets in most common use today are Al and Mg. Sometimes, for further narrowing the X-ray beam and elimination of stray radiation, an X-ray mono-chromator is used. However, with some mono-chromators, the alignment of the samples becomes extremely critical, and a drastic loss in excitation beam intensity must be expected from all such devices. The spectrometer used in present study, was not equipped with any monochromator.

The second part of a spectrometer (Figure 4.5) is the electron analyser. This is a 150° hemispherical electrostatic analyser, a schematic diagram of which is given in Figure (4.7).

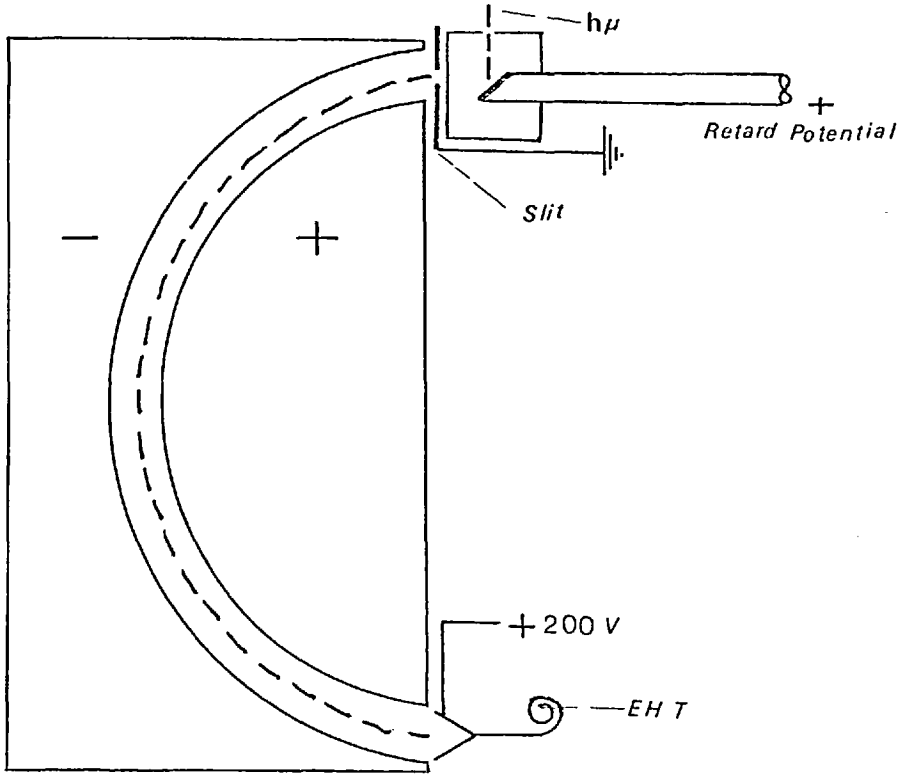


Figure (4.7) Schematic Diagram of an Electrostatic Electron Analyser

The technique used to energy analyse the electrons operates by keeping the potentials on both sections of the analyser constant, and hence focussing a constant electron

kinetic energy, while decreasing the positive retard voltage placed between the slit and the sample in a linear manner. Once a photo-electron has enough energy to both escape from the retard field, and traverse the path through the analyser as shown by the dots in Figure (4.7), then it is collected by a 200 V positive potential applied to the electron multiplier cup, and is detected. By scanning the retard voltage over, say 1000 V, several peaks may be recorded when core level photo-excited electrons have the correct energy. The potential across the two faces of the analyser may be changed to alter its sensitivity and resolution.

Finally the data were accumulated by employing a PDP-8f mini-computer. The computer is interfaced with a digital cassette system for recording data, an x-y plotter for final manipulation of output data, and an oscilloscope for a visual display of the spectra. Besides recording data, the computer may be used to process spectra, and it has some useful programmes such as curve substration, smoothing.

In order to provide a UHV environment, which is desirable for reliable surface sensitive studies (see below) and good resolution, the spectrometer is contained within a vacuum chamber pumped by two diffusion pumps charged with Santovac 5 oil, through anti-creep liquid nitrogen traps. The instrument is also equipped with several other devices such as an argon ion gun for ion sputtering (etching and sample cleaning) and a quadruple mass spectrometer for residual gas analysis.

4.4 Surface Sensitivity

The reason for the application of XPS to surface studies lies in the low mean free path that photoexcited electrons can travel through a solid without suffering energy losses. The graph below, Figure (4.8), taken from Prutton (16) demonstrates that electrons of around 100 eV k.e. have the smallest mean free path and hence the greatest surface sensitivity.

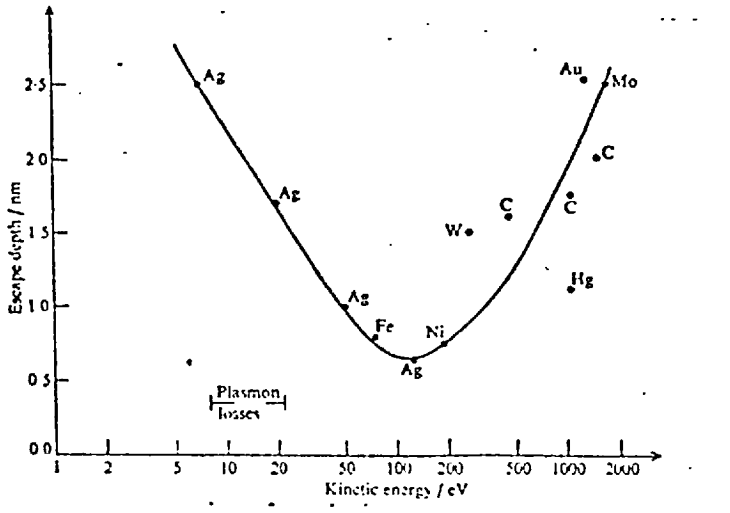


Figure (4.8) The Variation of Mean Free Path with Kinetic Energy

Most useful lines in XPS lie in the energy range 500-1100 eV k.e. for which the mean free path is still very small, having a value of approximately 2.5 nm. These low values mean that only photoelectrons from the very outer layers of a solid can contribute to the total photo-emission from the sample under study, and this fact forms the basis of the usefulness of the technique for surface analysis.

Not only is the technique sensitive to the surface layers, but within those layers small quantities of a minor constituent can be detected. This was amply demonstrated by Siegbahn et al (14) who found they could detect the presence of only 10^{13} atoms of iodine, a figure which represents only 1 or 2% of a monolayer coverage of the surface.

Studies or analyses may be performed on a given atomic species even if it is present as a minor constituent in the presence of many other atoms in the molecule. For example, Sighbahn et al (14) observed the cobalt signal in a 100 Å layer of vitamin B-12 in which the cobalt was present as 1 atom in 180 atoms of carbon, hydrogen, nitrogen, and oxygen. In yet another study, the disulfide bridges could be studies in insulin (mol. wt. 6000), though only three such bridges exist in the molecule.

Although the sensitivity quoted is quite good, one must remember that the figures relate to samples in which the entire amount of material is deposited in a small area (0.5 cm^2). If the material to be studied is dispersed in a large amount of another material, the total amount of contaminant that will be able to be placed into the sample holder will be much less than the minimum detectable quantity. Thus, ESCA, though sensitive to an extremely small amount of many species, is not yet a technique for trace analysis.

4.5 The Chemical Shift

The binding energy for a particular core level is influenced by the chemical environment in which that atom finds itself. More specifically, the effective

nuclear charge which an electron experiences is a function of the type and extent of bonding that the atom is taking part in. It is possible, using XPS to detect shifts in the binding energy of a particular core level, and hence yield chemical information concerning that atom. The diagram below, Figure (4.9), shows that the four different chemical environments of the carbon atoms in the structure shown gives rise to four distinct carbon 1s peaks in the spectrum.

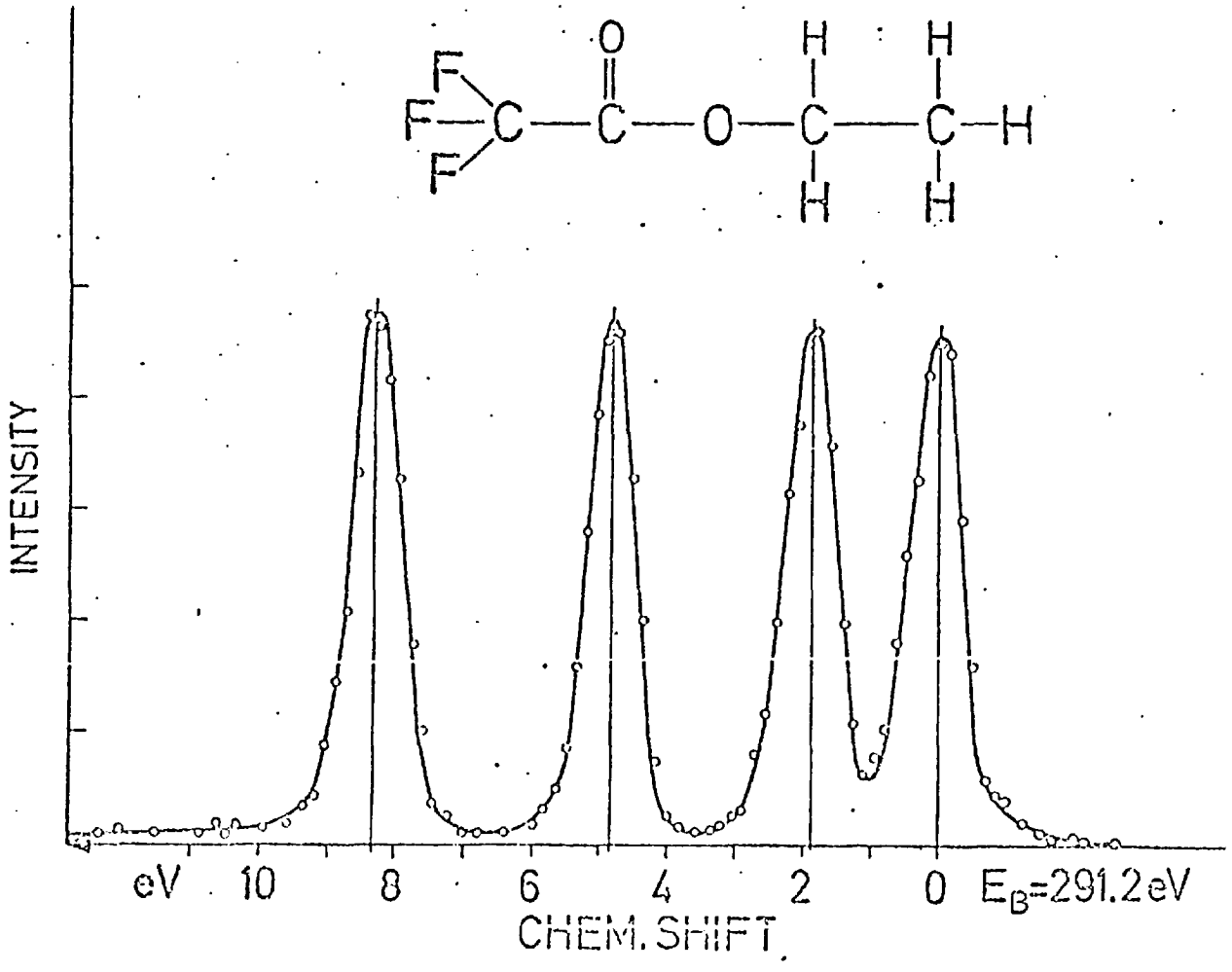


Figure (4.9) The ESCA Shifts of C1s in Ethyl Trifluoracetate (Siegbahn et al (95)) in the Gas Phase

Also important is the fact that the more electron deficient individual atoms become, the greater the chemical shifts will be. This is because the effective nuclear

charge has increased and so the binding energy also increases. Similar behaviour is found in the various oxidation states of most elements, allowing the qualitative analysis of a sample in terms of chemical structure. For the oxidation of metals, shifts to higher binding energies of the order of up to five electron volts are usually encountered for the substrate peaks when oxide nucleates.

To a simple approximation, the binding energy of an electron may be expressed as:

$$E_b = k_A\, q_A + \Sigma\, q_B/r_{ab} + E_R^o \qquad (4.4)$$

where $k_A\, q_A$ represents the contribution from the net formal charge on the atom considering that, in bonding, the electron is not removed to an infinite distance. The charge environment of an atom is not confined to its own electrons and those of atoms to which it is bonded. The second term takes into consideration the molecular and lattice potentials i.e. the field contribution from nearby atoms within the molecule or within the lattice. E_R^o is a reference level.

Several approaches have been used in an attempt to arrive at atomic charges that correlate with observed chemical shifts. The first and simplest of these uses Pauling electronegativity calculations.

$$q_i = Q_i + \sum_{i \neq j} n\, I_{ij} \qquad (4.5)$$

where Q_i is the formal charge on atom i, n is the number of bonds in which it is involved and I_{ij} is the partial ionic character of the bond between atoms i and j. I_{ij} may be expressed as

$$I_{ij} = i - e^{-0.25(\chi_i - \chi_j)^2} \qquad (4.6)$$

where χ_i and χ_j are the Pauling electronegativity values of i and j, respectively. However, the uncertainty in the bond numbers affects the calculation of charges. The absolute values of the charges calculated by this treatment should therefore be regarded as very approximate. They should only be used for comparing bonding effects in a series of similar compounds, i.e. only their relative values are significant.

The correlation of chemical shifts with independently estimated charges constitutes an interesting contribution to the discussion of the character of the bonds. Provided that ESCA shifts reflect the atomic charge in molecules in a constituent manner, agreement of a calculated charge with the general pattern implies that the structure on which the calculation of charge has been based is correct. Deviation from the general correlation would mean that the structure chosen for the calculation has been incorrect. Deviation can therefore serve to single out interesting cases for study, and may provide useful information on chemical structure.

Because of the importance of nitrogen and sulphur in present study, electronegativity values of elements involved in nitrogen and sulphur bonds as well as partial ionic character for bonds derived from the Equation (4.9) are given in Table (4.1), (4.2), (4.3) and (4.4) later in this Chapter. Tables (4.7) and (4.8) show the calculated charge and measured binding energies (E_b) for a series of nitrogen and sulphur

containing compounds. Calculation of charge from partial ionic character data is carried out using Equation (4.2) (14).

Element	Electro-negativity	Element	Electro-negativity
H	2.1	N^+	3.3
C	2.5	O	3.5
C^-	2.2	O^-	3.2
N	3.0	S	3.2
N^-	2.7		

Table (4.1) Electronegativity Values of Elements involved in Nitrogen Bonds (K. Siegbahn et al (14))

Bond	Partial ionic character	Bond	Partial ionic character
N - H	-0.18	N - O	+0.06
N^+ - H	-0.30	N - O^-	+0.01
N - C	-0.06	N^+ - O	+0.01
N - C^-	-0.15	N^+ - O^-	≈0.00
N^+ - C	-0.15	N - S	-0.06
N^+ - N	-0.02	N^+ - S	-0.15
N^+ - N^-	-0.09		

Table (4.2) Partial Ionic Character for Bonds

Element	Electro-negativity	Element	Electro-negativity
S	2.5	Cl	3.0
S^-	2.2	F	4.0
S^+	2.8	Na	0.9
S^{2+}	≈3.1		

Table (4.3) Electronegativity Values of Elements involved in Sulphur Bonds

Bond	Partial ionic character	Bond	Partial ionic character
S - Na	-0.47	S^{+} - O	+0.12
S - H	-0.04	S^{2+} - O	+0.04
S - C	0	S^{+} - O^{-}	+0.04
S^{+} - C	0.02	S^{2+} - O^{-}	≈0.00
S^{2+} - C	-0.09	S - Cl	+0.06
S - N	-0.06	S^{+} - Cl	+0.01
S - N^{+}	+0.15	S^{2+} - Cl	≈0.00
S^{+} - N	+0.01	S - S	0
S^{2+} - N	≈0.00	S - S^{-}	-0.02
S - O	+0.22	S - S^{+}	+0.02
S - O^{-}	+0.12	S - S^{2+}	+0.09
S - O^{+}	+0.35	S - S^{2+}	+0.18
		S - F	+0.43

Table (4.4) Partial Ionic Character for Bonds (K. Siegbahn et al (14))

4.6 Shake-up

When a core electron is photo-ejected, the coulombic potential experienced by the outer shell electrons is suddenly altered. This sudden perturbation may induce a "shake-up" transition, involving the excitation of a valence electron to a higher previously unoccupied orbital. The shake-up process is thought of as taking place simultaneously with core electron photo-ejection. If shake-up occurs, the kinetic energy of the ejected core electron will be less than that of an electron ejected from a corresponding core orbital in another molecule where shake-up has not occurred. Consequently, shake-up satellites always appear on the higher binding energy side of the main peak.

Shake-up satellite in the XPS spectra of many molecules have been reported, e.g. first row transition metal complexes. These peaks typically appear less than 10 eV away from the main peaks and in some cases e.g. Cu F_2 (17, 31) and Mn I_2 (18) are almost as intense as the main peak. Several suggestions have been made concerning the exact nature of the valence excitation corresponding to the shake-up, it has been variously described as 3d → 3d, or to 3d → 4S, 3d → 4p (17, 19, 20, 21) or as a charge transfer (C-T) type transition (22, 23). The balance of the evidence, however, seems to support the charge-transfer assignment as first proposed by Kim (22) and Pignataro et al (23). According to Kim (22) a Metal→Ligand (M→L) charge-transfer shake-up will give rise to a satellite structure in the ligand core electron spectra, while a L→M C-T transition will result in satellite(s) appearing in the metal core electron spectra.

It is interesting that XPS data alone support the charge-transfer mechanism as being responsible for the appearances of satellite peaks. For example, satellite structure has been observed in the 2p photo-electron spectra of some Sc^{III} complexes (24). A 3d → 4s, 4p, electron shake-up is therefore impossible because of the lack of 3d electrons.

Frost et al (17, 31) studied 46 Cu(II) and Cu(I) compounds and noted satellites only in the spectra of divalent copper. Since Cu(I) has a d^{10} configuration, C-T transitions of a ligand to metal d orbital nature are impossible. Any other allowed transition would be of very large energy and thus improbable. The only probable

transition for Cu(II) complexes would be of a L-M nature.

Shake-up satellites appear in the spectra many gases such as noble gases (25), or in organic molecules such as C 1s in thiophen, pyrolle and furan (26).

4.7 The Auger Process

The ejection of either a valence or a core electron by the action of an X-ray photon, leaves the ion in an excited state. The relaxation process then can take place via two different pathways. If an outer electron drops to fill the vacancy in the inner orbital, dissipating its energy by releasing a photon, the process is called X-ray fluorescence. Alternatively, when that higher orbital electron falls into the hole, it may transfer its energy to another electron. If this energy is sufficiently large, the electron will be emitted from the atom with a kinetic energy characteristic of that transition, leaving the atom in a doubly ionized state. This second process is termed the Auger process. This process is shown in Figure (4.10) for the singly ionized Si atom. The electronic energy levels are listed on the left (eV) with the zero of energy at the Fermi level E_F; E_C is the bottom of the conduction band.

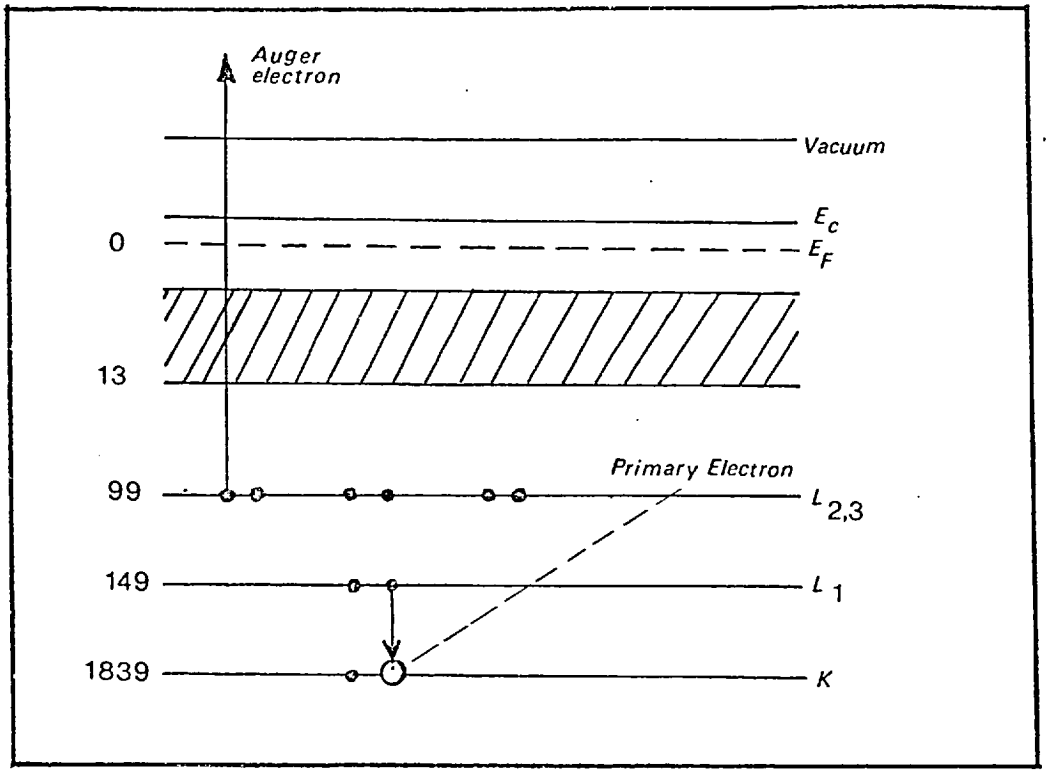


Figure (4.10) The Auger Process in the Singly Ionized Si Atom

The energy E of the ejected electron can be estimated by assuming the diagram of Figure (4.10), to be approximately valid. The energy released is $E_K - E_{L_1}$ (exactly), but the ejected electron must expend the energy $(E'_{L_{2,3}} + \phi)$ to escape the atom, where ϕ is the work function and $E'_{L_{2,3}} \neq E_{L_{2,3}}$ due to the extra positive charge of the atom. Because of this positive charge, $E'_{L_{2,3}}$ should be approximately equal to the $L_{2,3}$ ionization energy of the next heavier element, or $E'_{L_{2,3}}(Z) = E_{L_{2,3}}(Z+\Delta)$, where Z is the atomic number and $\Delta \simeq 1$ to account for the extra charge, therefore

$$E(Z) = E_K(Z) - E_{L_1}(Z) - E_{2,3}(Z+\Delta) - \phi \qquad (4.7)$$

Equation (4.7) is useful because E is expressed in terms of single ionization energy level which can be found in the X-ray and photoelectron energy tables. Equation (4.7) can be generalized to any Auger event involving the levels $W_o\ X_p\ Y_q$; also, the actual measured

energy will have an additional term - $(\phi_{sp} - \phi)$, which is the difference between the work functions of the energy analyser ϕ_{sp} and the material under investigation. This gives

$$E_{wxy}(Z) = E_W(Z) - E_X(Z) - E_Y(Z + \Delta) - \phi_{sp} \quad (4.8)$$

Experimental values of Δ are generally between $^1/_2$ and $^3/_2$.

The observed kinetic energy is dependent only upon the energies of the initial and final states of the species, as in X-ray fluorescence. The kinetic energy of the Auger electrons are therefore not dependent upon the energy of the exciting radiation or electron beam, but is constant. Auger lines, as a consequence, may serve as a convenient standard in an ESCA spectrum.

Since the final state of an Auger process involves coupling of the two remaining holes, this gives rise to various lines in the spectra. Each line is designated according to the energy levels involved in the transition. Thus a KLL Auger electron is generated by the creation of a hole in the K shell, the 1s level, followed by the collapse and emission of electrons from the L shell, either 2s or 2p. For example, X-ray induced Auger transition are visible in the photo-electron spectrum of copper, (see Figure (4.4)). Chemical shifts of Auger lines are also found when the effective nuclear charge changes from one chemical environment to another. However, since many important Auger lines include the valence band in the transition, simple interpretation in terms of oxidation state is made more difficult. For instance the

Cu(II) LMM line falls between those derived from Cu(O) and Cu(I) oxidation states. This will be discussed later in this study.

Finally this must be stated that, Auger emission and X-ray fluorescence do not occur with equal probability in all elements. In the lighter atoms, i.e. below atomic number 11, X-ray fluorescence is virtually non-existent, whereas Auger emission occurs with a probability of about 1.0. Above atomic number 11, the probability of Auger emission decreases as that for X-ray fluorescence increases, the 50% probability point being at about atomic number 33 (arsenic). X-ray fluorescence therefore is not a useful technique for the study of the lighter elements.

4.8 Calibration

In order to compare results for binding energies with those obtained by other workers, a calibration against some known standard is necessary. The choice of a suitable standard is not easy, however, and disagreement on procedures to be used, exists amongst various workers.

Binding energies for good conducting samples are usually referred to the Fermi edge of the metal or alloy in question. Unfortunately for a sample with a poor defined Fermi edge this is not an accurate procedure, and so this may be overcome by placing some gold in electrical contact with the sample and accurately determining the kinetic energy of the gold core levels. Usually this level is the $4f_{7/2}$ level peak since it is quite intense and has a narrow line-width, and its binding energy relative to the Fermi level is known.

Sample charging effects occur when electrons are omitted from the surface of an electrical insulator. A positive net charge might be formed, causing a decrease in the measured electron kinetic energy. During irradiation with X-rays, the radiation might cause an increased conductivity of the sample and secondary electrons might tend to neutralize the surface charge. In most cases, the observed charging effects were small, of the order of one electron volt, but sometimes effects of several electron volts have been reported (27). In calibrating non-conducting material, the effect of charging must be determined or eliminated. The charging influence can be controlled by calibrating the sample spectrum against an electron line from a thin surface layer on the sample. A noble metal layer e.g. gold (28) or the hydrocarbon contamination layer, which is usually present in spectrometers, have been shown to be useful for calibration.

An intra sample calibration, in which the sample is mixed with a non-conducting material is reported (27) unreliable, while mixing the sample with graphite can be useful.

In this study the binding energy scale was chosen such that the C 1s level was 285.0 eV. This is because carbon is present as a contaminant in virtually all measurements. The C 1s line has been used by many researchers with reasonable accuracy (27, 29).

4.9 Applications of ESCA

The most important use of the ESCA technique undoubtedly is in surface studies. However, the potential of ESCA for other practical applications is extensive.

These applications fall into the areas of analytical chemistry, biological systems, geology, polymers and alloys, catalysis, environmental studies, etc. ESCA application in corrosion science has been carried out successfully, mainly because corrosion is basically a surface phenomenon. An excellent review by Castle (8) considers the advancement of the ESCA technique in corrosion studies. For details of ESCA application in different areas see references (13,14).

4.9.1 ESCA study of copper and copper compounds

X-ray photoelectron spectroscopy has been applied to study copper and copper compounds by many workers (30, 31, 32, 33). Novakov and R. Prins (30) studying the spectra of solid Cu_2O, Cu Cl, Cu O, Cu S and Cu SO_4, reported the existence of satellite having various degrees of complexity, adjacent to the Cu 2p photolines in all cases. In an extensive study of copper compounds, Frost et al (31) discovered the importance of air oxidation and photo reduction. They reported that all cupric compounds measured had intense satellites on the higher binding energy sides of the $2p_{1/2}$, $2p_{3/2}$, 3s, and 3p peaks, with the last being much the weakest. All cuprous compounds examined had no satellites associated with any of these bands. Another difference found was that the width of the main peaks from the cuprous compounds was narrower than that of cupric. Frost et al (31) explained the spectra recorded by Novakov (30) as arising from surface contamination (oxidation) of cuprous species. The binding energies of 34 cupric and 12 cuprous compounds are reported for L_{II}, L_{III}, M_I, M_{II}, $_{III}$ photoelectron

bands of the copper, and K band of C, N, O and most intense bands of the other elements. This table is re-produced in Table 4.5.

The chemical shift between homologous compounds of different oxidation states were reported to be 1.3 eV for CuO and Cu_2O, 1.9 eV for $CuBr_2$ and CuBr and 1.9 for $CuCl_2$ and CuCl. The chemical shifts of the co-ordination complexes with the neutral ligand molecules were more complicated and difficult to predict on the basis of simple electronegativity concepts. According to these workers (31), qualitatively, there are two factors which determine the binding energies in the co-ordination complexes. One is the effect of charge transfer between ligand atoms and the counter anion on the charge of the copper atom. Another effect comes from the change in lattice energies of the different compounds. Frost et al reported a 1.8 eV increase in binding energy of the N 1s electrons of di-dipyridyl complexes compared with the neutral di-dipyridyl (N 1s 399.1 eV).

In a determination of photoelectron and Auger chemical shifts, P.E. Larson (32) reported data for metallic copper, Cu O, Cu_2O and Cu_2S. Of the four Cu 2p spectra, only Cu O exhibited multiplet line broadening and the shake-up satellites. The spectra of the cuprous compounds were found to be almost identical with the copper spectrum in terms of line width, binding energy, and absence of satellites. The Cu 2p chemical shifts, referenced to the metal, are given in Table (4.6). Larson reports in addition to its other features, that the Cu O spectrum has a substantial chemical shift of

	Cu L II($2p_{1/2}$)		Cu L III($2p_{3/2}$)		C	N	O	X	
	Satellite	Main peak	Satellite	Main peak					
CuF_2	6.2	959.6	6.7	939.7				F	687.9
$CuF_2.2H_2O$	7.2	957.9	7.5	938.1			534.9	F	686.7
$Cu(OH)_2$	7.6	957.3	7.6	937.4					
$CuCO_3$	7.3	957.1	7.8	937.2	287.5		533.9		
$Cu(AcO)_2.H_2O$	7.7,5.2	956.6	9.0,5.8	936.7	287.0		534.0		
$Cu(AcO)_2.2en.H_2O$	8.7	956.0	8.8	936.2		401.6	533.1		
CuO	8.5	956.3	9.4,7.8	936.2			532.9		
$K_2Cu(C_2O_4)_2$	8.5	956.1	9.2,6.2	935.8	286.2, 289.9		533.2	K	294.4
$Cu(NO_3)_2.3H_2O$	8.5	956.0	9.3,6.2	935.9		408.3	533.5		
$Cu(\emptyset COO)_2$	8.5,5.2	955.9	9.4,5.9	935.7	285.6, 289.7		532.1		
Cu(acac)$_2$†	9.3,5.0	955.3	9.5,5.1	935.4	285.9, 287.8		532.6		
$CuSO_4$	7.3,4.6	957.3	8.4,4.6	937.2			534.0	S	171.2
$CuSO_4.H_2O$	8.4,3.8	956.3	8.6,5.0	936.7			533.8	S	170.8
$CuSO_4.3H_2O$	6.8	957.7	7.2	937.9		[illegible]	533.5	S	170.3
$CuSO_4.5H_2O$	7.0	957.9	8.0	937.8			533.9	S	170.4
$CuSO_4.dip2H_2O$	8.0	955.7	8.2	935.5	286.0	400.6	532.1	S	169.1
$CuSO_4.3dip.7H_2O$	9.2	955.0	9.8	935.2	285.9	400.4	532.2	S	169.9
$CuSO_3.en.H_2O$	8.0	956.6	8.4	936.6	286.0	401.3	533.3	S	170.3
$CuSO_4.2en.H_2O$	8.0	956.3	8.4	936.1	286.8	401.0	532.4	S	169.4
$CuCl_2$	8.6	956.2	8.5	936.4				Cl	201.2
$CuCl_2.2H_2O$	8.0	956.6	8.4	936.6			533.7	Cl	200.8
$CuCl_2.dip$	8.5	955.2	8.3	935.4	286.3	401.0		Cl	199.7
$CuCl_2.2dip.3H_2O$	9.0	955.0	8.5	935.4	286.0	400.7	533.6	Cl	199.4
$CuCl_2.en.H_2O$	8.1	956.4	8.4	936.5	286.8	401.8	533.5	Cl	200.7
$CuCl_2.2en.H_2O$	8.1	955.9	9.0	935.7	286.4	400.7	533.3	Cl	199.1
$CuBr_2$	9.5	955.6	9.7	935.8				Br	71.5

The energies of the satellites are given in reference to the main peaks which in the case of C, N, O and F_1 refer to the 1s orbital, K = $2p_{3/2}$, S = 2p, Cl2p, Br = $3d_{3/2,5/2}$ I = $3d_{5/2}$ and P = 2p.

† acac = acetylacetonate

Table (4.5) The Binding Energies and the Satellite Splittings of the Copper Compounds (Frost et al (31))

	Cu L II($2p_{1/2}$)		Cu L III($2p_{3/2}$)		C	N	O	X	
	Satellite	Main peak	Satellite	Main peak					
$CuBr_2$.dip	8.8	954.9	8.9	935.1	286.5	401.3		Br	70.1
$CuBr_2$.2dip.$2H_2O$	8.3	955.2	8.7	935.3	286.2	400.9	533.3	Br	69.2
$CuBr_2$.en.H_2O	8.6	956.2	9.0	936.3	287.0	401.9		Br	71.0
$CuBr_2$.2en.H_2O	8.5	955.7	8.7	936.0	286.7	401.0	533.3	Br	69.7
$CuBr_2$.2en.$5H_2O$	8.4	955.9	8.4	936.0	286.7	401.5	533.4	Br	70.0
$Cu(ClO_4)_2.2H_2O$	8.2	957.3	8.4	937.1			534.6	Cl	210.2
$Cu(ClO_4)_2.4H_2O$	7.0	958.2	7.5	938.3			534.2	Cl	209.8
$Cu(ClO_4)_2.6H_2O$	7.0	958.5	7.3	938.5			534.6	Cl	210.1
CuCN		955.0		935.2	286.8	401.0			
CuI		955.0		935.2				I	622.2
Cu_2O		954.7		934.7			533.6		
CuSCN		954.4		934.6	287.0	401.0		S	165.9
Cu_2S		954.3		934.6				S	164.5
Cu_3P		954.1		934.3				P	136.2
CuBr		954.0		934.2				Br	79.6
CuCl		954.5		934.6				Cl	201.3
CuCl.$Ø_3P$		953.8		934.1	285.6		P 132.2	Cl	199.1
CuCl.$(Ø_3P)_3$		953.7		934.1	285.6		P 132.0	Cl	199.4
CuCl.$(Ø_2PH)_3$		953.9		934.0	285.6		P 133.8	Cl	199.7
CuCl.$(Ø_3P)$(O-phen)*		953.0		933.0	285.6	400.2	P 132.0	Cl	198.4

The energies of the satellites are given in reference to the main peaks which in the case of C, N, O and F_1 refer to the 1s orbital, K = $2p_{3/2}$, S = 2p, Cl2p, Br = $3d_{3/2,5/2}$ I = $3d_{5/2}$ and P = 2p.

* o-phen = o-phenanthroline

Table (4.5) *Continued* The Binding Energies and the Satellite Splittings of the Copper Compounds (Frost et al (31))

1.2 eV. The cuprous compounds appeared to have chemical shifts so small as to be nearly insignificant since error limits of $\pm$ 0.1 eV must be attached to these measurements. These results are essentially in agreement with Frost et al. According to Larson, Cu 2p spectrum readily identifies Cu(II), species, but fails to distinguish between Cu(O) and Cu(I).

Species	$2p_{1/2}$ and $2p_{3/2}$	$L_2M_{4,5}M_{4,5}$ and $L_3M_{4,5}M_{4,5}$
Cu	0	0
CuO	1.2	1.0
Cu_2O	0.1	2.3
Cu_2s	0.1	1.8

Table (4.6) Chemical Shifts (P.E. Larson (32))

The Auger chemical shifts are listed in Table 4.6 along with photoelectron shifts. Cu O has a shift of 1.0 eV, but the cuprous compounds appeared to have even larger shifts averaging 2.0 eV. On the basis of this limited data, Larson concluded that the Auger - photoelectron energy difference is about the same for Cu(O) and Cu(II), but about 2 eV for Cu(I). This could be the basis for a useful diagnostic technique.

A. Rosencwaig and G.K. Wertheim (33) independently reported that the Novakov (30) spectrum for Cu_2O is not that for Cu_2O but rather a combination of both Cu_2O and CuO spectra, suggesting that Novakov's material was partially oxidized to CuO. In an attempt to demonstrate the differences between CuO and Cu_2O, a fresh CuO sample was prepared by heating a Cu sample to 250^{o}C in an atmosphere of oxygen for 5 minutes. An adherent black layer was produced.

The Cu(2p) region exhibited strong satellites associated with both the $2p_{3/2}$ and $2p_{1/2}$ lines. There appeared clearly two satellites associated with the $2p_{3/2}$ line, one 8 eV and the other 10 eV from the primary line. On the $2p_{1/2}$ line the 10 eV satellite appeared to be very weak. The valence spectrum of CuO consisted of a broad 3d line under which lay an unresolved O(2p) level centred at about 5 eV. There appeared also a satellite 8 eV from the 3d line. When the CuO was heated to 250°C in the 10^{-7} Torr vacuum of the spectrometer for only a short time, the Cu spectra changed dramatically. In the Cu(2p) region the satellites completely disappeared, while the primary lines themselves have become much sharper and were shifted by about 1.2 eV to lower binding energy. The valence region was also considerably changed, the 3d line now being sharper with a shoulder near the top of the valence ~~bond~~ band, while the satellite at 8 eV disappeared. These changes were identical to those of directly prepared Cu_2O. The 1.2 eV shift to lower binding energy of the core levels exhibited the sign and magnitude expected for reduction of Cu^{2+} to Cu^{+}. The narrowing of the lines in Cu^{+} relative to those in Cu^{2+} was due to absence of multiplet broadening in ~~diagrametic~~ diamagnetic $3d^{10}$ Cu^{+}.

The observation of the shake-up satellites and chemical shift about 1.5 eV to higher binding energy (compared to metallic copper), is now considered to be indicative of the presence of Cu(II) species. Satellites are absent from the spectra of Cu(I) compounds.

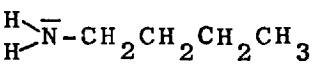
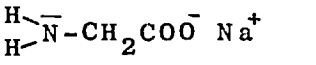
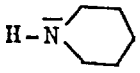
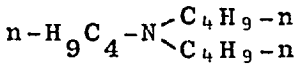
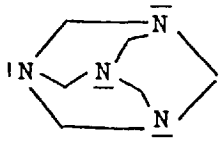
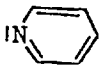
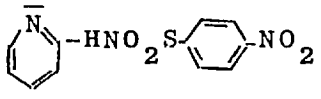
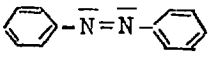
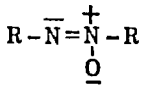
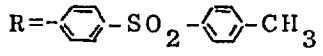
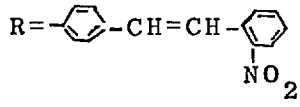
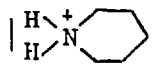
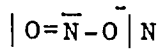
From the above discussion, it is now clear that the Cu 2p spectrum can distinguish between Cu(I) and Cu(II),

and Cu LMM Auger spectrum between Cu(I) and Cu(O). Combination of the two techniques enables one to distinguish between Cu(O), Cu(I) and Cu(II). The X-AES Cu LMM spectrum was found to be very useful in the present corrosion inhibition studies which will be discussed later in Chapter 6.

4.9.2 Structure determination of organic compounds using ESCA technique

Electron spectroscopy has been used with considerable success for structure determination of various organic compounds. In extensive chemical binding and molecular structure studies by K. Siegbahn et al (14), thirty-nine organic nitrogen compounds were studied and the N(1s) level was measured from the electron spectra. Twenty-seven of the compounds studied in this investigation are listed in Table (4.7). It gives the measured N(1s) binding energies, E_b, the calculated charge for the nitrogen, and the number of measurements made on each compound, n. From Table (4.7) it can be seen that the binding energies of nitrogen in various nitro compounds fall within a small range. In compounds Nos. 9, 22 and 23 Table (4.7), the binding energies of the nitrogen in the sulfonamido groups are significantly higher than that of ordinary aliphatic amino group. This is consistent with the known high electron attracting power of the sulfonyl group.

The calculated charge is related to partial ionic character for bonds from the electronegativity values given by Pauling. It is clear that introduction of one or more electronegative atoms in a nitrogen compound, results in an increase in binding energy of

Nr	COMPOUND	n	Calculated charge	E_b N 1s
1		2	-0.72	399.2
2		2	-0.45	399.2
3		5	-0.42	398.1
4		1	-0.42	397.3
5		3	-0.30	397.8
6		6	-0.18	398.1
7		2	-0.18	398.6
8		3	-0.18	398.0
9		3	-0.18	398.0
10		4	-0.18	398.4
11		2	-0.06	399.3
			-0.02	
12		2		399.3
13		5		399.4
14		2	+0.10	400.4
15		1	+0.13	404.3

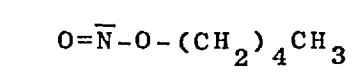
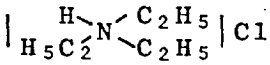
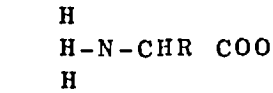
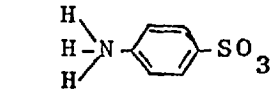
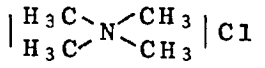
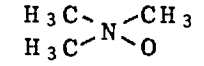
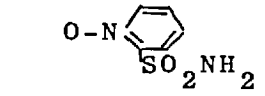
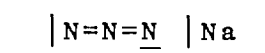
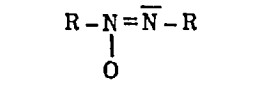
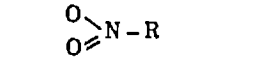
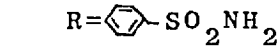
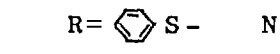
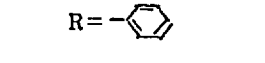
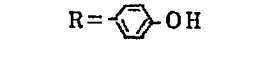
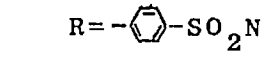
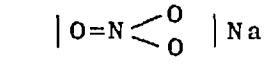
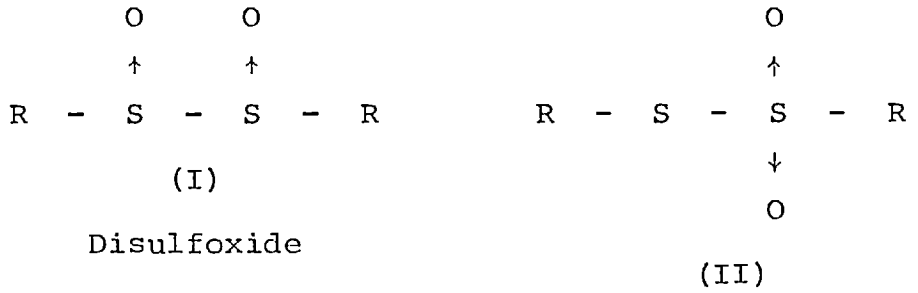
Nr	COMPOUND	n	Calculated Charge	E_b N 1s
16		2	+0.18	403.7
17		3	+0.25	400.4
18		10	+0.27	400.3
19		3	+0.27	401.0
20		3	+0.40	401.5
21		2	+0.55	402.2
22		2	+0.55	402.2
1		2	+0.64	403.7
			+0.81	
12	R=12	2		403.6
13	R=13	5		403.4
			+0.87	
23		2		404.9
24		2		405.1
25		10		405.1
26		3		405.3
13	R=13	5		405.3
9		3		405.5
27		2	+1.02	407.2

Table 4.7: Calculated charges and measured binding energies (E_b) for a series of nitrogen containing compounds.

nitrogen.

Since the character of the bonds between sulphur and other elements, especially carbon, nitrogen, oxygen, and halogens is an important subject in organic chemistry, electron spectroscopic measurements on a large number of organic sulphur compounds has been carried out. Table (4.8) gives the measured binding energies and calculated charge for a series of sulphur compounds by K. Siegbahn et al (14). Some interesting information can be obtained using the qualitative aspects of the electron spectra. For instance, the thiolsulfonate structure of cystine S-dioxide has been studied (14). The two possible structures of the disulfide dioxides, i.e. the disulfoxide (I), and the thiosulfonate (II) structures, have both received support.



(I)

Disulfoxide

(II)

Thiosulfonate

The cystine molecule contains two equivalent sulphur atoms:

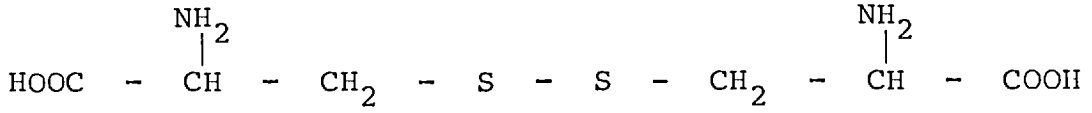
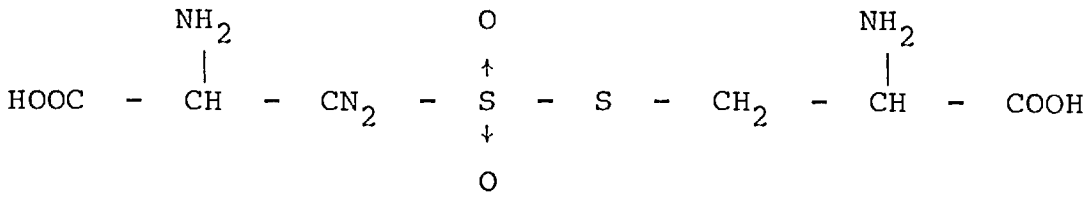
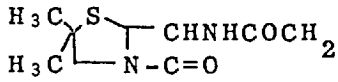
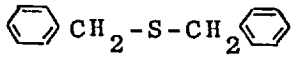
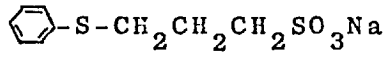
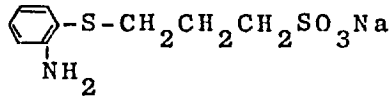
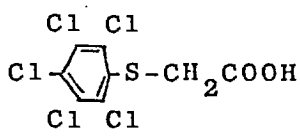
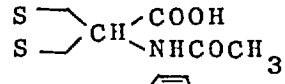
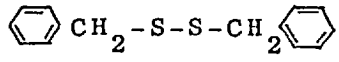
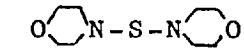
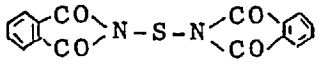
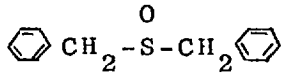
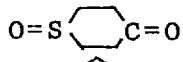
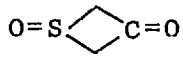
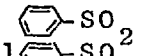
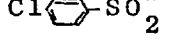


Figure (4.11(b)) shows the photoelectron spectrum of this compound in S(2p) region. The sulphur 2p shell is a single line which has a full width at half-maximum intensity of 2.5 eV. This is consistent with the equivalence of the two sulphur atoms in the cystine molecule. In the disulfide dioxide in which two oxygens are attached

to sulphur, two different structures may be formulated. If one oxygen is attached to each of the two sulphur atoms (I), the resulting symmetry with equivalent sulphur atoms would give rise to single lines in the electron spectra of the sulphur atoms. If both oxygens are attached to one of the sulphur atoms, i.e. if the disulfide dioxide has the thiosulfonate structure (II), the two sulphur atoms having non-equivalent structural positions, would give rise to two different lines in electron spectra of the sulphur atoms. This is actually the case. Figure (4.11(a)) shows the electron spectrum of the 2p subshell of sulphur in cystine S-dioxide, recorded with Al K_α (14). Instead of one single line as in the symmetrical cystine, two lines are now obtained from the 2p subshell in sulphur. One of the lines has approximately the same energy as the cystine S line and the other line has an energy 4.0 eV lower. Each line has a half width of about 2.5 eV. The separation is of the same order of magnitude as the shifts observed for sulphur atoms with comparable differences in the oxidation states. The electron spectrum of cystine S-dioxide obtained by ESCA therefore gives conclusive evidence for the thiosulfonate structure:



Similar results were obtained for atmospheric oxidation of Cu(I)-2-~~mer~~mercaptobenzothiazole and Cu(I)-2-mercaptobenzimidazole complexes which will be discussed in Chapter 7.

Nr		COMPOUND	q	S2p	O1s
1		Na_2S	-0.60	160.8	530.7
2	1	$H-S-CH_2CH(NH_3)COO$	-0.04	161.8	530.6
	2	$H-S-CH_2CH(NH_3^cCl)COON$		162.2	530.9
3	1	$H_3C-S-(CH_2)_2CH(NH_3)COO$		162.1	530.6
	2			161.9	530.9
	3			162.4	
	4		0	162.8	531.3
	5			162.5	531.8
	6			161.5	532.0
4	1	$OOC(NH_3)CHCH_2-S-S-CH_2CH(NH_3)COO$		162.7	530.3
	2			162.7	531.8
	3			162.8	
5		S_8	0	162.2	
6	1			162.5	531.8
	2		+0.13	164.3	531.7
7	1		+0.44	164.9	530.5
	2			164.9	531.4
	3			165.0	530.9
8	1		+0.56	165.4	530.9
	2			165.5	531.2

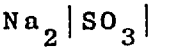
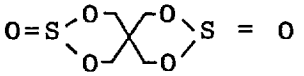
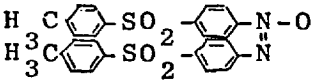
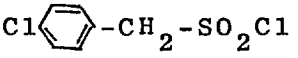
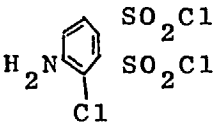
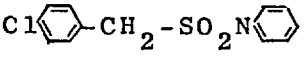
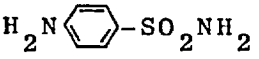
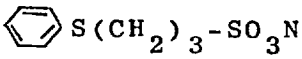
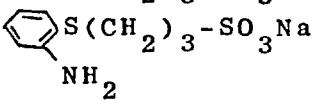
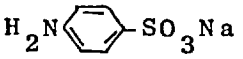
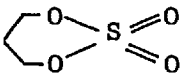
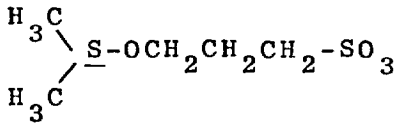
No		COMPOUND	q	S2p	O1s
9			+0.68	165.8	531.3
10			+0.88	167.0	531.5
11			+0.88	167.2	531.6
12	1			167.3	531.5
	2		+0.95	167.3	531.4
13	1		+0.95	167.2	531.7
	2			167.3	531.9
14	1			167.1	531.3
	2		+1.00	167.5	531.8
	3			167.0	531.6
15	1	$Na_2\|SO_4\|$		167.7	531.6
	2	$Fe\ \|SO_4\|$	+1.22	168.0	531.8
	3	$(Fe)_2(SO_4)_3$		168.3	531.1
17		Dextran-OSO_2ONa	+1.22	168.7	531.4
18			+1.32	168.6	532.5
19			+1.07	167.6	531.3

Table 4.8: Calculated charges (q) and measured binding energies for a series of sulfur compounds.

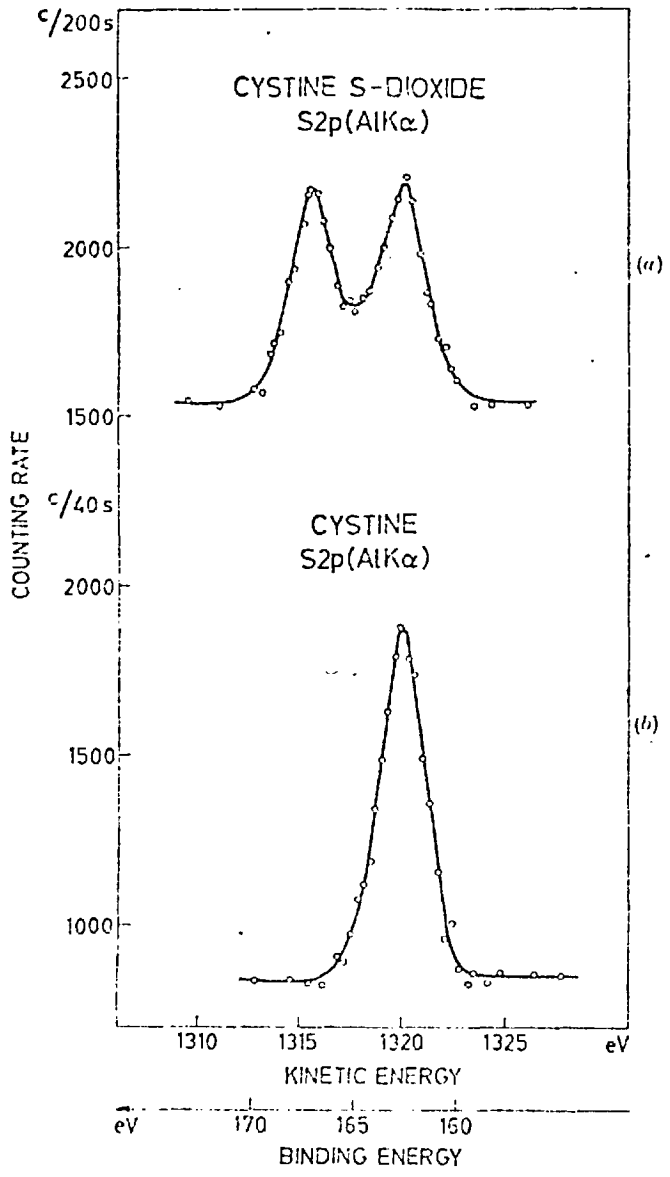


Figure 4.11: XPS spectra of(a) cystine S-dioxide ; (b) cystine (Siegbahn et al (14)).

4.9.3 ESCA as an analytical tool

Electron spectroscopy is sensitive to all elements except hydrogen and helium. Since the measured electron binding energies of most elements are sufficiently unique, a broad range scan of the electron energy spectrum provides a good means of qualitative analysis. Although accidental overlap of some peaks does occur, in general the electron signals from adjacent elements are quite well separated.

The integrated intensities of the electron signals are directly proportional to the number of similar atoms in the sample, representing a convenient quantitative tool. After correction for various effects, e.g. variation in photoelectric cross-section, and the shake-up effects, the relative peak intensities show good agreement with the stoichiometric formula. However, peaks with widely differing kinetic energies will have different effective sampling depths which will result in an unreliable analysis. On the other hand, this effect may be used to examine surface vs bulk composition.

According to Wagner (34), the variability in response amongst compounds make it doubtful that the technique is capable of better than semi-quantitative application on a routine basis. Nevertheless, he reports its ability to analyse certain surfaces which it is not possible to analyse by other methods, makes it of considerable potential value.

According to Jørgensen and Berthau (35), although the electrons arrive from a volume containing only a few micrograms of the sample, only high concentration, above

1% of most elements, can readily be detected. Furthermore, the signal intensities of a given sample decrease slowly, by one third or more, during measurements extending over a few hours. However, it can be of analytical interest to obtain even semi-quantitative information about the relative concentrations of elements in the outermost 20 Å of a solid sample.

Table (4.9) shows data obtained for relative intensities of atoms which comprise the various compounds used in this study, by Wagner (34) and Jørgensen (35). Values in parentheses are according to Wagner.

Element	1s	2s	2p	3s	3p	3d
C	0.27(0.27)	-	-	-	-	-
N	0.4 (0.42)	-	-	-	-	-
O	0.6 (0.52)	0.02	0.01	-	-	-
F	1.00	0.04	0.02	-	-	-
S	-	-	0.35(0.46)	-	-	-
Cl	-	0.25	0.42(0.55)	0.04	0.05	
Cu(I)	-	-	3	-	0.4	0.15
Cu(II)	-	-	1.5	0.15	0.3	0.12

Table (4.9) Relative Signal Intensities with F 1s as Unit

In the present study the strongest signal of each element was chosen for calculation stoichiometry e.g. Cu 2p and Cl 2p.

4.9.4 Limitations and problems

Although ESCA can be extremely valuable in different areas of research, there are certain problems associated with this technique which severely limits the use of ESCA. For instance, molecules to be analysed must be strong

enough to resist X-ray bombardment and must be resistive towards the vacuum necessary for analysis i.e. of low vapour pressure. There are several reports dealing with photo-reduction effect during the analysis of samples (14, 36).

Another major disadvantage of ESCA in studying films formed on copper by organic inhibitors is the sample transfer problem. Corrosion inhibitors are used mainly in preventing corrosion at the metal-solution interface whereas ESCA is an ultra-high vacuum technique. Thus, it is not possible to study adsorption of corrosion inhibitors at the metal-solution interface "in situ" and there necessarily exist a transfer problem in any experimental programme.

Despite these problems, the acquisition of valuable information with the ESCA technique is not precluded.

CHAPTER FIVE

A REVIEW OF PREVIOUS WORK ON INHIBITION OF COPPER CORROSION

5.1 Copper Corrosion

Copper is the only engineering metal that is a noble metal. Because it is noble, the hydrogen evolution process is not part of the corrosion reaction. For this reason, copper is not corroded by acids unless oxygen or other oxidizing agents (e.g. HNO_3) are present. For example, reaction between copper and sulphuric acid is not thermodynamically possible; but corrosion proceeds in the presence of oxygen, and the products are copper sulphate and water. Reduction of oxygen to form hydroxide ions is the predominant cathodic reaction for corrosion of copper and its alloys.

Generally, the lower (cuprous) series of copper compounds are less soluble than the higher (cupric) series. Cuprous chloride, for instance, is sparingly soluble, and it might be expected that copper immersed in, say, potassium chloride solution would escape corrosion, since any weak spots in the air-formed oxide would be healed with cuprous chloride. In a study of copper corrosion (37), a copper specimen placed in potassium chloride solution showed rapid change, although for some days this takes the harmless form of surface coloration, the liquid remaining free from precipitate. The changes start at isolated spots, which are most plentiful near the cut edges, but instead of producing loose matter, as on iron or zinc, they lead to oval areas of bright interference tints on the finely ground specimen, or rather dirty brownish patches on coarsely ground specimens. It is believed (37) that solid cuprous chloride,

formed by the anodic reaction, being only very slightly soluble, is converted "in situ" into cuprous oxide by the cathodically formed alkali; the oxide film thus formed is responsible for coloration. During this early period, the liquid remained clear; the corrosion-products were entirely adherent. However after about 3 days, green basic cupric chloride appeared, relatively loose, probably formed by the action of oxygen on the small amount of cuprous chloride in solution, and the liquid became cloudy.

The pitting of copper is a relatively exceptional phenomenon; it has been investigated by R. May (38). He pointed out that the copper surface covered with a uniform scale of oxide may become faulty locally, either through the existence of crevices in the metal, the settlement of small particles on the surface during film-formation, mechanical scratching or some similar cause. Sometimes the fault may heal itself by the anodic formation of solid cuprous chloride, but sometimes the cuprous chloride, which is slightly soluble, will diffuse out into the liquid as soon as it is formed, and be converted either to the basic cupric chloride by oxidation, or perhaps to cuprous oxide by the action of cathodically formed alkali. If this occurs, the repair of the film by plugging with cuprous chloride will not occur, and the cuprous chloride will prevent fresh oxygen from reaching the metal, so that repair by oxide-formation will now be impossible; thus attack, once started, will continue.

Water containing carbonic or other acids may corrode

copper and copper base alloys sufficiently to cause blue staining, and if such water comes into contact with iron, galvanized steel, or aluminium surfaces, it causes an increase in their corrosion rate. Accelerated corrosion in this instance is caused by a replacement reaction in which copper metal is deposited on the base metal, forming numerous small galvanic cells. Treatment of acid waters with lime or sodium silicate reduces the corrosion rate sufficiently to overcome both staining and accelerated corrosion of other metals, except aluminium. Aluminium is an exception because of its sensitivity to extremely small amounts of Cu^{++} in solution, the usual water treatment being inadequate to reduce Cu^{++} pick up to non-damaging levels. The presence of adequate Cu^{++} ions in presence of Cl^{-}, represents a highly corrosive environment for copper itself, as will be discussed later in detail.

It is possible to avoid the damaging effects of Cu^{++} contamination of water by using copper piping coated on the inside surface with tin (so-called tinned copper).

5.2 Corrosion Inhibition of Copper

The inhibition of corrosion of metals in contact with aqueous solution at a pH not far from neutrality has in many cases been achieved by the use of inorganic substances such as chromates, phosphates etc. The sodium salts of organic acids, such as the benzoate, salicylate, phthalate, and tartrate, have been suggested as alternatives to these compounds, particularly with ferrous metals. The action of these substances appears to be due to the adsorption of the organic anion on the metal surface or

to the formation of the complexes with the metal ions, which in some cases can be found in corrosion product. In recent years, investigators have shown that a system of tarnish or corrosion control for copper, brass and bronze can be built around the organic compound 1, 2, 3 benzotriazole (39). Besides benzotriazole, the use of 2-mercaptobenzothiazole and benzimidazole and its mercapto derivative has been suggested for the inhibition of copper corrosion (40). The dissolution of copper in acid solutions has been inhibited by sulphur containing organic compounds, benzyl thiocyanate, and furfural. Furfural has been found (41) to be an excellent inhibitor for copper in hydrochloric acid solutions. This inhibitor affords protection to copper at all concentrations of HCl, the efficiency being 90-100%. The amounts of furfural required to bring about efficient inhibition in dilute acidic solutions is greater than that required at higher concentrations of HCl solutions. According to Desai (41), the resin - forming tendency of furfural appears to be responsible for the inhibiting power.

Desai (42) has also studied the effect of 30 organic substances on corrosion of copper in more basic solution containing NaOH. Among the most effective inhibitors are resorcinol, phloroglucinol, pyrogallol, tannin, aminophenols, furfuraldehyde, 8-hydroxy-quinoline, and quinalizarin. In many cases the action of the additives is explained by assuming the formation of a surface reaction product between the inhibitor, the metal, and the corrosive medium.

5.3 Corrosion Inhibition of Copper and its Alloys by Benzotriazole

Benzotriazole (BTA) has been found very effective in preventing the corrosion of copper and its alloys and of some other metals and alloys such as cadmium (43) and some steels in aqueous media. Because of its effectiveness many investigations have been carried out. Although these studies are very different from each other, it is possible to divide them into two categories, namely practical studies and fundamental studies. Practical studies are those studies concerned with the inhibition efficiency of the BTA, the optimum amount of BTA in different environments etc. Fundamental studies contain those studies which deal with inhibition mechanisms, film formation and its properties, etc. In this section, practical studies will be reviewed first, and then fundamental studies will be discussed.

5.3.1 Practical studies

There are so many papers dealing with this aspect of BTA corrosion inhibition that a comprehensive review of them would be extremely lengthy. In view of this, only a few important works are reviewed. The effect of different concentrations of BTA on the rate of corrosion of copper and steels have been studied (44). In tests lasting 60 to 90 days, 0.001% benzotriazole completely protected copper. Corrosion of grey cast iron was reduced 8 to 10 times by 1% benzotriazole. In a 0.1% buffer solution containing BTA and its sodium salt at a pH of 7.3 to 7.5, the corrosion rate for grey cast iron and for steel were the same as in a solution containing 1% BTA at a pH of 5.9 to 6.2. The buffer solution

appeared to be most effective. Concentration of 0.5% eliminated corrosion of grey cast iron; 0.2% solution protected steel; 0.6% protected steel in contact with copper and 0.001% protected copper.

In other work (45) on the protective properties of BTA with respect to the corrosion of copper and steel in neutral and acid solution, it was concluded that despite a certain inhibiting action, BTA could not be considered an efficient anti-corrosive agent for ferrous metals in neutral media. It proved effective, however, in preventing the corrosion of copper by itself and in contact with steel. In acid media, benzotriazole prevented the corrosion of copper, but visible compounds formed on the surface of the metal.

Cotton (39) has studied the tarnishing of copper and copper alloys exposed to humid environments, and the possibility of the prevention of staining by reaction with triazole-type compounds. Cotton (39) reports that bright copper directly treated by aqueous solution or by exposure to the concentrated vapor of benzotriazole will withstand staining upon exposure to 0.25 percent salt mist for 24 hours or to 0.1 percent SO_2 for 5 days. Vapour treatment is particularly suitable for components such as electrical contacts which cannot be wetted.

In Great Britain a major industrial atmospheric contaminant is sulphur dioxide and it has been confirmed that the presence of between 0.05 percent and 0.5 percent v/v sulphur dioxide can result in stress corrosion of brass. The prevention of staining in sulphur dioxide atmospheres afforded by benzotriazole treatment also controls stress

corrosion of brass in this environment (39). In tests upon a cold drawn brass component exposed to moist 0.1 percent SO_2, cracking occurred in 3 days with the untreated component, but the treated components had not cracked after 43 days (39).

A comparison has also been made by Cotton (39) between benzotriazole-type compounds such as indazole ($C_7H_8N_2$), benzimidazole ($C_7H_8N_2$), indole (C_8H_9N), methylbenzotriazole ($C_7H_8N_3$) and BTA itself. Copper complexes are formed with benzotriazole, indazole and benzimidazole but not with indole and methyl benzotriazole. For the structure of these compounds see Appendix A. This investigation had confirmed that from this range of different types of compound, benzotriazole is the most effective one.

Study of inhibition of copper corrosion in chloride solution by heterocyclic compounds by G. Trabanelli et al (46) showed that among the various heterocyclic compounds such as benzotriazole, 2-mercapto benzimidazole, 2-mercapto benzthiazole, benzimidazole and sulphthiazole, BTA is the most efficient. 2-mercapto benzthiazole in the second place and 2-mercapto benzimidazole is the third in the list (see Appendix A for structural formula). R. Walker (47) studied triazole, benzotriazole and naphthotriazole as corrosion inhibitors for copper. It appeared that triazole was a poor inhibitor, while benzotriazole and naphthotriazole were superior. Naphthotriazole gave the best result. When used as a pre-treatment for Cu surfaces, the inhibitors increased the time before atmosphere staining occurred.

V.P. Dobrovol'skaya and co-workers (48) studied the

effect of benzotriazole, 2-mercapto benzothiazole, acetanilide, cupron and some other inhibitors on corrosion of Cu in 3% NH_4OH and in a mixture of 0.5 N NaOH + N/1 $(NH_4)SO_4$. The effect of protective action of benzotriazole was 96% efficient, mercapto benzothiazole 99% and the rest of the inhibitors were between 95 and 91%. The corrosion rate of Cu in contact with Fe in the 3% NH_4OH solution was a few times higher than for Cu alone. The presence of BTA or MBT reduced the corrosion of Cu in contact with steel by 97 and 98% respectively.

K.H. Wall and I. Davis (49) demonstrated that BTA is a satisfactory corrosion inhibitor for copper in closed-circuit, water-cooled stators. Laboratory and plant tests indicated that conductivity increases and copper pick-up is significantly reduced at concentration levels greater than 20 ppm of BTA. In order to confirm that BTA is an effective inhibitor for copper in neutral solution, a 2 in. length of ¼ in. i.d. copper tubing was immersed in 100 ml of BTA solution of concentration 100 ppm. A similar length was also immersed in 100 ml of distilled water. After 3 months at room temperature, the copper concentration of the BTA solution was 27 $\mu g/l$ and that of water was 400 $\mu g/l$.

5.3.2 Fundamental studies

In one of the earliest studies, Cotton (39) suggested that a polymeric chains or monomolecular plate-like complexes form on the copper surface due to interaction between copper and inhibitor, affording excellent protection. Cotton suggests that the nitrogen-hydrogen group, and at least one of the other nitrogen in the ring, is involved in the complex molecular arrangement. Cotton also

concluded that benzotriazole forms a strongly bonded chemisorbed two-dimensional barrier film less than 50 Å thick. It is this insoluble film which protects copper and its alloys in aqueous media, various atmospheres, lubricants and hydraulic fluids.

The simplest method of achieving a strong bond would be by the production of a co-ordination compound of benzotriazole with cuprous ions. Thus, the copper would be bonded using sp orbitals, with a covalent link formed by replacement of the hydrogen atom, and a co-ordinate bond formed by the lone pair of electrons on one of the nitrogen atoms. Thus, a polymeric chain (39) of alternate copper atoms and benzotriazole molecule would be built up as indicated in Figure (5.1).

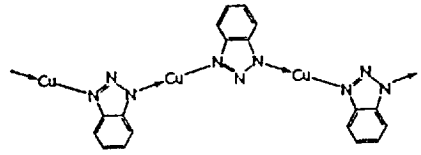


Figure (5.1) Cuprous BTA Complex (39)

From an elemental analysis of a chemically prepared cuprous complex, Cotton (39) concluded the complex has a composition of metal/organic ratio of one atom of copper to one molecule of BTA ($C_6H_4N_3$ Cu).

On the other hand, Cotton suggests it is not possible to describe the cupric complex so simply. It is evident that at least two cupric derivations exist, but it seems that they require the presence of a fifth element such as chlorine or oxygen. Physical data, such as electron spin resonance indicated that the cupric compound

has an unusual structure. The possible structure suggested by Cotton (39) is indicated in Figure (5.2).

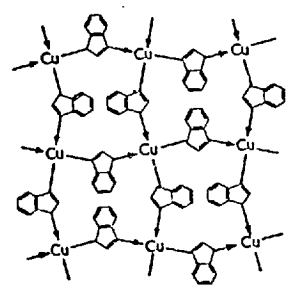
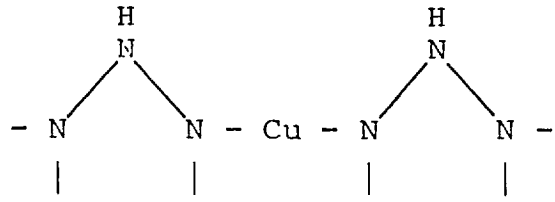


Figure (5.2) Cupric-BTA Complex (Cotton (39))

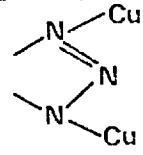
J.K. Prall and L.L. Shreir (50) in a study of benzotriazole as an additional agent for acid copper sulphate solutions have reported pH titration of Cu(I) vs. benzotriazole have shown that proton release does not occur, suggesting that imido group (=N-H) of the benzotriazole remains intact during the complex formation. According to them (50), this has been confirmed by infra-red spectroscopy which had also indicated that cuprous benzotriazolate may be polymeric and the following structure was suggested.



In addition, they found strong evidence which supports the view that surface film is present as Cu(I)-BTA. This structure is incompatible with results reported by Poling (51).

Poling (1970) (51) using infra-red reflectance spectroscopy has shown that the protective films formed on copper by benzotriazole are composed of a highly inert

copper benzotriazole (Cu - BTA) polymer. All of the films studied had a thickness equivalent to many molecular layers of the Cu - BTA monomer. Therefore, reaction of benzotriazole at copper surface is not limited to formation of a chemisorbed, two dimensional polymer layer as previously reported by Cotton (39). The multiple reflectance spectrum of a copper sample treated with BTA appeared to be close to the transmission spectrum of Cu BTA in a KI pellet. Based on the intensity of 745 Cm^{-1} band, the average film thicness over the two mirrors was determined to be 3100 Å (51). Multiple reflectance spectra of different samples treated with BTA also revealed that no >N-H groups were retained in the Cu-BTA surface film, therefore Cu was bonded to the amino nitrogen in the BTA complex, possibly having a "bidentate structure" of



Poling suggested that the mechanism for growth of Cu BTA film beyond the chemisorbed monolayer stage usually involved transport of copper ions through the surface films. These ions then reacted with physically adsorbed BTA molecules to precipitate insoluble Cu BTA complexes on the film surface. With a reservoir of BTA maintained in the treatment solution, the availability of Cu ions at the solid/liquid interface controlled the growth of the Cu BTA films.

Finally Poling (51) reports that Cu-BTA films afforded excellent protection of Cu in near neutral solutions. Cu-BTA films were found also to be protective in mildly acidic (pH = 3) solution that were free from O_2.

The basic discrepancy between the results of the above mentioned investigators is the reported film

thickness. According to Cotton (39) reaction of BTA at Cu surfaces is limited to formation of a chemisorbed, two dimensional polymer layer with an approximately 50 Å thickness. On the other hand, Poling's early studies showed that such films continued to grow beyond the chemisorbed monolayer stage to form films up to several thousand Å thick. Certain aspects are left in doubt in both reports. The role of chloride ion and also of Cu_2O is not clear. The question of detailed structures of the Cu-BTA complexes remains unanswered because it is not clear why some chloride was retained in Cu-BTA precipitate (Poling), despite repeated washing, while no chloride was reported by Cotton (39). The mechanism suggested by Poling (51) does not explain all observations. For instance, why in some environments, such as distilled water, the film thickness stays low (51).

F. Mansfield et al (52) using ellipsometry have concluded that in neutral media BTA is chemisorbed on the copper surface and this chemisorbed layer prevents adsorption of oxygen and oxide formation. The film thickness stays low in neutral solutions containing BTA according to Mansfield et al. In acidic solutions, film thicknesses appear to be high, but for a short exposure time this is a result of a porous salt film which can be easily wiped off. The underlying film is thin (60 to 140 Å) but different from Cu_2O as indicated by the lower index of refraction. For longer exposure times, this underlying film becomes thicker and cannot be wiped off.

Mansfield et al (52) found that on a cathodically reduced surface in de-aerated solution containing BTA, the optical constants were similar to those obtained in BTA free solution. This seems to indicate that BTA interacts

with the Cu surface only when this is covered with some oxide layer. According to these authors, this seems to argue against a pure adsorption mechanism and more work has to be done to understand these results. In fact, the results on cathodically reduced surfaces proved to be not completely reproducible (52), because in a second experiment only some parts of the specimen remained clean, while the rest was covered with a thicker film. This suggests that probably immersion of a copper sample in a solution of BTA, even for a short period of time, may result in film formation so that reaction of BTA with a cathodically reduced copper surface does not really take place. Although the authors did not suggest any mechanism involving Cu_2O or its importance in film formation, nevertheless the finding that a cathodically reduced surface remains clean most of the time in BTA solution is of great importance.

R.F. Roberts (36) using X-ray photoelectron spectroscopy indicated that the rate of adsorption of BTA onto a Cu_2O surface is more rapid than that of BTA onto a CuO surface. Thus the immersion of a Cu_2O surface in aqueous BTA at 60°C in the absence of Cl^- for 3 minutes results in the formation of both cuprous and cupric-benzotriazole surface compounds whereas neither of these is formed on a CuO surface treated in the same manner. The most important observation was that the Cu(I)-BTA surface compound which is formed initially upon the immersion of a Cu_2O surface in aqueous solution of BTA, gradually oxidized to Cu(II)-BTA as the immersion time is increased. The ratio of the areas of the Cu(II)-BTA Cu ($2p_{3/2}$) peak to that of the Cu(I)-BTA Cu ($2p_{3/2}$) peak

was plotted as a function of immersion time. Figure 5.3 shows this graph. From the Figure it appears that oxidation proceeds for immersion times up to 2 hours and essentially ceases for immersion times in the range of 2-21 hours (Figure (5.3)). Roberts (36) suggested that the thickness of the film initially formed upon the adosrption of BTA onto Cu_2O surface has a range of 15-60 Å. The Cu(II)-BTA surface films, formed by oxidation of Cu(I)-BTA on Cu_2O substrates in solution, grew to a maximum thickness of less than 7 ± 3 Å for immersion times in BTA for 24 hours.

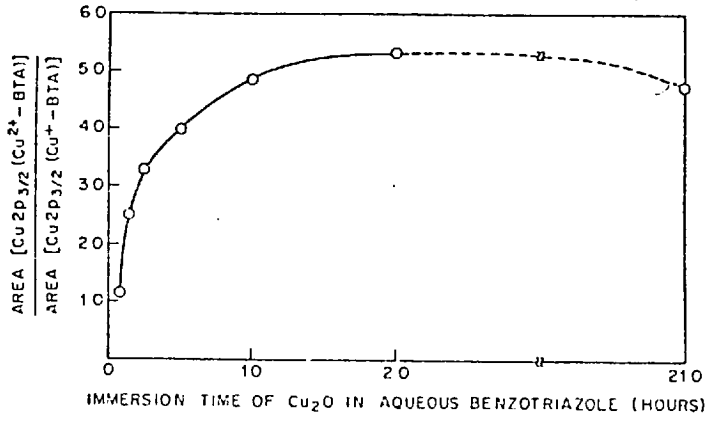


Figure (5.3) Plot of Ratio of the Areas of the Cu $2p_{3/2}$ photoline of Cu^{2+}-BTA to that of Cu^{+}-BTA vs. Immersion Time in Aqueous BTA (Roberts (36))

Finally, as a possible structure for copper-benzotriazole surface film, Robert suggests with Cu^+ having a co-ordination number of four, the first layer of Cu(I)-BTA might be anchored to the copper oxide substrate by two bonds between a single Cu^+ ion and two lattice oxygen atoms, with the remaining two Cu^+ co-ordination position occupied by BTA. Succeeding layers of Cu^+-BTA could then involve Cu^+ bonded to BTA with some co-ordination positions

occupied by H_2O molecules.

The mechanism by which benzotriazole inhibits the corrosion of Cu in aqueous chloride environment has been investigated by Ogle and Poling (53) using infra-red reflectance, X-ray photoelectron spectroscopy and electrochemical methods. Composition and thickness of protective Cu-BTA films were determined by reflectance spectra. X-ray photoelectron spectroscopy yielded additional data regarding composition of films and indicated the valence state of Cu in these surface films. Polarization curves were recorded during both treatment of Cu mirrors and corrosion of pretreated mirrors. The topographies of films and of underlying Cu after varied conditions of pre-treatment and corrosion were examined by electron microscope techniques. Ogle and Poling (53) have classified the Cu-BTA surface films formed on Cu into two types. The films which are formed in a solution with a pH greater than a limiting pH, where $4>pH_{lim}>3.5$ and those which are formed at pH less than the limiting pH. Infra-red reflection-absorption spectra of these films were almost identical to spectra of cuprous benzotriazolate. However, X-ray photoelectron spectra (ESCA) of both types of films indicated the presence of about 10% of total Cu, existed as cupric ions. A weak 2p chlorine (Cl) peak at 197.1 eV was also observed in spectra of the thin and thick films. They concluded that the small proportion of Cu detected in the divalent state by ESCA was probably present as Cu(II)-BTA rather than $CuCl_2$, because the Cl binding energy was in the range of CuCl. The authors then suggested (53) that although the presence of Cu(II)-BTA in surface films on Cu had not been previously reported by Poling (51), the

varying magnetic susceptibilities of Cu(I)-BTA precipitates showed the possible presence of Cu(II). Hence, it is likely that the Cu(II) in surface films on Cu resulted from partial oxidation of Cu(I) in the Cu(I)-BTA films formed initially. Although it is not clear from this report whether they envisaged this oxidation as taking place "in situ" or from exposure to air, it becomes apparent from Poling's next report (54), to be reviewed later, that they are referring to an "in situ" oxidation. Although Poling (53) reports minor cupric present in Cu-BTA film, he does not see any discrepancy between his results and those of Roberts (36). No attempt was made to explain the reason for chlorine existence in the surface film as it was reported as a weak peak (53).

Ogle and Poling (53) concluded that treatment of Cu in solutions containing BTA resulted in the formation of two distinctly different types of Cu-BTA films depending on solution acidity and substrate. In near neutral environments, then (<60 Å) multilayer films grew on top of Cu_2O interlayers. In contrast, thick films (up to several thousand Å) resembling a network of acicular crystallites formed on Cu substrates in acidic environments. The suggested mechanism is basically the same as Poling's previous report (51) in which a chemisorption process follows by nucleation and growth of Cu-BTA film and thicknesses to which films grow is controlled by their ability to resist outward diffusion of Cu ions.

The difference in limiting thickness to which thin and thick films grow is associated with the presence or absence of a Cu_2O interlayer, respectively. When present, it augments the overall resistance to diffusion of Cu

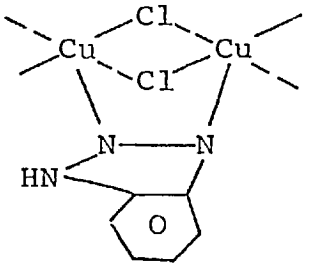
to the solid-solution interface. Again it is not clear from this report why the very presence of Cu_2O interlayer facilities film formation and film growth. Moreover, although the authors have noticed two distinctly different types of Cu-BTA films depending on solution acidity and substrate, no attempt is made to clarify the structure of these two different films. Finally, in determination of the degree of protection, they reported that the role played by Cu_2O interlayers in the protection of Cu by pre-treatment with BTA was complex (53). In acidic environments, coherency between Cu metal, Cu_2O interlayer, and pretreated Cu-BTA surface film appeared to determine the degree of inhibition.

T. Notoya and G.W. Poling (54) using scanning electron microscopy (SEM) technique, examined the topographies of thick copper benzotriazole (Cu-BTA) films. Relations to crystallographic orientations of substrate copper crystals have also been shown. Cu-BTA crystallites formed on relatively thin Cu_2O films all adopted the form of star-like structures of acicular crystallites which were large in size compared with those formed on thick oxide film. Also they appeared to be less protective. On the other hand, the Cu-BTA crystallites formed on Cu_2O films more than 200 Å thick have more matted structures, which might act to protect both the underlying oxide and substrate copper. In addition, the density of the Cu-BTA crystallite cluster or average Cu-BTA film thickness depends on the underlying oxide thickness: the thicker the oxide film, the finer and more dense the Cu-BTA crystallites. However, the structures of thick Cu-BTA films formed on top of the oxide appeared

to be less dependent on the crystallographic orientation of the substrate copper crystal. No mechanism is given.

At this stage, the study of N. Morito and W. Suetaka (55) must be mentioned. Using infra-red (4000 - 400 cm^{-1}) and ultra-violet-visible (50,000 - 12,500 cm^{-1}) reflection spectroscopy of BTA treated copper, they concluded that the film consists of Cu(I)-BTA formed by substitution of a H atom in the N-H group with Cu(I) ion. From the relative intensity of the adsorption bands of C-H stretching vibration they concluded that the plane of the Cu(I)-BTA molecule is parallel to the Cu surface. Far infra-red reflectance spectra (400 - 200 cm^{-1}) suggest the presence of N-Cu-N deformation vibration and that the surface film may be a polymer. The electronic reflectance spectra of the Cu immersed for 150 seconds are in near agreement with the spectra of Cu(I)-BTA. The spectra of very thin films (< 10 Å) are a little different from that of Cu(I)-BTA, but are quite different from that of BTA cupric salt and BTA. Therefore, the thin film seems to be composed of a compound similar to Cu(I)-BTA.

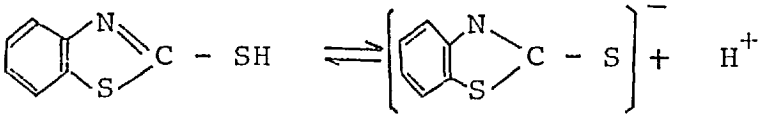
Several investigators have dealt with this problem to a lesser extent, nevertheless their studies are worth mentioning. S. Thibault (56) using multiple reflectance infra-red spectroscopy studied the inhibition properties of benzotriazole, benzimidazole, indol and indazole on the corrosion of copper. Based on the work done by Jarvis and Wells (57) he suggests that in the presence of chlorine ions (Cl^-), the surface complex has the following structural formula:-



5.4 Corrosion Inhibition of Copper and its Alloys by 2-Mercaptobenzothiazole

Besides benzotriazole, the use of 2-mercapto-benzothiazole has been suggested (40, 46) for the inhibition of copper and copper alloy corrosion. There are a large number of reports dealing with practical aspects of corrosion inhibition properties of 2-mercaptobenzothiazole and some related compounds, and excellent protection has been reported. Surprisingly very little work is reported concerned with the mechansim of MBT interaction with copper and alloy surface and the nature and structure of the protective film.

Bregman (40) has suggested that in aqueous solution, mercaptobenzothiazole ionizes as a weak acid as illustrated below.



The ionic species form insoluble salts with metal ions, such as copper and conceivably the protective coating consists merely of insoluble copper salt of MBT. However, a more plausible structure for the protective coating would take into account the fact that the MBT possesses not only an ionized sulphur group but also a ring sulphur and a ring nitrogen, both capable of forming co-ordinate

bonds with the metal or the metal ion.

If the surface of the copper becomes partially oxidized, one mode of attachment of MBT to the surface can be visualized (40) as shown in Figure (5.4).

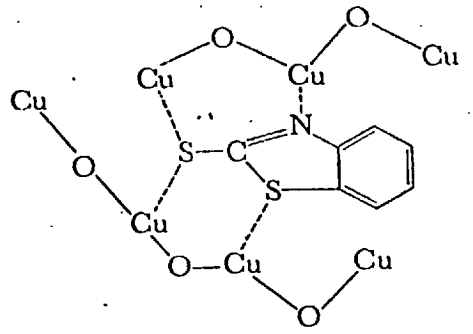


Figure (5.4) Possible Structure of Cu-MBT Complex Film (40)

This structure is a pictorial presentation only; the precise geometry would be dependent upon the structure of the oxide film and the geometry of the MBT molecule. It does show, however, that it would be firmly bonded to the surface by several bonds and a similar type of bonding to the unoxidized metal surface may also be visualized.

According to G. Trabanelli (46), the action of MBT consists of the formation of an adherent and protective film. The binding characteristics of MBT can be interpreted by substituting the hydrogen atom of the sulfydryl group by copper cations and by means of bonds co-ordinated with the electron pairs of the other sulphur atom or of the nitrogen atom.

S. Thibault and J. Talbot (58) compared three closely related compounds, 2-mercaptobenzothiazole (MBT), 2-mercaptobenzimidazole and 2-mercaptobenzoxazole, with respect to their use as Cu corrosion inhibitors in weak acids. The threshold of efficiency corresponds to the formation of a surface coating ($>2 \times 10^{-4}$) for MBT and mercaptobenzoxazole and $>5 \times 10^{-5}$ for mercaptobenzimidole).

M. Bassoli et al (59) reported corrosion of Cu tubes pretreated with a solution of 3.3% sea salt containing varying amounts of MBT for 24 hours, was prevented for 3-4 weeks, when placed in a circuit in which a 3.3 gram salt solution (without MBT) was pumped at different speeds.

S. Thibault and J. Talbot (60) studied the compound formed on the surface of copper by MBT, 2-mercapto-benzoxazole and 2-mercaptobenzimiazole, in 10^{-3} M HCl. The complex of Cu with the organic compound seems to form at the surface of the metal and protects it. The benzene ring makes the molecule heavy and renders the complexes which are formed more insoluble, but it does not seem to play any other role in the corrosion prevention. Only the part bearing the N atoms seems active. Thus, the complex between Cu and the organic compound may be formed by the intermediary of the N atom of the pentagonal ring as in the case for BTA.

M.M. Patel et al (61) studied corrosion inhibition of 63/37 brass in acetic acid solution by MBT. They reported a 98% protection. N.K. Patel (62) reported the MBT inhibits corrosion of Cu in a variety of aqueous solutions. The inhibitive power of MBT is related to the formation of a thin adherent film of a complex compound on the metal surface. The infra-red spectra of the corrosion product was similar to that of $Cu(MBT)_2$.

Finally, S. Jeanin et al (63) studied crystals of Cu. MBT complexes using infra-red spectroscopy. Spectra of complexes were similar to that of protected Cu surfaces. Extracyclic S atoms were considered to bond MBT to the Cu surface.

5.5 Electrochemical Polarization of Copper in Brine Solutions

5.5.1 Cathodic and anodic behaviour of copper in NaCl solution

The $Cu-H_2O-Cl^-$ system under neutral, acidic and alkaline conditions has been investigated by many workers (64-70). Hedges (64) carried out an extensive investigation of the kinetics of the anodic behaviour of copper in hydrochloric acid solutions when polarized by the passage of a fairly large current. Hickling and Taylor (65) studied the behaviour of copper in alkaline solutions. They showed that copper passivates in alkaline solutions forming the oxides Cu_2O, and CuO, while in acid solutions, copper dissolves to give soluble salts and does not develop a protective passive film. Hedges (64), however, showed that copper could be passivated in acid solutions by lowering the temperature. At -11^oC copper becomes passive in concentrated nitric acid due to the formation of a dark grey film of cupric oxide. A four-part paper concerning the thermodynamic, kinetic, and electrochemical aspects of the corrosion of copper has been written by Ives and Rawson (66).

Lal and Thirsk (67) have studied the anodic behaviour of copper in NaCl solutions, both in the presence and in the absence of oxygen, by observing changes in the overpotential occurring during constant-current polarization and after the current has been interrupted. In their experiments, in neutral sodium chloride solutions, a range of current densities from 1×10^{-5} to 1×10^{-1} A cm^{-2} were employed in 0.1, 0.5, 1.0, 2.0 and 4.0 M NaCl. It was realized that when a certain current density was exceeded,

dependent on the concentration of the electrolyte and the temperature, a precipitate is formed on the electrode. In neutral chloride solutions the precipitate was shown to be cuprous chloride. The plot of log (current density) against potential, gave an almost linear relation up to a critical value of the current density corresponding to the formation of insoluble deposits (67). By repeating a selection of these experiments in the absence of oxygen it was shown that the results in neutral sodium chloride were unaffected by the presence of air above the solutions (67).

H.P. Lekie (68) has studied the anodic polarization characteristics of copper in a variety of environmental conditions. According to Lekie, in dilute acid solutions at room temperature, copper may dissolve at a rate limited by a diffusion-controlled current; increasing the acid concentration results in an increased tendency for passivation. At 25°C, anodic polarization curves for copper in 1M H_2SO_4, only a maximum diffusion-controlled current was observed at noble potentials with no decrease in the current density usually associated with passivity. At 0°C, however, there is some evidence of partial passivation. As the sulphuric acid concentration is increased to 10M, a pronounced passivation reaction is observed even at 25°C. Lowering the temperature to -11°C further increases the tendency for passivation.

Passivation was observed, Leckie reports (68), at all concentrations of NaOH. Both potentiodynamic and galvanostic curves were obtained. An active/passive transition characterized by a critical current density and a passivation potential, can be shown more clearly

in potentiodynamic polarization curves. According to this investigator, passivation of copper in high concentrations of H_2SO_4, may well be associated with the formation of Cu_2O. The absence of passivity in more dilute acid solutions may be attributed to the increased solubility of the corrosion products. Similarly, the passivation tendency of copper in dilute H_2SO_4 at 0^oC may be attributed to the reduced solubility of the corrosion product film at lower temperature. Bacarrella and Griess (69) reported the electrochemical polarization behaviour of copper in de-aerated 1.24 M NaCl solution at 30^oC. The anodic process consists of the oxidation of copper and has a Tafel slope of 60 mV/decade which corresponds to 2.3 $RT/_F$. The cathodic process, in this case, is primarily the reduction of water to hydrogen. Polarization near the corrosion potential was difficult to interpret because of contributions from unknown cathodic processes. For this reason corrosion potentials at a given temperature were not always reproducible. No passivation under these conditions has been reported.

The rotating ring-disk technique was used by A.H. Taylor (70) to investigate the corrosion mechanisms of pure copper and naval brass in de-aerated 0.5 M NaCl at ambient temperature. Pure Cu corrodes only via Cu^+ over the range ~ 2.5×10^{-6} to ~ 900×10^{-6} A cm^{-2} corrosion current. He found no evidence for Cu^{2+} species or for film forming reactions.

5.5.2 Electrochemical polarization behaviour of copper in the presence of organic inhibitors

Dudgdale and Cotton (71), reported a study of polarization behaviour of pretreated copper samples in 3%

neutral NaCl solutions. They noted quite significant differences in the cathodic behaviour of the treated samples together with smaller but reproducible differences in the anodic behaviour. Benzotriazole, therefore, falls into the general category of cathodic inhibitors. Furthermore, it appeared that the inhibition is specific to the oxygen reduction reaction and does not operate for the hydrogen reduction reaction. In fact they noticied that when visible hydrogen evolution takes place, the difference between the treated and untreated copper sample is reversed. No explanation for this phenomenon is given. Also, no passivation due to film formation on the sample in the anodic part was noticed for untreated samples. The anodic process, according to them, is copper oxidation to produce the tarnish film, possibly with copper dissolution as an intermediate step. There is no evidence whether this oxidation process is the formation of Cu_2O or CuO and if there is a dissolution, whether it is via Cu^+ or Cu^{2+} species. However, it has been reported in this work that the corresponding cathodic reaction is almost certainly oxygen reduction, and is less vigorous on a benzotriazole treated surface than on an untreated surface.

F. Mansfield et al (72) studied the effect of BTA on the corrosion of copper in 5% NaCl by potentiostatic polarization and some other methods. They disagree with Dudgdale and Cotton (71) concerning the anodic behaviour of treated copper. According to them (72), some of the BTA adsorbed during dipping into a solution containing the inhibitor, desorbs again in solutions free of BTA. The remaining film of BTA prevents tarnishing but cannot prevent

copper dissolution. In contrast with Dudgdale and Cotton (71) who suggested a precipitation mechanism consisting of the formation and deposition of a Cu-BTA complex on the surface, Mansfeld et al (72) proposed a chemisorption mechanism. According to them, the good electronic conductivity of the film formed on copper, the decreased double layer capacity, the small film thickness and the decreased current on anodic polarization indicated that BTA is chemisorbed on the surface. They also suggested that the behaviour of copper samples at extreme cathodic potentials (1.2 V) observed by Dudgdale and Cotton (71) is due to dissolution of BTA adsorbed on the surface. In the cathodic cycle, on the other hand, BTA strongly decreases the rate of oxygen reduction accompanied by a shift of the corrosion potential in the negative direction.

Poling (51, 53) in his two papers showed the difference between the polarization behaviour of the Cu samples in solution with and without BTA. Also, pretreated samples were compared to those fresh unprotected samples. Polarization behaviour of copper samples in the inhibited and uninhibited, H_2 purged, 3% NaCl solution at 26^{o}C and pH 3 showed that the Cu-BTA films acted primarily as a cathodic inhibitor of the hydrogen evolution reaction at this pH. When oxygen was available for reduction (i.e. solution exposed to air), the Cu-BTA film appeared to have a minor effect on the cathodic part. The effect on the anodic branch was the same as de-aerated solution. In neutral aerated 3% NaCl solution, growth of Cu-BTA films caused pronounced inhibition of both the anodic and cathodic reactions. Results similar to these were obtained in H_2 purged neutral NaCl solutions and in the absence

of O_2 the Cu-BTA films exert even greater influence on the electrode reactions. According to Poling (51) these results indicate that the Cu-BTA films act as highly impermeable physical barriers, which provide exceptional protection to Cu in near-neutral solutions.

There are some obvious problems with this report (51). There are no indications of any shift in the corrosion potential due to the addition of BTA to the solution, which is definitely the case for inhibited aerated solution of NaCl. For a high concentration of BTA (0.02M) this is not less than 0.2 V in the negative potential direction (71, 72). In fact, in a curve drawn for inhibited solutions, a shift in corrosion potential twoards positive potential is shown (51). Similarly no shift in corrosion potentials of copper in aerated and de-aerated solutions is reported (51). This is mainly because when oxygen is removed from the solution the predominant cathodic process (i.e. oxygen reduction) is prevented, resulting in movement of corrosion potential towards negative potentials. Also, no passivation in uninhibited NaCl solution has been reported, which may be expected to occur in the range of potentials and current densities Poling has used. At the end, in contrast to Dudgdale and Cotton (71), he (51) suggests that the Cu-BTA films inhibit the hydrogen evolution reaction rather than O_2 reduction reaction. Similar results were reported in another paper by Poling (53) dealing with pre-treatment of copper samples before electrochemical polarization.

G. Trabanelli et al (46) studied the inhibition of copper corrosion in chloride solutions by heterocyclic

compounds. The anodic and cathodic polarization curves were recorded for copper in 0.1M NaCl solution in the presence and absence of inhibitors. A comparison of the efficiency of different inhibitors is given.

CHAPTER SIX

STUDY OF FILM FORMATION BY BENZOTRIAZOLE ON COPPER AND ITS ALLOYS

There are two principal reasons for studying surface films formed by BTA on copper, through which this inhibitor exercises its protection. These are to elucidate the structure of the films and the mechanism by which they are formed, in the hope that this will lead to a fuller understanding of the corrosion inhibition process and the development of more efficient treatment procedures. Previous investigations of film structure and formation mechanism have left considerable uncertainties, which have been discussed earlier in detail. For example, the oxidation state of copper in the surface film, which has an importance in film structure and film stoichiometry has been subjected to several studies. U.V. and infra-red techniques (51, 55) marginally favoured copper in its monovalent state, whereas in another work (36) it has been shown that there exists a correlation between the ratio of Cu(II)/Cu(I) in the film and immersion time to BTA solution. As well as the oxidation state of copper in the film, its stoichiometry and chemical structure have not been elucidated satisfactorily under all conditions. This applies also to the mechanism of film formation. No satisfactory model has been proposed to cover all the observations.

This chapter is devoted to the results obtained from a study of such films using ESCA and I.R. reflectance spectroscopy. Since results obtained from these techniques are complementary, both sets of results are presented in

this chapter. A model based on these results concerning the nature and the structure of the films is then proposed. The mechanism by which BTA interacts with copper surfaces, and as a result, inhibits the corrosion of copper is discussed.

6.1 Structure of the Films

6.1.1 Oxidation state of copper in the films

The first step in determination of the structure of the films is to investigate the oxidation state of copper. Although it should be possible to determine this using I.R. spectroscopy, it is not reliable for this purpose. ESCA, which has been fully described in Chapter 4, is a powerful technique for surface studies and can distinguish different oxidation states via the "chemical shift". Extensive use has been made of this technique.

Since any polished copper sample is inevitably covered with thin film of cuprous oxide, (73) and it is the Cu_2O which is initially in contact with any BTA treatment solution, it is important to investigate the effect of BTA on thick layers of Cu_2O. For this reason two types of copper samples were used in this study. In one set, the copper samples were polished with diamond paste of different sizes, the last one being 1 μ. In order to remove possible contamination arising from diamond paste, these samples were washed with acetone, methanol and triply-distilled water and dried in air. This washing routine was done for every sample prepared this way in order to have a reproducible surface. On another set of copper samples, films of Cu_2O were grown

electrochemically in KOH solution (for details see Appendix A).

Before studying the reaction with BTA, the substrate was fully characterized. An oxide-free copper sample was prepared inside the spectrometer using argon ion bombardment. Argon ion bombardment of a polished sample produced a relatively clean surface with no oxide on the surface judging from disappearance of oxygen 1s peak from ESCA spectrum. The spectra obtained from a clean metallic surface were used as reference spectra. The XPS spectra of all these three types copper samples in Cu 2p region were identical. The results are in agreement with previously reported spectra (17, 32, 36). Figure (6.1a) shows a typical XPS spectrum of a polished and argon etched copper sample in the Cu 2p region. Figures (6.1b) and (6.1c) show typical Cu 2p spectra of polished samples and Cu_2O covered (grown electrochemically) copper samples respectively. Apparently, there are no remarkable differences between the three spectra. No detectable chemical shift could be detected on the other XPS peaks either. So the immediate conclusion is that XPS fails to distinguish between Cu(O) and Cu(I).

Fortunately, Cu $L_{3,4}$ $M_{4,5}$ $M_{4,5}$ Auger lines in the X-ray induced Auger spectra of metallic copper and Cu_2O are quite distinguishable and there is a shift of about 2.5 eV between them. Figures (6.2a), (6.2b) and (6.2c) demonstrate X-ray induced Auger spectra of argon etched, polished and Cu_2O covered copper samples. These correspond to samples in Figures (6.1a), (6.1b) and (6.1c) respectively. Examination of the spectrum in Figure (6.2b) shows the polished sample must be covered

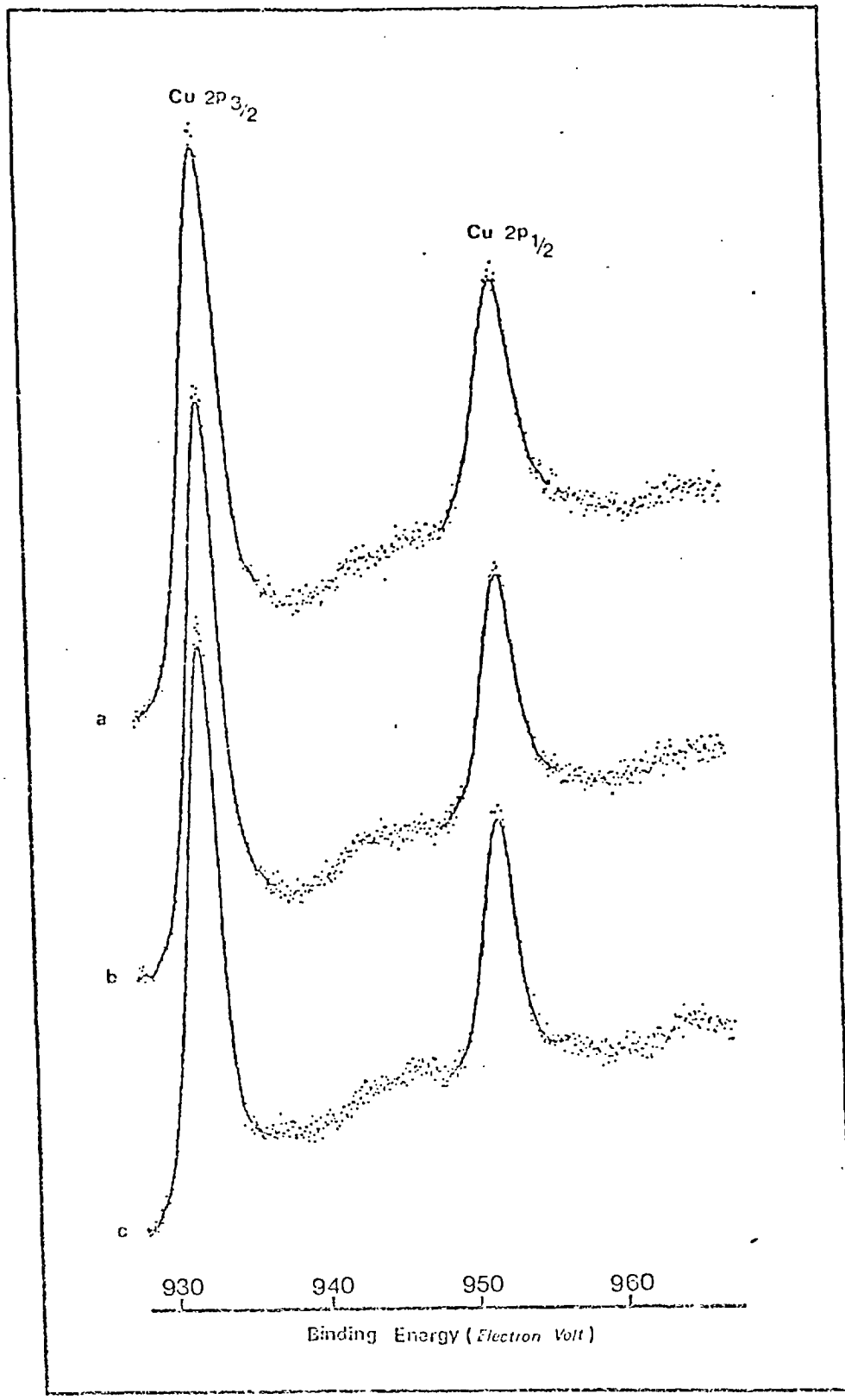


Fig. 6.1: X-ray photoelectron spectra of Cu (a) polished and argon etched (b) polished (c) with an electrochemically grown Cu_2O surface.

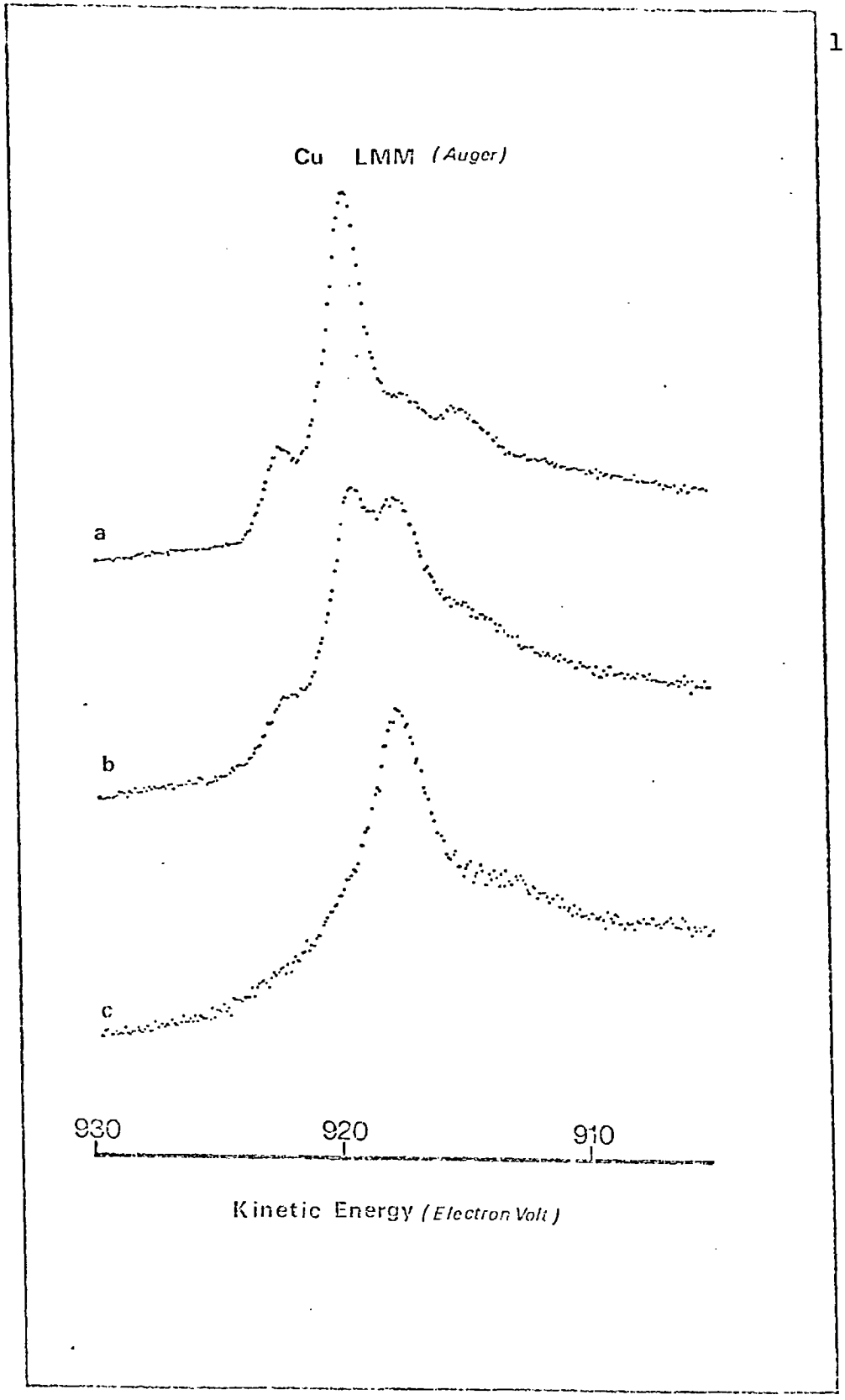


Fig. 6.2: X-ray induced Auger spectra of Cu (a) polished and argon etched (b) polished (c) with an electrochemically grown Cu_2O surface.

with a thin layer of cuprous oxide whose thickness is within the escape depth of the Auger electrons of Cu, which is not greater than say 15 Å. This proved to be the case for all polished samples studied, no matter how soon the samples were transferred to the spectrometer after polishing and washing processes. This Cu_2O layer grows to a certain limit due to prolonged exposure to air at room temperature, never exceeding from escape depth of the Cu Auger electrons.

The Cu 2p XPS spectra of copper samples which proved to be handicapped in differentiating between Cu(O) and Cu(I) proved to be most useful for identification of Cu(II) compounds. In all Cu(II) compounds examined by XPS, a chemical shift of about 2.7 eV towards the higher binding energies, and relatively strong satellites have been observed. These satellites appear at 6-10 eV higher binding energy of the main peak (31). Although some conflicting data have been reported in early publications (30) concerning the presence or absence of satellites in the Cu 2p spectra of cuprous compounds, it is now accepted that the observation of these satellites can be taken to be indicative of the Cu(II)species (see Chapter 5). Also a broader and less intense signal, is characteristic of the Cu(II) compounds.

The X-AES spectra of Cu(II) compounds, on the other hand, showed no remarkable difference with those of Cu(I) compounds. A small shift towards higher kinetic energies (about 0.9 eV) is associated with Cu(II) compounds. It is concluded at this stage, that XPS spectra at 2p region together with X-AES spectra at Cu L MM can identify uniquely Cu(O), Cu(I) and Cu(II).

The reaction of BTA with the copper was carried

out simply by immersion of the specimens in aqueous solution containing BTA. The samples were treated with BTA in a variety of conditions with respect to the concentration of BTA, NaCl concentration, pH and temperature. However a standard treatment was developed which consisted of the immersion of samples for a certain period of time in an aqueous solution of 0.02 M. BTA, and 0.5 M NaCl, at pH ~3 and at 25°C with N_2 purging, followed by washing with triply-distilled water and drying in air. The photoelectron spectra of copper samples after being treated with the standard solution showed no major differences in the Cu 2p region from Cu or Cu_2O, despite prolonged exposure to the solution. Figure (6.3a) shows an XPS spectrum of a polished sample treated with the standard solution for 10 minutes and Figure (6.3b) shows the spectrum of a similar sample treated with standard solution for 16 hours. Identical results were obtained for many exposure times. The minor presence of cupric compounds in Figure (6.3a) which is evidenced from the appearance of a small shoulder at higher binding energy side of the Cu 2p peak, and also the possible presence of shake-up satellites is due to atmospheric oxidation of the surface film which will be discussed in detail later. That the surface film contained BTA, is not clear from Cu 2p photoelectron spectra alone, but in each case the strong N 1s peak and the enhanced intensity of the C 1s peak over untreated surfaces was taken as evidence of a surface Cu-BTA complex. This is shown in Figure (6.3c) which demonstrates the XPS spectrum of a copper treated with standard solution in C 1s, N 1s, O 1s and Cu Auger region. Although the existence of a N 1s peak and an increased intensity in the C 1s peak is an indication of the existence

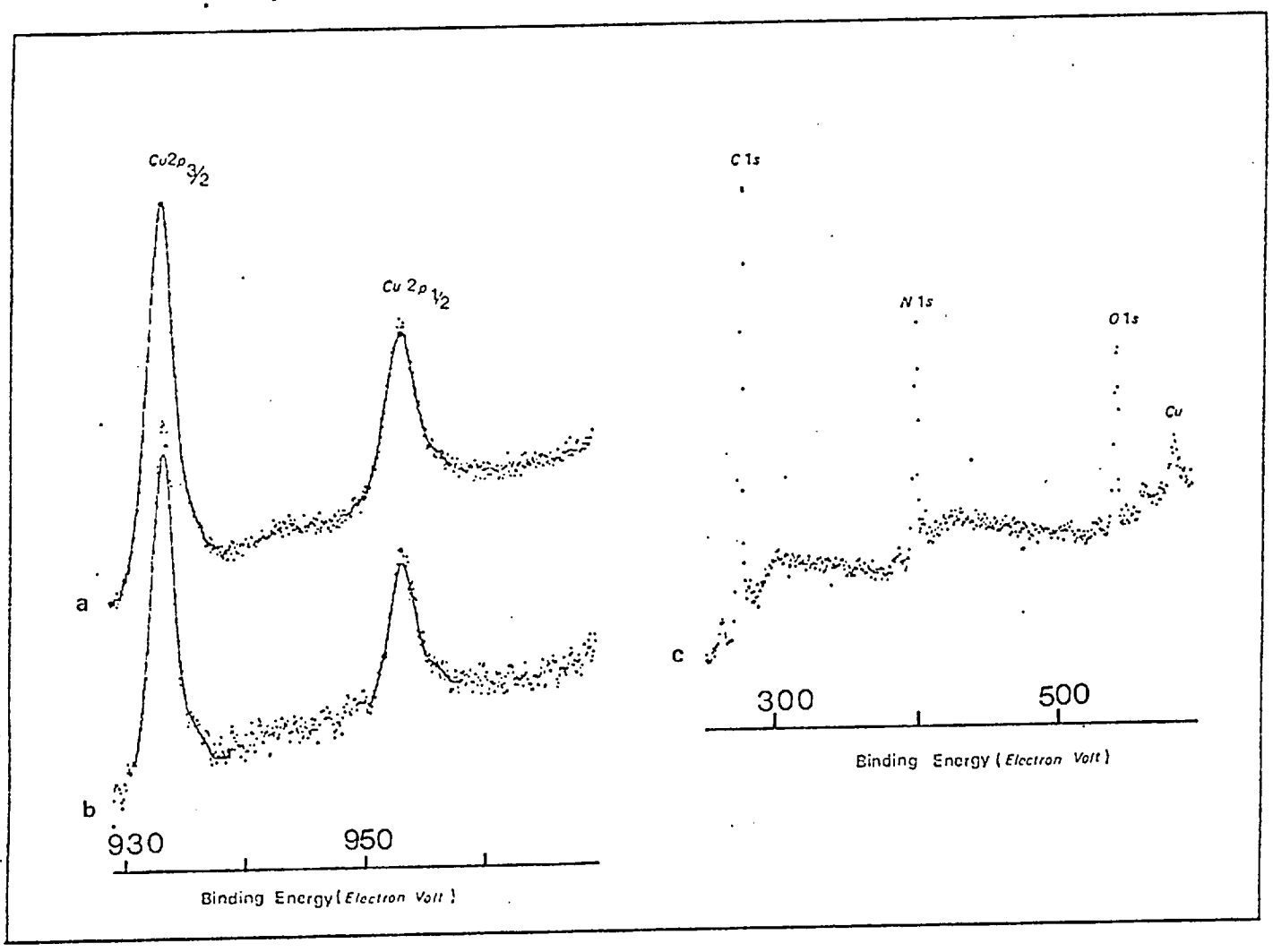


Fig. 6.3: XPS spectra of Cu (a) treated with standard BTA solution for 10 minutes (b) for 16 hours, (c) C 1s, N 1s, and Cu LMM Auger peaks after BTA treatment.

BTA on the surface, it does not distinguish between a copper-BTA complex and physically adsorbed BTA molecules.

It is already established that X-ray induced Auger spectra can distinguish easily between Cu(O) and Cu(I), however, it was further found that the Cu Auger spectra provide a reliable way to identify the formation of a Cu-BTA surface complex. Figure (6.4a) shows an X-AES spectrum of a copper sample polished and etched, in Cu LMM Auger region and Figure (6.4b) shows the spectrum of a copper sample covered with Cu_2O (electrochemically grown). Figure (6.4c) shows the result of treatment of such a sample with a standard solution of BTA for 5 hours. Obviously there is a shift in kinetic energy of the peak due to Cu-BTA complex from 917.1 eV k.e. for Cu_2O to 915.6 eV k.e. for the complex which enables one to distinguish easily between metallic copper, Cu_2O and the copper involved in a BTA complex. The results obtained with polished samples were similar to those with electrochemically grown Cu_2O surfaces, except in the resultant film thickness. Since the Cu Auger peaks of these samples before BTA treatment showed that the surface is covered with a thin layer of Cu_2O, it is not surprising that these samples behaved in a similar manner with respect to BTA adsorption as those with electrochemically grown Cu_2O surfaces.

Following these results, a variety of conditions for the BTA treatment were investigated. In each case a series of sample immersion times were examined and both polished copper samples and samples with electrochemically grown Cu_2O surfaces were used. The various conditions were:

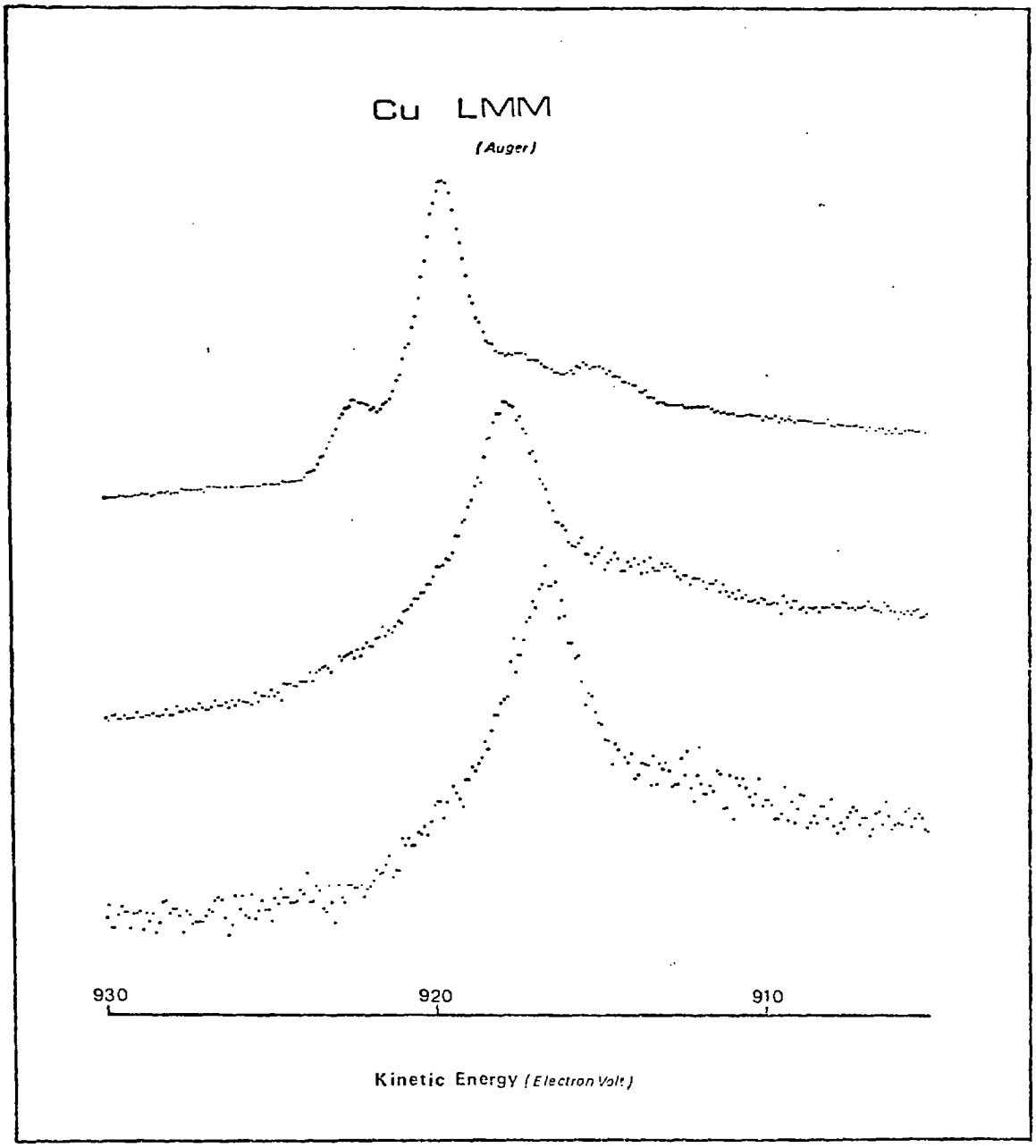


Fig. 6.4: X-AES spectra of Cu (a) polished and etched, (b) Cu_2O surface, (c) treated with standard solution of BTA for 5 hours.

a) 0.02M BTA, 0.5M NaCl at pH varying from neutral to 1.

b) Various BTA concentrations (2×10^{-5}M - 2×10^{-2} M).

c) Various temperatures (15°C - 80°C).

d) Various NaCl concentration (from none to 2M).

e) Variation in the degree of agitation of the solution.

f) Adsorption from organic solutions of BTA, e.g. dry CH_3Cl which is one of the few organic solvents in which BTA is appreciably soluble.

In all cases the Cu 2p spectra of the surface film produced were similar to Figure (6.3a) or (6.3b), indicating that there is no substantial increase in Cu(II) peaks intensities due to different conditions and exposure times. In all cases copper was found to be in its monovalent state from XPS and X-AES spectra.

The above results differ from the results obtained by Roberts (36), in which he found a correlation between the ratio of Cu(II)/Cu(I) and exposure time to the solution. For this reason similar conditions:- pH ≈ 5.25 amd 25-60°C in the absence of NaCl with N_2 purging were reproduced, and Cu_2O samples for a wide range of BTA concentrations were studied. The resulting spectra were similar to Figure (6.3a) or (6.3b) regardless of immersion time, in complete agreement with the results obtained for BTA solutions containing NaCl. Although in general N_2 purging was carried out throughout, it was found that even if air was blown through the BTA solutions during treatment, no increase in the amount of Cu(II) resulted. The possible conversion of Cu(II) to Cu(I) by photoreduction was shown not to occur in the spectrometer (see below) and therefore the observations genuinely reflect the oxidation state in the surface film.

However, in all cases the BTA treated copper specimens proved to be very sensitive to exposure to air, during which oxidation of Cu(I) to Cu(II) was observed to take place. This is demonstrated in Figure (6.5b-d), for the sample which had originally been given 20 hours immersion in a BTA solution and whose spectrum is shown in Figure (6.5a). The spectra were obtained after 2, 3 and 18 hours exposure to air and indicate the progressive oxidation of Cu(I) in the surface film to Cu(II). This is evident from the increasing intensity of the high binding energy shoulders and the shake-up satellites. This sequence of spectra was typical of all the BTA treated copper samples studied. A check was also made to see if running the spectra at intermediate times during the oxidation process accelerated the process through radiation damage, but no effect was observed. Photo-reduction effects, which have been reported for some Cu(II) compounds during which Cu(II) converts to Cu(I), were absent from the present study, perhaps because the Al X-ray anode was operated at the lowest possible power level. Since the spectra were obtained by digital accumulation, it was possible to verify that no photo-reduction took place during acquisition of the spectra. In fact, no evidence for photo-reduction of Cu(II) to Cu(I) was obtained from any spectrum under the prevailing conditions in the spectrometer and the short time taken to collect data.

A reasonable explanation for the small amount of Cu(II) present in the surface film (Figure (6.5a)) is that this arises from oxidation of the film during the finite time (5-15 minutes) needed to dry the sample in air before insertion into the spectrometer. Subsequent drying time in

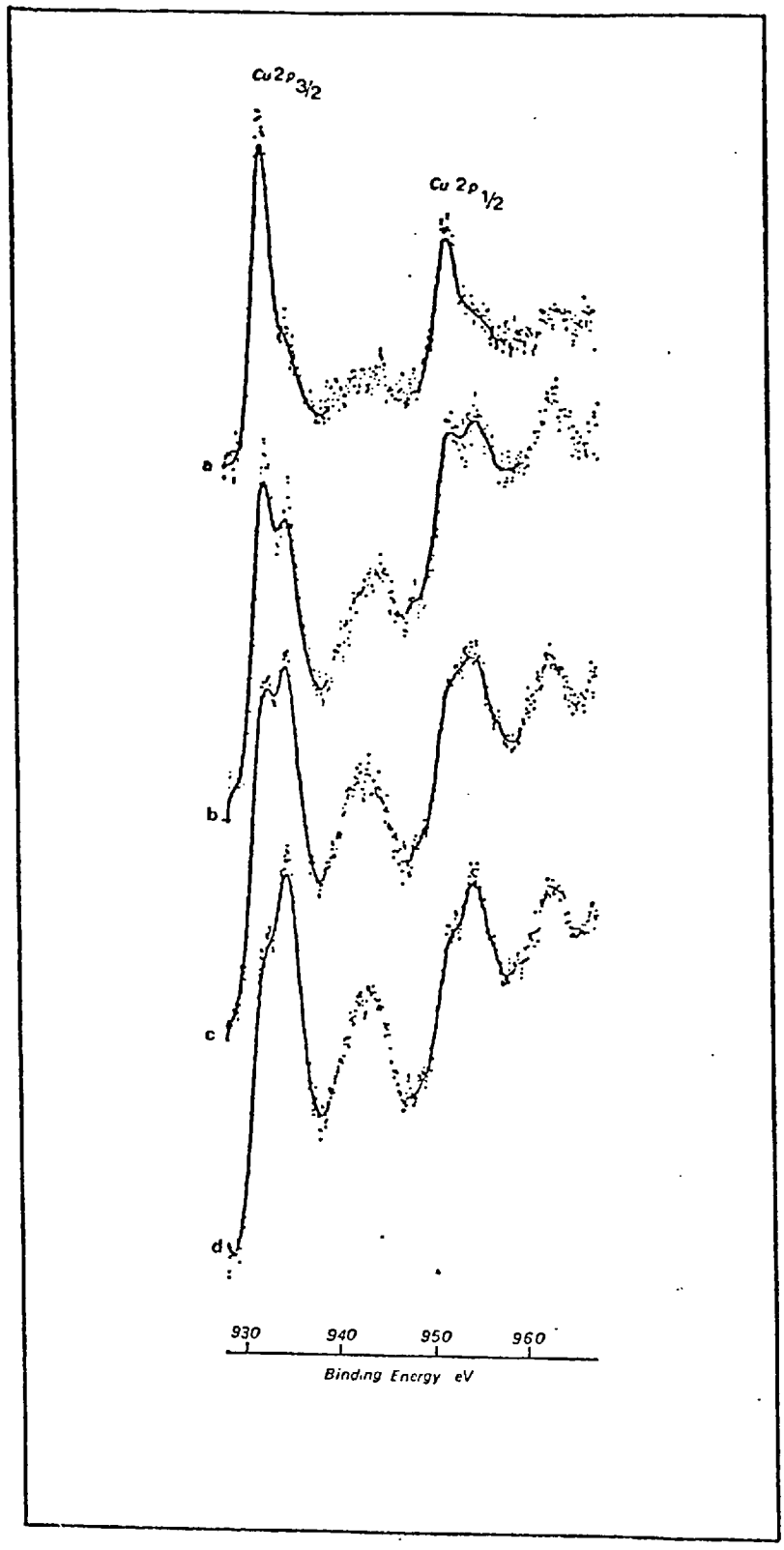


Fig. 6.5: XPS spectra of a Cu (a) treated with standard solution of BTA for 20 hours. Exposure of this sample to air for (b) 2 hours, (c) 3 hours, (d) 18 hours.

view of this fact was kept to a minimum. Finally it must be stated that the oxidation of some Cu(I) compounds to Cu(II) due to air exposure has been noticed previously and has been reported by several workers (36, 74).

Considering the above results, it is now quite clear that the films formed on copper surfaces by BTA, from both aqueous and non-aqueous solutions, consist of a Cu(I)-BTA complex. When the sample is removed from the solution, this complex reacts with air and a Cu(II) overlayer is produced. Obviously the structure of an overlayer produced by such an oxidation process would not be the same Cu(II)-BTA complex as may be formed in solution and referred to by previous workers (36, 53).

From the point of view of corrosion inhibition, it is very important to determine the properties of this Cu(II) overlayer since O_2 is clearly degrading the surface film. For this purpose samples with relatively thick Cu(I)-BTA complex films were exposed to air for a long period of time (say a few days) and then tests were made to determine the properties of the Cu(II) layer. These films could be easily wiped off with a tissue and examination of the underlayer films showed that they are Cu(I)-BTA complexes. This in its turn, on exposure to air, can undergo oxidation to form a new Cu(II) overlayer. Figure (6.6Aa) and (6.6Ca) shows the XPS and Auger spectra of a sample treated with BTA after a significant amount of surface oxidation has taken place. If the sample is wiped gently with a dry tissue, the outer layers are removed and the spectra in Figure (6.6Ab) and (6.6Cb) are obtained. The ESCA spectrum of the sample in the Cu 2p region indicates that the Cu(II) had been almost removed. The existence of an inner layer

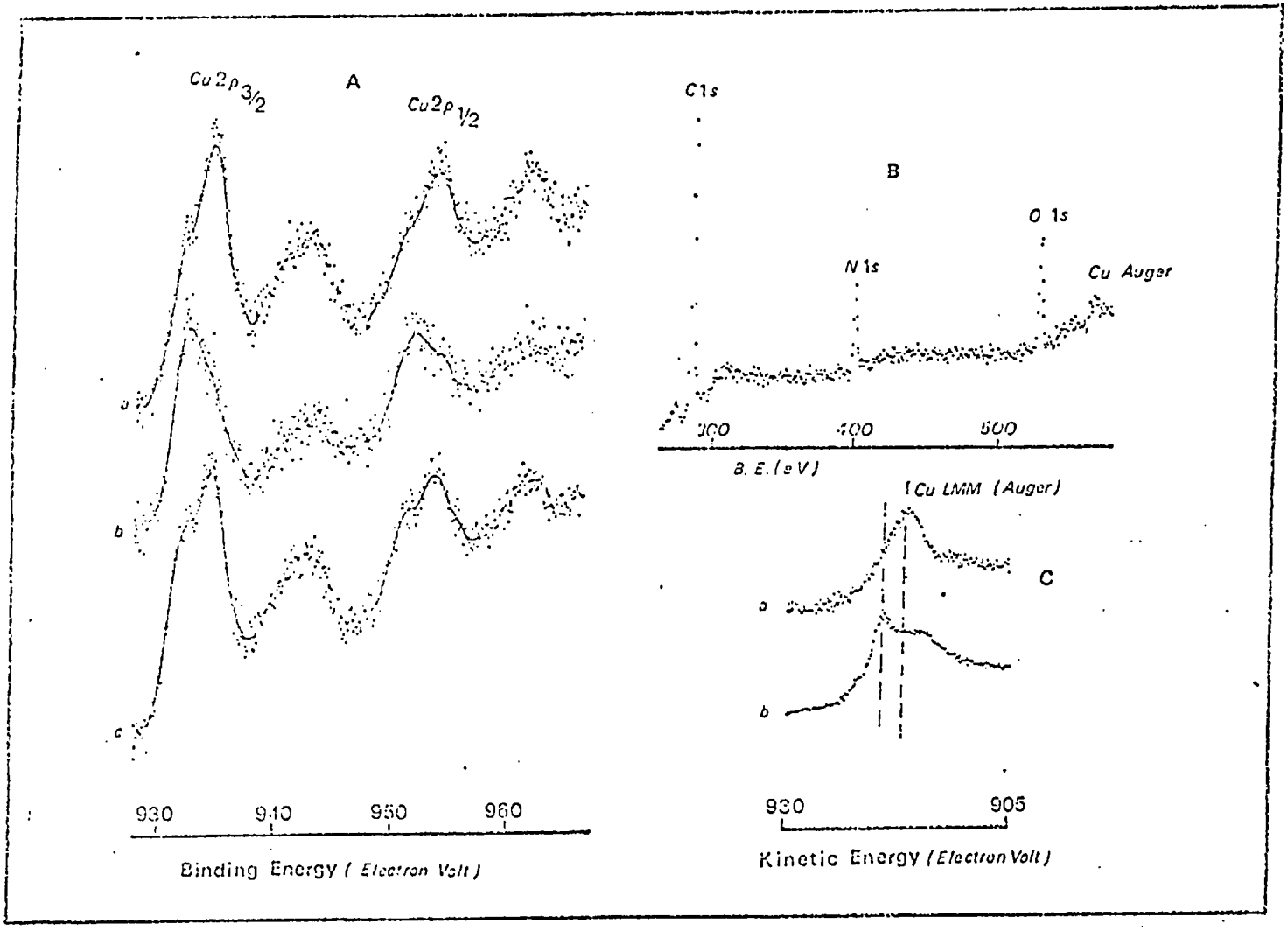


Fig. 6.6: Effect of wiping the oxidized Cu-BTA surface film A(a) original Cu2p spectrum;A(b) above dample after wiping; A(c) the same sample after being exposed to air again; B C 1s, N1s, O1s and CuLMM Auger peaks after wiping; C(A) X-AES spectrum of above sample before wiping, C(b) after wiping.

of Cu(I)-BTA complex is proved by Cu Auger peak, Figure (6.6Cb) and also by the C 1s and N 1s peaks (Figure (6.6B)).

It was also found that if surface oxidised samples were immersed for a short time in water, the amount of Cu(II) was substantially reduced relative to Cu(I). Results obtained from samples exposed to air and then washed, and repeating this, for several cycles, indicate that there remains a very thin film at the end. This shows that the Cu(II) overlayer resulting from air oxidation dissolves in water, and as a result the complex film thickness decreases. Figure (6.7a) shows an XPS spectrum of a sample covered with Cu-BTA film after being exposed to air for a long time, and Figure (6.7b) the same sample after being washed. Exposure of this sample to air results in oxidation of underlayer film shown by Figure (6.7c).

These results indicate that a degradation of the surface film takes place on exposure of the sample to atmosphere. This degradation might be significant from corrosion inhibition point of view and could be an indication that a copper pretreated with BTA on exposure to air will lose its protection after some time.

6.1.2 ESCA investigation of Cu-BTA complexes

Since it was established in the last section that a complex of Cu(I)-BTA forms on the surface of BTA treated copper samples, and precipitated complexes of copper and BTA are known, a study of these precipitates in order to compare them with the surface complexes seemed necessary. In view of this, both Cu(I) and Cu(II) complexes prepared from the solution were examined by ESCA. For details of the preparation procedure see Appendix A . XPS results showed that the Cu(II)-BTA complex exhibited a spectrum (Figure (6.8f))

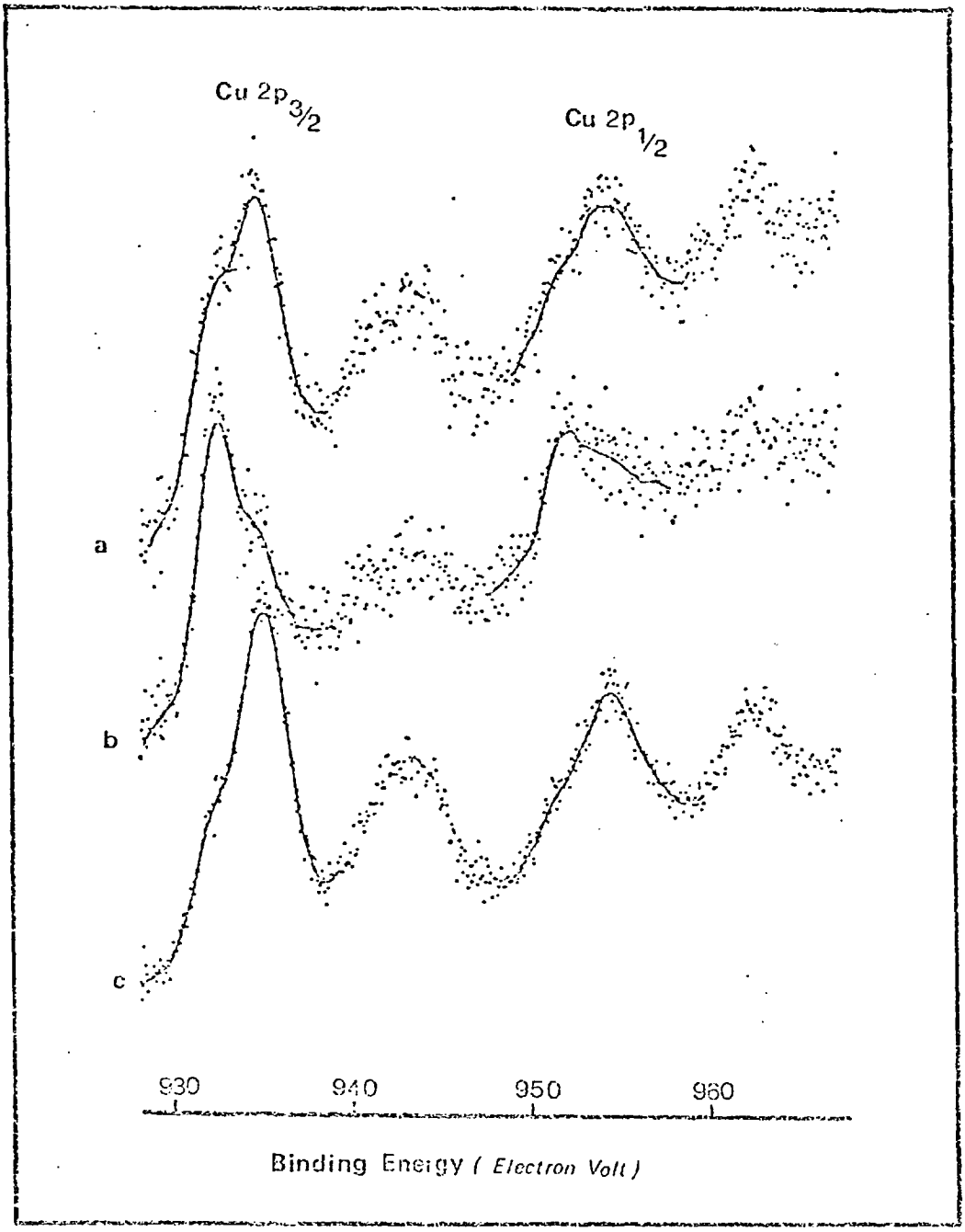


Fig. 6.7: Effect of washing the oxidized Cu-BTA surface film (a) original Cu2p spectrum; (b) the same sample after being washed; (c) sample (b) exposed to air again.

typical of cupric compounds (see Chapter 5). Binding energies are given in Appendix B . Cu(I)-BTA complexes prepared from solution exhibited a variation in stoichiometry due to the method of preparation which will be discussed in detail later in this chapter. However, the spectra in the Cu 2p region proved to be identical irrespective of preparation method. Measurement of binding energies of Cu(I)-BTA complex showed no differences from those of the surface films. Figure (6.8a) shows the spectrum of the Cu(I)-BTA complex prepared from the solution in Cu 2p region. There is a high Cu(II) content in this spectrum evidenced by higher binding energy shoulder of the main peak and existence of shake-up satellite. This is almost certainly caused by oxidation during the long drying time required for the precipitates. As for the surface films reported earlier exposure to air gradually converts the Cu(I)-BTA complex to a Cu(II) compound. This is evident from Figure (6.8b-e) indicates XPS spectra of above sample exposed to air for 5, 16, 26 and 48 hours and show the gradual increase in the peak due to Cu(II). These results are consistent with those derived already for the surface films. Both the surface films and solution prepared complexes showed similar behaviour towards atmospheric oxidation and this might suggest that they have a similar structure. X-AES spectrum of this complex before exposure to air (corresponding to Figure (6.8a)) showed a broad peak at 915.6 eV kinetic energy (after being corrected for charging effect) because of high Cu(II) content in the original sample.

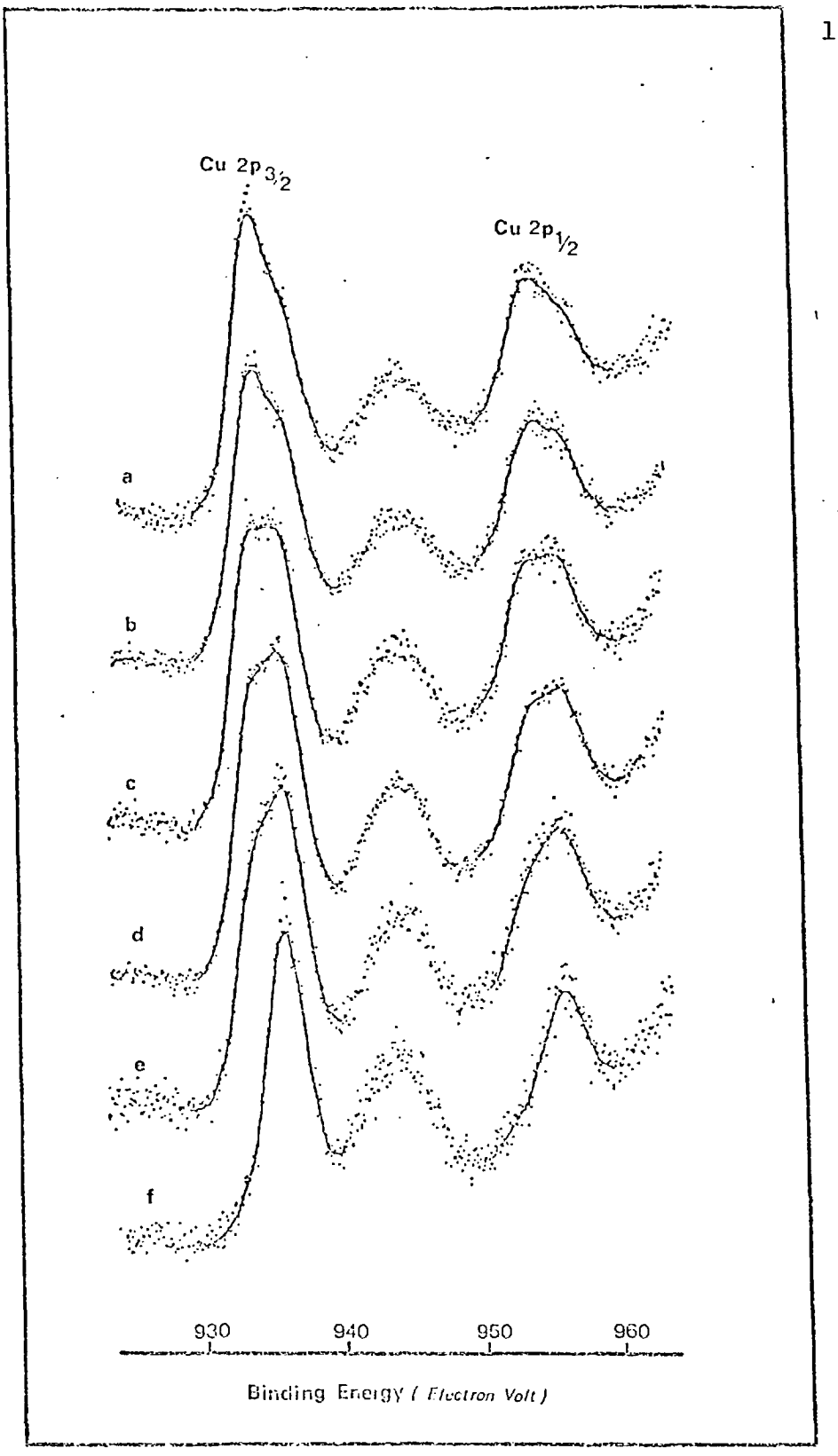


Fig. 6.8: XPS spectra of Cu(I)-BTA precipitated complexes; (a) Cu(I)-BTA. Exposure of Cu(I)-BTA to air for (b) 5 hours; (c) 16 hours; (d) 26 hours; (e) 48 hours; (f) Cu(II)-BTA complex.

6.1.3 I.R. reflectance spectroscopy of surface films and complexes

Another useful method of studying the BTA surface film on copper is infra-red reflectance spectroscopy (51, 55). This enables one to compare directly the spectra obtained for the surface films with the transmittance spectra of unreacted BTA and chemically prepared Cu-BTA complexes. Lack of high sensitivity, samples sizes and reflectivity severely limits the use of this technique. Nevertheless the technique can be used together with other methods, such as ESCA, to help understand the system more accurately. From the point of view of this study, the important region of the I.R. spectrum is 2500-3500 cm^{-1} where the C-H and N-H stretching vibrations occur. The spectrum of BTA and Cu-BTA complexes were obtained in the solid phase, using a KBr disc containing small amount of the compounds. There are some disadvantages in using this solid state method. The absorption bands in solid state are broader than for liquid samples. Moreover, the pressure applied to press the discs, in some cases, can lead to an alteration in chemical nature of the substance to be analysed. This is for instance the case for some Cu(II) compounds, which due to high pressure convert to Cu(I). This was the case for a chemically prepared Cu(II)-BTA complex when pressed to form a pellet for ESCA analysis. Apart from these limitations, the technique is quite reliable with good reproducibility. Figure (6.9a) shows a reflectance spectrum of Cu mirrors and (6.9b) shows a typical spectrum of BTA obtained in solid phase. The latter spectrum shows a broad, multi-peaked band between 2500-3450 cm^{-1}. This arises from the >NH and C-H stretching

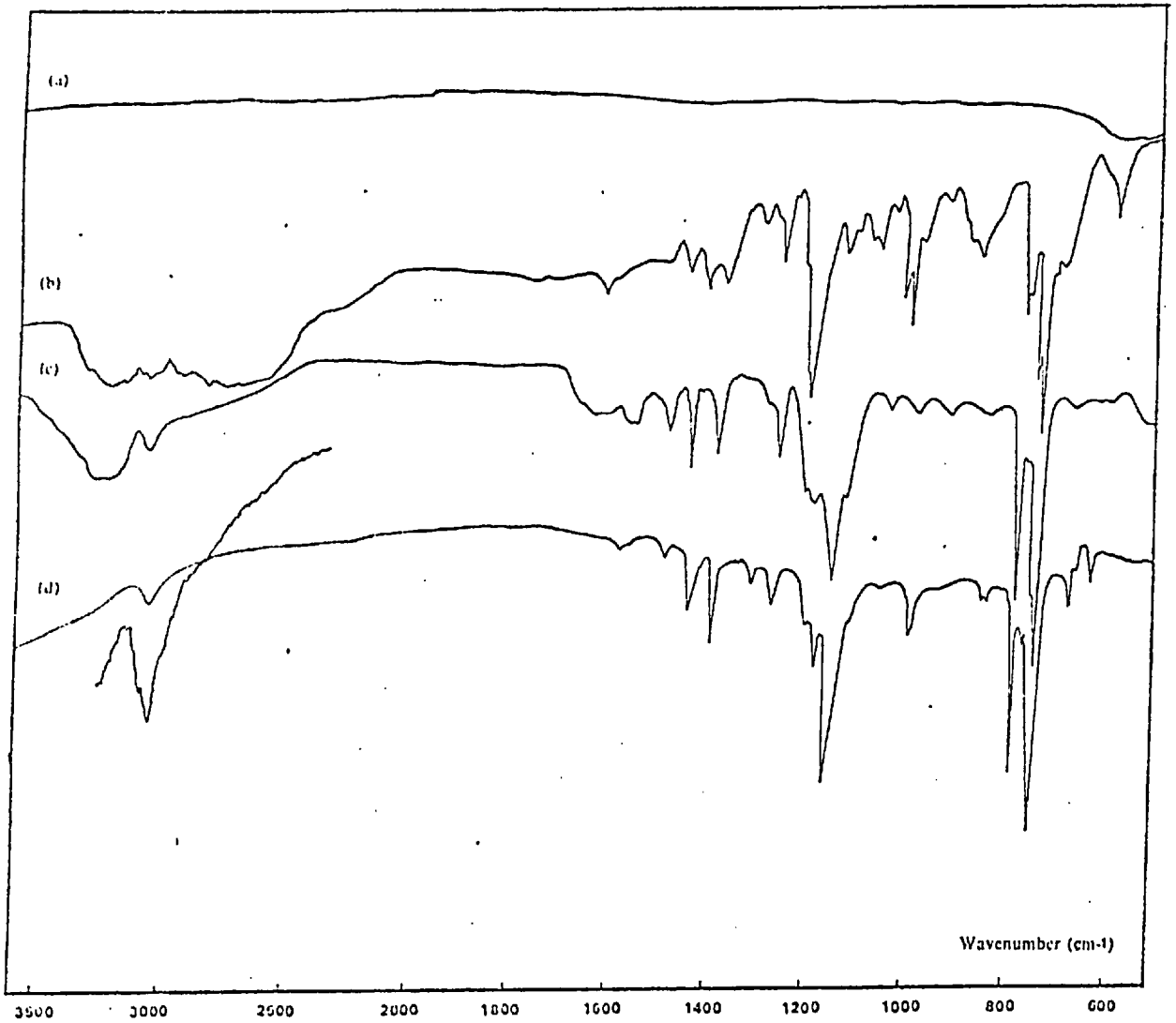


Fig. 6.9: Infrared spectra of : (a) blank Cu mirror, (b) solid BTA in K Br pellet (c) Cu-BTA complex (d) Cu-BTA surface film

vibrations. Stretching frequencies of C-H bands appear as weak bands near 3000 cm^{-1} but, being weak, they are usually obscured by the stronger N-H absorption. The N-H stretching band has been placed around 3200 cm^{-1} by O'Sullivan (75) and near 3450 cm^{-1} by Morgan (76), for benzotriazoles. The broad bands in this region of the BTA spectra are observed in most benzotriazoles between 3200-3100 cm^{-1} and is consistent with hydrogen bonds of moderate strength of the type N-H ... N.

In the region between 1000-2000 cm^{-1} bands related to heterocyclic ring systems appear near 1460, 1420, 1390, 1315, 1280, 1210, 1150, 1120, 1100, 1070, 1030 and 1012 cm^{-1}, according to Harzel (77) and Leiber (78). The strong band around 1200 cm^{-1} may arise from -N-N- vibration (51).

Many bands below 1000 cm^{-1} are due to deformation vibration of the benzene ring. Out-of-plane C-H bending vibrations in the aromatic ring, give rise to the strongest band in the benzotriazole spectrum around 745 cm^{-1} (51)

Infra-red spectrum of a Cu(I)-BTA complex (Figure (6.9c)) prepared from the solution showed a resemblance with BTA spectrum with two major differences namely the disappearance of a band around 2800 cm^{-1} and a shift in the band around 1215 cm^{-1} in benzotriazole to 1150 cm^{-1} in the complex. Figure (6.9c) shows an infra-red spectrum of a Cu(I)-BTA complex prepared from acidic solution in the presence of chloride ions and pressed in KBr disc.

A multiple reflectance unit with two copper mirrors (see Chapter 5) was used to obtain Cu-BTA surface film spectra. The spectra were obtained from samples treated in different

conditions of temperature, concentrations etc. as described for ESCA (section 6.1.1). Apart from differences in band intensities, the spectra were almost identical. Figure (6.9d) shows a multiple reflection spectrum from copper mirrors covered by film formed by reaction with BTA. The spectrum is typical of dozens of others recorded for films formed on copper by BTA. Comparison of the BTA infra-red spectrum Figure (6.9b) and reflectance spectrum of complex film on copper Figure (5.9d) shows that in this case also, there are two major differences between the spectrum of BTA and the spectrum of the surface film, namely the disappearance of band around 2800 cm^{-1} and a shift in the band at 1215 cm^{-1}. The disappearance of broad bands around 2800 cm^{-1} indicates that there are no N-H group retained in the Cu-BTA complex and surface film. The band around 3000 cm^{-1} in the spectra in both cases, is characteristic of aromatic CH group stretching vibrations.

In an attempt to deuterate the surface complex, the copper sample was treated with a D_2O solution of BTA. I.R. reflectance spectrum of the resultant surface did not show any N-D vibration indicative of complete replacement of N-H (or N-D) with N-Cu. Attempts by Poling (51) to deuterate the surface complex after being formed from aqueous solution also showed no N-D vibration in the I.R. spectrum.

Many similar heterocyclic compounds are reported to exhibit the same behaviour with respect to replacement of N-H group with N-M in which M is a monovalent metal such as copper, Na, Ag etc. 2-mercaptopyrimidin-4-Ol (2-thiouracil) which has two - NH groups in the molecule has been reported to exhibit N-H bands of moderate strength at 3100 cm^{-1} (79).

This band disappeared in the spectrum of the complex of this compound with copper. In another work (80), Cu(I) complexes with 2-imino-4-oxo-1,3-thiazolidine have been studied. The cyclic-NH for the free ligand appears as a broad band with strong intensity at 3100 cm^{-1}. The appearance of this band at 3100 cm^{-1} is attributed to the intermolecular hydrogen bonds (81). In the spectra of the complexes, the cyclic NH is absent. This indicates the deprotonation of the cyclic NH and its bonding to the metal. The lowering of intensity and decrease in the frequency of C-S stretching mode in the complex is attributed to the co-ordination of the sulphur to the metal in addition to nitrogen.

In addition to the above compounds, another series of compounds with N-H group in the molecule is 2-mercapto-benzothiazole and its related compounds. In the formation of complexes with copper, the N-H was similarly eliminated. This will be discussed later in Chapter 7.

Comparison of Cu-BTA complex I.R. spectrum with the reflectance spectrum of the surface film shows that these two spectra are very similar. The similarity between the two spectra has been previously reported (51). Minor differences might be due to different techniques used to obtain these spectra. This strongly suggests that the BTA surface film has the same chemical nature as the Cu-BTA complex prepared chemically. This might be taken as evidence for a precipitation mechanism for formation of the surface film.

6.1.4 Structure of Cu(I)-BTA complexes

The chemical structures of Cu(I)-BTA complexes both on the surface and prepared from the solution, are

of importance, because they enable one to compare the surface film and solution prepared complexes, which may help to elucidate the mechanism of film formation. Although it is possible with some accuracy to measure the stoichiometric ratio of the complexes prepared from the solution by standard chemical analysis techniques, this is not true for the surface film. ESCA can offer a unique way to investigate the stoichiometry of the surface films and analogous chemically prepared complexes (see Chapter 4 for details).

Previous chemical analyses of solution prepared Cu(I)-BTA precipitates by Cotton (39) and by Poling (51) support a stoichiometric ratio of one copper atom to one BTA molecule. Table (6.1) shows both sets of results.

		C%	H%	N%	Cu%	Cl%
Poling	calc.	39.7	2.2	23.1	35.0	-
	found	37.6	2.7	20.8	32.1	7.7
Cotton	calc.	39.67	2.22	23.13	34.98	-
	found	39.67	2.37	22.49	33.71	-

Table (6.1) Chemical Analysis of Cu(I)-BTA Complex (Cotton (39) and Poling (51))

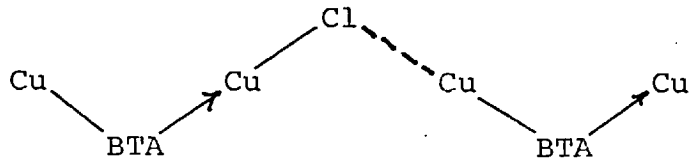
However, Poling (51) noticed the existence of chlorine in the precipitate despite several washes in distilled water. The proposed structure for both Cu(I) and Cu(II) complexes by Cotton (39) is shown in Chapter 5.

In the course of the present study it was found that there are two types of Cu(I)-BTA complexes, depending upon the methods of preparation. The complexes obtained in the absence or only small quantities of chloride ions, have a stoichiometric ratio of one Cu to one BTA, determined using standard chemical analysis techniques (see Appendix A.)

These results are similar to those of Cotton (39) and Poling (51), as discussed above. Results from ESCA analysis of peak intensities of these complexes supports this stoichiometry, [illegible], using Wagner (34) and Jørgensen (35) relative intensity factors.

However, in higher concentrations of chloride ions, i.e. in NaCl containing solutions, ESCA analysis of the complexes showed that the ratio of Cu to BTA is 2, and for each two atoms of copper there is only one chlorine atom. Therefore, the stoichiometry of this complex appears to be Cu_2Cl BTA. Chemical analysis of this complex supported this ratio. Results of the chemical analysis for Cu, C, N and H, are given in Table (6.2) and the analytical details in Appendix A.

Based on this information, the following structure for this complex is proposed:-



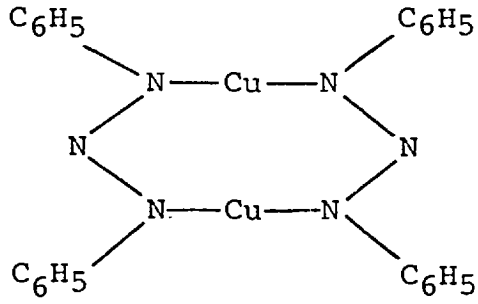
In this structure, copper is in cuprous state, having the co-ordination number 2. The atoms of copper, are bridged together by BTA molecules and chlorine.

Co-ordination number 2 in Cu(I) compounds is found frequently, for example cuprous azide occurs with a zig-zag polymeric chain in which Cu is in co-ordination number 2 (82). The planar, dimeric diazo aminobenzene-copper (I), is another example in which copper is in co-ordination number 2 and two diazo aminobenzene groups are held together by linearly co-ordinated copper atoms to form an eight member ring (83):-

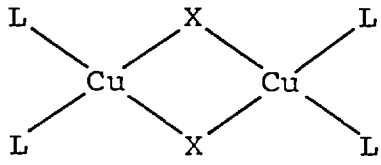
Element	Sensitivity Peak Height (Wagner)	Sensitivity Peak Area (Wagner)	Peak Heights (found) mm	Peak Area (found) corresponding wt.mg.	Ratio (2 atom) Cu	Chemical Analysis[c] (Calculated) %	Chemical Analysis (found) %
C	0.27 (0.27)[a]	0.24	9.3 16	166.6	7.7 (7.9)[b]	25.5	25.0
N	0.42 (0.4)[a]	0.41	11 32	199.2	3.03 (2.7)[b]	14.8	11.6
H	-	-	-	-		1.7	1.6
Cu(I)	- (3)[a]	3[d]	13 8	26.1	2 (2)[b]	45.3	43.8
Cl	0.55 (0.42)[a]	0.46	9.4 64	200.3	0.988 (1.2)[b]	12.6	-

Table 6.2: ESCA and Chemical Analysis for Cu(I)-BTA complex.

(a) Values are given by Jørgensen (35)
(b) Values are calculated for peak areas.
(c) calculated based on Cu_2Cl_2BTA
(d) Sensitivity factor for Cu has not been determined by Wagner. The value given by Jørgenssen was used to calculate atom ratios.



Linear 2-co-ordination is also found in Cu_2O and KCuO (84). Many of the compounds having a combination L Cu X, where L = ligand, X = halogen, might be expected to contain 2-co-ordinate copper, according to Bailer et al (82). Also when halogen is present, halogen bridging can occur in Cu(I), complexes (85), for instance:-

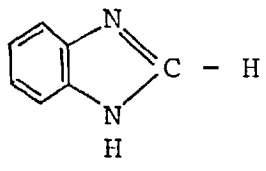


ESCA examination of the Cu(I)-BTA surface films which were prepared "infinitely thick" to make sure there are no contributions to the signal intensities from copper substrate, revealed that the stoichiometry of the films are identical to that of their analogous precipitates prepared under similar conditions, Table 6.2 . In the surface complexes two different complexes due to presence or absence of Cl^- were identified. Surface complexes were found to be identical to those prepared chemically in every respect; stoichiometry and binding energies. Thus, taking into account the previous results obtained from the oxidation behaviour of the surface complexes and precipitates and also their similar infra-red spectra, it can safely be concluded that the surface film is indeed a Cu(I)-BTA complex identical to Cu(I)-BTA prepared chemically. This suggests a dissolution and re-precipitation mechanism

which will be discussed later in more detail.

6.1.4.a Electron spectra of N 1s in BTA and in Cu(I)-BTA complexes

Because of the instability of BTA at spectrometer conditions of pressure and temperature (10^{-9} Torr and room temperature), it is not possible to obtain reliable BTA electron spectra. This is because at pressure less than 10^{-5} Torr and room temperature BTA sublimes almost instantaneously. However, at a low temperature (say -150°C), it is possible to prevent BTA from evaporation (sublimation) and hence to obtain its ESCA spectrum. The electron spectrum of N 1s of BTA obtained at less than -150°C (for experimental detail see Appendix A), showed a broad peak at a binding energy of 398.3 eV, in contrast with the previously reported binding energy of 400.2 eV. A comparison of binding energies given in Table (4.7) by Siegbahn et al (14) with BTA, shows the 400.2 eV binding energy for N 1s in this molecule is probably incorrect. Calculation of the charge on the N-H group of BTA using Pauling electronegativity values (see Tables (4.1) and (4.2)) showed an approximate value of -0.24 which corresponds to a binding energy of less than 398.0 eV (see Chapter 4). A closely related compound to BTA, namely benzimidazole with the following structure



, was investigated by ESCA, for the purpose of comparison. This compound was found to be resonably stable at low pressures. The N 1s binding energy of the benzimidazole was determined to be 397.8 eV. The fact that in the previous study (36), the problem of evaporation associated with obtaining the BTA electron spectrum has not been mentioned,

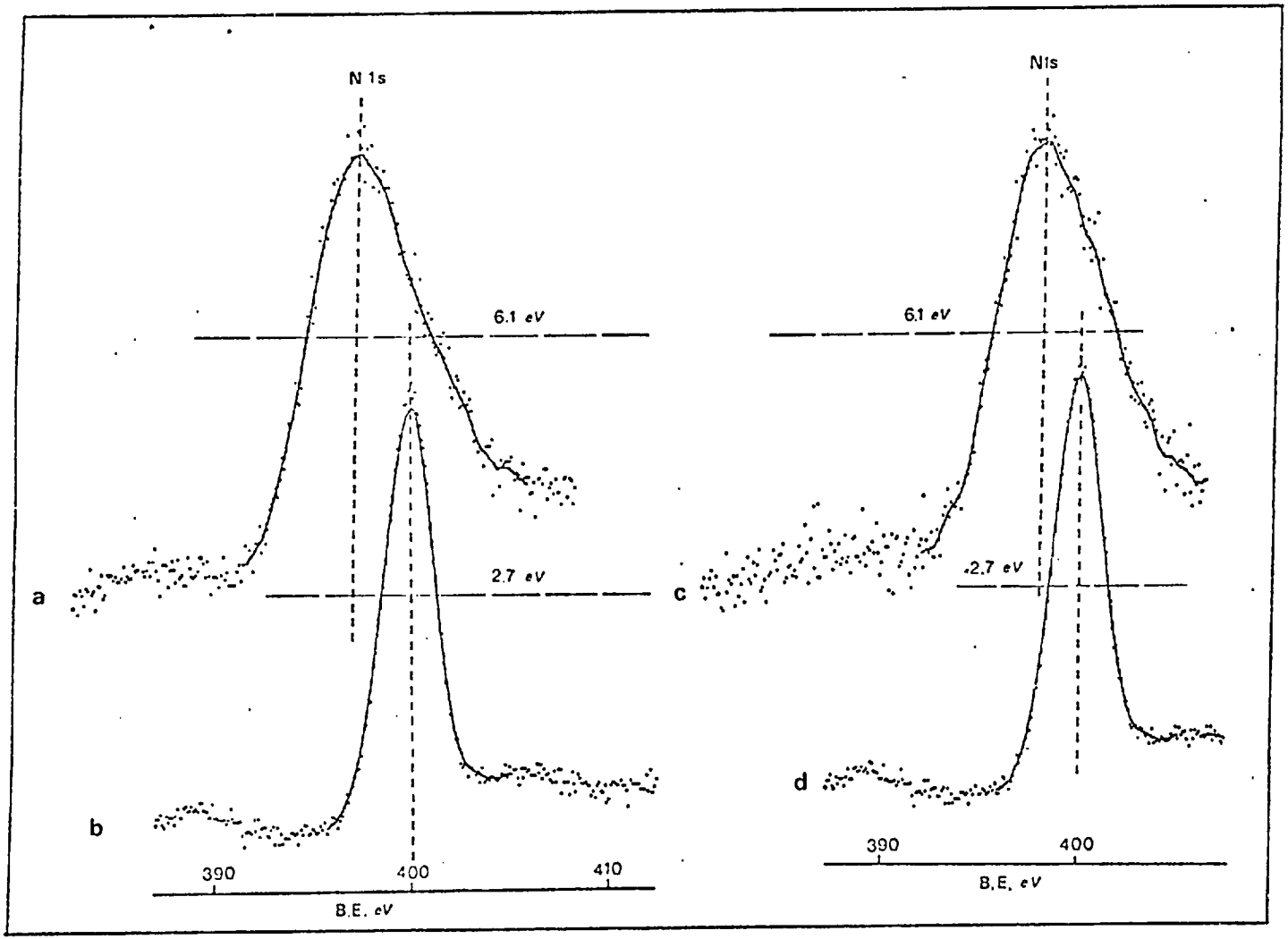
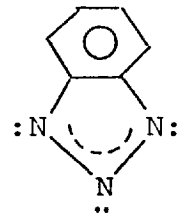


Fig. 6.10: XPS spectra of N 1s in (a) BTA; (b) Cu(I)-BTA, (c) benzimidazole, (d) Cu(I)-benzimidazole

suggests that the N 1s peak observed by Roberts (36) may be due to impurities or arise from the double-sided adhesive tape which had been used to mount the samples.

In the complex with copper (both surface and solution prepared complexes), changes take place in both binding energies and the shape of the N 1s peaks for both BTA and benzimidazole. The binding energies of the N 1s in copper complexes of BTA and benzimidazole were found to be 399.9 eV and 399.4 eV respectively, and in both cases the peaks are significantly narrower, from about 6.1 eV FWHM in BTA and benzimidazole compared to 2.7 eV in the complexes. Figure (6.10a) shows N 1s XPS spectrum in BTA and Figure (6.10b) the N 1s peak in Cu(I)-BTA complex. Figure (6.10c) and (6.10d) show N 1s peaks in benzimidazole and its copper complex respectively. No change was observed due to different ways of complex preparation for example presence or absence of the Cl^-.

The small value of FWHM for the N 1s peak in the complexes shows that the charge is distributed evenly on the three nitrogen atoms. Looking at the structure of the Cu(I)-BTA complex proposed by Cotton (39) and Poling (51), in which two copper atoms are bonded to nitrogen 1 and 3 of BTA molecule (Chapter 5), the charge differences are smeared out by delocalization. The narrowness of the N 1s peak in the complex is consistent with this interpretation. In fact, when BTA dissolves in water, some molecules lose a proton, becoming a BTA^-, leading to the following structure:



In this structure, charge is distributed over the three nitrogen atoms and because of the delocalization the molecular anion is more stable. Copper ions in solution now can form a chemical bond with BTA^{θ}. The same argument is also valid in the case of benzimidazole.

The formation of BTA^{θ}, however, is not the only possible route for BTA to co-ordinate with copper ions in solution. Another possibility is the hydrated cuprous ion reacts directly with BTA according to:

$$H_2O - \overset{\overset{H_2O}{|}}{\underset{\underset{H_2O}{|}}{Cu}} - H_2O + BTA \rightleftharpoons H_2O - \overset{\overset{BTA}{|}}{\underset{\underset{H_2O}{|}}{Cu}} - H_2O + H_3O^{+}$$

The nitrogen atoms serving as the electron donor atoms in a great variety of ligands has been reported (14). Some of which are:

$$:NH_3, \quad :N \equiv C - S^{-}, \quad N:, \quad \text{etc.}$$

6.1.4.b Oxygen 1s electron spectra

The oxygen 1s peak in the XPS spectrum of the Cu(I)-BTA surface film is always present in films prepared in standard solutions. Since at pH = 3 this peak could be due to oxygen or water adsorbed onto the surface, and not associated with the complexed molecule, attempts were made to remove thin layers from the top of the surface film to examine the inner layers. Argon ion bombardment of the surface for a short time (e.g. 30 sec.), using the lowest possible energy (e.g. 1 kv and 6 μA), resulted in the removal of a thin layer. This reduced the C, N and O 1s peak at a similar rate, within experimental accuracy. However, for untreated polished copper samples, argon ion

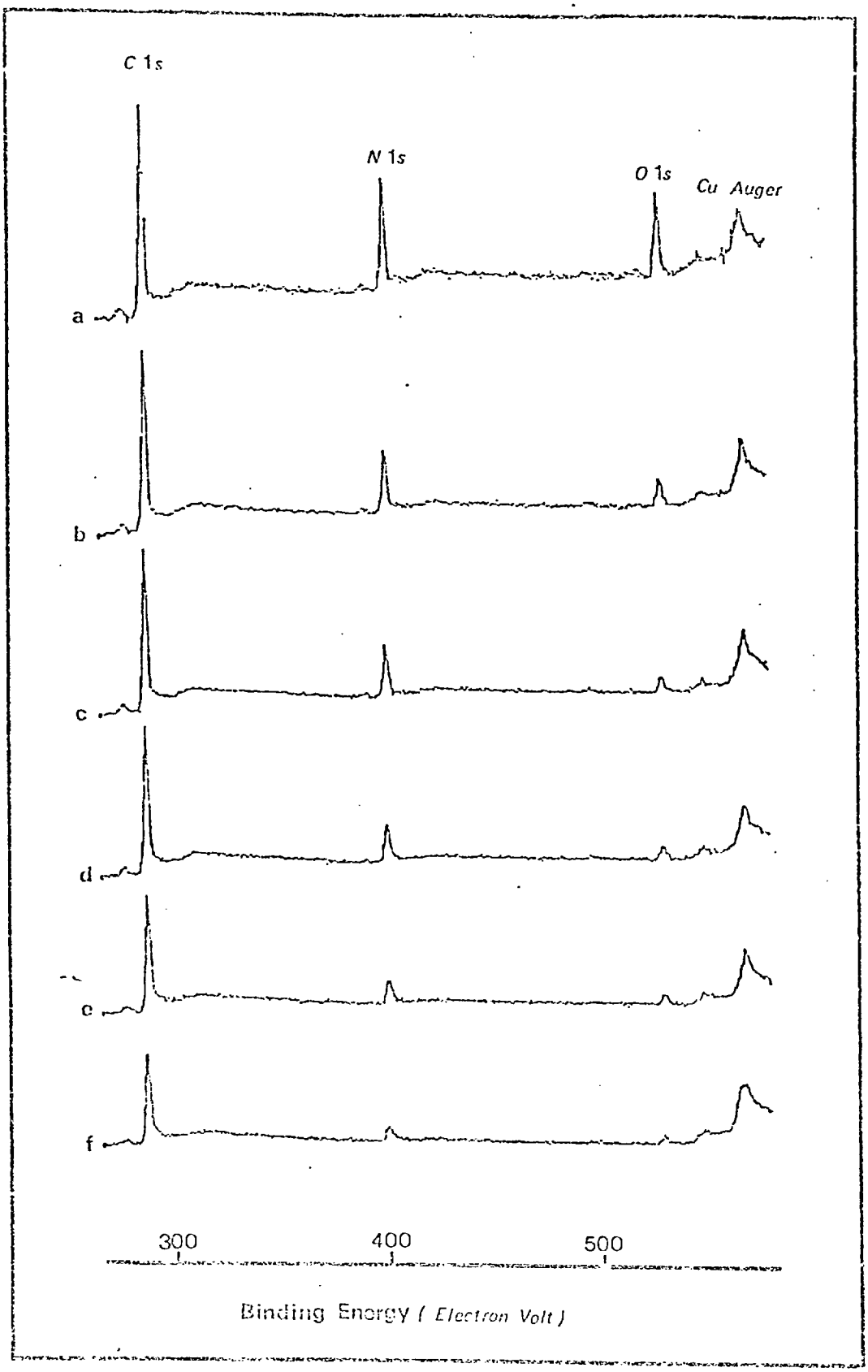


Fig. 6.11: XPS spectra of a Cu sample covered with Cu-BTA complex, (a). This sample after being argon ion etched for (b) 30 secs., (c) 1 min; (d) 1.5 min. (e) 2 min, (f) 3 min.

spluttering reduced the O 1s peak to a negligible intensity in a comparatively short time. Figures (6.11a-f) show the XPS spectra of a copper specimen covered with complex film, (6.11a), and after removing thin films from the surface (6.11b-e). The reproducibility of these results argues against patchy absorption as a possible explanation for the persistance of the O 1s peak in the spectra of BTA treated samples. The observation of O 1s peak in this series, can be taken as an indication that oxygen or more probably H_2O is in fact involved in the surface film throughout its depth.

6.1.4.c Chlorine and bromine electron spectra

Formation of Cu-BTA complexes in the presence of bromide ions instead of Cl^-, showed that bromine behaves in an identical manner to chlorine. Examination of both surface films and the complex prepared from the solution showed that these two are identical and they are also similar to those formed in the presence of Cl^-, having stoichiometric formula of Cu_2Br BTA. Because of the sharp and intense nature of bromine XPS spectrum, it is easy to determine the binding energy of bromine with great accuracy even in small quantities. This is not the case for chlorine because of the small separation between Cl $2p_{3/2}$ and Cl $2p_{1/2}$, and it is not possible to determine the binding energy of Cl^- in the complex with great accuracy. Binding energy measurement of Br 3d in Cu Br and in the complex showed however that there is a slight shift of about 0.7 eV towards lower binding energy in the BTA complexes. This is also the case for Cl $2p_{3/2}$. The binding energies of Cl $2p_{3/2}$ and Br 3d in the complexes and the surface film before and after atmospheric oxidation did not show a significant change. Binding energies are listed in Appendix B.

6.1.5 Depth profile of the surface films

The relationship between the structure of the Cu-BTA films, Cu_2O, and the metallic copper substrate is of importance because it helps to elucidate the mechanism of film formation and corrosion inhibition. T. Nateya and G.W. Poling (54) studied the topography of complex films and the relationship with the Cu_2O interlayer. Ogle and Poling (53) showed the stability of Cu_2O in solution depends upon the pH. They have shown that at pH > 4, Cu_2O is stable and virtually no dissolution takes place. On the contrary, at pH < 3, the Cu_2O dissolution is almost instantaneous and complete. In a 4 > pH > 3, however, it is possible to observe a partial dissolution. That is to say, if the original Cu_2O film is thick enough at a pH between 3-4, some Cu_2O may dissolve and leave a copper surface which is still covered with Cu_2O (see Chapter 5 for details). In the BTA treatment of samples covered with Cu_2O at different pH, it was shown (53) that an interlayer Cu_2O is retained only when the pH of the solution is greater than 3. The results obtained in the present study using different techniques are consistent with previous results.

Argon ion bombardment was used to investigate the depth profile of the surface films, and in particular examine the underlayers. Very low beam energy and low etching rates were used for argon ion bombardment and the X-AES spectra of the sample in the Cu LMM region were obtained at frequent intervals throughout the etching process. The samples were covered originally with thick Cu_2O films, grown electrochemically. In one set, samples were treated with standard solution of BTA at pH ~ 3 for a long period of time (say 10 hours) and in another set samples were

treated in a similar solution, but at pH ~ 7. Samples treated with solution at pH ~ 7, despite prolonged exposure to the solution (e.g. 48 hours), were found to be covered with a very thin film of Cu BTA, which immediately disappeared after argon ion bombardment for 30 seconds at lowest rate, leaving a Cu_2O underlayer. Further bombardment of the surface, gradually resulted in the disappearance of the underlayer Cu_2O, with the appearance of metallic copper. Figure (6.12a) shows an X-AES spectrum of Cu_2O sample in Cu LMM region. Treatment of this sample with BTA, results in formation of a thin film which is evidenced by slight broadening to lower kinetic energy, Figure (6.12b). In addition, the presence of a Cu-BTA film was established by the XPS spectra of C 1s and N 1s. Argon ion bombardment of this sample for 30 seconds at 1.5 kv and 6 μA results in the disappearance of this Cu-BTA film, which is evidenced by slight shift in Cu X-AES spectrum to higher kinetic energy, the kinetic energy corresponds to untreated Cu_2O. It is clear from Figure (6.12c) that all the Cu-BTA film has been removed leaving Cu_2O. This is also supported by the disappearance of the N 1s signal and decreased intensity of C 1s peak, and an increase in O 1s peak intensity in the XPS spectrum. Further bombardment for another 3 minutes results in the appearance of Cu metallic peak, Figure (6.12d) and after 3 more minutes, almost all the Cu_2O signal has disappeared, Figure (6.12e). XPS spectrum of O 1s showed that there is hardly any oxygen left on the surface.

Samples treated with a standard BTA solution at pH ~ 3 exhibited completely different behaviour. Argon ion bombardment of these samples showed that there are no

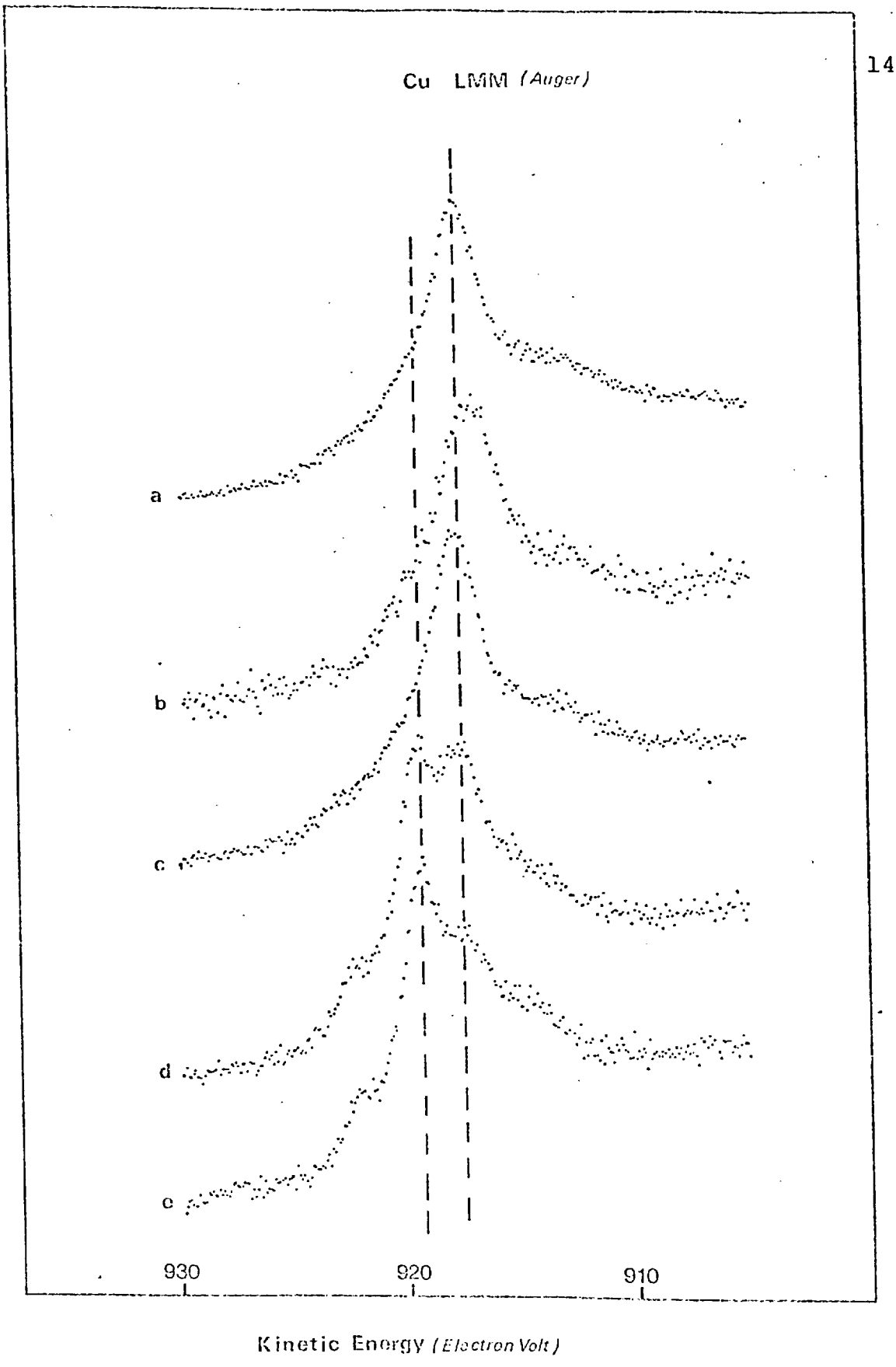


Fig. 6.12: X-AES spectra of (a) Cu_2O sample ; (b) This sample exposed to BTA solution at pH = 7; (c) above sample being etched for 30 sec; (d) further bombardment for 3 min.; (e) further bombardment for 3 min.

intermediate layers of Cu_2O and that the thick surface films were Cu(I)-BTA. Figure (6.13a) shows X-AES spectra of a copper sample covered with a thick Cu(I)-BTA film and Figure (6.13b) shows the result of argon ion bombardment of this sample for 1 minute at the previous rate. The spectra are virtually identical, though there may be a slight shoulder due to a metallic Cu signal. 3 minutes more bombardment results in appearance of an intense metallic Cu peak while still there exists some Cu(I)-BTA. Figure (6.13c). No Cu_2O intermediate layer appears to be retained during BTA treatment under these conditions Argon ion etching of the surface for longer times eventually results in Figure (6.13d) which may be compared to X-AES spectrum of a clean Cu surface. Figure (6.2) and also XPS spectrum of sample showed no N 1s and O 1s peak. It could be argued that argon ion bombardment might damage the film, giving misleading results. However, X-AES spectra obtained earlier by wiping off part of the surface film showed no evidence for the presence of Cu_2O (see Figure (6.6)). It can be concluded that at pH < 3 there is no Cu_2O underlayer and the thick surface films produced under these conditions are entirely Cu(I)-BTA. The presence of an O 1s peak in XPS spectrum of films prepared in this fashion as discussed in 6.1.4.b might be due to the existance of H_2O in the surface film.

These results are consistent with those of Ogle and Poling (53), for pH > 4 and pH < 3. Between pH 3-4 the situation is more complex and will be discussed later in the context of the mechanism of film formation.

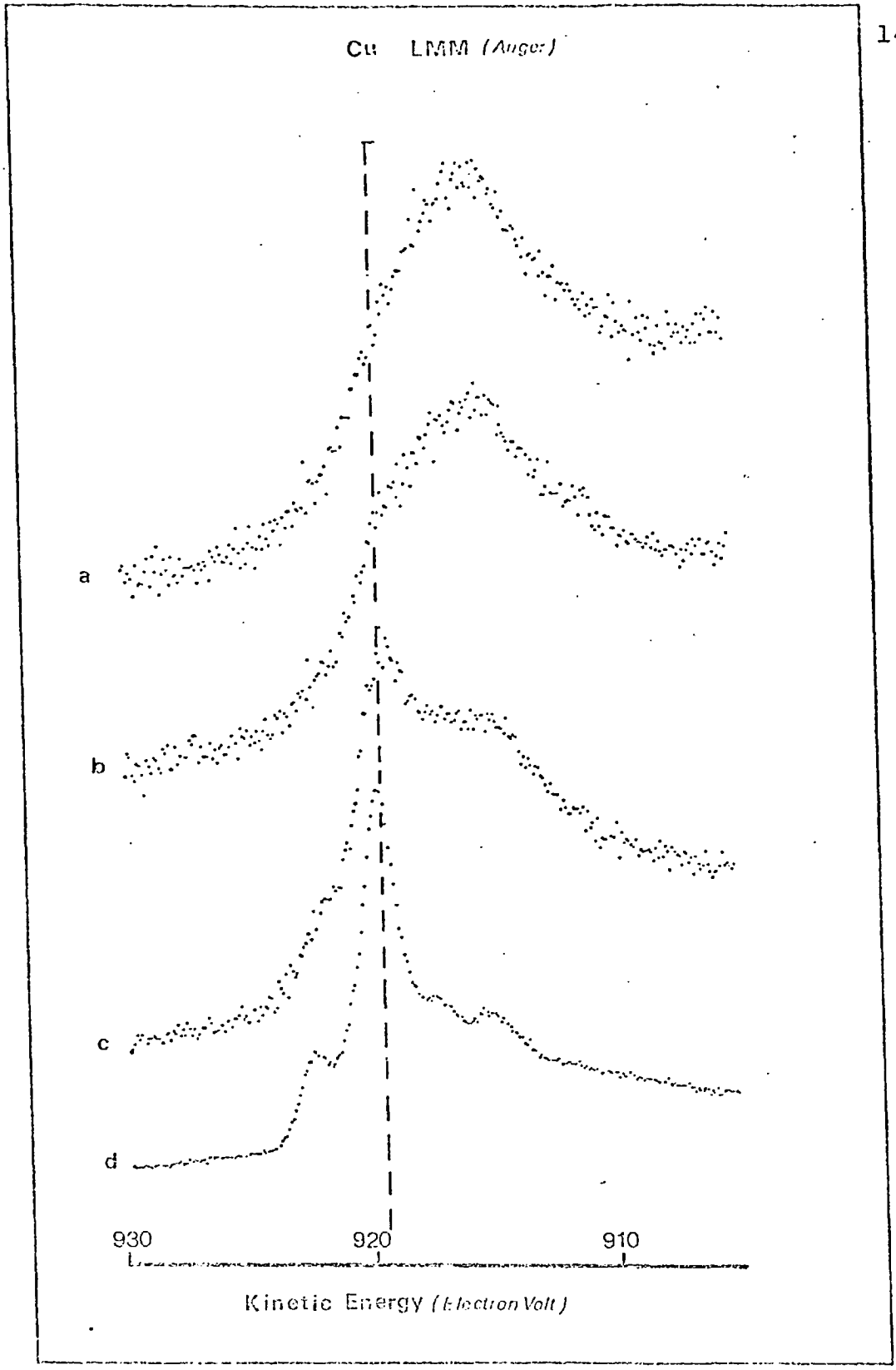


Fig. 6.13: X-AES spectra of a Cu sample being treated with BTA at pH ≃ 3 (a); (b) argon etching of the above sample for 1 min.; (c) argon ion etching for 3 min,;(d) argon ion etching for 5 min.

6.2 Mechanism of Cu-BTA Film Formation

During more than ten years extensive study of the Cu-BTA system, many data from different aspects have been reported by several authors, but the mechansim of film formation is far from being clarified. As discussed earlier in Chapter 5, Cotton (39), Poling (51) and Mansfield and Smith (52) have proposed mechanisms by which certain aspects of film formation are explained. However, to date, no model has been proposed which can explain satisfactorily the entire set of observations. The reasons for this are the wide range of conditions and the limited applicability associated with different techniques, such as infra-red spectroscopy and ellipsometry. This has produced results which cannot be directly compared. ESCA with its potential for surface analysis seemed initially to suffer similar limitations. That is to say, at an early stage of using the ESCA technique for this problem, the only way to establish the presence of a Cu-BTA surface film, was the observation of peaks from the N 1s and C 1s of the inhibitor. These are the criteria which have been used by Roberts (36) to prove the existence of the Cu-BTA film, and also by the author at the early stages of the present work. This is certainly is a limitation of the XPS methods, and because of it the technique cannot go beyond determining the oxidation states of elements in the complexes, and the stoichiometric ratios of the elements in the film. The evidence for formation of the surface Cu-BTA complex is indirect. However, during the course of this study, it was found that X-ray induced Auger spectroscopy can provide valuable information about the film formation in different

environments, because it can distinguish the Cu-BTA complex itself. The X-AES method enables one to differentiate an extremely thin, say a few Å, Cu-BTA film from the substrate. The combination of X-AES and XPS as discussed earlier (section 6.1), has been found to be a most powerful method for the study of the Cu-BTA system, and other related systems.

In this section the results of an investigation of film formation, its thickness, and the effect of different conditions of the treatment solutions and surfaces are presented. Among the various variables in the film formation process, such as acidity of the solution, the BTA concentration, the temperature of the solution, and so on, the most important factors were found to be the pH of the treatment solution, the concentration of chloride ions in the solution, and the original cuprous oxide surface film. This section then, is divided into three parts which consider the effect of pH, Cl^- and Cu_2O on film formation and its thickness in the first two parts and in the last part, a model based on these facts is proposed.

6.2.1 The role of Cu_2O in film formation

Copper oxides are shown to be important in Cu-BTA film formation (52, 53). The ellipsometric results of Mansfield and Smith (52) discussed in Chapter 5 suggest that the presence of copper oxide is essential for film formation. Although aspects of their experimental work on oxide-free surfaces was not quite satisfactory, the implication that the presence of Cu_2O is important is clear. Roberts (36) has shown that reaction with a Cu_2O surface is much faster than adsorption onto CuO, and

Ogle and Poling (53) made an extensive study of Cu_2O behaviour in different pH solutions with and without BTA. Some aspects of this work were discussed previously. The relationship determined by Ogle and Poling (53) between the Cu_2O thickness, the pH of the treatment solution, the exposure time, and the thickness of resultant Cu-BTA film is given in Table (6.3) and Table (6.4).

pH	Immersion time (min.)	Cu_2O Thickness (Å) Initial	Final
3.00	2	282	92
3.00	10	318	75
5.35	300	177	326

Table (6.4) Stability of Cu_2O in Different pH (53)

pH	Cu_2O Thickness (Å) Initial	Final	Cu-BTA Thickness (Å)
3.51	25	8	189
3.51	90	58	47
2.99	56	not detected	1320

Table (6.5) Effect of Cu_2O Films on Cu-BTA Formation (53)

This data shows that the thickness of the Cu-BTA films are related to the thickness of Cu_2O which has either dissolved or disproportionated, although this fact does not seem to have been recognized by Ogle and Poling (53). Furthermore, the most important single factor in determining the amount of oxide dissolved, is the pH of the solution. The question still remains, however, as to how the copper oxide is involved in complex formation, i.e. the mechanism of its involvement and the role played by the oxide substrate in complex film thickness.

In an attempt to assess the role of the surface oxide in film formation and in influencing the final film thickness, film formation on an oxide-free surface was studied at early stages of the present study, using I.R. reflectance spectroscopy. For details of experimental see Chapter 3 and Appendix A . The polished copper mirrors prepared for this experiment were etched mildly in a diluted HNO_3 solution for a short time (e.g. 20 seconds), and then were polarized in a pure NaCl electrolyte at -0.90 V vs. S.C.E. using a potentiostat, under a nitrogen atmosphere. After some time at that potential to make sure all surface oxides were reduced to copper metal, a solution containing the inhibitor was subsequently injected from a side arm while allowing the sample potential to vary freely. Figure (6.14a) shows an infra-red reflectance spectrum obtained from a sample after cathodic reduction of the oxide followed by inhibitor injection and exposure to the same solution for ½ hour. Comparison with Figure (6.9d) indicates that no trace of Cu-BTA complex is evident in this spectrum. Interestingly, the same sample after running the I.R. spectrum, was left exposed to air for some time and then placed in the same BTA solution for a short period of time (say ½ hour). Examination of the infra-red reflectance spectrum, Figure (6.14b), showed that the sample surface was now covered with a relatively thick Cu-BTA complex, indicating the importance of Cu_2O in Cu-BTA film formation.

The validity of these results was examined later using XPS and X-AES method and will be discussed below. It is clear now, that although BTA does form a complex on the oxide-free copper surfaces, the film

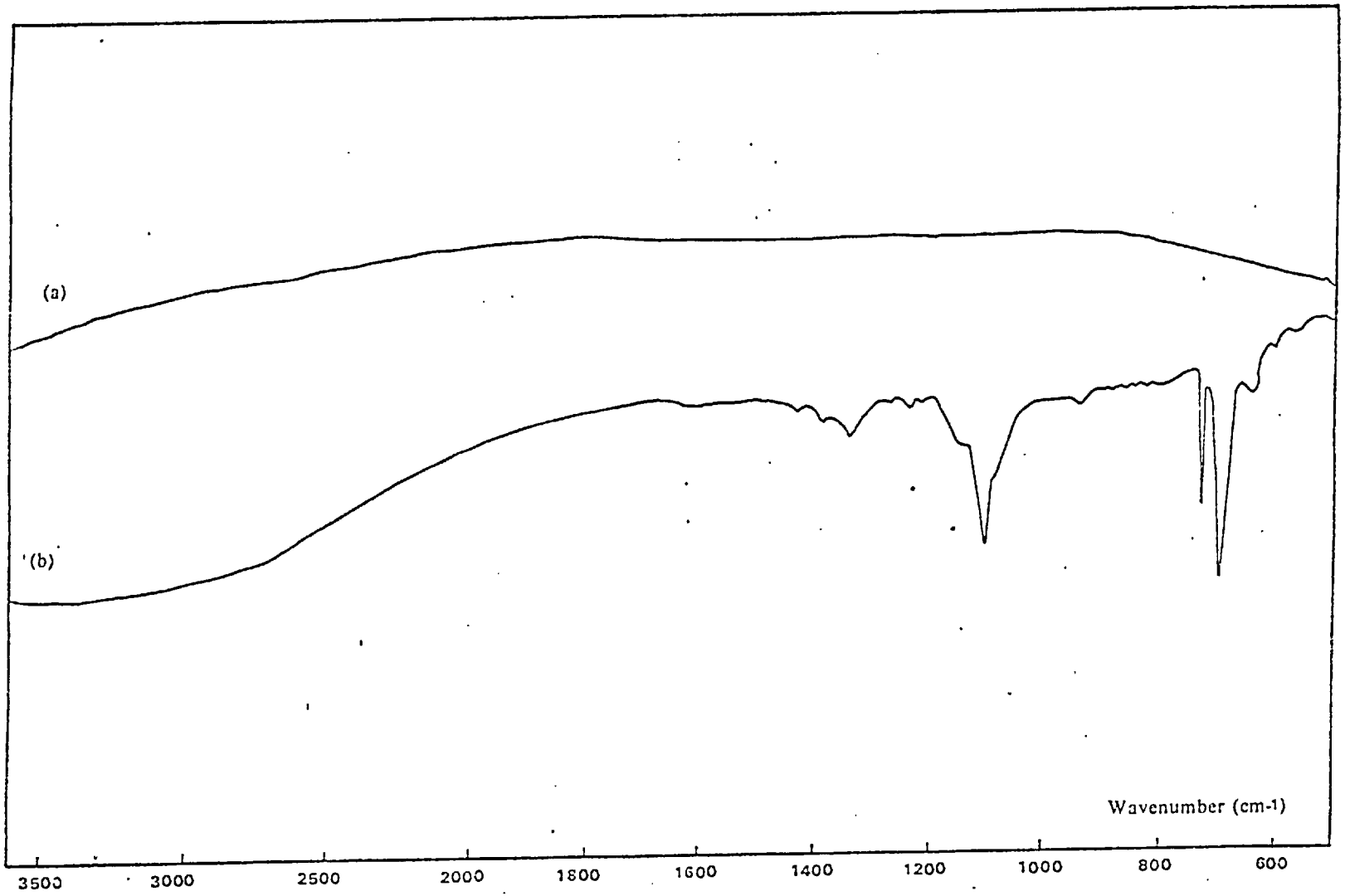


Fig. 6.14: Infrared reflectance spectra of a copper sample (a) cathodically reduced followed by injection of BTA and exposed to this solution for ½ hour; (b) the same sample exposed to above solution after being exposed to air.

thickness stays extremely low. Therefore, although the inability to detect the Cu-BTA surface complex after a cathodic reduction is probably due to the lack of sensitivity in the I.R. technique, the general picture is still valid.

Having established that Cu_2O is important in film formation and in determining film thickness, a detailed study seemed necessary to elucidate the mechanism of film formation.

a) Behaviour of Cu_2O samples in inhibitor-free solutions

When a Cu_2O sample is immersed in an aqueous solution free from the inhibitor, the following reaction greatly depends upon the pH of the solution. This is demonstrated by Equation (6.1) (86).

$$Cu_2O + 2H^+ \rightleftharpoons 2Cu^+ + H_2O;\ \log (Cu^+) = -0.84 - pH \qquad (6.1)$$

The conditions governing the stability of Cu^+ salts are defined by the alternative electrode processes (6.2) and (6.3).

$$Cu \rightleftharpoons Cu^+ + e \qquad (6.2)$$

$$Cu \rightleftharpoons Cu^{++} + e \qquad (6.3)$$

At equilibrium, in the presence of metallic copper, $\frac{(Cu^{2+})}{(Cu^+)^2} = K$, at 20°C, K has the magnitude 1×10^6. Hence copper will dissolve in a solution of a Cu^{2+} salt until enough Cu^+ ion has been formed to establish equilibrium in the system. Conversely, Cu^+ ions, would undergo disproportionation, according to Equation (6.4), until equilibrium was reached.

$$2Cu^+ \rightleftharpoons Cu^{2+} + Cu \qquad (6.4)$$

The numerical magnitude of K implies that appreciable concentrations of Cu^+ ions cannot exist in a solution at all, and the known copper (I) compounds are limited to those

which are extremely insoluble (the oxide, sulfide and halides), so that the Cu^+ ion concentration in equilibrium with the solid cannot rise to a value involving appreciable disproportionation and the Cu^+ ion concentration is held at a low figure. Other Cu(I) salt such as Cu_2SO_4 are unstable.

From Equation (6.1), the concentration of Cu^+ ion at different pH can be calculated. For example, at pH = 7 (Cu^+) is equal to $10^{-7.84}$ M. The amount of the disproportionation can be determined by $\frac{(Cu^{2+})}{(Cu^+)^2} = 10^6$, so $(Cu^{2+}) = 10^{-9.68}$ M, which is smaller than (Cu^+) by a factor of almost 100. Let us compare this value for the one which is calculated at pH = 3. At pH = 3, (Cu^+) was calculated according to Equation (6.1) to be $10^{-3.84}$ M, and (Cu^{2+}) has a value of $10^{-1.68}$ M, more than 100 times greater than the value of (Cu^+). It is quite clear that at pH = 7, an extremely small amount of Cu^+ dissolves and contribution of the disproportionation reaction is almost negligible. In contrast, at pH = 3, disproportionation reaction becomes exceedingly important by which Cu^+ ions can disproportionate by a magnitude of $2 \times 10^{-1.68}$ M. This figure shows, for samples with surface areas of a few cm^2, thousands of Å of Cu_2O can disproportionate in 1 litre of acidic solution at pH = 3. Cu_2O disproportionates by dilute solution of acids (H_2SO_4, HF, etc.), to a Cu(II) salt and free metal (87);

$$Cu_2O + H_2SO_4 \rightleftharpoons CuSO_4 + H_2O + Cu \qquad (6.5)$$

In the present work, the presence of Cu^{2+} ions in H_2SO_4 solution was established by U.V. absorption spectroscopy of the solution. No Cu^{2+} ions could be detected when hydrochloric acid was used, or when Cl^- were present. The

reason lies in the fact that immediately after disproportionation according to (6.4), a second reaction occurs (Equation 6.6).

$$Cu^{2+}_{(aq)} + Cu_{(M)} + 2Cl^{-} \rightarrow 2CuCl_{(S)} \qquad (6.6)$$

CuCl is a colourless precipitate and has no absorption band in U.V. region.

Examination of the surface of a Cu_2O sample (grown electrochemically) treated with a solution of HCl at pH = 3, by ESCA revealed that after a few minutes treatment, the resultant surface becomes an oxide-free metallic surface. Figure (6.15a) shows an X-AES spectrum of a copper sample covered with thick Cu_2O. Figure (6.15b) shows the result of treatment of this sample for 30 seconds with a solution of HCl at pH = 3. It is clear from this spectrum that the thickness of Cu_2O film after 30 seconds, has been reduced to a few Å (within the escape depth of Auger electrons), evident from appearance of a metallic peak in the spectrum. Results of 5 minutes treatment of an identical sample is shown in Figure (6.15c). This spectrum represents an oxide-free metallic surface and very small amount of Cu_2O present is due to the atmospheric oxidation during transfer from the solution to the spectrometer prior to measurement.

At pH= 7, as calculated already, only an extremely small amount of Cu_2O dissolves as Cu^{+} ion in solution and disproportionation plays only a negligible role. So, introduction of a Cu_2O sample in an aqueous solution at pH = 7 does not result in complete dissolution of Cu_2O even after a long period of time and the Cu Auger spectrum remains unchanged. pH = 7 and pH = 3, represent two extremes

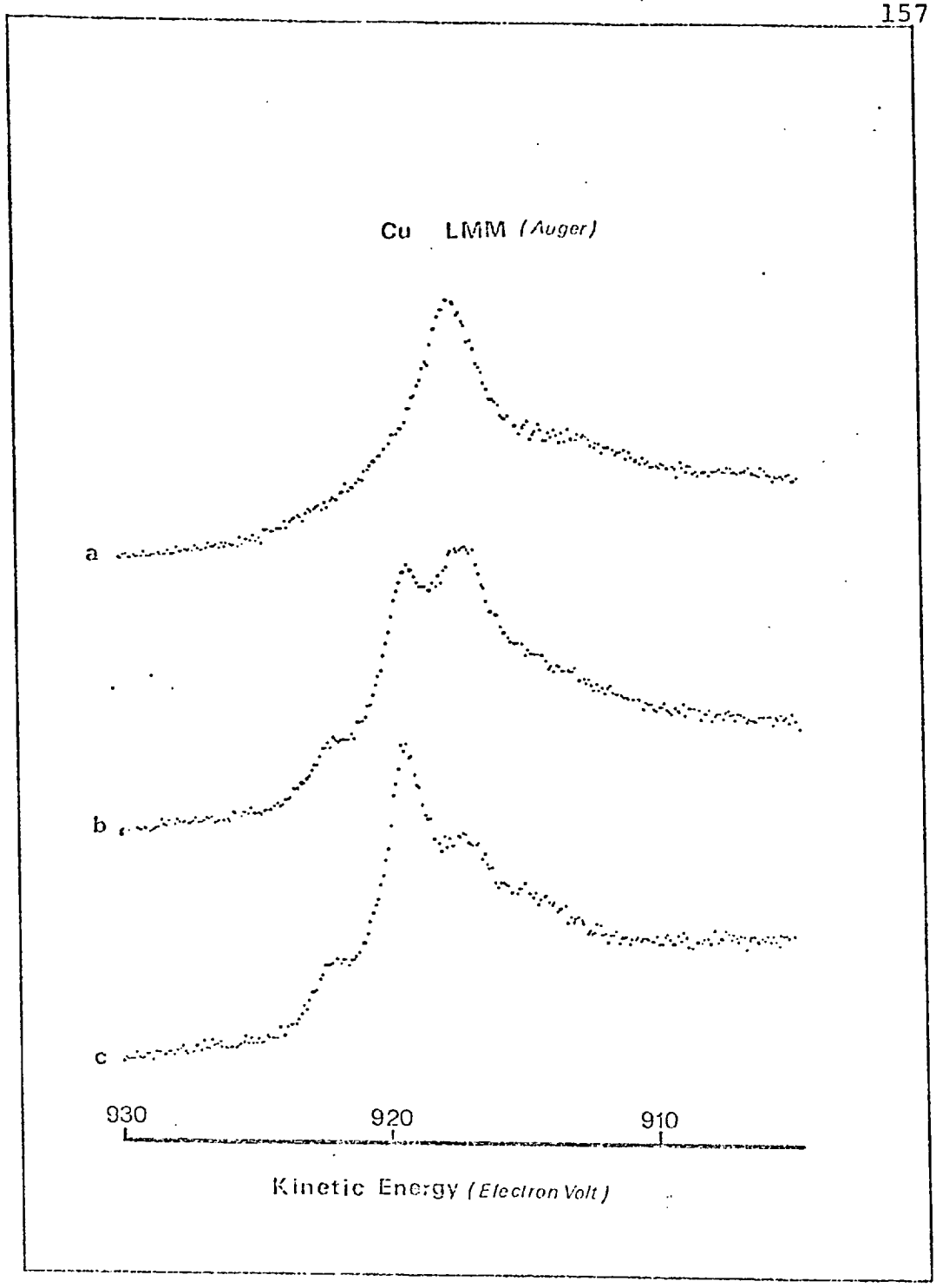


Fig. 6.15: X-AES spectra of : (a) a Cu_2O sample, (b) above sample exposed to HCl solution at pH=3 for 30 seconds; (c) treatment of similar sample with similar solution for 5 min.

in the present study. At pH = 7 virtually no dissolution takes place, so Cu_2O samples remain intact, in contrast at pH = 3 all Cu_2O dissolves (disproportionates) leaving a clean metallic copper. The situation between the two extremes is not difficult to visualise. At any pH, it is possible to calculate how many Cu_2O atoms enter the solution, and thus by knowing the Cu_2O original thickness, determine the resultant thickness of Cu_2O. Thus it follows that by chosing the correct pH, it is possible to remove some of the Cu_2O surface film, or all of it. This has been demonstrated experimentally by Ogle and Poling (53) (Table (6.3), see also section 6.1.5).

b) Cu-BTA films formed at pH ~ 7

Cu-BTA films formed on Cu_2O with different thicknesses were produced by exposure of the samples to a solution of BTA at pH ~ 7, 0.5M NaCl, 0.02M BTA at 25°C and N purging. Films on air-formed oxide layer, although formed readily, stayed low in thickness and did not change due to prolonged exposure to the treatment solution. Figure (6.16a) shows an X-AES spectrum of a copper polished sample which has been exposed to air for two hours. Figure (6.16b) shows the result of ½ hour treatment of this sample with BTA solution at pH ~ 7, and Figure (6.16c) shows the result of an identical sample treated with the above solution for 2 hours. In both Figure (6.16b) and (6.16c) film formation is evident from the broadening and the appearance of a shoulder on the lower kinetic energy side of the Cu_2O peak. Existance of a Cu-BTA complex was also confirmed by appearance of a N 1s peak and the enhancement of C 1s peak in XPS spectrum of the surface. In both Figure (6.16b) and (6.16c) peaks corresponding

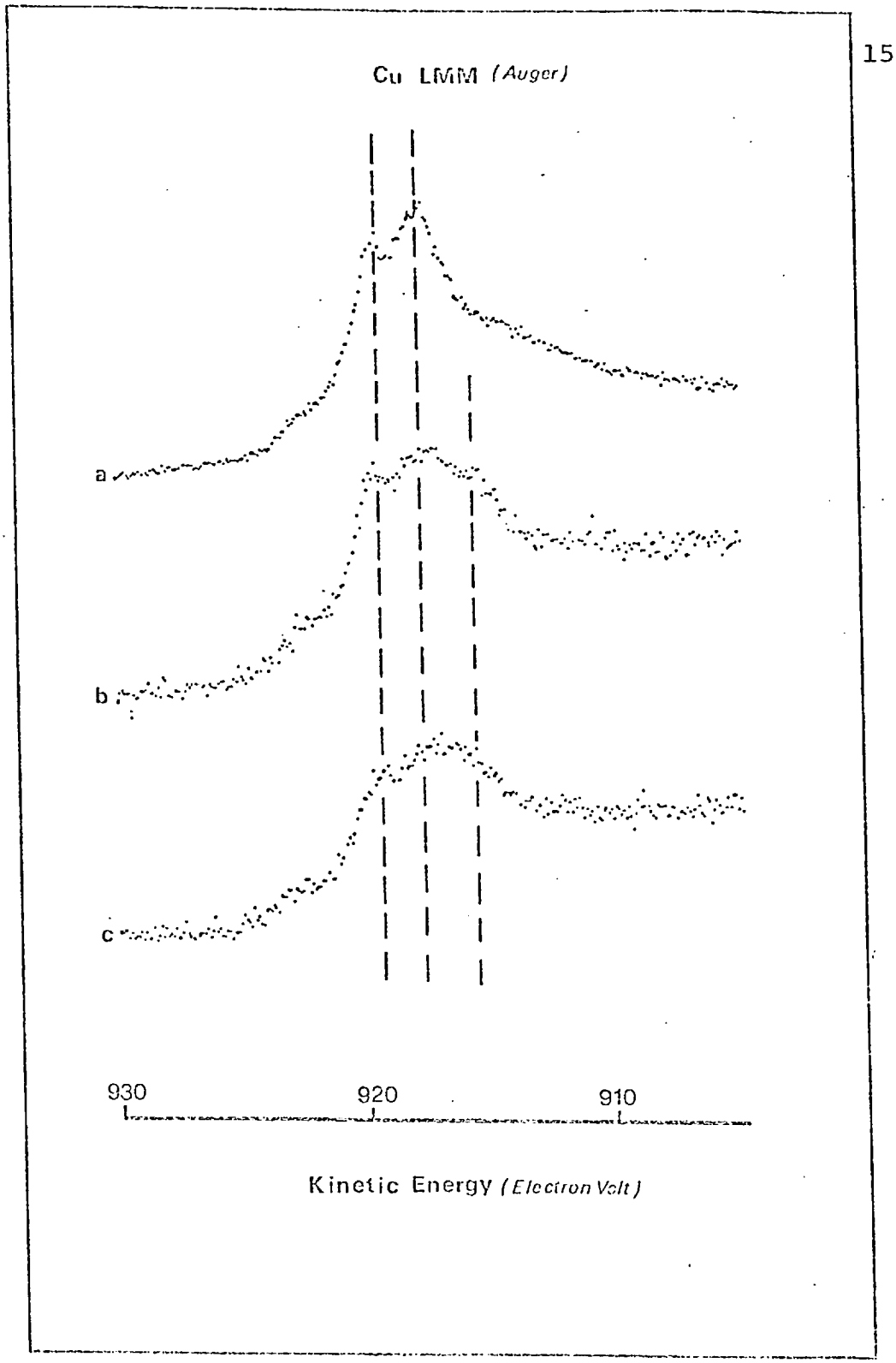


Fig. 6.16: X-AES spectra of a Cu polished sample: (a) exposed to air for 2 hours; (b) treated with BTA solution (pH≃7) for ½ hour; (c) a similar sample treated with similar solution for 2 hours.

to metallic Cu and Cu_2O are still present, indicating the Cu-BTA film is very thin.

Cu-BTA film formation on samples with thick Cu_2O (grown electrochemically) by treatment of these samples with a solution of BTA at pH = 7 (similar to above mentioned solution), was already discussed in (6.1.5) in determining depth profile of the surface films. Cu-BTA films formed in this way, stayed thin and no increase in the thickness was found due to prolong exposure to the solution (see Figure (6.12b)).

c) Cu-BTA films formed on Cu_2O samples at pH ~ 3

Results from X-AES and I.R. reflectance spectroscopy showed that for samples with electrochemically grown Cu_2O films, relatively thick Cu-BTA complex films are formed when the pH of the treatment solution is less than 3, provided chloride ion is present. The role of chloride ion will be discussed later. Figure (6.17a) shows a Cu LMM Auger spectrum of a sample with a thick Cu_2O film and is identical with earlier spectra. Figure (6.17b-d) show the X-AES spectra of these samples treated with standard BTA solution at pH < 3, for progressively longer periods of time, namely 30 seconds, 2 minutes and 20 minutes treatment respectively. The last spectrum in Figure (6.17d) shows that there are no peaks due to Cu at 919.7 eV k.e. or Cu_2O at 917.9 eV k.e., indicative of formation a relatively thick Cu-BTA film which its thickness is greater than Cu Auger electron escape depth. Results from I.R. reflectance spectroscopy of similar samples treated in the same way, supported these conclusions. It is clear that thick Cu-BTA complex films are formed in a relatively short period of exposure time.

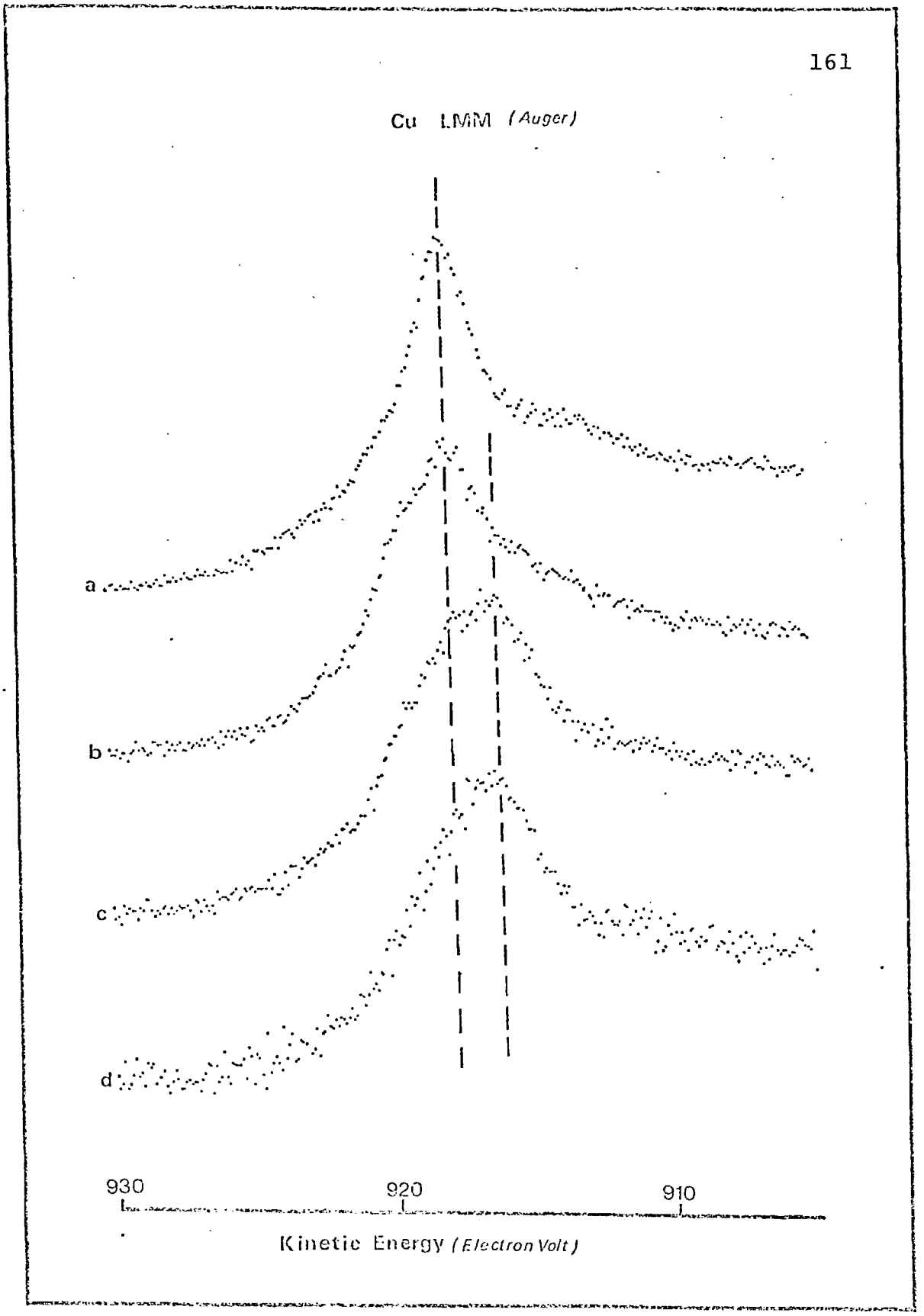


Figure 6.17: X-AES spectra of Cu_2O samples treated with BTA solution at pH≃3; (a) fresh Cu_2O sample; (b) treated for 30 sec.; (c) 2 min.; (d) 20 min.

An important fact from the point of view of film formation mechanism is that the rate of Cu_2O dissolution (disproportionation) is greater than the rate of Cu-BTA complex formation. A 30 seconds treatment with solution (Figure (6.17b)) results in the appearance of a shoulder at higher kinetic energy of the main Cu_2O peak, indicative of Cu metal (919.7 eV). Cu-BTA complex film formation then appears only after a couple of minutes (Figure (6.17c)).

Treatment of samples with air-formed oxide with BTA solution at pH = 3, resulted in the Cu-BTA film formation, but the film thickness stayed low (within escape depth of Auger electron). These results are consistent with the hypothesis that for relatively short exposure times of Cu_2O covered samples in a solution of BTA, the oxide original thickness determines the thickness of the resultant Cu-BTA complex film and not anodic dissolution of Cu metal.

d) Cu-BTA films formed on oxide-free surfaces

I.R. reflectance spectroscopy of oxide-free surfaces treated with BTA solution showed no Cu-BTA film formation (see section (6.2.1)). The XPS spectra of samples treated in a similar manner, however, revealed those peaks characteristics of BTA namely C 1s and N 1s, although substantially reduced in relative intensities compared to those samples exposed to BTA solution without cathodic reduction of the oxide. This suggested that the Cu-BTA film was extremely thin, say the order of a monolayer. In order to investigate this further, similar studies were made using the X-AES copper spectrum rather than XPS. The oxide-free surfaces were

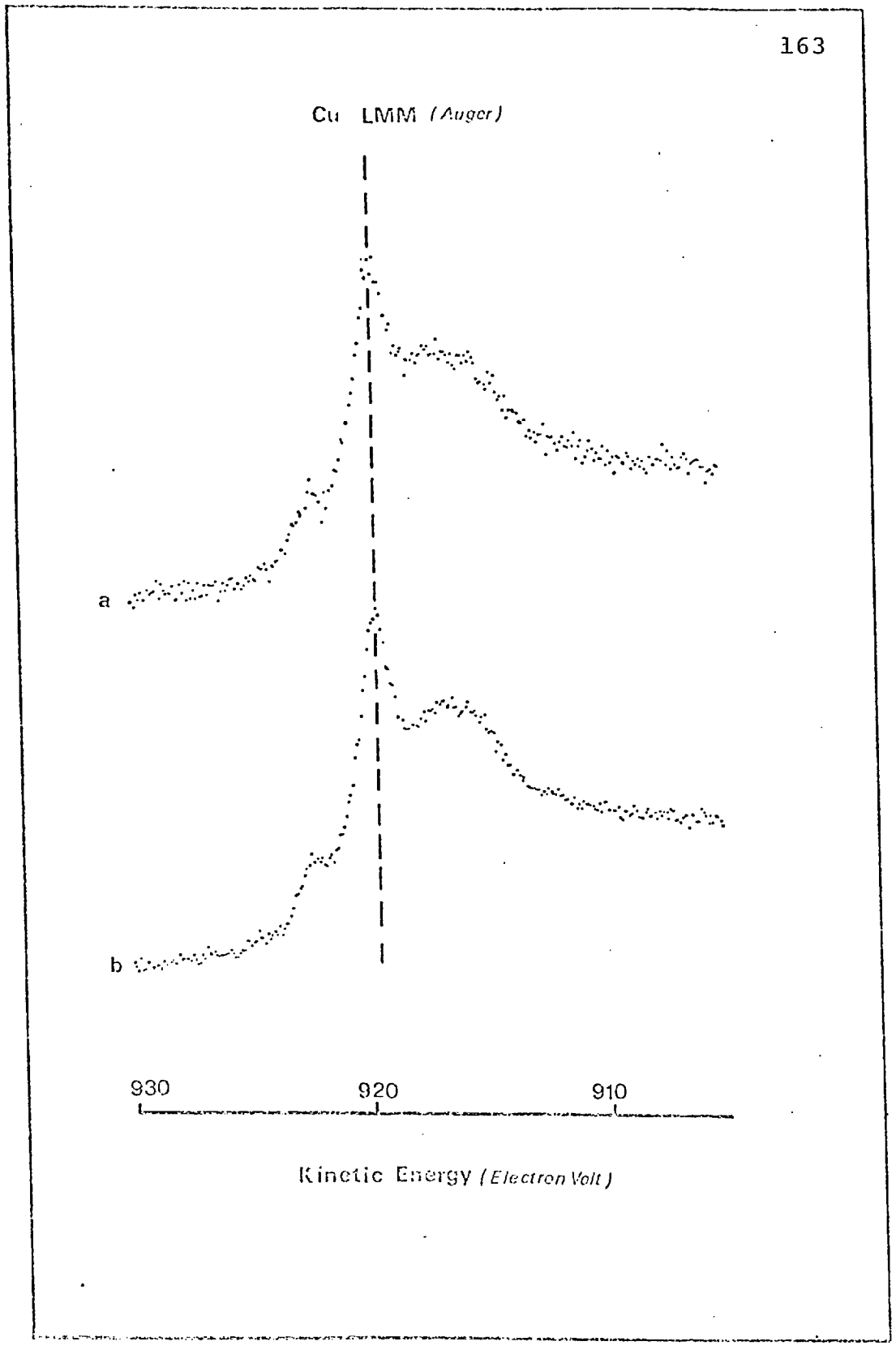


Figure 6.18: X-AES spectra of a copper sample after being cathodically reduced followed by inhibitor injection. Exposed to the solution for: (a) 10 min.; (b) ½ hour.

produced in an identical fashion to those described earlier. For details of experiment see Appendix A. Figure (6.18a) shows an X-AES of a copper sample after being cathodically polarized followed by inhibitor injection and exposure to the solution for 10 minutes. Figure (6.18b) shows the result of an identical sample exposed to the solution for ½ hour. In both spectra the metallic peaks (919.7 eV k.e.) are very intense, indicating that the complex film thickness must be much less than the escape depth of the Auger electrons. There is evidence for some Cu-BTA complex formation from the appearance of a broad peak at smaller kinetic energy side of the main peak. This experiment was repeated with solutions at different pH varying between 7 and 3 but the results always appeared to be similar.

6.2.2 The mechanism of film formation

The mechanism of film formation, based on the results obtained in this study and also other reported observations, cannot be a single chemisorption process as suggested previously (52). Nor is it a simple single process of precipitation particularly in the presence of chloride ions. In fact, several chemical processes with different rates take place "in situ", which eventually result in the formation of the Cu-BTA complex films. The model for the mechanism of film formation which will be proposed below will be explained for the most complicated case, i.e. copper samples with thick Cu_2O treated with solution of BTA at pH ~ 3 in the presence of chloride ions. The model then will be extrapolated to the simpler cases.

The first process which takes place when a Cu_2O sample is immersed in an acidic solution (pH < 3), is the

disproportionation of Cu_2O according to Equation (6.5) as discussed earlier. If chloride ions are present, the second process is formation of cuprous chloride (see Equation 6.6). The two reactions are repeated again here:-

$$Cu_2O + 2H^+ \rightleftharpoons Cu^{2+} + H_2O + Cu \qquad (6.5)$$

$$Cu^{2+}_{(aq)} + Cu_{(M)} + 2Cl \rightarrow 2CuCl_{(S)} \qquad (6.6)$$

Due to the small solubility of CuCl, 1.1×10^{-3} M, the solution becomes saturated if the amount of Cu_2O on the original sample is sufficiently large. In such cases CuCl precipitates mainly on the surface of the copper. Equation (6.6) represents a highly corrosive media for copper. In fact with a sufficiently large reservoir of Cu^{++}, i.e. added artificially, in the presence of chloride ion, reaction (6.6) takes place until the entire copper sample has dissolved. The reaction takes place at a tremendously high rate despite the formation of a CuCl layer on the surface which has certain protection properties. Introducing BTA into such a solution does inhibit the corrosion of copper to some extent. However, reaction (6.6) followed by formation of Cu-BTA complex as will be discussed later, does not stop even after BTA introduction and as long as there are Cu^{++} and Cl^- ions, the reaction takes place, though at a much lower rate.

Since the amounts of Cu_2O on the samples are normally limited, the amount of Cu^{2+} produced by the disproportionation reaction is only small and thus little CuCl is produced by reaction (6.6). In this case, even if CuCl is precipitated because of the high localized concentration near the copper surface, it will be soon washed away. Examination of the copper sample with

electrochemically grown Cu_2O on exposure to acid solutions containing Cl^- ions, revealed that the surface becomes clean soon after being inserted in the solution. Exposure of a Cu_2O sample in a solution of HCl at pH ~ 3 as discussed earlier (Figure (6.15)), revealed that after 5 minutes exposure to such solution the surface becomes a clean metallic copper. No trace of chlorine was found in XPS spectrum of this surface. When BTA is present in solution there are two possible ways for complex formation. It could form a complex via the intermediate stage of CuCl formation or directly from using Cu^{2+} ions in solution. The ability of CuCl to form complexes with certain organic compound has been reported by many workers (88, 89). However, whether or not the complex formation is via an intermediate stage, the overall reaction in the presence of Cl^- will be:

$$Cu_{(M)} + Cu^{2+}_{(aq)} + BTA_{(aq)} \xrightarrow{Cl^-}{}_{(aq)} Cu_2Cl\ BTA_{(S)} \qquad (6.7)$$

The second possible way of complex formation is through the formation of Cu(II)-BTA. In fact, it was found that Cu(II)-BTA complexes prepared from a solution of Cu^{2+} and BTA, in the presence of Cl^- and copper metal, convert to a Cu(I)-BTA complex. The net result is the precipitation of Cu_2Cl BTA complex on the copper surface. Examination of the solution by U.V. spectrophotometry showed that after a certain period of time no Cu(II) complex was retained in the solution. This reaction takes place most probably via an intermediate stage i.e. CuCl formation, since it is not observed in the absence of chloride ion.

To establish the effect of CuCl as an intermediate, an attempt was made to divide the reaction (6.7) into different stages. In the first stage, CuCl was grown on

the copper samples up to a few thousand Å, by inserting the copper samples in a solution of Cu^{2+} + Cl^-, which was already saturated with CuCl. It was found that a couple of minutes was sufficient to grow an extremely thick layer of CuCl on the surface. Samples prepared this way were then immersed in a solution of BTA at pH = 3, in the presence of Cl^-, for a short period of time (e.g. 15 minutes). Examination of the resulting surface by ESCA and Ar ion sputtering showed that the entire film of CuCl had converted to a Cu_2 BTA Cl complex. Using this technique, it is possible to grow Cu_2 BTA Cl complex films on the surface with any desired thickness. Argon ion sputtering was used to determine the thicknesses of the CuCl and resultant Cu_2 BTA Cl complex. In fact, it took a long time to remove a layer of complex formed in this fashion. The time taken to remove this top layer with the highest rate of etching, using estimations of sputtering rates for pure metals (see Appendix A), was sufficient to remove thousands of Å of such a film.

Figure (6.19Aa) and (6.19Ba) show a CuCl surface prepared as explained above, in Cl (2p) and N (1s) regions respectively. 20 seconds treatment of this sample with BTA solution resulted in decrease in Cl 2p peak and appearance of a nitrogen peak, Figure (6.19Ab) and (6.19Bb). It must be noted that the spectra obtained in this series of experiments were all at the same condition of X-ray power and the same number of scans. Five minutes exposure to the BTA solution resulted in spectra presented in Figure (6.19Ac) and (6.19Bc) which are clearly similar to (6.19Bb) except in peak intensities. Figure (6.19Ca) shows the Cu LMM Auger spectrum of CuCl surface and (6.19Cb) the same sample

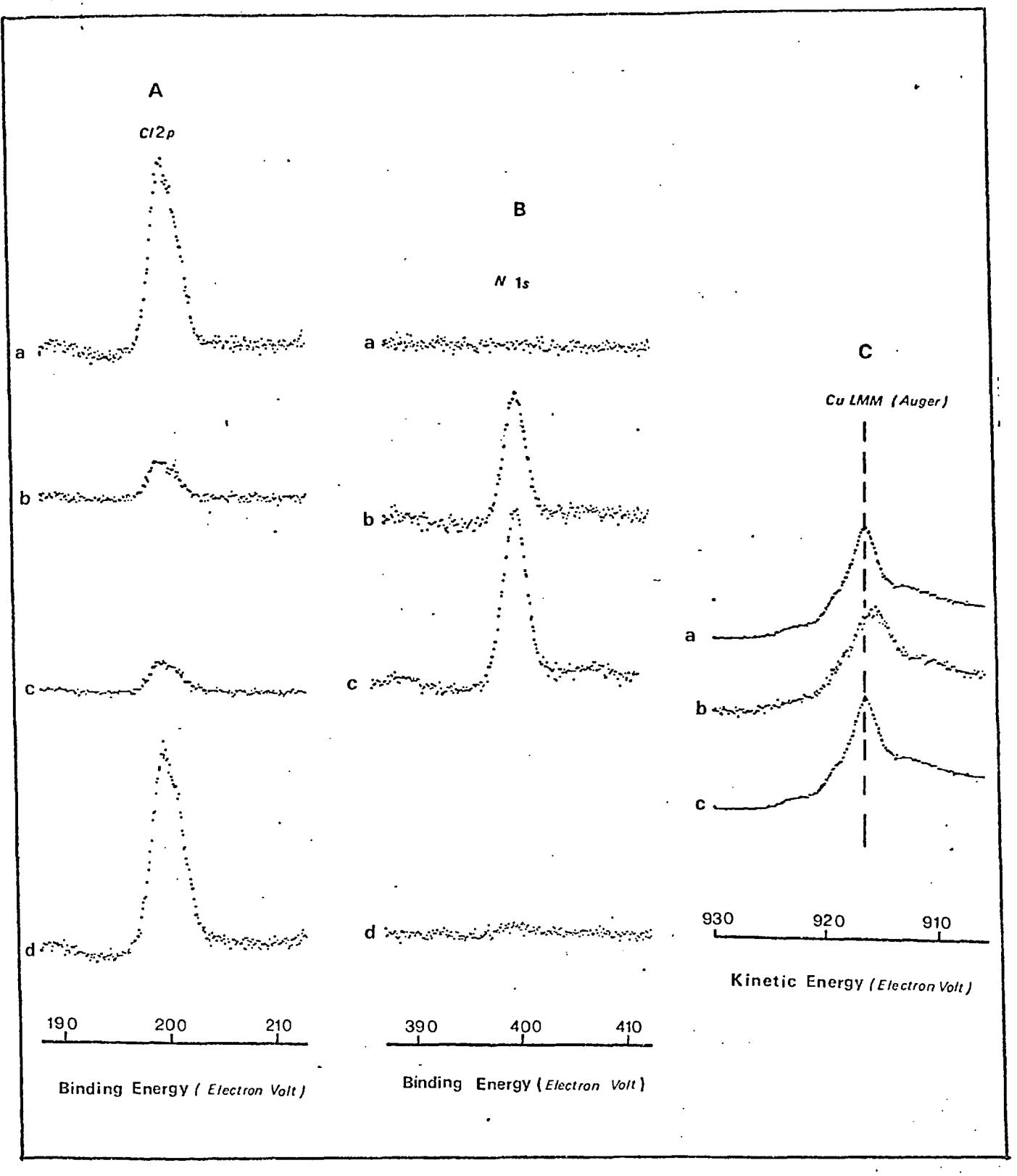


Figure 6.19: ESCA spectra of a CuCl surface A(a), B(a) and C(a), treatment of this sample with BTA solution for 20 sec. A(b) and B(b); treatment of this sample with BTA for 5 min. A(c), B(c), C(b); This sample etched for 20 min. A(d), B(d) and C(c).

after being treated for 5 minutes with BTA. A small shift towards lower binding energy in (6.19Cb) is because of complex formation. From these sets of spectra it is obvious that the surface is now completely covered with a Cu_2 BTA Cl complex. To find out how deep the Cu-BTA film is and also to see whether or not any CuCl underlayer is retained, argon ion bombardment of the surface was employed to remove layers from the surface. It took a very long time with relatively high rate of etching (say 20 minutes with 3 kv and 10 μA) to remove the Cu_2 BTA Cl film completely from the surface, indicative how thick a Cu_2 BTA Cl layer was formed. Figure (6.19Ad) and (6.19Bd) show the results after 20 minutes argon ion bombardment. Figure (6.19Cc) shows the Cu LMM Auger spectrum of the resultant surface. It is quite obvious that the underlayer film is CuCl. For exposures much longer than 5 minutes to BTA solution (say two hours), the entire film appeared to be converted to Cu_2 BTA Cl complex. Taking into consideration the above results, it is clear that formation of a Cu_2 BTA Cl complex film on the surface is more than likely via an intermediate stage of CuCl formation.

An important feature of two reactions (6.6) and (6.7), which effects the film thickness, is the difference in the rate of reaction between (6.6) and (6.7). Figure (6.17) as described earlier, indicates that the disproportionation of Cu_2O takes place within seconds after sample being immersed in acidic solution, whereas the formation of a complex film has taken a few minutes. Thus, the soluble Cu^{2+} ions entering the solution form a $Cu(I)_2$ BTA Cl complex (Eqn. 6.7), with the maximum concentration close to the sample surface. Having a

small solubility, it immediately precipitates onto the surface. In this way the maximum film thickness can be obtained. Immersion of a Cu_2O sample in an acidic solution for a certain period of time (e.g. 20 minutes), followed by injection of inhibitor, resulted in formation of only a thin complex film. This indicates that the products of reaction (6.5) i.e. Cu^{2+}, have dispersed in the solution and thus only a small amount of Cu^{2+} ions are available for film formation at the metal surface, (Eq. (6.6)). Figure (6.20a) shows a Cu Auger spectrum of a Cu_2O sample immersed in a solution of HCl at pH ~ 3 for some time (say ½ hour), followed by injection of BTA, and then left exposed to the solution for 15 minutes. Figure (6.20b) shows the result of an identical sample left for 30 minutes exposed to the solution. Figure (6.20c) shows an identical sample which was inserted into the same BTA containing solution for 6 minutes. Obviously in this case a thicker complex film is formed more rapidly.

The model, now, can explain the entire different observations. From Equations (6.5) and (6.6) in all cases the resultant surface complex films will be Cu(I) complexes. Relatively thick films can be obtained if the samples are originally covered with thick Cu_2O in the presence of enough Cl^- in acid solutions. The film thickness depends on exposure time because of inevitable dispersion of the Cu^{2+} ions produced in (6.5).

When there are no Cl^- ions present, films thickness stays relatively low either because of elimination of intermediate stage of CuCl formation, or because the difference in complex structure, or both.

In a neutral solution in which according to

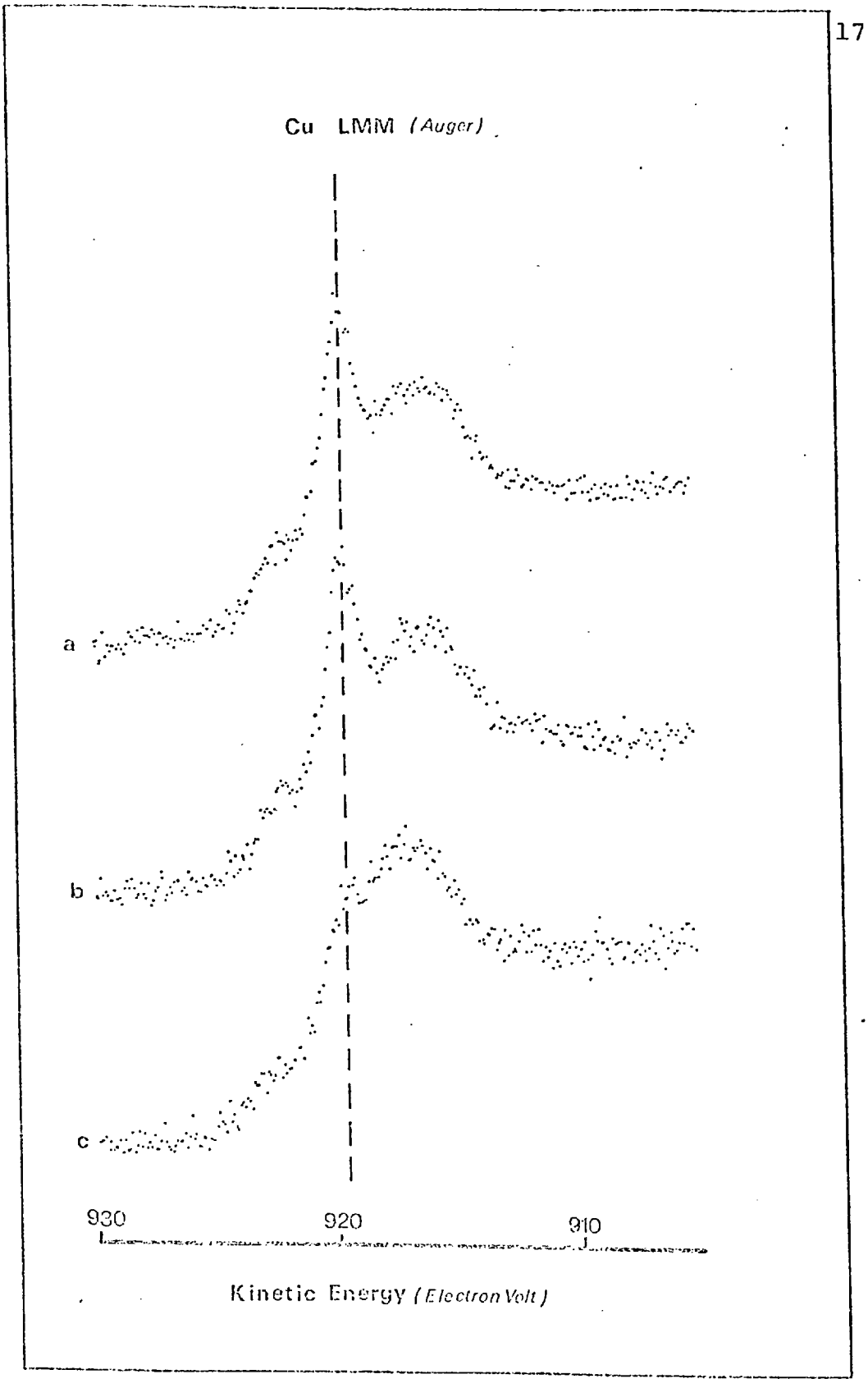


Figure 6.20: X-AES spectra of: (a) Cu_2O sample exposed to a solution of HCl (pH≃3) for ½ hour, followed by injection of inhibitor and left exposed to solution for 15 min; (b) a similar sample exposed to above solution for ½ hour; (c) a Cu_2O sample exposed to above solution for 6 min.

Equation (6.4) Cu_2O dissolution takes place through formation of Cu^+ in a very limited amount and the disproportionation reaction (Equation (6.5)) takes place only at a negligible rate, the resulting complex film will be very thin as is indeed observed to be the case, Figure (6.12). The same is true when there is no Cu_2O, i.e. cathodically reduced surfaces, where there is also no Cu^{++} ions in solution.

One important aspect of copper corrosion and its interaction with BTA which must be taken into account is the anodic dissolution of copper. This anodic process, as will be discussed in Chapter 8 in detail, is not particularly important in Cu-BTA film formation for short exposure of less than ½ hour. For longer exposure times, i.e. when the corrosion cell has been established, copper dissolves in solution as Cu^+, and in the presence of Cl^-, it forms CuCl. The role of Cu_2O in the corrosion of copper is quite important. If the copper is covered with a thick layer of oxide, and as long as the oxide is stable, i.e. in near neutral solutions, the rate of corrosion will be very small. On the other hand, a clean copper surface exposed to high concentration sodium chloride solution, even without Cu^{++} ions present, undergoes a slow corrosion process. This was observed particularly when the concentration of NaCl is greater than 1 M. Copper treated this way, is, after some time (say a couple of days), surrounded by a white cloud of CuCl. In a small volume of electrolyte, once the solution is saturated with CuCl, it precipitates (mainly onto the surface) and this affords some protection. This decreases the rate of Cu dissolution, although by no means stops corrosion completely (see Chapter 8 for

Copper active/passive transition in NaCl solutions).

6.3 Films formed by BTA on Copper-Nickel Alloys

Elemental copper has found small use in industry. However, copper alloys such as copper-nickel or copper-zinc (brass) alloys are widely used. So it is of interest to study the effect of BTA on such alloys. The interaction of BTA with copper-nickel alloys was studied in order to investigate whether preferential interaction with one alloy constituent takes place. If both metals, i.e. Cu and Ni, are responsible for film formation (if there is any), one might expect to observe signals from both elements in the ESCA spectrum of the film. Alloys of compositions 70Cu:30Ni, 55Cu:45Ni, and 30Cu:70Ni were chosen as typical copper-nickel alloys for use in this part of the study.

6.3.1 Characterization of Cu/Ni alloy substrate

In order to study the interaction of inhibitor with Cu/Ni alloys, it is important to study and characterize the surface of the substrate in both clean and oxidized form. Argon ion etching of these alloys produced relatively clean surfaces in which the relative peak heights of Cu and Ni in 2p region were close to their nominal bulk composition. Figure 6.21 shows XPS spectra of Cu $2p_{3/2}$ and Ni $2p_{3/2}$ for 70Cu:30Ni (6.21(a)), 55Cu:45Ni (6.21(b)) and 30Cu:70Ni (6.21(c)). In this study, however, it is only the relative intensities of peaks after being treated with BTA which is of interest.

The oxidation behaviour of copper-nickel alloys has been investigated previously by Castle (90). Castle in

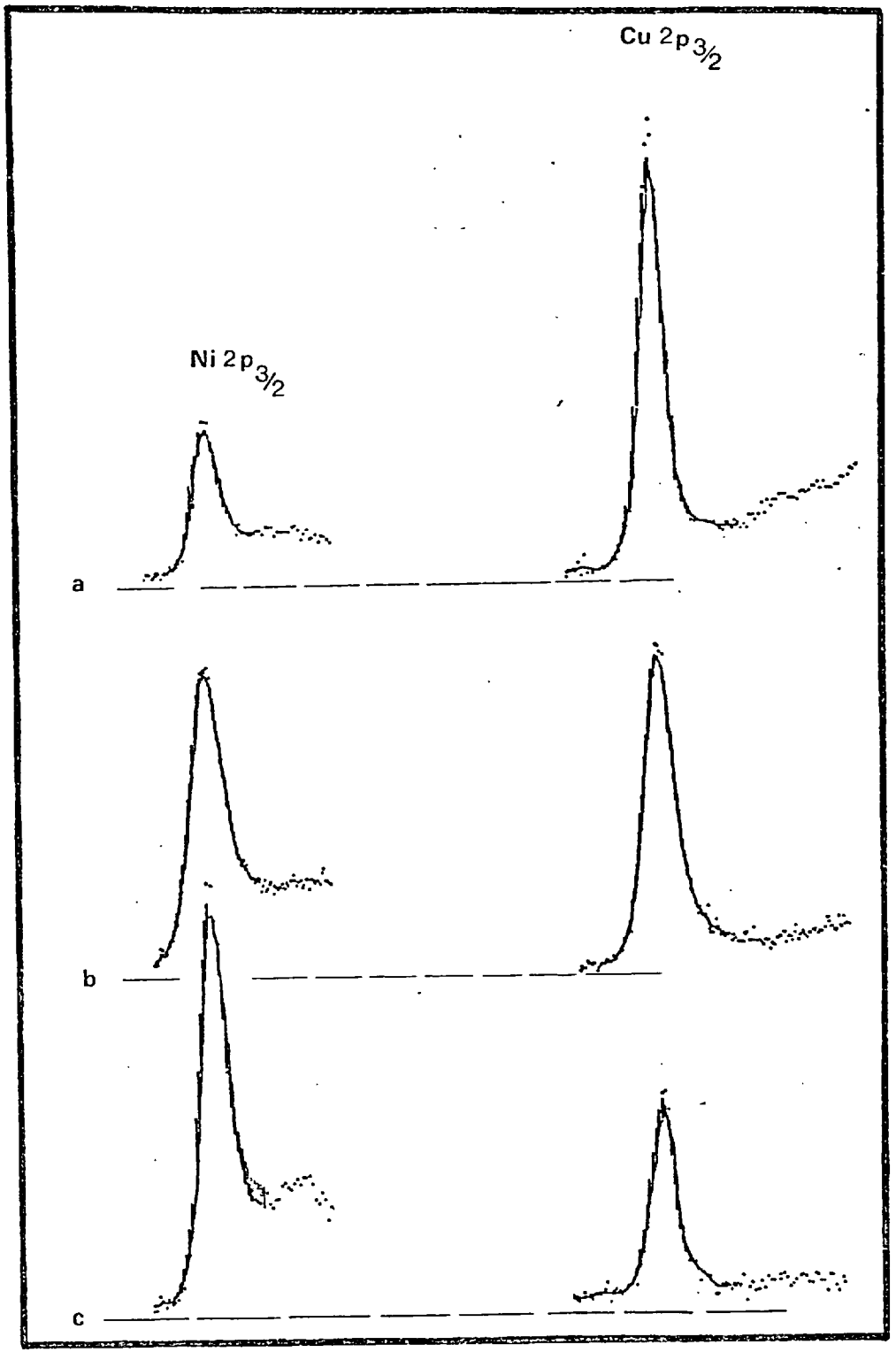


Figure 6.21: XPS spectra of (a) 70Cu:30Ni; (b) 55Cu:45Ni; (c) 30Cu:70Ni.

his first report concluded that at room temperature, the oxide film on copper-nickel alloy is a nickel oxide. The Cu spectrum ($2p_{3/2}$) was shown to be due to copper metal and the oxide layer on a copper nickel alloy is predominantly nickel oxide. This conclusion was supported using CuLMM Auger spectra to detect cuprous oxide formation, in Castle's later reports (91, 92).

Results obtained in the present study using both XPS and X-AES techniques were in full agreement with Castle's findings. The spectra obtained for polished, oxidized samples and those treated with BTA solution, showed a very sharply rising background, with a large decrease in peaks intensities. This sharply rising background has been observed by Castle (90) and according to him this is a typical of alloys surfaces which have not been prepared by evaporation or argon ion stripping within the spectrometer itself.

Examination of the polished surfaces of Cu/Ni alloys showed that the samples are predominantly covered with Ni oxide after exposure to air for some time. The XPS spectra of a 55Cu/45Ni alloy which was polished and argon ion etched, then exposed to air for 3½ hours, showed the formation of nickel oxide by the appearance of a higher binding energy shoulder at 856.2 eV on the Ni $2p_{3/2}$ peak, as well as shake-up satellites which are associated with NiO (93). Prolong exposure to the air (say 3 days) resulted in an increase in NiO thickness, while virtually no changes was observed in copper state, evidenced from X-AES CuLMM spectrum.Figure 6.22(a) shows an XPS spectrum of a Cu55/Ni45 alloy, polished and argon ion etched in Ni $2p_{3/2}$ region. Figure 6.23(a) shows the corresponding CuLMM Auger spectrum.

Figures 6.22(b) and 6.23(b) show the result of exposure of this sample to the air for 3½hours and Figure 6.22(c) and 6.23(c) show the result of 3 days exposure to air. While there is hardly any change in CuLMM peak, a progressive oxidation is evident from the appearance of the Ni $2p_{3/2}$ spectra.

These results confirm that the predominant oxide layer on the Cu/Ni alloys formed by oxidation in air at room temperature is NiO. This was the case for all three compositions of alloys which were used in this study. The thickness of NiO oxide stays low (within escape depth of Ni photoelectron) at room temperature even after long exposure to air (e.g. 24 hours). All binding energies are given in Appendix B .

6.3.2 Interaction of BTA with Cu/Ni Alloys

No attempt was made to investigate the behaviour of alloys in acidic solutions of BTA because acid attacks Ni while Cu remains unchanged, and this inevitably results in great changes in surface compositions. This effect would mask any preferential interaction and therefore samples were treated at pH = 7. Polished and cleaned samples were immersed in a solution of 0.02M BTA at pH~7 with 0.5M NaCl at 25^{o}C for different period of times, then taken out, washed and air dried. Samples treated with BTA solution showed a sharply rising background in their ESCA spectra, with a drastic decrease in peak intensities, which made it almost impossible to obtain any reasonable Cu Auger spectrum, after the samples were treated with BTA. However, since it is assumed that the ratio of peak heights in 2p region is a reasonable estimate of the surface compositions of the alloy constituents, the

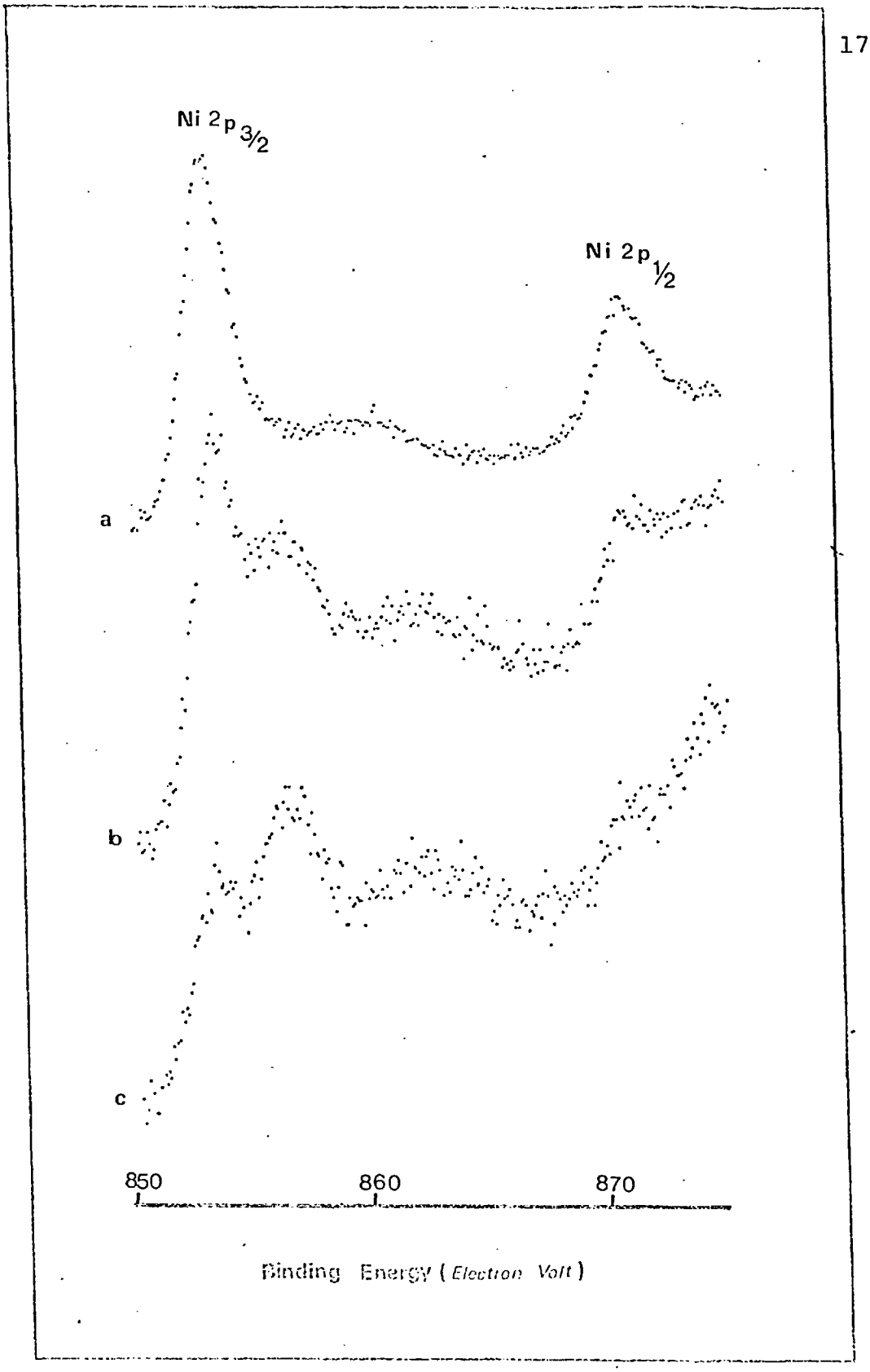


Figure 6.22: XPS spectra of 55Cu:45Ni alloy in Ni 2p region (a) polished and etched; (b) exposed to air for 3½ hours; (c) exposed to air for 3 days.

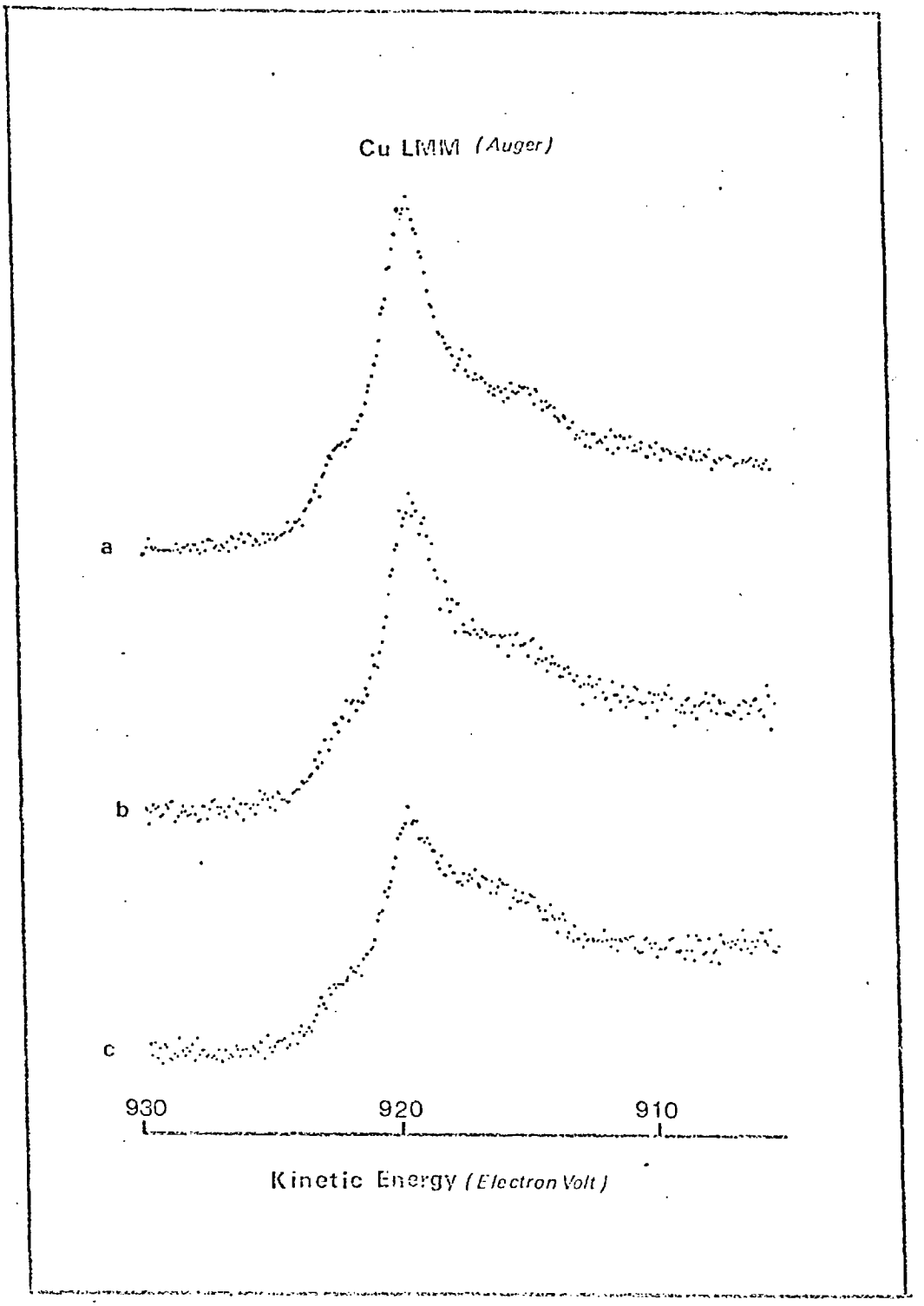


Figure 6.23: XPS spectra of 55Cu:45Ni alloy in Cu 2p region (a) polished and etched; (b) exposed to air for $3\frac{1}{2}$ hours; (c) exposed to air for 3 days.

relative changes caused by treatment with the inhibitor could be determined. Treatment of the polished samples with BTA resulted in the formation of a Cu(I)-BTA complex on the surface, while there was no evidence for the formation of a nickel complex. Figure 6.24(a) shows the XPS spectrum of an etched, clean 70Cu:30Ni sample in Ni and Cu $2p_{3/2}$ region, Figure 6.24(b) shows this sample before etching and Figure 6.24(c) the same sample after being treated with BTA for 5 minutes. The disappearance of Ni $2p_{3/2}$ peak from the spectrum indicates thatthe alloy now has a surface which consists largely of copper in the form of a Cu(I)-BTA surface complex since the Cu Auger proved to be not particularly informative, the presence of a Cu-BTA complex was inferred by the presence of strong C 1s and N 1s peaks.

To check whether or not the same changes occur in a similar solution without BTA, a sample was exposed to such a solution for a long period of time (say 24 hours). Except for minor changes in the NiO peak intensity and associated shake-up satellites, no change took place and the Ni $2p_{3/2}$ peak was quite detectable. Therefore the changes described above were due to BTA.

In the case of 30Cu:70Ni, the Ni 2p peak was observed to be still strong after 5 minutes exposure to a similar BTA solution. Figure 6.25(a) shows an XPS spectrum of an etched sample in 2p region and 6.25(b) is the same sample before being etched. Figure 6.25(c) showsthe same sample after being treated with BTA solution for 5 minutes. This shows that after 5 minutes exposure to the solution the surface composition looks similar to that of the original polished surface. Again, the C(1s) and N(1s) peaks indicated the

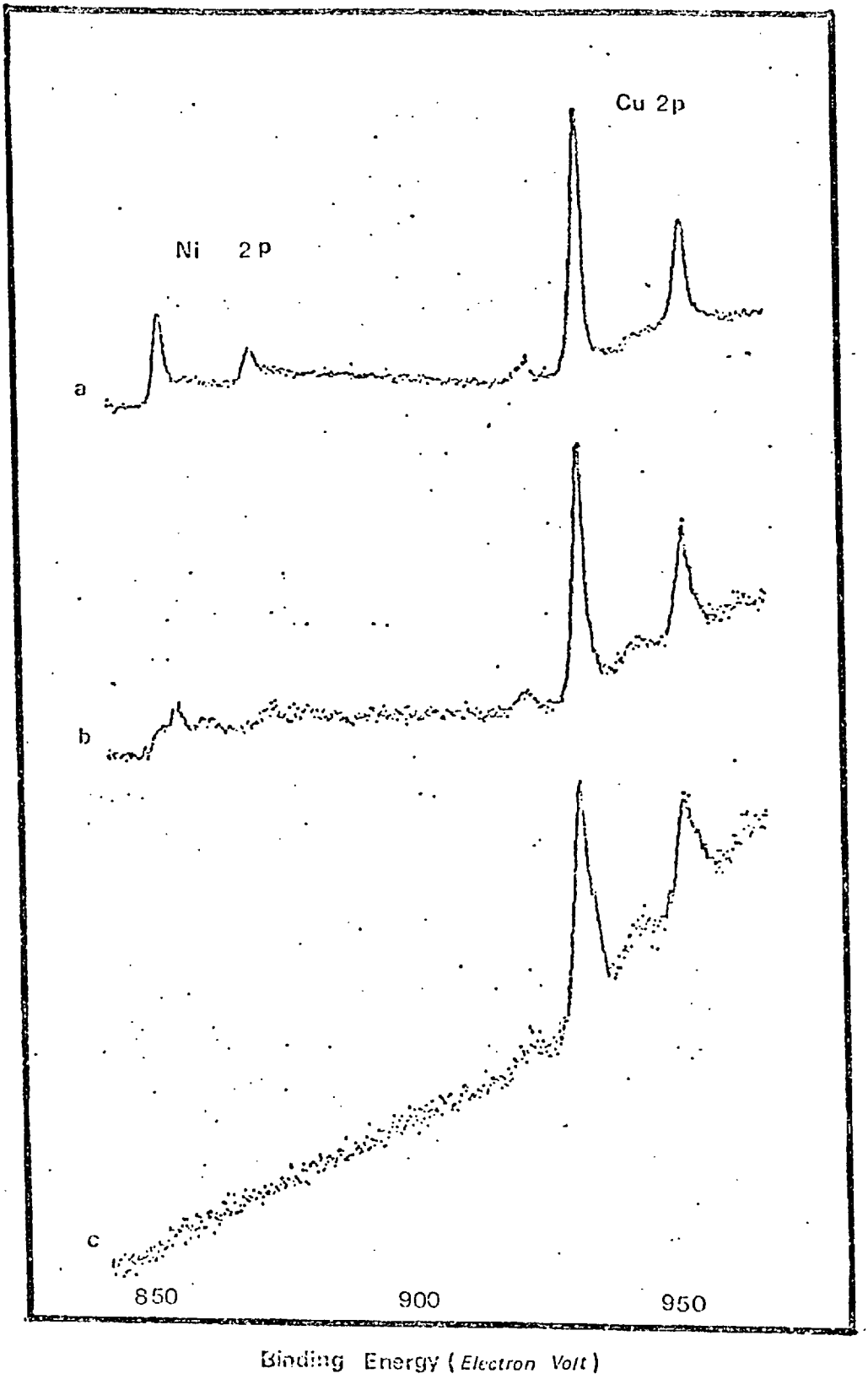


Figure 6.24: XPS spectra of 70Cu:30Ni alloy : (a) polished and argon ion etched; (b) polished; (c) after immersion in BTA solution for 5 min.

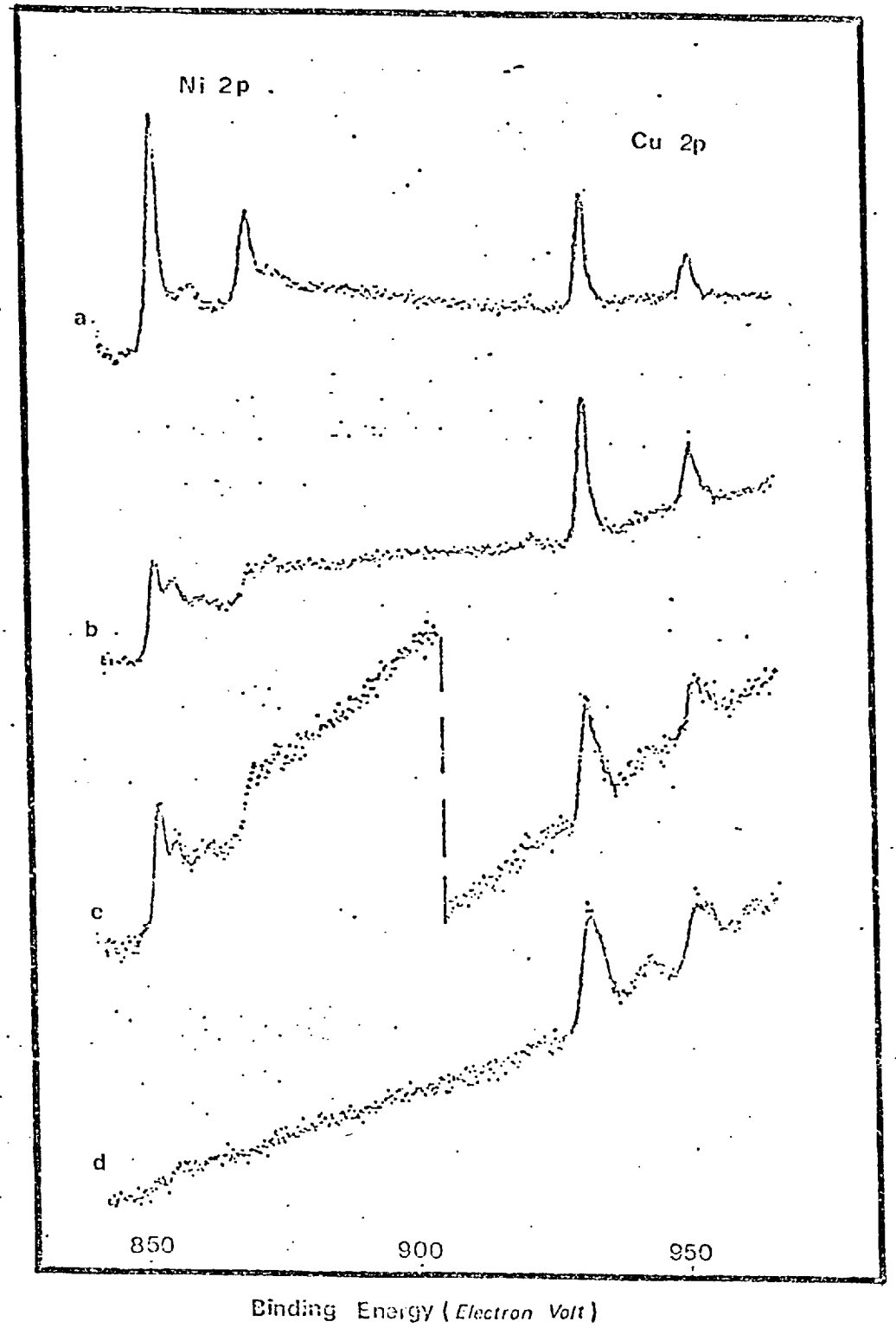


Figure 6.25: XPS spectra of 30Cu:70Ni alloy : (a) polished and argon etched; (b) polished; (c) after exposed to BTA solution for 16 hours.

presence of a BTA complex. However, after 16 hours BTA treatment, the surface becomes similar to the 70Cu:30Ni alloy treated for 5 minutes, being now almost completely Cu(I) BTA (Figure 6.25(d)). Again no significant changes were observed in the surface composition due to exposure of the polished sample in a BTA-free solution for comparable times.

In all these studies, the Cu(I)-BTA surface complex rapidly oxidized to Cu(II), after removal from the solution as was found for the BTA treated copper samples. The explanation of the trace of Cu(II) in the spectra of Cu/Ni samples treated with BTA is again oxidation during the finite drying and transfer time.

The binding energies of the various peaks are given in Appendix B, but they proved to be not particularly informative. The Cu 2p binding energies remain unchanged on BTA treatment and so do those of Ni, i.e. compared to Cu_2O on copper and NiO. Nitrogen 1s binding energies are the same as for the treated copper samples.

Evidence for compound formation involving nickel is slight since a study of pure nickel indicated that BTA only weakly interacts with Ni. The Cls and Nls photoelectron peaks which were observed in the case of treated nickel were quite weak in comparison with their relative strength in the spectra of treated copper samples. The fact that nickel salts can form a complex with BTA, suggests that a Ni-BTA complex could be formed on the surface. Despite this, the above results show that there is no detectable nickel complex formation.

The Ni $2p_{3/2}$ binding energies for the treated copper-nickel alloys could not be determined accurately because of the weak nature of the nickel peaks except for a very short exposure times for the 30Cu:70Ni alloy, which is identical to that of pure nickel.

6.3.3 Mechanism of Film Formation

Since it established that copper-nickel alloys on exposure to air, are covered with a NiO film with a thickness not more than Ni photoelectron escape depth, and that the surface film after being treated with BTA solution at pH~7 is a complex of Cu and BTA, the mechanism by which the complex films are formed is either through diffusion of copper ions through NiO film or dissolution of NiO,which leaves the copper directly in contact with solution. The stability of NiO at different pH is given by equation (6.7) (86):

$$NiO + 2H^{+} \rightleftarrows Ni^{++} + H_2O \qquad (6.7)$$

$$\log[Ni^{++}] = 12.18 - 2pH$$

At pH = 7 $[Ni^{++}] = 10^{-1.82}M$. This figure indicates for a sample of 1 cm^2 surface area and in 1 litre of solution, thousands of $\mathring{A}$ of NiO surface film can dissolve. It is clear that the second possibility for Cu-BTA film formation of Cu/Ni alloys in which copper ions dissolve after dissolution of the NiO film is the more likely mechanism. The mechanism of Cu-BTA film formation would appear to be, (a) dissolution of NiO; (b) dissolution of copper ions in solution; and (c) precipitation of Cu(I) BTA complex on the surface. The Cl 2p peaks were present in XPS spectra of BTA treated

alloys when NaCl was added to the solution. Being very thin, no attempt was made to determine stoichiometry of Cu-BTA films on Cu/Ni alloys.

In order to study the behaviour of Cu:Ni alloys in solution containing Cl^- and Cu^{2+} ions, samples were inserted in a solution of 0.5M NaCl with addition of some Cu^{++} ions, for different periods of time and the resultant surfaces were examined by ESCA. This investigation showed that the alloys behave in exactly the same manner as pure copper, with copper dissolving into the solution to form cuprous chloride which then precipitates on the surface. Even though the rate of copper dissolution is high, it is much less than that of pure copper. Examination of the surfaces showed that the samples treated this way are covered with thick films of cuprous chloride. When BTA is present, very thick Cu_2-BTA-Cl complex films were obtained.

The results presented above show that on copper-nickel alloys BTA acts as a corrosion inhibitor for this alloy by forming a predominantly Cu(I)-BTA surface complex. The mechanism by which this complex forms is identical to that for pure copper, i.e. dissolution of copper and precipitation of the complex on the surface. In case the sample is covered with NiO (on exposure to air), the first reaction is dissolution of NiO followed by the dissolution of copper and finally precipitation of the Cu(I)-BTA complex.

6.4 Films Formed on Brass

The brass 70Cu:30Zn was chosen to investigate the interaction of BTA with other copper alloys besides Cu-Ni alloys. Brasses are widely used in industry and 70Cu:30Zn

is a typical example. This study was carried out to investigate the films formed by BTA interaction and once again as for the Cu-Ni alloys, to see whether preferential interaction with one alloy constituent takes place.

The relative Cu and Zn $2p_{3/2}$ peak heights for heavily argon ion etched samples correspond closely to the nominal bulk composition as was the case for Cu/Ni alloys, and should therefore give a reasonable estimate of the relative surface composition.

The spectra of Cu and Zn in the 2p region from brass samples treated with BTA for different periods of times, showed that on exposure to BTA solution, although the copper peak intensity increased relative to zinc, it is not as marked as was the case for the copper-nickel alloys. Indeed, it was found that even very long exposure times do not result in a further decrease of the relative intensity of the zinc signal. Fig. 6.26(a), shows an XPS spectrum of a polished and etched brass sample, in the Cu and Zn 2p region. Figure 6.26(b) shows the same sample before being etched and 6.26(c) is after immersion in BTA solution at pH~7 with 0.5M NaCl for 20 hours. The presence of C(1s) and N(1s) peaks indicated that there are some complex film formation. The Cu(I)-BTA surface complex on brass, rapidly oxidized to Cu(II), after removal from the solution as was the case for copper or copper-nickel alloys. The reason for the trace of Cu(II) in the spectra of the samples treated with BTA is oxidation during the finite drying and transfer time. A small peak between two sets of Cu2p and Zn2p peak is due to the O KLL Auger transition. In this case also, a sharply

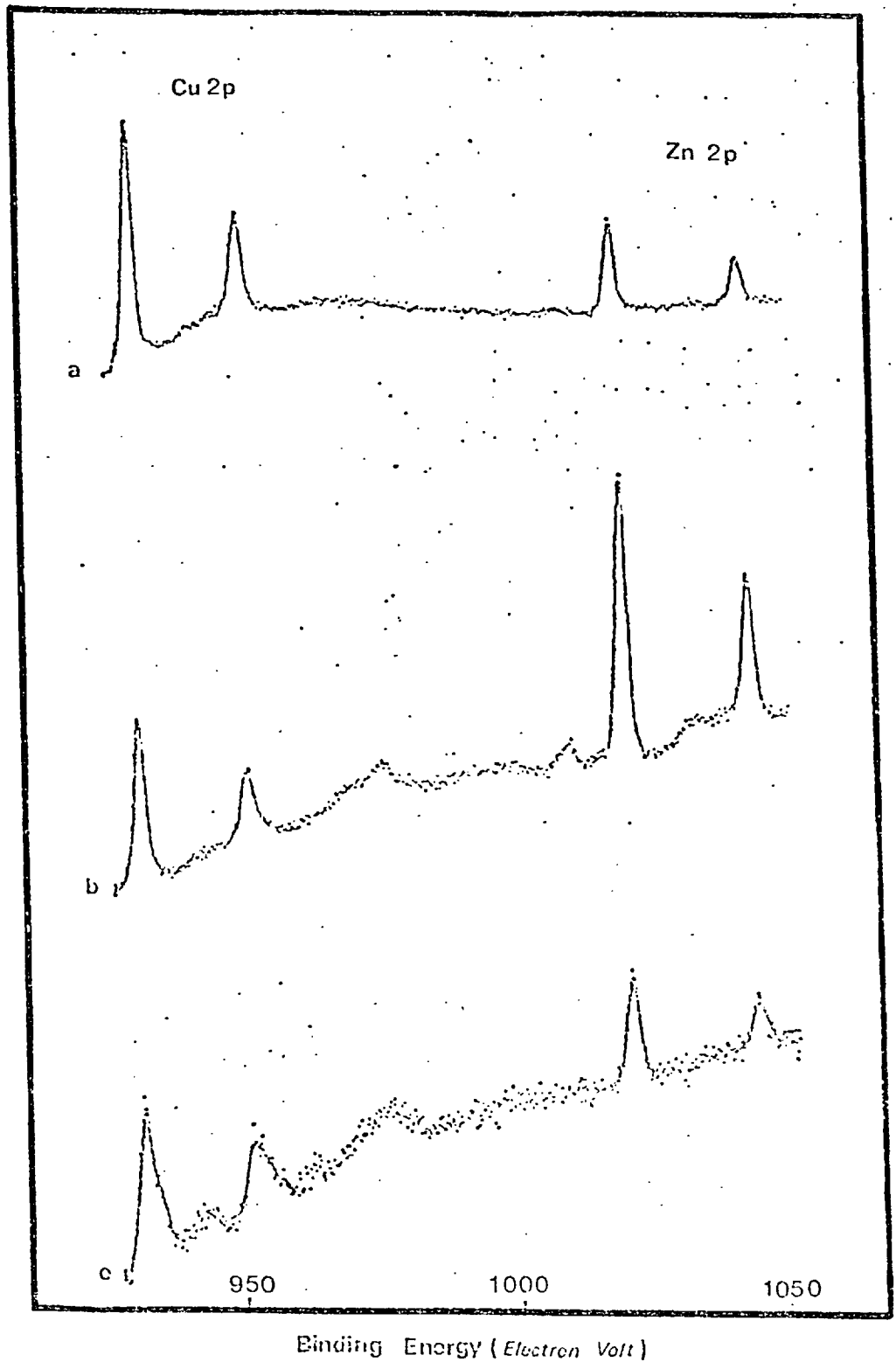


Figure 6.26: XPS spectra of 70Cu:30Zn brass: (a) polished and argon ion etched; (b) polished; (c) after exposed to BTA solution for 20 hours.

rising background (although not as much as copper-nickel), and a decrease in peak intensities, makes it difficult to use the metal Auger peaks to determine the surface chemistry. Nevertheless it was found possible to use this method with a reasonable accuracy especially for short exposure times (i.e. less than ½ hour).

Considering the above results, it is clear that unlike nickel in Cu/Ni alloys, zinc is involved in the surface complex in some way. In view of this, it seemed logical to investigate the interaction of pure zinc with BTA in order to find out whether a complex film is formed on the surface.

Studies of pure zinc showed that BTA adsorbs strongly onto the zinc surface. The XPS and X-AES spectra of the treated samples showed that the $Zn2p_{3/2}$ peak shifts to a higher binding energy by 0.7 eV, even after a short period of treatment with BTA (say five minutes) and the ZnLMM Auger peak also showed a shift of about 0.8eV, to the lower kinetic energy, compared to the ZnO Auger peak (94). The solution prepared Zn-BTA complex, showed exactly the same characteristics for details of experimental see Appendix A . Figure 6.27(a) shows an X-AES spectrum of a polished and argon ion etched Zn sample. Figure 6.27(b) and 6.27(c) show the result of exposure of this sample to the air for 10 minutes and ½ hour respectively. A progressive oxidation has taken place which is evident by appearance and an increase in its intensity of a peak on the lower kinetic energy side of the main peak at 988.4 ke. This corresponds to ZnO (94) 30 seconds treatment of this sample with a solution of BTA, results in Fig. 6.27(d) in which the X-AES peak is

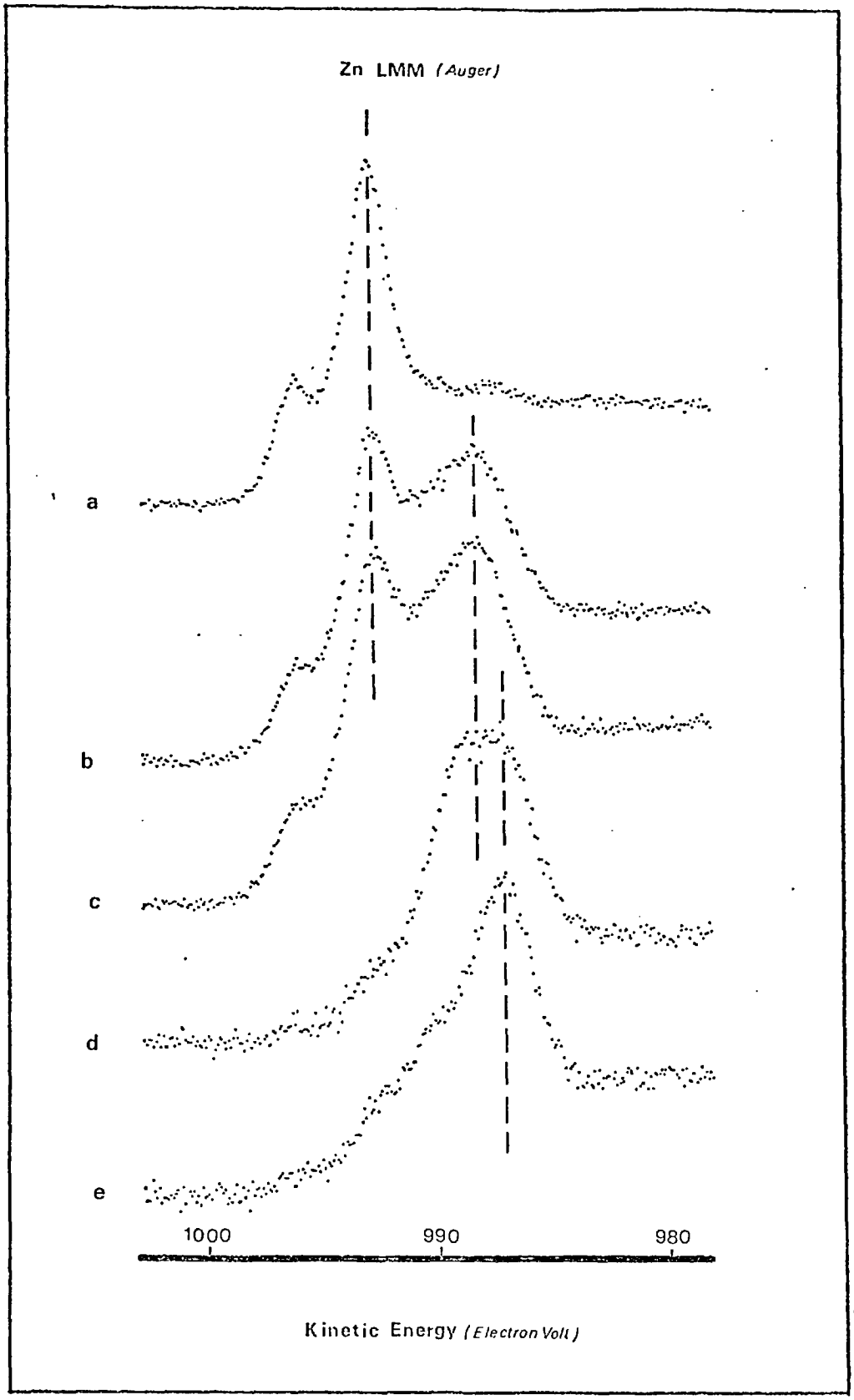


Figure 6.27: X-AES spectra of Zn sample : (a) polished and argon etched; (b) this sample exposed to air for 10 min.; (c) exposed to air for 30 min.; (d) exposed to BTA solution for 30 sec.; (e) similar sample exposed to BTA solution for 5 min.

observed to be broadened at low kinetic energy due to formation of a Zn-BTA complex. Presence of complex, was also supported by observation of a N 1s XPS peak and enhanced C 1s peak. Immersion of a sample in a solution of BTA for longer time i.e. 5 minutes, results in formation of relatively thick Zn-BTA complex which gives a sharp new peak at 987.2 eV kinetic energy, Fig. 6.27(e). It can now be seen that the broadening evident in Fig. 6.27(d) is due to the presence of the complex peak.

Above results show that the X-AES spectrum of Zn is a reliable way to determine the involvement of Zn in complexes with BTA. A study of the Auger spectra of Zn and Cu X-AES spectra in Cu/Zn alloy after being treated with BTA for a short period of time (say ½ hour) showed that again in this case it is mainly copper which is responsible for the film formation. Exposure time for more than ½ hour, results in a large decrease in signal to noise ratio in which it is not possible to obtain good quality Cu and Zn Auger spectra.

Results obtained for Cu/Zn alloys also showed that the oxidation behaviour of this alloy is different from that of Cu/Ni alloys. Cu and Zn Auger spectra of oxidized samples showed that both Cu and Zn undergo oxidation. Fig. 6.28(a) and 6.29(a) show X-AES spectra of Zn and CuLMM Auger transitions respectively of a polished and heavily argon ion etched sample. Exposure of this sample to the air for ½hour results in spectra shown in Figures 6.28(b) and 6.29(b). As is evident from these spectra, both Zn and Cu have undergone an oxidation although the rate of the oxidation of the Zn appears greater, judging by intensive peak due to ZnO at 988.4 eV k.e. Treatment of these samples with BTA for

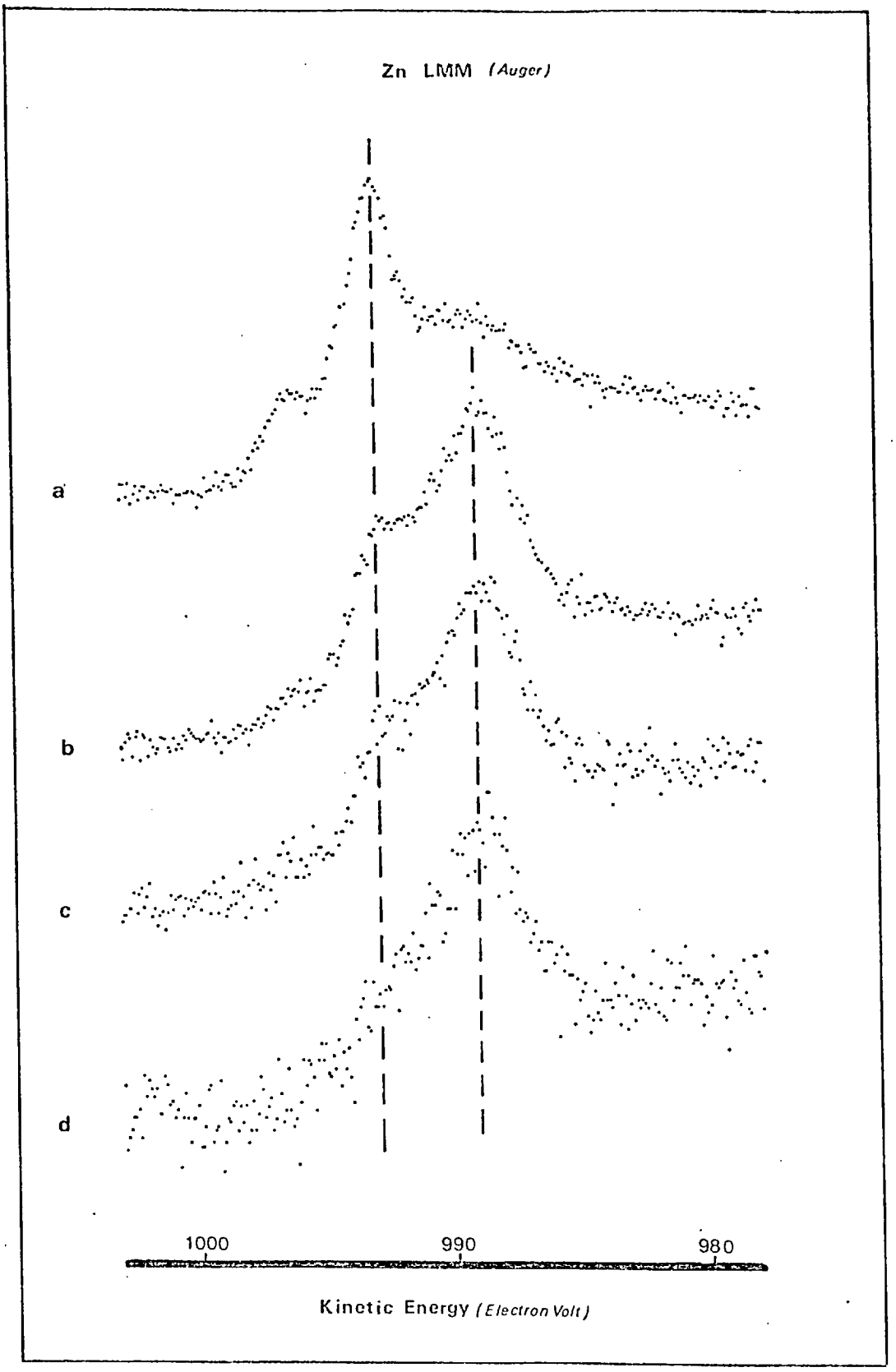


Figure 6.28: X-AES spectra of 70Cu:30Zn brass (a) polished and argon ion etched; (b) exposed to air for 30 min.; (c) exposed to BTA solution for 3 min.; (d) exposed to BTA solution for 30 min.

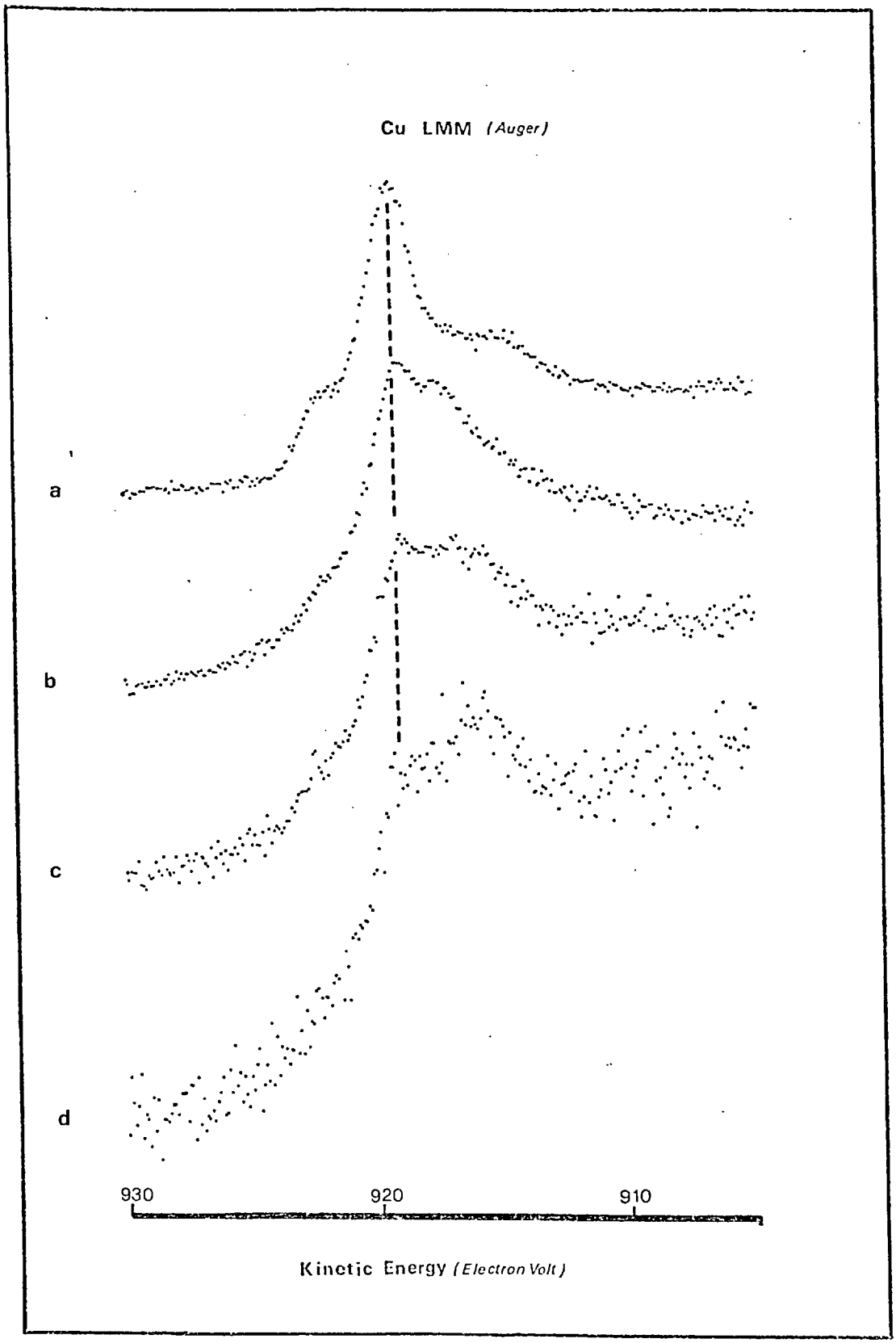


Figure 6.29: X-AES spectra of 70Cu:30Zn brass (a) polished and argon ion etched; (b) exposed to air for 30 min.; (c) exposed to BTA solution for 3 min.; (d) exposed to BTA solution for 30 min.

3 minutes results in Fig. 6.28(c) and 6.29(c), in which formation of a Cu-BTA film is evident by the appearance of considerable broadening at lower kinetic energy (see Fig. 6.27) The Zn Auger peak has change little so that the contribution of Zn to the film formation must be very small. Exposure to the BTA solution for ½ hour results in Fig. 6.28(d) and 6.29(d). The signals are becoming weak, but they are still possible to observe, and the film mainly consists of a Cu-BTA complex. However, the presence of Zn-BTA complex is not evident from the Zn Auger peak which cannot be distinguished from ZnO. However a 0.5 eV shift in the $Zn2p_{3/2}$ XPS peak is indicative of some Zn complex formation.

6.4.1 Mechanism of Film Formation

The stability of ZnO at different pH is given by equation (6.8) (86).

$$ZnO + 2H^{+} \rightleftharpoons Zn^{++} + H_2O, \quad \log [Zn^{++}] = 10.96 - 2pH \qquad (6.8)$$

At pH = 7, $[Zn^{++}] = 10^{-3.04}M$. This value shows that ZnO films of order of thousand Å can readily be dissolved. Cuprous oxide dissolves in a much smaller amount ($10^{-7.84}M$) which represents a value not more than few Å. In the presence of BTA, copper ions precipitate as Cu-BTA complex on the surface. The same mechanism is valid for formation of a Zn-BTA complex. When Cl^{-} is present (i.e. addition of NaCl), a peak due to Cl2p in XPS spectrum of the treated surface is detectable. In this case again like Cu/Ni case, because of the very small thickness of these films, it is not possible to determine the stoichiometry of the films.

These results suggest that the mechanism of Cu(I)-BTA film formation is basically the same as for pure copper. Addition of Cu^{++} ions in presence of Cl^{-} once again represents a highly corrosive media towards brass. Introducing BTA in such a solution, slows down the corrosion process and a very thick Cu-BTA complex film forms on the surface.

6.5 Films Formed From Non-Aqueous Media

Adsorption from non-aqueous media was carried out in order to investigate the possibility of complex film formation from such media, using suitable solvents, such as dry CH_3Cl or benzene, etc., in which BTA is appreciably soluble. Care was taken to use a dried-solvent to reduce the effect of aqueous media as much as possible. These experiments showed that although complex films form from non-aqueous solutions on copper and its alloys, the thickness of the film stays very low regardless of exposure time. This can easily be explained by the model suggested for the film formation mechanism. Since the mechanism is a dissolution of copper followed by precipitation, and this can not take place in a dry solvent, the film thickness as a result stays low and is probably no more than a monolayer. This also proved to be the case for copper-nickel alloys treated with organic solutions of BTA. No matter how long the sample is exposed to such solutions, the $Ni2p_{3/2}$ peak never disappears from the XPS spectrum, as is the case for aqueous solution of BTA. These results strongly support the mechanism of film formation in aqueous solution proposed in Section (6.2.3).

6.6 Summary

The major findings in this part of current study is as follows:

1. The corrosion inhibition properties of benzotriazole are due to formation of a protective film on the copper surface.

2. The nature of this film proved to be a complex between copper and BTA. The surface film proved to be a Cu(I) complex and identical to the complexes prepared by precipitation from the solution.

3. Two different kinds of Cu(I)-BTA, were identified. When the solution is free from Cl^- as a small amount of Cl^- is available, the complex has a stoichiometric formula of one atom copper to one BTA molecule. In the presence of large amount of Cl^- ions, however, the complex formed has a stoichiometric formula of Cu_2Cl BTA.

4. Infrared spectroscopy of these complexes showed that the hydrogen bonded to nitrogen in BTA molecule is replaced by copper atoms.

5. The complexes proved to be sensitive to atmospheric oxidation. The oxidation degrades the protective film and the oxidized film could be washed or wiped off easily.

6. The mechanism by which complexes are formed is disproportionation of cuprous oxide to copper metal and cupric ions. In the presence of chloride ions, the complex film probably forms via an intermediate stage of CuCl formation. The thickness of the film, in the case of sufficiently large reservoir of inhibitor and chloride ions, depends upon

concentration of cupric ions in the solution and hence the thickness of Cu_2O on the original surface. Artificially addition of Cu^{++} ions in such a solution results in formation of extremely thick films. Therefore, it is concluded that the important factors affecting the film thickness are: (a) pH of the solution; (b) thickness of the Cu_2O; (c) and concentration of chloride ions.

7. Treatment of copper-nickel alloys and brass with BTA solution showed that the predominant protective film is a copper complex, hence the only copper is responsible for film formation, particularly in the case of copper-nickel alloys. In the case of pure zinc and brass, it was found that BTA is capable of forming a complex of Zn-BTA on pure zinc and to smaller extent on brass.

CHAPTER SEVEN

STUDY OF THE FILMS FORMED BY 2-MERCAPTOBENZOTHIAZOLE ON COPPER AND ITS ALLOYS

This chapter describes a study of films formed on copper, brass, and copper-nickel alloys by the interaction of 2-mercaptobenzothiazole (MBT) with the relevant surfaces, using X-ray induced photoelectron and Auger electron spectroscopy (XPS and X-AES), together with multiple reflection infrared spectroscopy. This study was carried out primarily in order to compare the behaviour of this inhibitor with that of BTA, in respect of film formation and film structure. Other related compounds such as 2-mercaptobenzimidazole (MBIA), have also been used to clarify the Cu-MBT interaction.

The procedure for obtaining XPS and X-AES spectra was identical to that used for BTA described in the previous chapter. In this case again, two types of samples were used, namely, those polished and those covered with electrochemically grown Cu_2O. Samples were immersed in a saturated solution of MBT in a variety of conditions and then the ESCA spectra were run. Since the solubility of MBT is very small, saturated MBT solutions were used throughout this study. The solutions were purged with nitrogen and the temperature of the solution was kept at $25^{o}C$, using a thermostatic water bath.

7.1 Structure of the Films

Since it is established in the case of BTA, that this inhibitor exercises its protection through formation of a Cu(I)-BTA film, the objection of the present study would be to establish the existence of a surface film on copper samples after being treated with MBT solution, the oxidation state of copper in the surface film, its stoichiometry and finally its mechanism of formation. Existence of a surface film was proved using XPS, X-AES and infrared reflectance spectroscopy as for BTA.

7.1.1 Oxidation State of Copper in Surface Film

The photoelectron spectra of MBT treated copper showed no major differences to untreated samples in the Cu2p region despite prolong exposure to the treatment solution. Figure 7.1(a) shows an XPS spectrum of a polished and argon etched copper sample in Cu2p region. Figure 7.1(b) shows an XPS spectrum of a Cu_2O sample and 7.1(c) shows the same sample after being treated with a saturated solution of MBT containing 0.5 M. NaCl, at pH~3 for 40 hours. The existence of a surface film on the last sample was proved by appearance of S 2p and N 1s and enhancement of C 1s peak in XPS spectrum. X-AES spectrum of this sample supported existence of a Cu-MBT film as will be discussed later. The spectrum shown in Figure 7.1(c) shows the nature of Cu in the film is either Cu(0) or Cu(I) but no trace of Cu(II) is observed in the spectrum. In fact, all samples treated with MBT solution in different conditions, showed no cupric species in the XPS spectra.

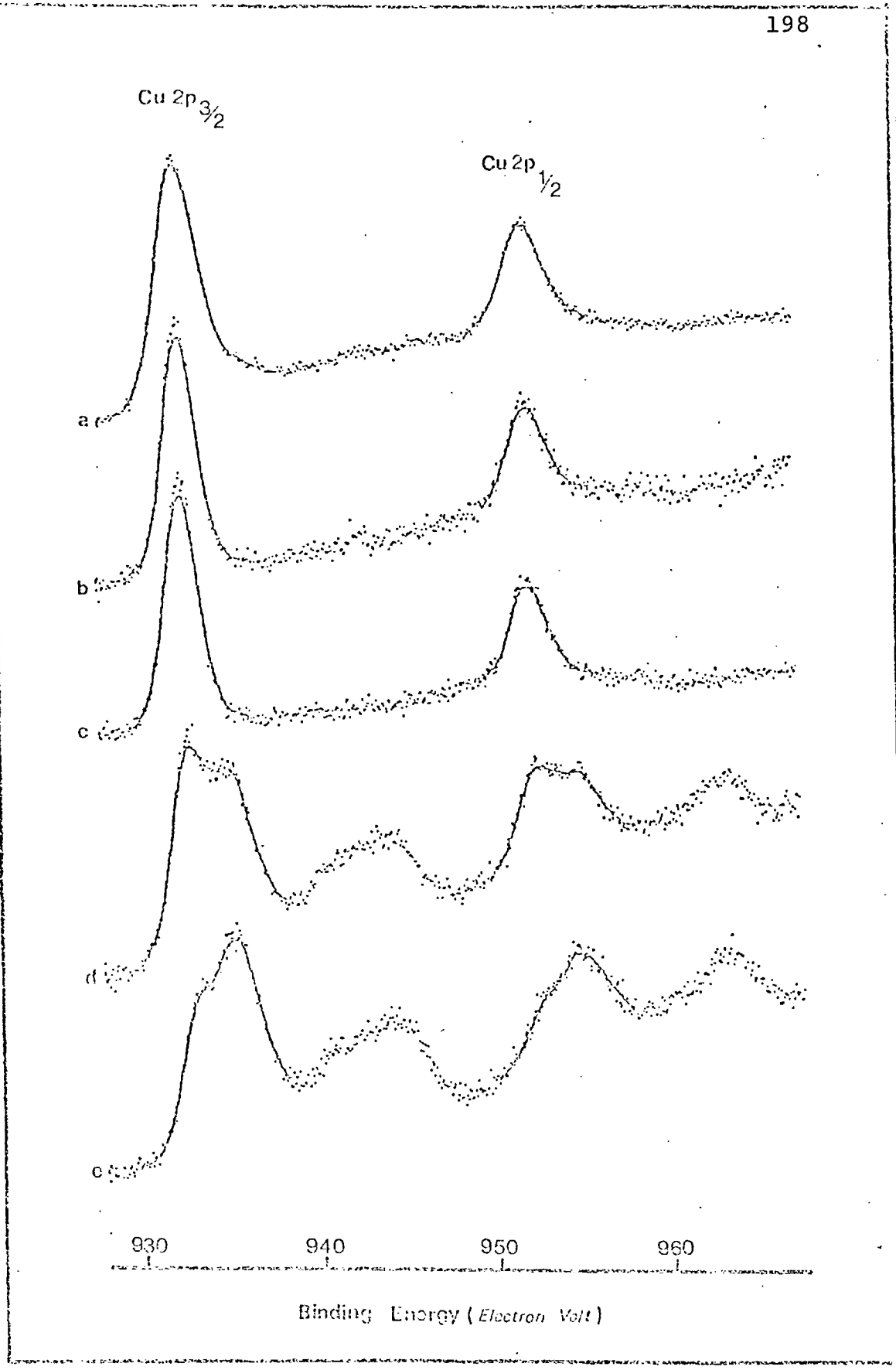


Figure 7.1: X-ray photoelectron spectra of copper sample (a) polished and argon etched; (b) Cu_2O; (c) treated with MBT solution (pH≈3) for 40 hours, (d) exposure of sample (c) to air for 48 hours; (e) exposed to air for 5 days.

In all these spectra, shake-up satellites which are characteristic of Cu(II) compounds were absent and binding energy of Cu2p XPS peaks showed values characteristic of Cu(I) compounds. In addition no correlation was found between the exposure time and the amount of CU(II) species, which are absent in all cases from the MBT treated samples.

Although XPS spectra can differentiate easily between Cu(I) (or Cu(O)) and Cu(II) compounds, it fails to distinguish between Cu(O) and Cu(I) as discussed in the previous chapter. In this case again, like BTA, X-AES spectra showed major differences between metallic copper, Cu(I) and the copper complex. Figure 7.2(a) shows an X-AES spectrum of a polished and Argon ion etched copper sample, Figure 7.2(b) shows X-AES spectrum of a Cu_2O sample and 7.2(c) shows the result of 10 minutes treatment of this sample with MBT solution at pH~3. Appearance of a new peak at 916.7eV k.e. is due to Cu-MBT surface film and its kinetic energy is in the range of Cu(I) compounds and not Cu(O)(see Appendix B).

Thus, the immediate conclusion is that the Cu-MBT surface film resulting from the interaction of MBT with copper sample is a Cu(I) compound which could be identified directly using the X-AES method. The surface film is always a Cu(I) compound regardless of conditions and exposure time.

7.1.2 Stoichiometry of Cu-MBT Surface Films

ESCA analysis of surface films grown "infinitely thick" using Wagner (34) and Jørgenssen (35) signal intensity ratios showed that there is one copper atom to

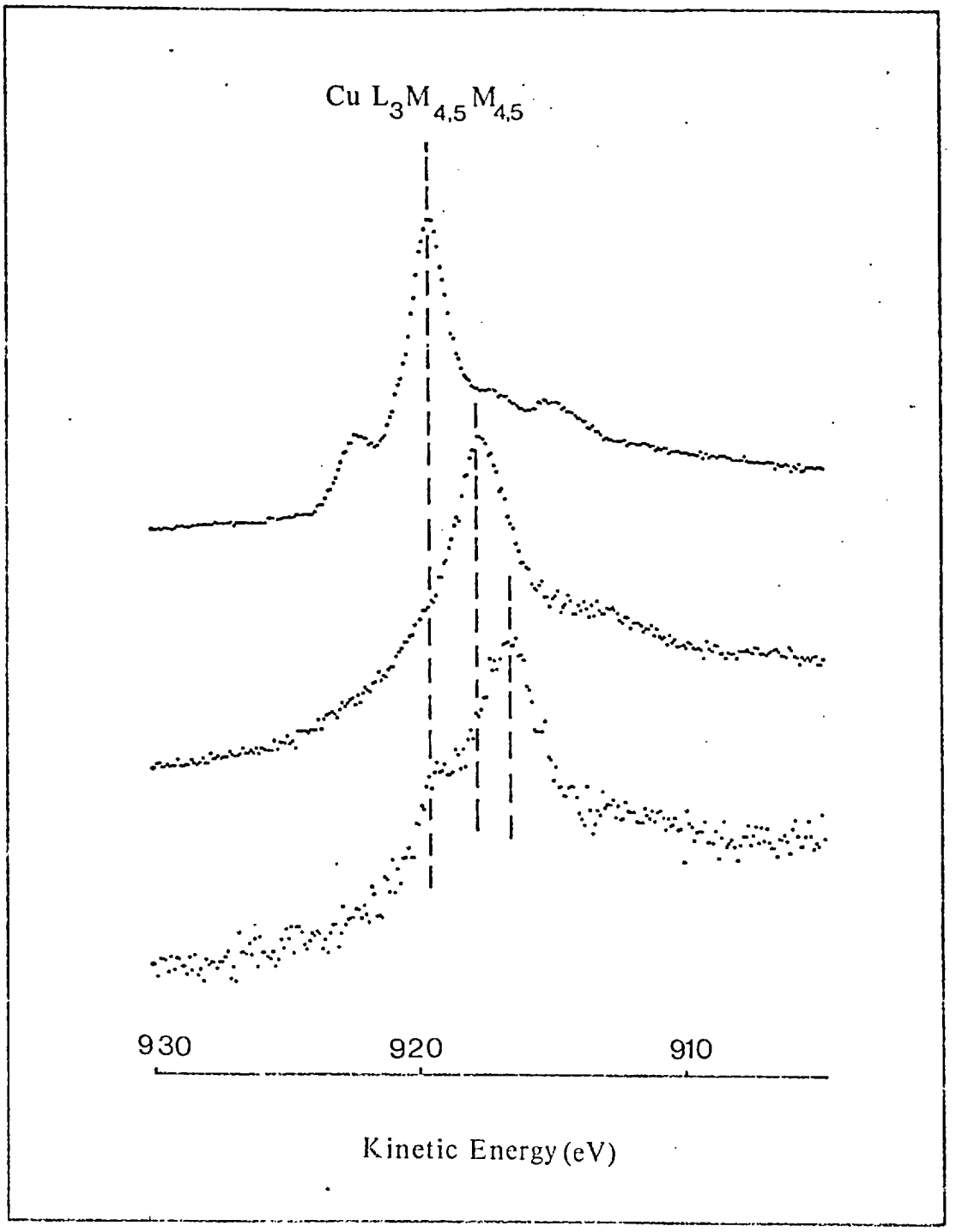
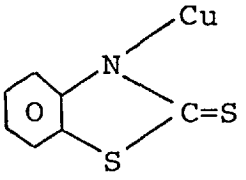


Figure 7.2: X-ray induced Auger spectra of copper sample: (a) polished and argon etched, (b) Cu_2O; (c) treated with MBT solution (pH≈3) for 10 min.

one BTA molecule in all cases (see Table 7.1). No chlorine was detected even when films were formed in the presence of high concentration of Cl^-, in contrast with BTA. Results from I.R. reflectance spectroscopy of these films as will be discussed later, showed that hydrogen in heteocyclic ring of MBT molecule is replaced with copper. This suggests a formula of



Inertness to the most chemical solvents suggests that perhaps the complex is not a salt but rather a "polymer".

7.1.3 Binding Energies of Surface Films

Binding energy measurements of S, N, and Cu based on C 1s at 285.0 eV for MBT, untreated copper samples, and treated samples showed no major differences. $Cu2p_{3/2}$ binding energies were measured to be 932.9 eV for both treated and untreated samples. S 2p binding energies in MBT and the surface film were found to be the same, having a value of 164.1 eV. The only difference was observed was between the N 1s binding energies, which was measured to be 399.8 eV for MBT and 400.1 eV for surface film. This indicates C=S bond probably remains intact, on film formation and replacement of H in -NH group of the MBT, gives rise to a difference in binding energy of N 1s. All binding energies for different peaks are given in Appendix B .

7.1.4 Air Oxidation of Cu-MBT Surface Films

The samples treated with MBT proved to be sensitive to exposure to air, during which, oxidation of Cu(I) to Cu(II) takes place, as was the case for BTA. However it appeared that for MBT the films were less sensitive to air, and it takes a longer time to reach a completely oxidized surface, compared to BTA. Figure 7.1(c) shows an XPS Cu2p spectrum of a copper sample after being treated for 40 hours with MBT. X-AES spectrum of this sample showed that it is covered with a Cu-MBT complex. Exposure of this sample to air for 48 hours results in the formation of some cupric compound on the surface as is evident by the appearance of a shoulder on the main peak at higher binding energy and also the appearance of shake-up satellites. Figure 7.1(d). Exposure to air for 5 days resulted in an increased intensity of the cupric peaks, Figure 7.1(c).

No change was observed in the other peaks except for S2p XPS spectrum due to atmospheric oxidation. Figure 7.3(a) shows an XPS spectrum of the S 2p for MBT (binding energy is corrected for charging effects). The slight assymmetry exists in this peak could be due to two different S groups. Figure 7.3(b) exhibits the S 2p spectrum of the above copper sample, which was treated with MBT for 40 hours. Next the sample was exposed to air for 48 hours. Figure 7.3(c) shows the result of this exposure, the main change being the appearance of a shoulder on the higher binding energy side of the main peak. Figure 7.1(d) shows the XPS spectrum of Cu2p of this sample at the same stage of oxidation. Finally 5 days exposure to air results in an increased intensity of this shoulder up to almost 1/3 of the main peak (Figure 7.3(d)). Prolong exposure to air

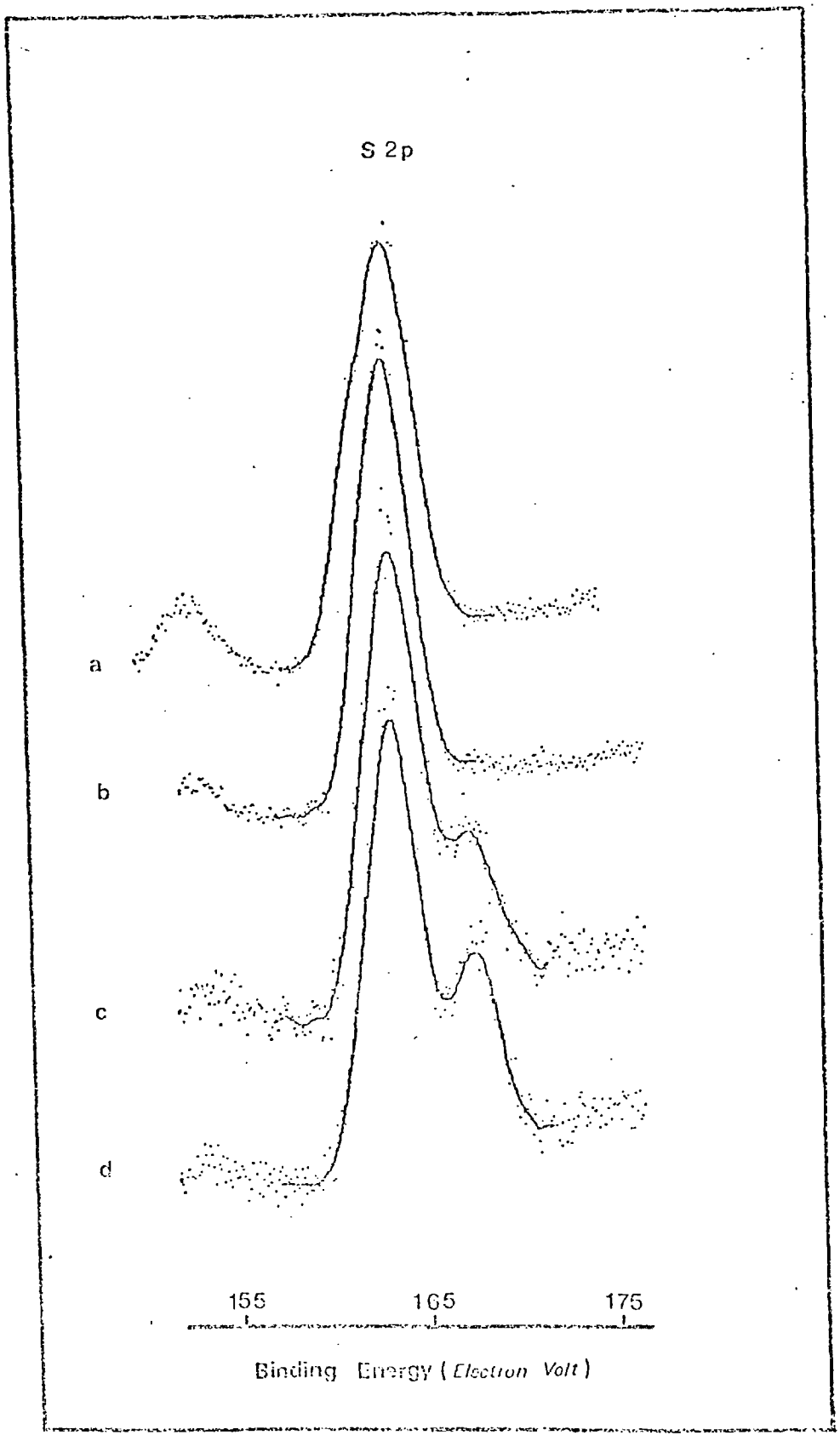


Figure 7.3: XPS spectra of : (a) MBT, (b) copper sample treated with MBT for 40 hours (corresponds to 7.1(c)); (c) exposed to air for 48 hours; (d) exposed to air for 5 days.

does not result in any further increase in the intensity of this peak. It was found that the relative intensity of this new peak never increases beyond 1/3 of the main peak whereas almost all Cu within escape depth of the Cu photoelectron was oxidized. The reproducibility of these results indicates that the difference in S 2p peaks intensities is a true reflection of surface chemistry and not because of S electron escape depth. In view of this, it can be safely concluded that only one atom sulphur out of four undergoes oxidation.

7.1.5 Oxidation of Chemically Prepared Cu-MBT Complexes

Solution prepared Cu(I)-MBT complexes from a solution of copper(I) salt with addition of MBT solution, were examined to determine the binding energies, stoichiometry and the behaviour of these complexes with respect to air oxidation. The complexes proved to be identical to surface films in every respect. ESCA quantitative analysis of Cu(I)-MBT complexes showed a stoichiometric ratio of one atom copper to one molecule of MBT as was the case for surface films (see Table 7.1 for ESCA and also chemical analysis).

Interestingly, the complexes prepared from cupric salts and MBT, showed XPS spectra characteristic of cuprous compounds. XPS spectra of complexes prepared from Cu(II) salts were identical to those prepared from Cu(I). This is not a unique property of MBT, since there are other organic compounds, such as triethylamine, which exhibit the same behaviour. It has been reported (96) that triethylamine forms a 1:1 complex with copper(I) salts, while at $-45^{o}C$ cupric salts form a yellow green complex $CuCl_2$ $2Et_3N$

Element	Sensitivity Peak Heights *	Peak heights (found)	Ratio for 1 atom) Cu	Chemical Analysis ** (calculated)	Chemical Analysis (found)
C	0.27	$\frac{14.7}{32}$	6.2	36.5	36.7
N	0.4	$\frac{7}{64}$	0.99	6.0	5.4
H	-	-	-	1.7	1.9
Cu(I)	3	$\frac{13.3}{16}$	~~0.2077~~ (1)	27.7	26.9
S	0.35	$\frac{12.4}{64}$	1.99	27.8	-

Table7.1: ESCA and Chemical Analysis of Cu(I)-MBT complex.

*- All values of sensitivities are given by Jørgensen (35)

**- Calculation based on Cu MBT

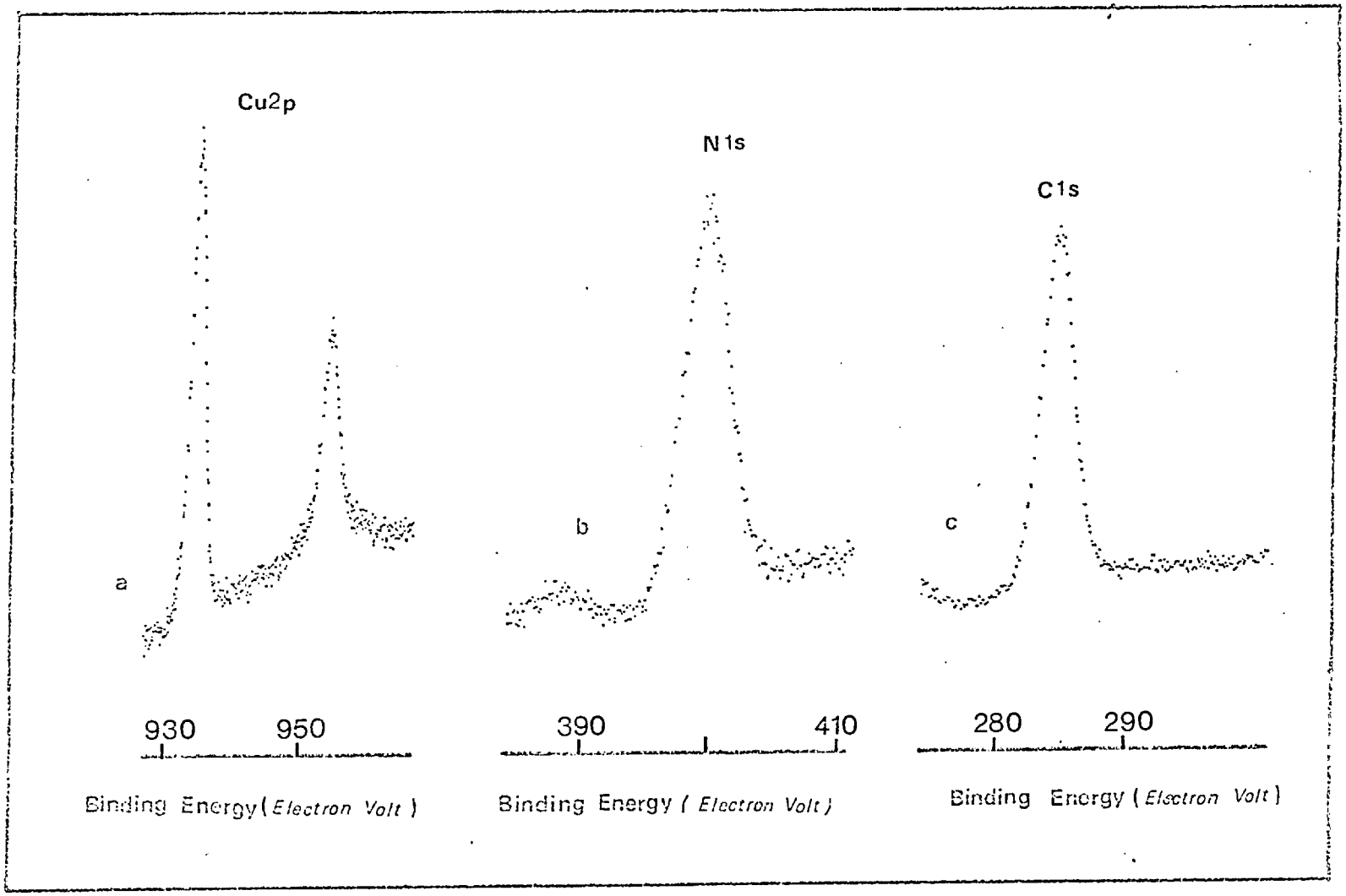


Figure 7.4: XPS spectra of Cu2p (a); N 1s (b) and C 1s (c) of a Cu(II)-MBT complex

which, on warming to $0^{o}C$, undergoes an internal electron transfer to give CuCl NEt_3.

Similar reaction must take place immediately after formation of a Cu(II)-MBT complex, since it transforms to a Cu(I)-MBT complex as demonstrated by its XPS spectra (Figure 7.4).

Solutions prepared Cu(I)-MBT complexes undergo oxidation on exposure to air. However it takes much longer for complete oxidation than the BTA case (about 20 days). Again it was shown in this case that only one sulphur out of four undergoes oxidation. Figure 7.5(a) and 7.6(a) show XPS spectra of Cu and S 2p of a Cu(I)-MBT complex before oxidation and Figure 7.5(b) and 7.6(b) shows the same sample after being exposed to air for 20 days. Prolong exposure to air did not result in any change in the ratio of two sulfur peaks. These sulfur peaks are very useful in clarifying the structure of Cu-MBT complexes, as will be discussed later in detail.

7.1.6 I.R. Reflectance Spectroscopy of the Cu-MBT Films

An I.R. absorption spectrum of solid MBT was obtained using a K Br pellet. Fig. 7.7(a) shows a typical spectra. The spectrum shows a broad, multipeaked band between 2500-3450 cm^{-1}. This arises from the N-H and C-H stretching vibrations. The stretching vibration of C-H band appears as a weak band near 3000 cm^{-1}. Most of the bands between 800-2000 cm^{-1} are due to the heterocyclic ring and those around 750 cm^{-1} probably arise from out-of-plane C-H vibrations in the aromatic ring.

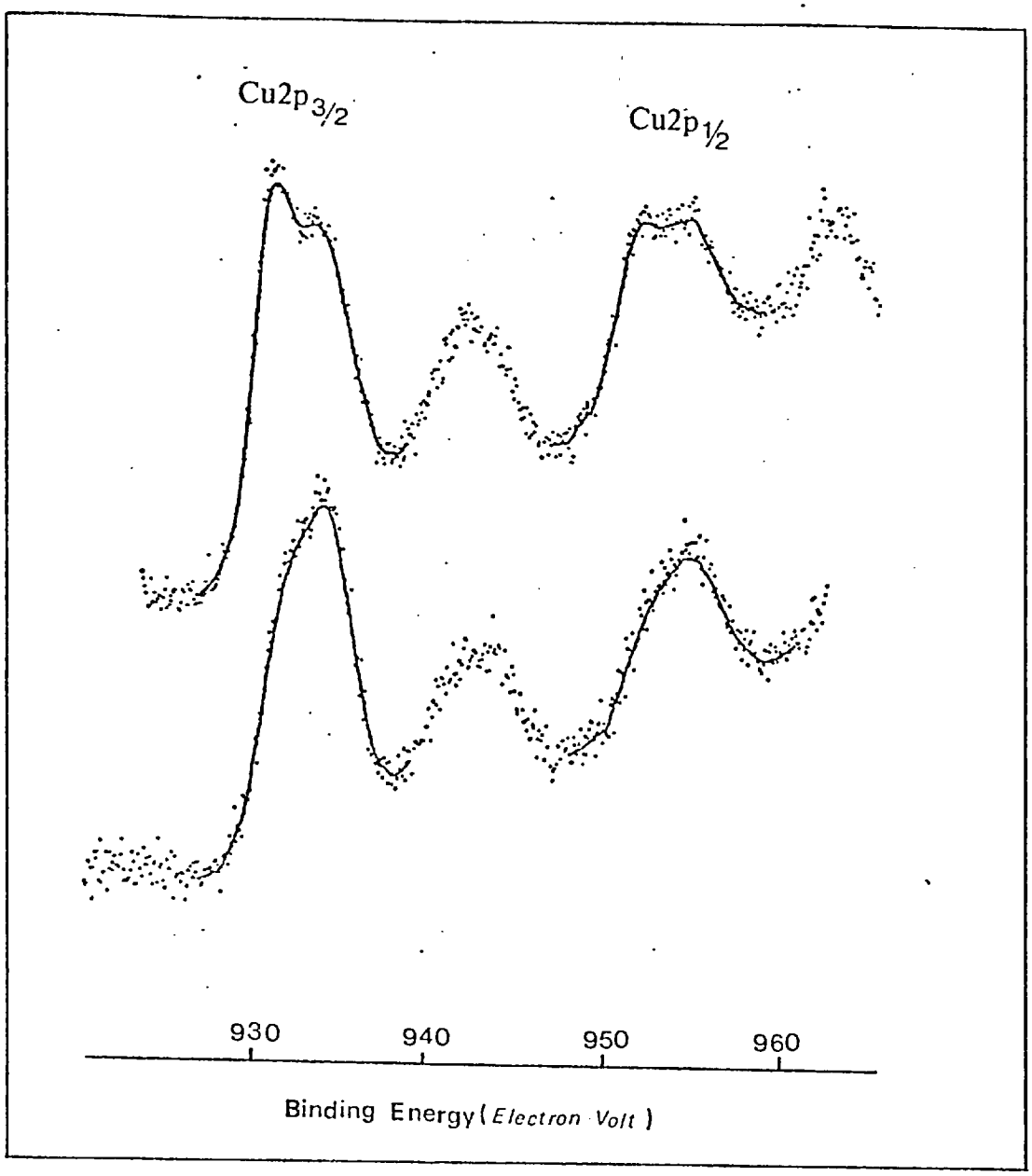


Figure 7.5: XPS spectra of Cu(I)-MBT complex: (a) before atmospheric oxidation, (b) after oxidation.

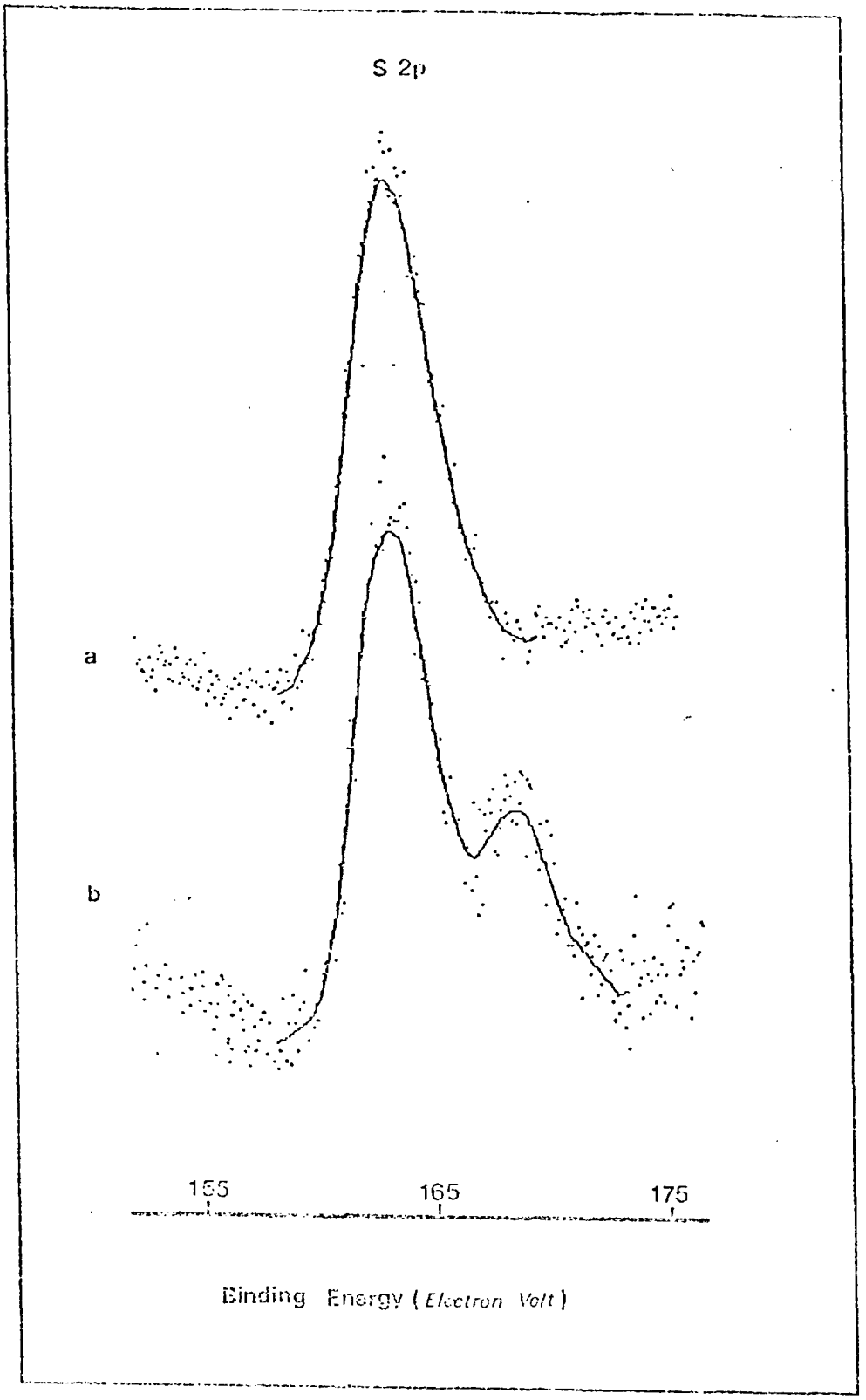
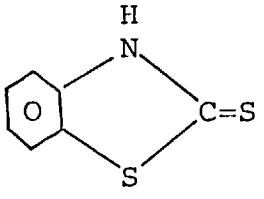


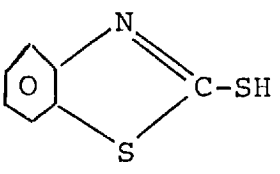
Figure 7.6: XPS spectra of Cu(I)-MBT complex; (a) Before atmospheric oxidation, (b) after oxidation.

No evidence is found foran S-H stretching band which would be expected to appear at about 2500 cm^{-1}. MBT is not an exceptional case in this respect. Many similar molecules show very weak bands due to the S-H vibrations. For instance, 2-mercaptobenzoxazole, 5-chloro-2-mercaptobenzothiazole, and 2-ethoxy-2-mercaptobenzothiazole show no band due to S-H vibration and 2-mercaptobenzimidazole shows a very weak band around 2500 cm^{-1} due to S-H stretching vibration.

Tamura and Co-workers (97) have investigated the adsorption from aqueous solution of 2-mercaptobenzothiazole onto silver bromide. This compound and other similar materials have important stabilizing properties on photographic emulsions, and infrared spectroscopy was applied in an attempt to determine the modes of adsorption onto silver halide surfaces. According to these workers (97), infrared spectroscopyreveals that compounds such as this exist in the thio-lactam form;



rather than as the mercapto form presented below:



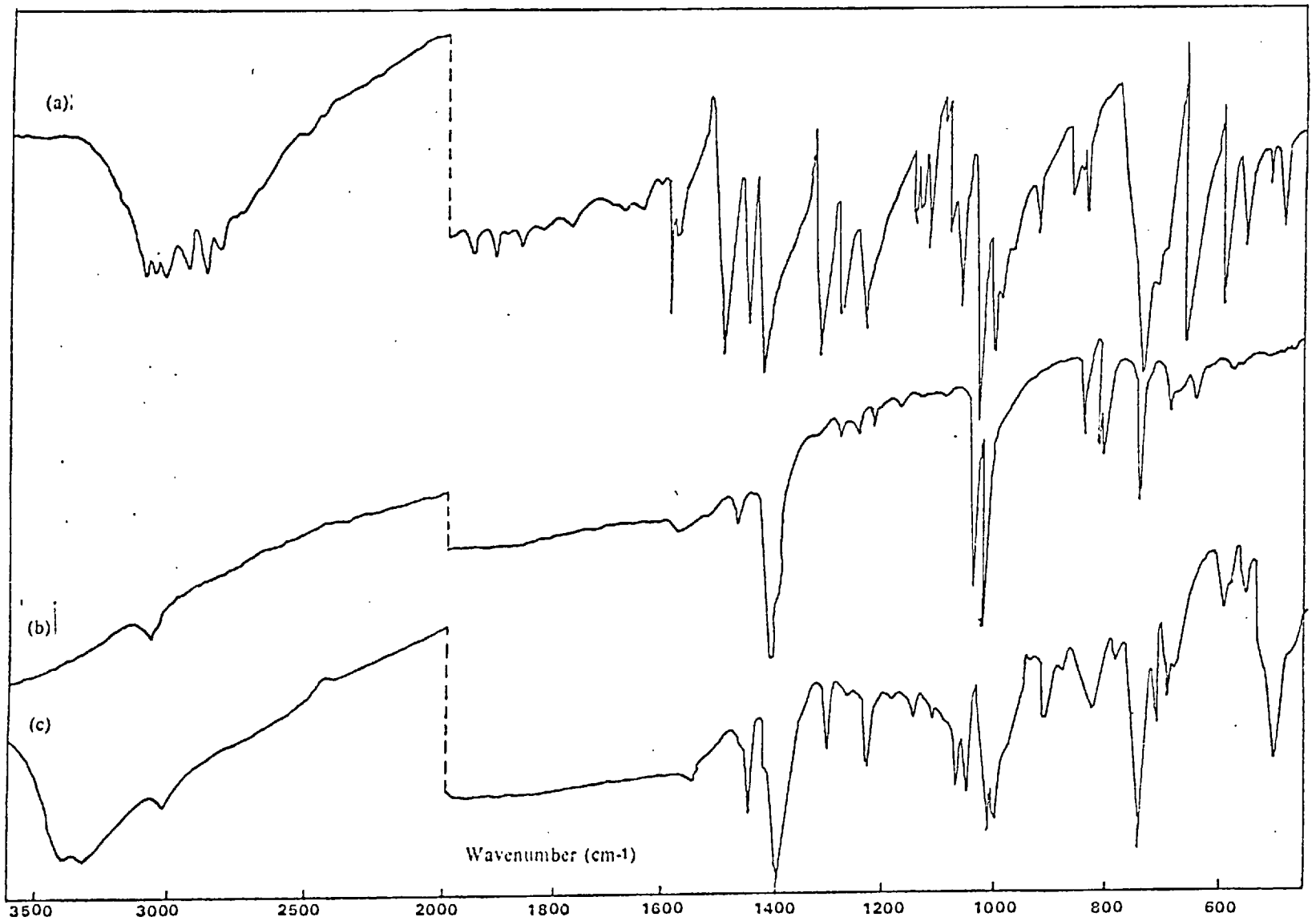
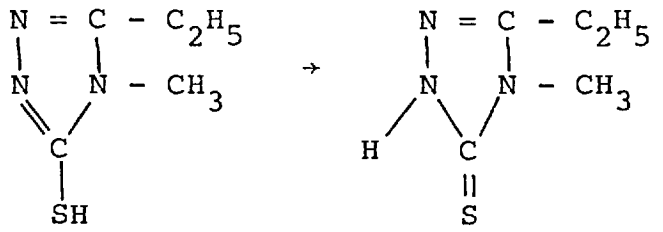


Figure 7.7: Infrared spectra of (a) solid MBT; (b) Cu(I)-MBT complex; (c) Cu(I)-MBT surface film.

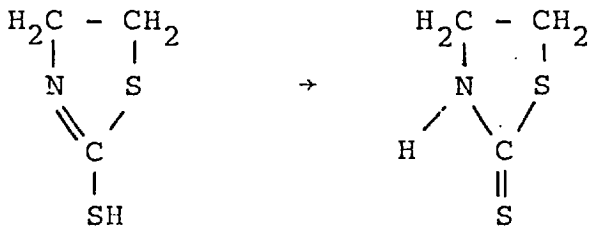
This is shown by the appearance of an adsorption band arising from the stretching of an NH group at about 31000 cm^{-1} for the solid and at about 3400 cm^{-1} for solutions in organic solvents. No S-H stretching band was observed.

When a solution containing silver ions was added to an aqueous solution of 2-mercaptobenzothiazole, a precipitate of silver-mercaptobenzothiazole was obtained. It was shown that the NH stretching band in the spectrum disappeared with the formation of the silver salt. Other changes occurred in the spectral region between 1600-1400 cm^{-1}.

Adsorption onto silver iodide of similar molecules, 3-mercapto-4-methyl-5-ethyl-,2,4-triazole(a) and 2-mercapto-thiazoline(b) has been reported by Little & Ottewill (98). The spectra showed that these compounds existed as the thiolactam form, since bands attributable to SH groups were missing, while other bands appeared which were associated with NH groups.



(a)



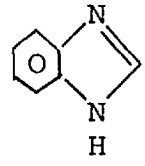
(b)

The infrared spectrum of the silver salts of these compounds showed that the hydrogen was replaced from the NH group by the silver in forming the salt. This was shown conclusively by the disappearance of the NH stretching band at 3140 cm^{-1}.

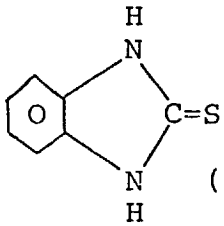
The same behaviour was observed in the case of copper salts in the present study. Complexes prepared from a solution of MBT and a Cu salt, showed the disappearance of N-H vibration stretching bands in the I.R. spectrum. Apparently, the hydrogens in these groups are replaced by Cu. Figure 7.7(b) shows an I.R. spectrum of Cu-MBT complex in K Br.

The spectra of Cu-MBT films formed on the copper sample after being treated with MBT solutions, closely resembled that of the Cu-MBT complex prepared by precipitation from solutions. In this case also, N-H stretching is absent from I.R. spectrum, showing the replacement of hydrogen by copper. Figure 7.7(c) shows an I.R. reflectance spectrum of a sample treated with a saturated MBT solution at pH~3 with 0.5M NaCl.

The reaction of related compounds such as benzothiazole, benzimidazole and its mercapto derivative with copper, showed the same behaviour. I.R. spectra of the complexes showed that in all cases, N-H stretching is absent from the spectra. I.R. spectrum of 2-mercaptobenzimidazole with structure formula of



or



(II)

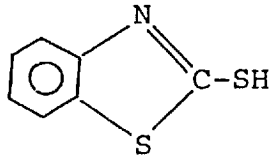
showed a small absorption due to the S-H vibration, which favours structure (II).

It is interesting to know that in reaction with copper,

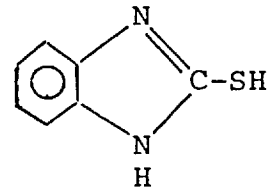
both hydrogens are replaced by Cu and no absorption band due to N-H (or possibly SH) was observed. Quantitative analysis by ESCA supported this replacement and showed there are two atoms of copper for one 2-MBIA molecule. All I.R. spectra of these compounds and of their complexes with copper are in Appendix D .

7.1.7 Structure of Cu-MBT Complex

The results obtaining from the oxidation of a Cu(I), MBT complex in air, Figure 7.6(a,b) showed that only one atom sulfur out of four undergoes oxidation. Since there are two sulfur atoms in a MBT molecule, this suggests a dimeric structure for the complex after being oxidized. However these results do not reveal which of the two sulfur atoms in the MBT molecule (shown below (I)), undergoes oxidation.



(I)



(II)

A similar compound 2-mercaptobenzimidazole (MBIA) in which the S atom in the heterocyclic ring is replaced by N, was used to clarify the oxidation situation, Cu-MBIA complexes were prepared and then exposed to air for a few months. At certain intervals, the sample was examined by XPS. Figure 7.8(a-c) shows the progressive oxidation of this sample using the XPS spectra in S 2p region, to

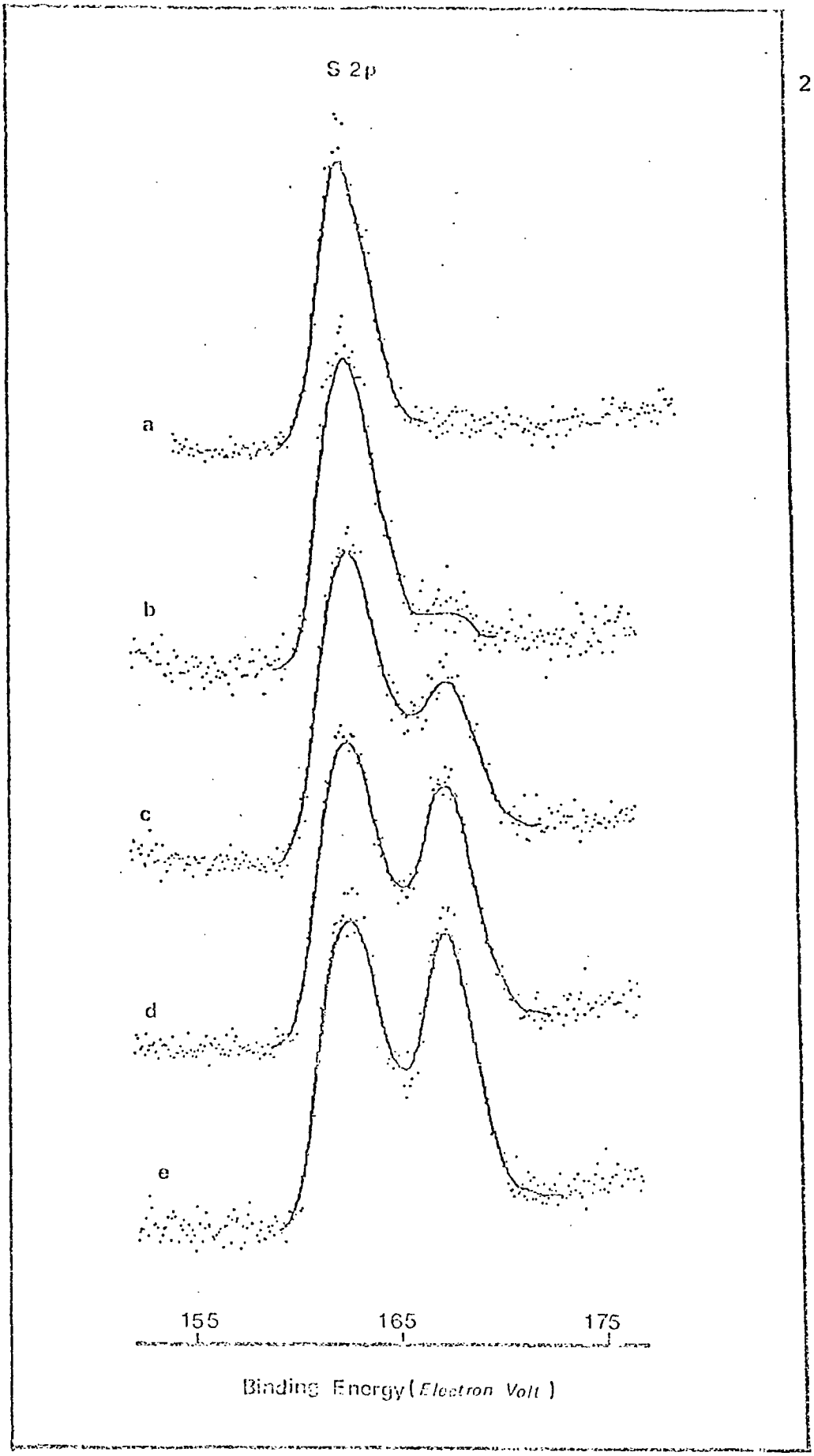


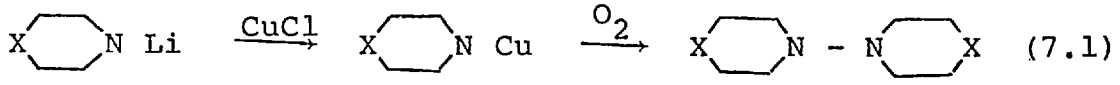
Figure 7.8: XPS spectra of (a) 2-MBIA; (b) Cu sample treated with MBIA and exposed to air for 2 hours; (c) exposed to air for 24 hours; (d) exposed to air for 10 days.

monitor the oxidation process. In this case, the intensity of the oxidized sulfur grows to an intensity almost equal to the unoxidized peak. This indicates that one out of the two atoms of sulfur has undergone oxidation. Prolong exposure to air does not result in any change in this ratio.

These results support the suggestions of a dimerization oxidation for both these complexes. Moreover, an important conclusion can be drawn from these results. That is to say that the S atom in the heterocyclic ring of the MBT molecule, remains intact on complex formation with Cu and after atmospheric oxidation. This is evident, when this S atom is eliminated as in MBIA, and subsequently this molecule reacts with copper. Quantitative ESCA measurements of the Cu-MBT complex dictate a stoichiometric formula of 1 Cu to 1 MBT. Thus, in order to satisfy the other results mentioned above, an oxidation-dimerization of Cu-MBT complex is proposed in which a copper atom is eliminated from the complex by the action of O_2, and two molecules of MBT subsequently form a dimerized molecule with structure of R-S-S-R where this compound in its turn can undergo oxidation to form either R-S(=O)-S(=O)-R or R-S-S(=O)-R. This oxidation process will be discussed later.

Oxidation and dimerization of organo-copper compounds have been investigated by Kauffmann et al (99). According to these investigators acetylenes can be dimerized by oxidizing their copper(I) compounds with oxygen. They also found that cyclic amines, imines and amidines, can be dimerized from their Cu(I) compounds on the reaction with oxygen. The amines were converted by phenyl-lithium into

the lithium amides, which on reaction at 20°C with one molar equivalent of CuCl, gave colourless Cu(I) compound (1). These suspensions became dark brown when oxygen is passed into them (1 h) and the reaction was lead to a hydrazine derivation of type (2) with elimination of copper from the molecule:

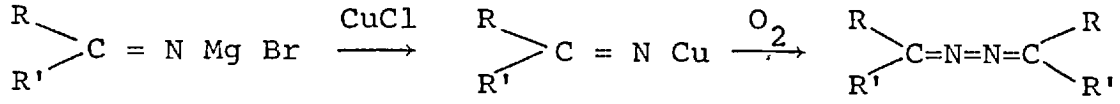


(1) (2) (7.1)

where

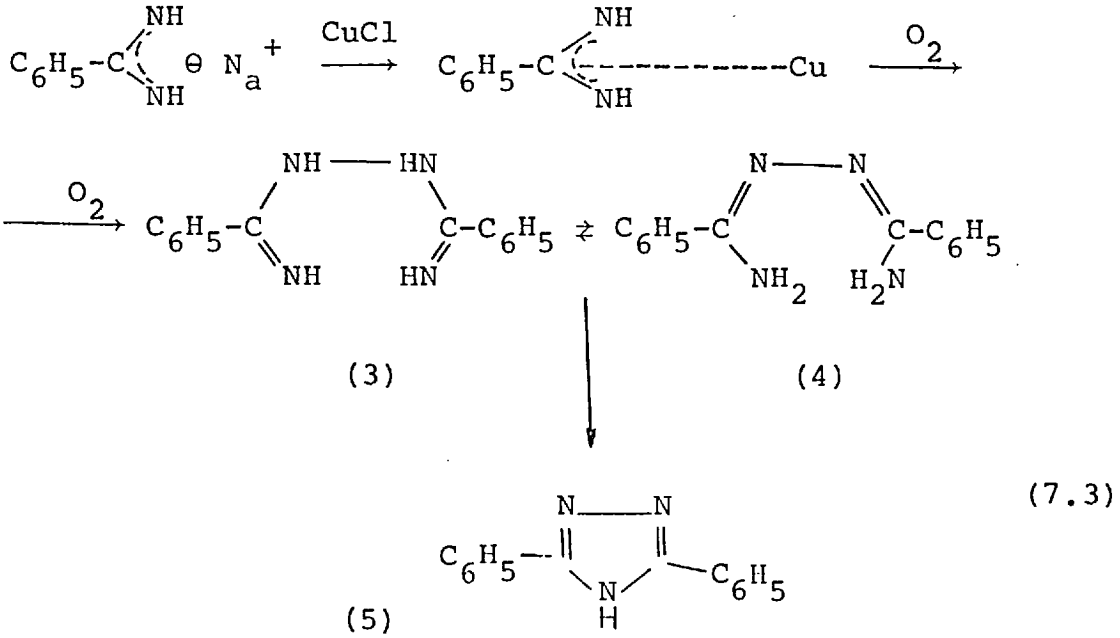
$X = O$ or $X = CH_2$.

Oxidation and dimerization of imines and amidines are similar to the reaction of amines, as are evident from equations (7.2) and (7.3).



(7.2)

where $R = R' = C_2H_5$ or C_6H_5

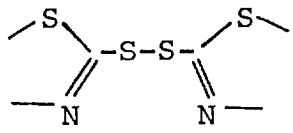


(3) (4) (7.3)

(5)

Dimerization of copper compound in this case results in formation of compound (3) or (4) which rapidly loses NH_3 to form a triazole of type (5).

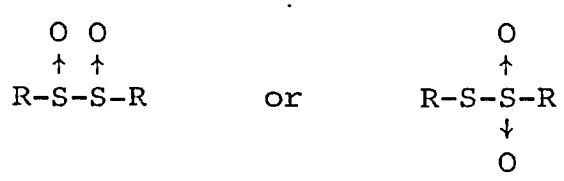
There are many more exmaples of oxidation-dimerization reaction (88), in which dimerization can take place through bond formation between C-C or N-N or S-S. Dimerization of MBT and also BMIA is through S-S bond formation with elimination of Cu from the molecule. Also there are reports (100) in which oxidative dimerization of MBT by oxidation agents such as H_2O_2 has been investigated. Ermakov et al (100) has shown that 30 minutes treatment of MBT in a Me_2CHOH solution at 60^oC with 5-10% H_2O_2 resulted in formation of a dimerized MBT with formula



It is interesting to note that a dimerized MBT, loses its ability to form a Cu complex. A purified dimerized MBT solution was added to a solution of copper salt, no complex formation was observed. Also no film formed on the copper samples treated with this compound.

The dimerized inhibitor, as stated already, can undergo oxidation, and this is the case for MBT and MBIA. Study of the S 2p XPS spectra of S groups in these compounds before and after oxidation and comparing them with Cu spectra showed that there is no correlation between the rate of the oxidation of S and Cu (compare Figures 7.5(a) and 7.6(a)). This is what one would

expect, because oxidation of copper takes place with dimerization, then S undergoes oxidation. The dimerized compound can be regarded as R-S-S-R. Clearly two possible structures could be suggested for the oxidation of the sulfur atoms



(I) (II)

Axelson and co-workers (101) using ESCA, studied the oxidation products of different disulfides, and reported that the oxidation of these compounds, to give either (I) or (II), would yield different spectra. In fact, structure (II) was confirmed. A shift of about 4.0 eV was reported as due to the oxidation of the S atom. (see also Chapter 4 for detail).

This is also the case for the oxidized Cu-MBT complex. There are four S atoms in the complex and the two mercapto-S atoms (after forming a bond), undergo oxidation and as a result, one of them reacts with two atoms of oxygen. In other words, one out of four S atoms oxidizes. The binding energy of this oxidized S shifts towards the higher binding energy by as much as 4.8 eV (see Appendix 1). The same is true in MBIA case.

To determine the properties of the surface films resulting from air oxidation of Cu(I) complexes, thick Cu(I) MBT films were grown on the surfaces and then exposed to air for a long period of time (say 5 days). This showed that, as in the case of BTA, these Cu(II) films

only form on the top of the Cu(I) films and can easily be wiped or washed off. Figure 7.9(a) and 7.10(a) show the XPS spectrum of Cu2p and S 2p of an oxidized surface film, and Figure 7.9(b) and 7.10(b) show the same sample after being washed with water. Apparently the amount of Cu(II) and oxidized sulfur is reduced to very small quantities. If the sample is exposed to air again, the under layer Cu(I)-MBT is now directly exposed to air and can undergo further oxidation. Figure 7.9(a) and 7.10(c) show the result.

Identical results were obtained for the oxidized surface when the outer layer is wiped off with a dry tissue. Figure 7.11(a) and 7.12(a) show the XPS spectra of an oxidized complex film on a copper sample in Cu and S 2p region. Figure 7.11(b) and 7.12(b) show the result of wiping this sample. On exposure to air the under layer Cu(I) complex, undergoes oxidation as is evident by reference to Figure 7.11(c) and 7.12(c).

These results are consistent with the oxidative-dimerization mechanism explained earlier, in which two molecules of inhibitor in the complex form a dimerized molecule, while Cu is eliminated from the molecule, and oxidizes to CuO. This process naturally takes place at the top of the film at the film-air interface. The thickness of this film even after a long exposure to air does not quite exceed the escape depth of Cu photoelectron (see Figure 7.1 and 7.5) and protects the under layer from being oxidized to some extent. On immersion in an aqueous solution (washing solution at pH~7) both dimerized inhibitor

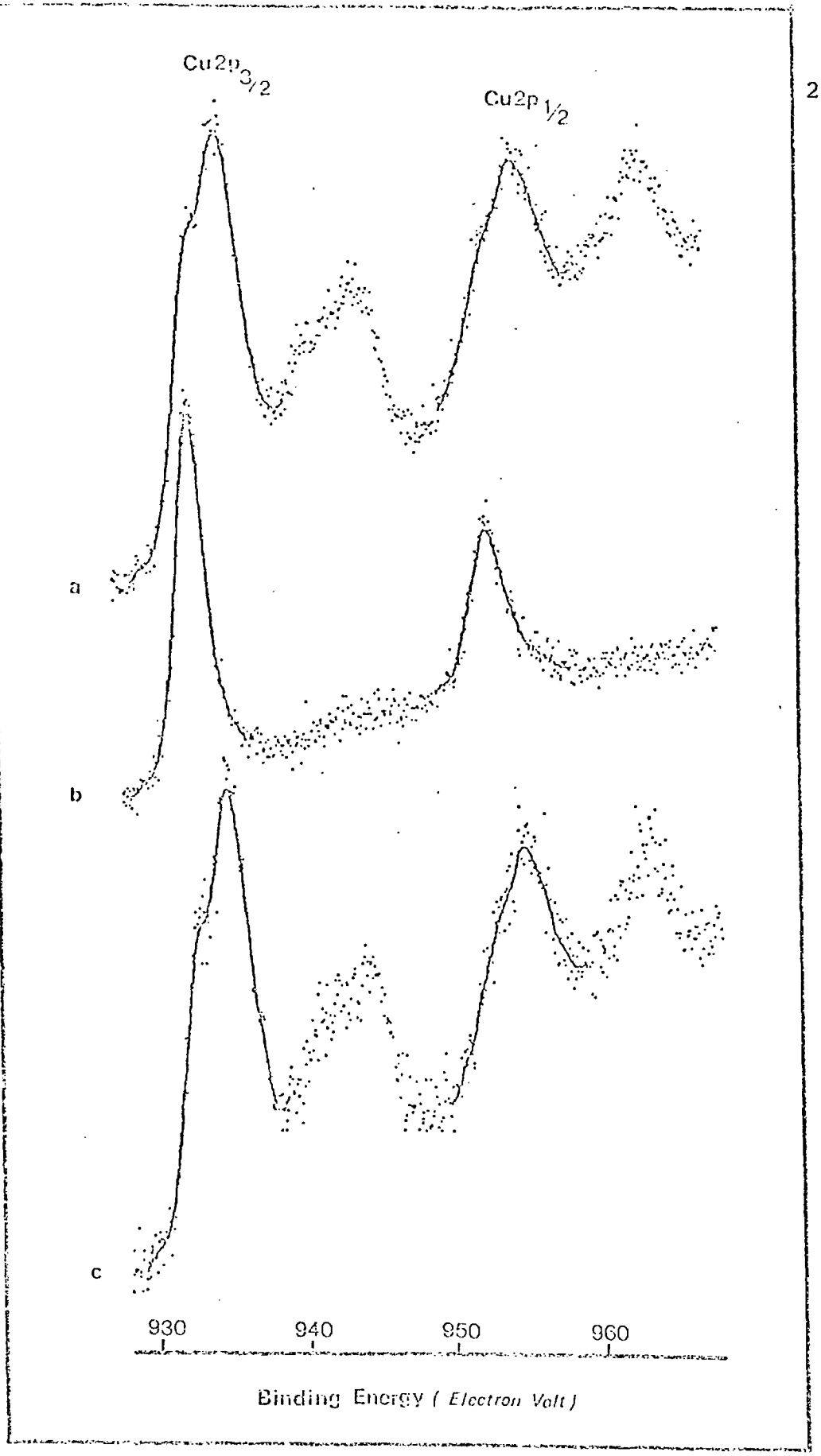


Figure 7.9: XPS spectra of: (a) oxidized surface film; (b) the same sample after being washed; (c) sample (b) exposed to air again.

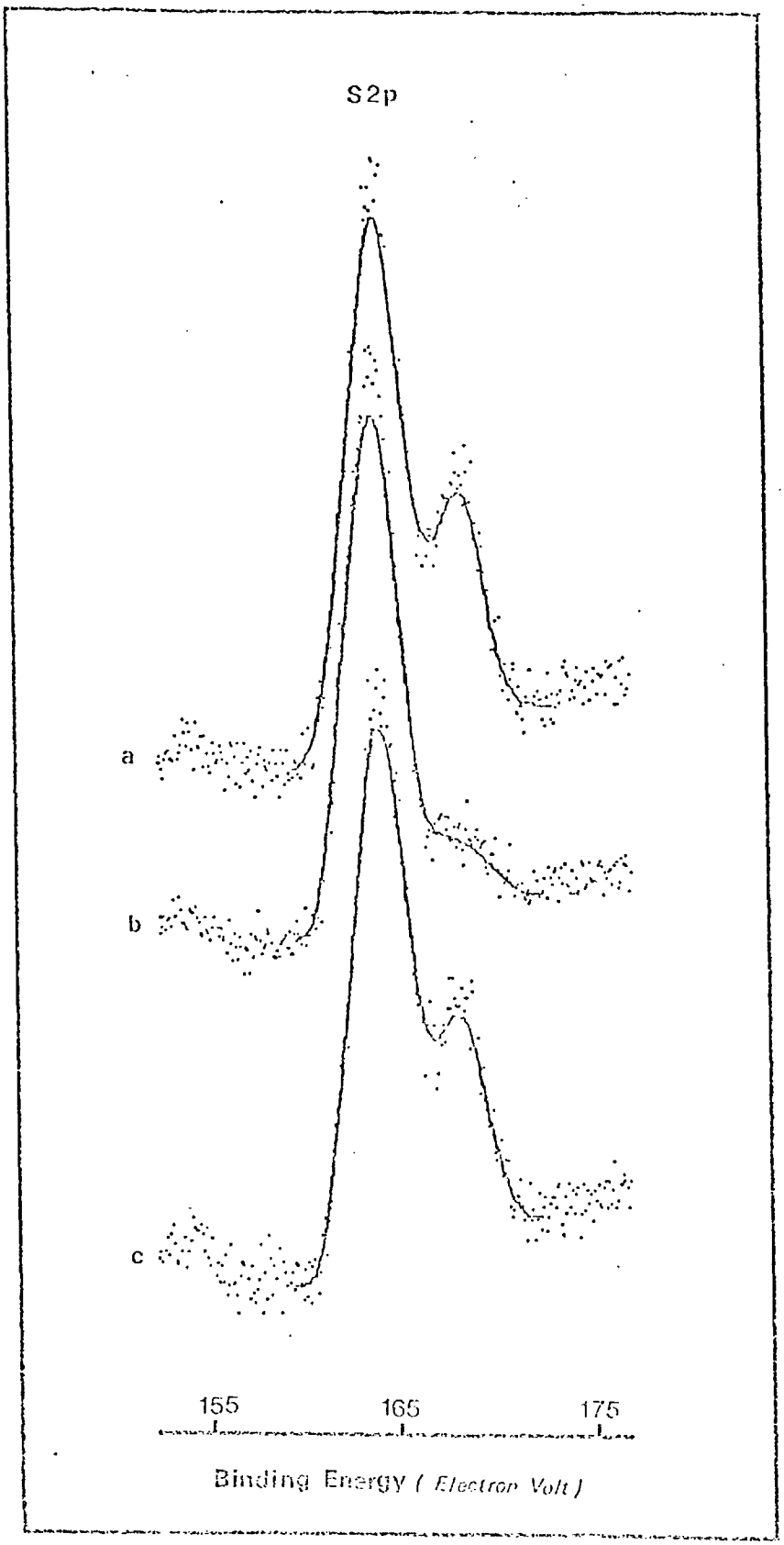


Figure 7.10: XPS spectra of : (a) oxidized surface film; (b) the same sample after being washed; (c) sample (b) exposed to air again.

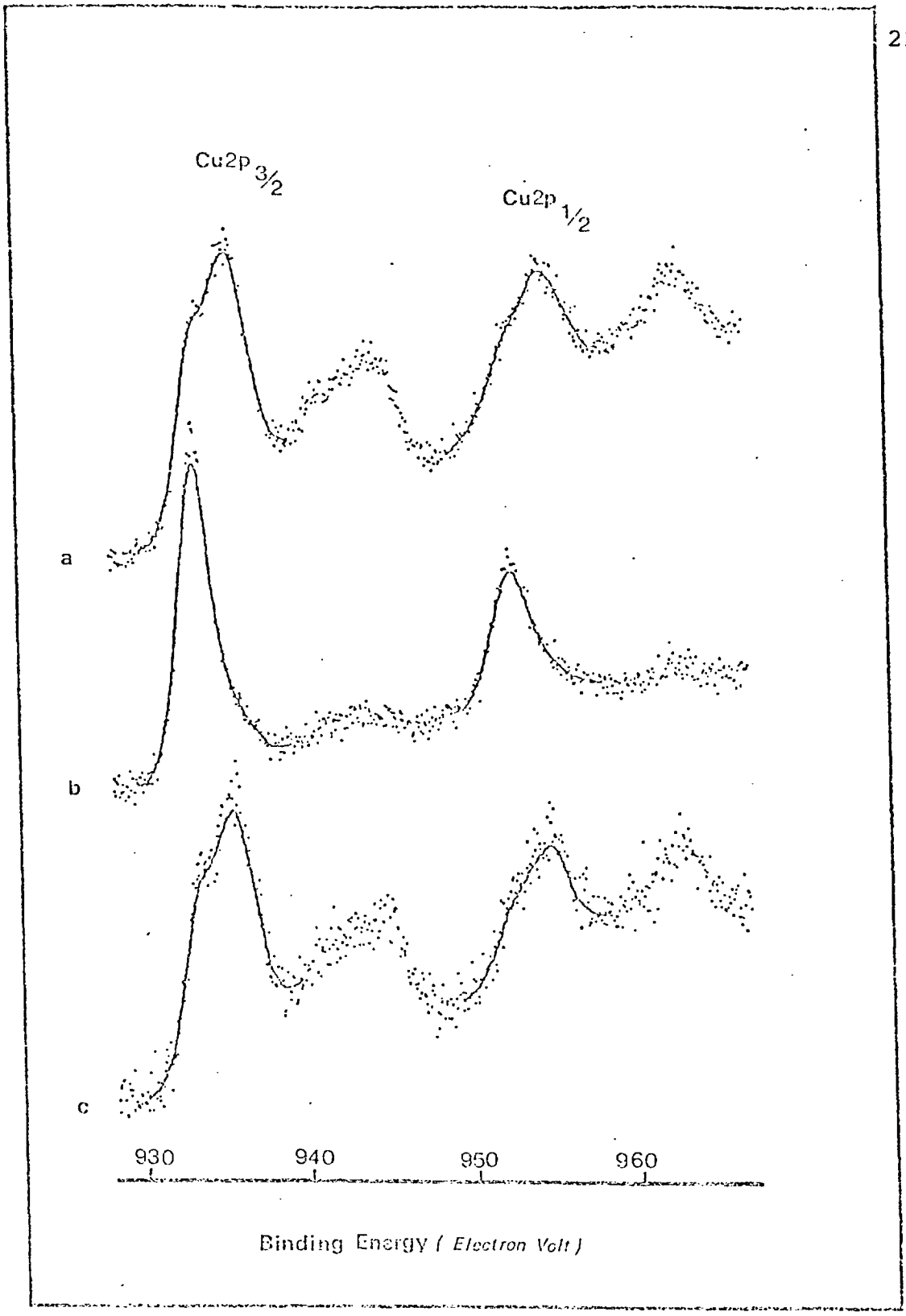


Figure 7.11: XPS spectra of : (a) oxidized surface film; (b) the same sample after being wiped; (c) sample (b) exposed to air again.

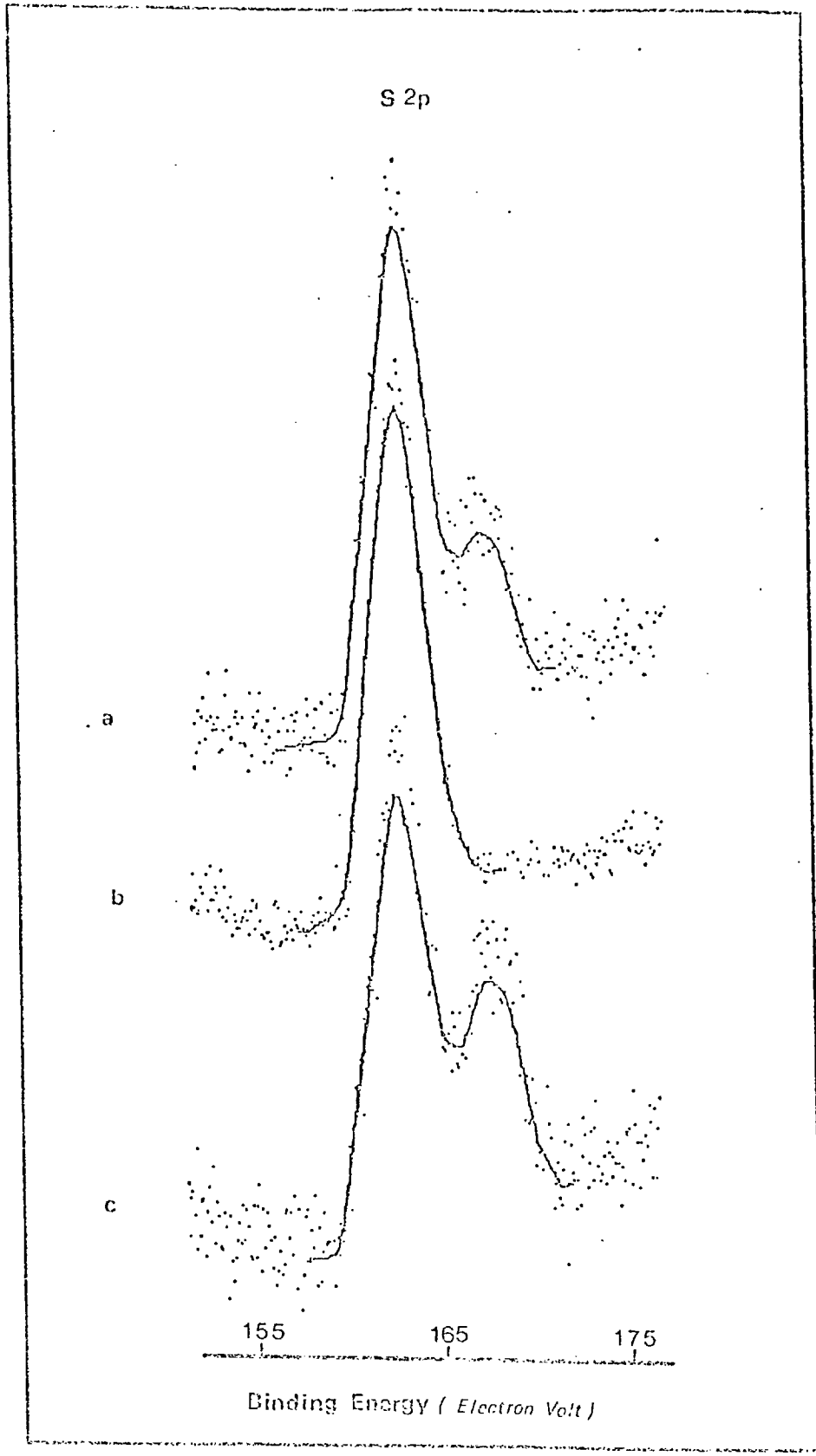


Figure 7.12: XPS spectra of : (a) oxidized surface film; (b) the same sample after being wiped; (c) sample (b) exposed to air again.

and CuO dissolve and leave a Cu(I)-inhibitor complex under layer. Solubility of CuO can be obtained from equation (7.1) according to Pourbaix (86)

$$CuO + 2H^{+} \rightleftarrows Cu^{++} + H_2O, \quad Log[Cu^{++}] = 7.89 - 2pH \qquad (7.1)$$

Therefore, at pH = 7,

$$[Cu^{++}] = 10^{-6.11} \text{ M}.$$

This figure shows that at least one thousand Å of CuO film from a 1 cm^2 sample immersed in 1 litre pure water can dissolve. This shows that a pre-treated sample which is exposed to air frequently, will lose its protection soon, if the protective Cu(I)-inhibitor complex film is not repaired.

7.1.8 O 1s XPS Spectra of Cu-MBT Complex Films

An oxygen 1s peak in the XPS spectra of the Cu-MBT complex is always present. Since this peak could be due to oxygen or water adsorbed onto the surface and not associated with the complex molecule, attempts were made to remove thin layers from the top of the complex films to examine the inner layers. Argon ion bombardment of the surface for a short time, using the lowest possible energy (i.e. 1 kv and 8μA for 30 seconds), resulted in the removal of a thin layer. This reduced the S 2p, Cls, Nls and Ols peaks at the similar rate. The persistence of the Ols peak in these spectra, and the reproducibility of the results suggests that H_2O is infact involved in the surface film. Figure 7.13(a) shows an XPS spectra of copper sample

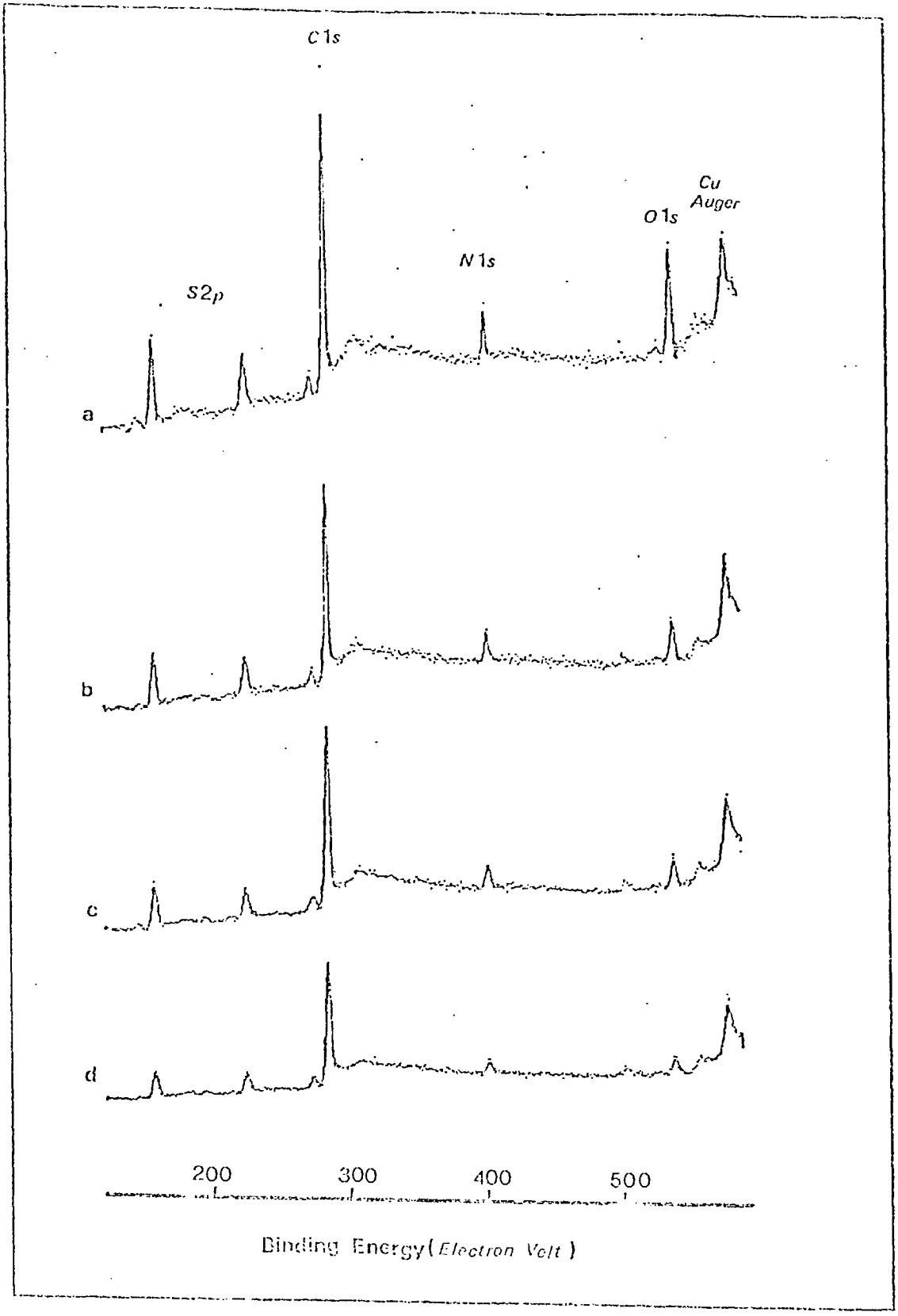


Figure 7.13: XPS spectra of copper sample covered with Cu(I)-MBT surface complex (a). This sample argon etched for 30 sec. (b)1 min.(b); 1.5 min (c); 2 min (d).

converted with Cu-MBT complex and Figure 7.11(b-e) show the sample after being etched by argon ions for different periods of time.

7.1.9 Depth Profile of the Surface Films

The results obtained by removing a thin layer from the top of a surface Cu-MBT film and examination under layer were identical to that of BTA. When a sample was treated with MBT solution at pH less than 3, no different under layer structure was formed. Figure 7.14(a) shows an X-AES spectrum of copper sample in CuLMM region, which is covered with a thick film formed in MBT solution at pH~3. Figure 7.14(b) and 7.14(c) show the result of removing a layer from the top by argon ion bombardment. Clearly there is no indication of any under layer from the appearance of a peak due to metallic Cu only.

In this case again, like BTA, the only time a distinct under layer could be detected was when a sample was treated with MBT solution at pH~7. Figure 7.15(a) shows an X--AES spectrum of a Cu_2O sample and Figure 7.15(b) and 7.15(c) show the spectrum of the sample sample exposed to this film is extremely thin when formed at these conditions. This film was then removed by argon ion bombardment, which left a Cu_2O underlayer (Figure 7.15(d)). Further bombardment of the surface resulted in removal of Cu_2O from the surface (Figure 7.15(e-f)).

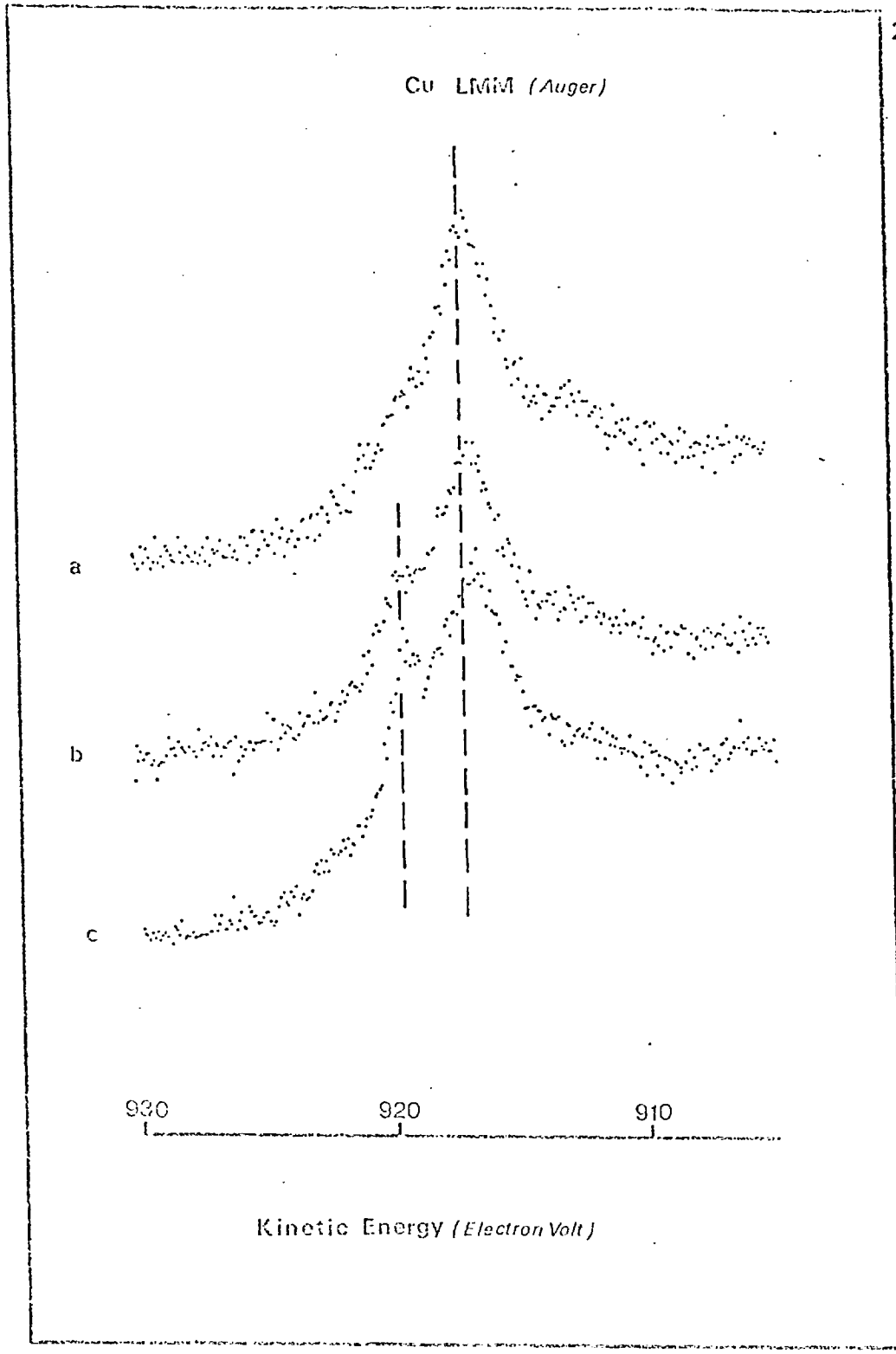


Figure 7.14: X-AES spectra of copper sample : (a) covered with thick Cu(I)-BTA film; (b) above sample after being argon etched for 1 min.; (c) etched for 2 min.

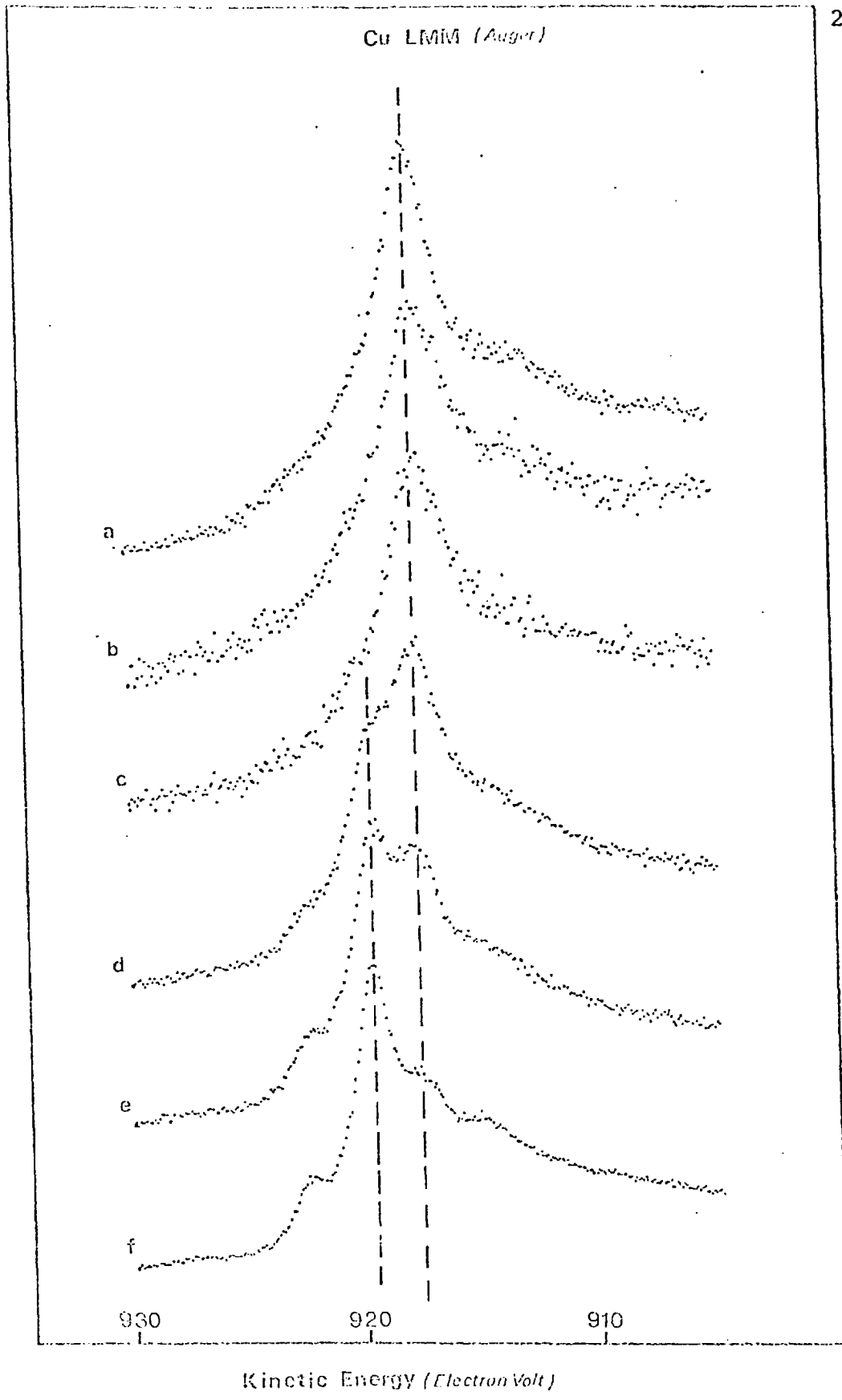


Figure 7.15: X-AES spectra of (a) Cu_2O sample; (b) exp to MBT solution (pH≈7) for 10 hours; (c) exposed MBT solution for 48 hours; (d) argon ion etched for 1 min.; (e) for 2 min.; (f) for 5 min.

7.2 Mechanism of the Film Formation

Study of films thicknesses formed under different conditions showed that the factors affecting the film thickness are the same as the BTA case. These factors, are; (a) the pH of the solution; (b) original Cu_2O film thickness; (c) presence or absence of chloride ions. Since the mechanism of film formation appears to be identical to that of BTA formed films which was described previously, this will not be discussed in detail. However, a few examples of film formation in different conditions are given.

Cuprous oxide is a determining factor in film thickness providing that the MBT solution is slightly acidic (pH~3) and chloride ions are present. Figure 7.16(a) shows an X-AES spectrum of a Cu_2O sample and Figure 7.16(b) shows the result of the treatment of this sample with a solution of MBT at pH~3 for 30 seconds. No, or very little, film formation has taken place after 30 seconds but all Cu_2O has dissolved. A two minute exposure of an identical sample to this solution results in formation of complex film evident from appearance of a new peak Figure 7.16(c). Figure 7.16(d) shows the result of a six minute treatment, in which the growing intensity of the new peak indicates the thickening of the film. Finally Figure 7.16(e) shows the result of a twenty minute exposure to MBT solution in which the film grows to an appreciable thickness which masks the signal from under layer metallic copper, results in a single peak due to Cu-MBT film.

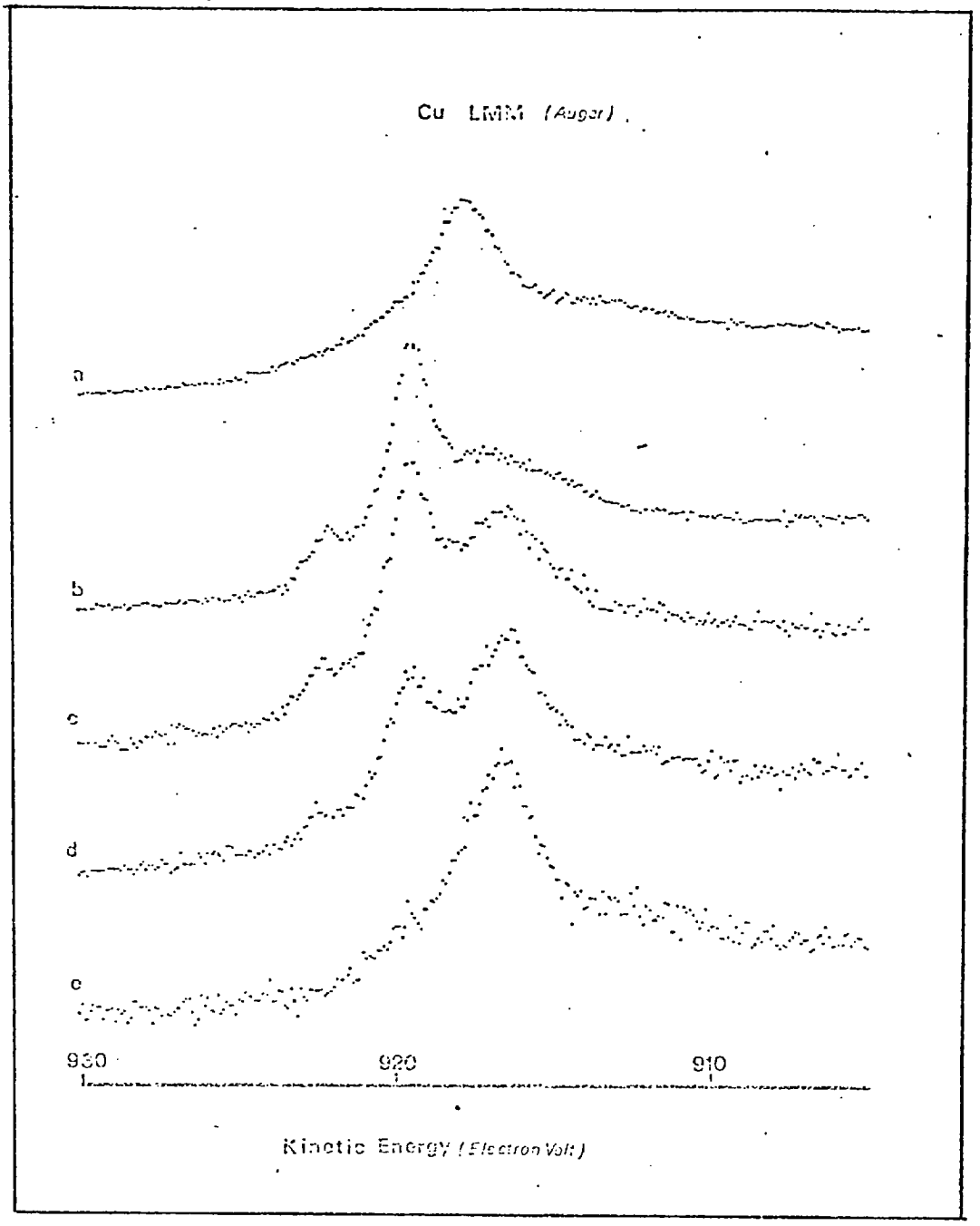


Figure 7.16: X-AES spectra of Cu_2O samples (a) exposed to MBT solution at pH≈3 for (b) 30 sec., (c) 2 min.; (d) 6 min.; (e) 20 min.

In the absence of any Cu_2O, film thickness stays extremely low as was the case for BTA. Figure 7.17(a) shows an X-AES spectrum of the surface of a copper sample after being cathodically reduced followed by inhibitor injection (see Appendix A for details of experiment). The sample then was left exposed to this solution for twenty minutes. A very thin film is formed which is evident from intensive metallic peak. A Cu_2O sample was exposed to the same solution for the same amount of time for the purpose of comparison Figure 7.17(b) shows the result.

When the solution is at pH~7, the film thickness stays low despite the prolong exposure to the solution. Figure 7.18(a), (b) and (c) shows the result of a Cu_2O sample (7.18(a)) exposed to MBT solution at pH~7 for 10 hours (7.18(b)) and 48 hours (7.18(c)).

If the sample is covered with a thin Cu_2O film (air-formed), on exposure to the MBT solution at pH 7 the film thickness stays low evident from Figure 7.19(a), (b) and (c). Figure 7.19(a) shows a polished copper sample exposed to air for ½ hour and then exposed to MBT solution at pH~7 for fourty minutes. Figure 7.19(b). Figure 7.19(c) shows an identical sample exposed to such a solution for 1½ hours. Clearly a complex is formed in this case but the thickness is still low because even after 1½ hours the peaks due to Cu and Cu_2O can be detected.

Finally, polished copper samples with air-formed oxide (Figure 7.20(a)) were exposed to a MBT solution at pH~3 for five minutes (7.20(b)), for 10 minutes (7.20(c)) for ½ hour (7.20(d)) and for 40 minutes (7.20(e)). Again

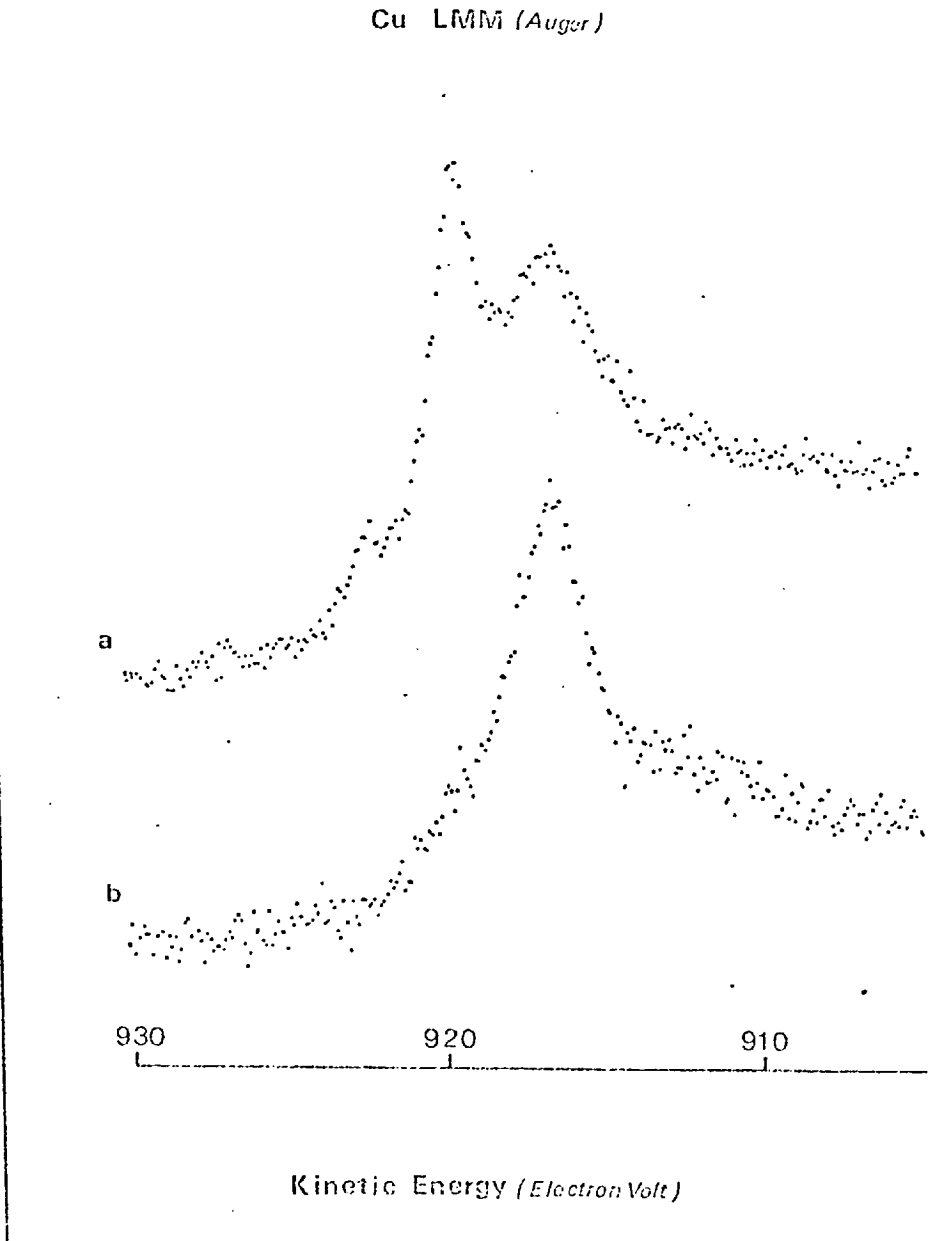


Figure 7.17: X-AES spectra of : (a) copper sample after cathodically reduced surface followed by injection of inhibitor; (b) Cu_2O sample exposed to the same solution for $\frac{1}{2}$ hour.

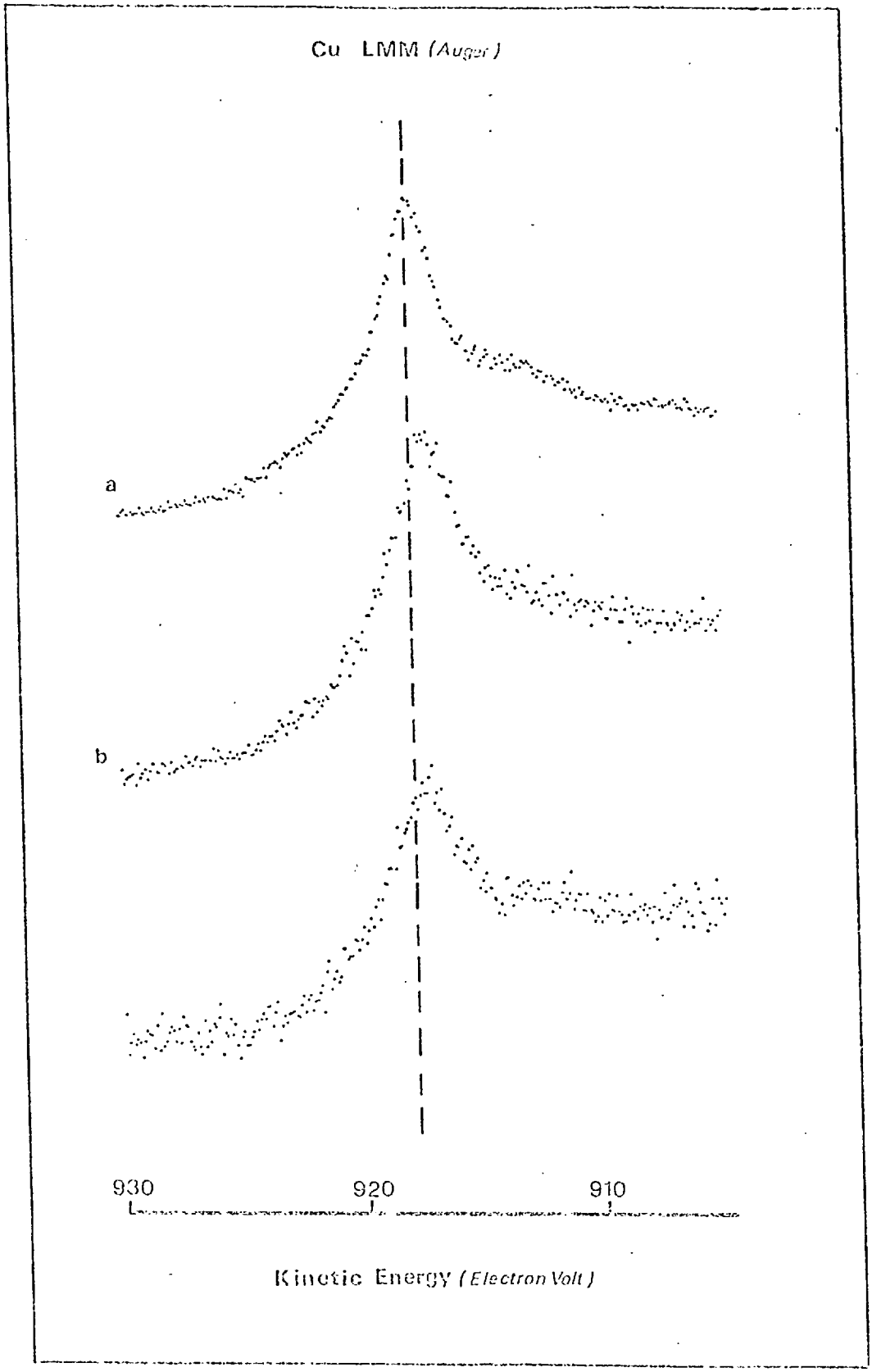


Figure 7.18: X-AES spectra of : (a) Cu_2O sample; (b) above sample exposed to MBT solution (pH≈7) for 10 hours; (c) for 48 hours.

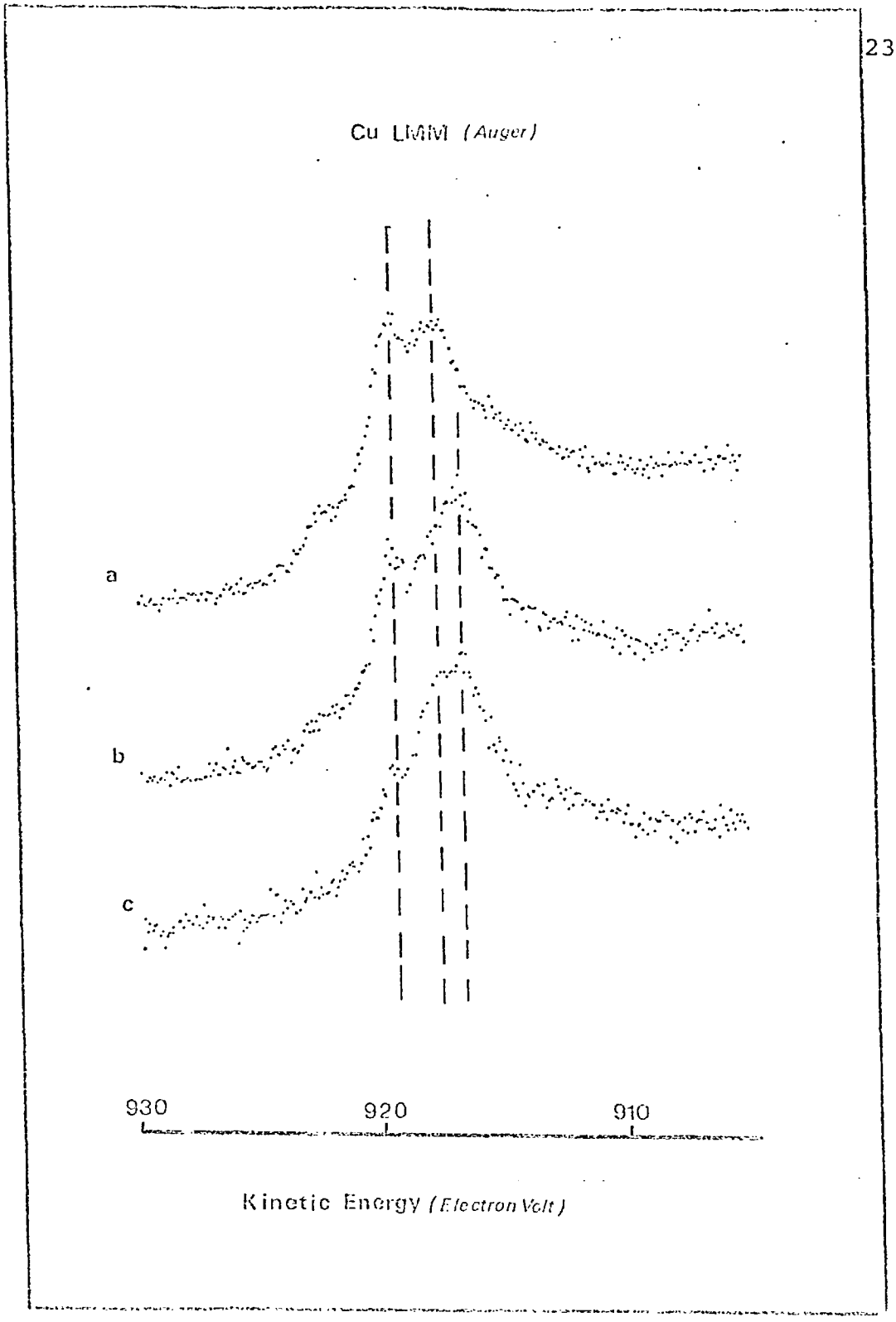


Figure 7.19: X-AES spectra of copper samples: (a) polished and exposed to air for ½ hour; (b) this sample exposed to MBT solution (pH≈7) for 40 min.; (c) similar sample exposed for 1½ hour.

it is clear that, although the film formation is instantaneous, it will stay low in thickness even after 40 minutes exposure to MBT solution.

These results indicate that the only time the film thickness grows to hundreds of Å in a relatively short time, is when a thick Cu_2O covered sample is treated with MBT solution at pH~3 containing Cl^- ions. This is because according to equation (6.1) (page154), disproportionation of Cu_2O takes place first and then after an intermediate stage of CuCl formation, Cu(I) MBT forms and precipitates onto the surface, in an identical manner to the BTA case. So the overall reactions after disproportionation will be:

$$Cu_{(m)} + Cu^{2+}_{(aq.)} + 2MBT_{(aq.)} \xrightarrow{Cl_{(aq.)}} 2Cu(I)\text{-}MBT_{(s)} \qquad (7.4)$$

In this case also, by adding Cu^{2+} ion artificially and in the presence of Cl^-, extremely thick films can be obtained.

Because of the low solubility of MBT, these processes i.e. disproportionation and film formation, are quite distinct and independent as is clear from Figure 7.16(a-e). This figure has been explained already, but comparison of Figure 7.16(a) and 7.16(b) shows two distinct stages.

A very intense metallic peak in this spectra and the lack of any other peaks, indicates that the disproportionation reaction takes place almost instantaneously after the sample has been introduced into the solution. Figure 7.16(c) shows the X-AES spectrum of a similar sample

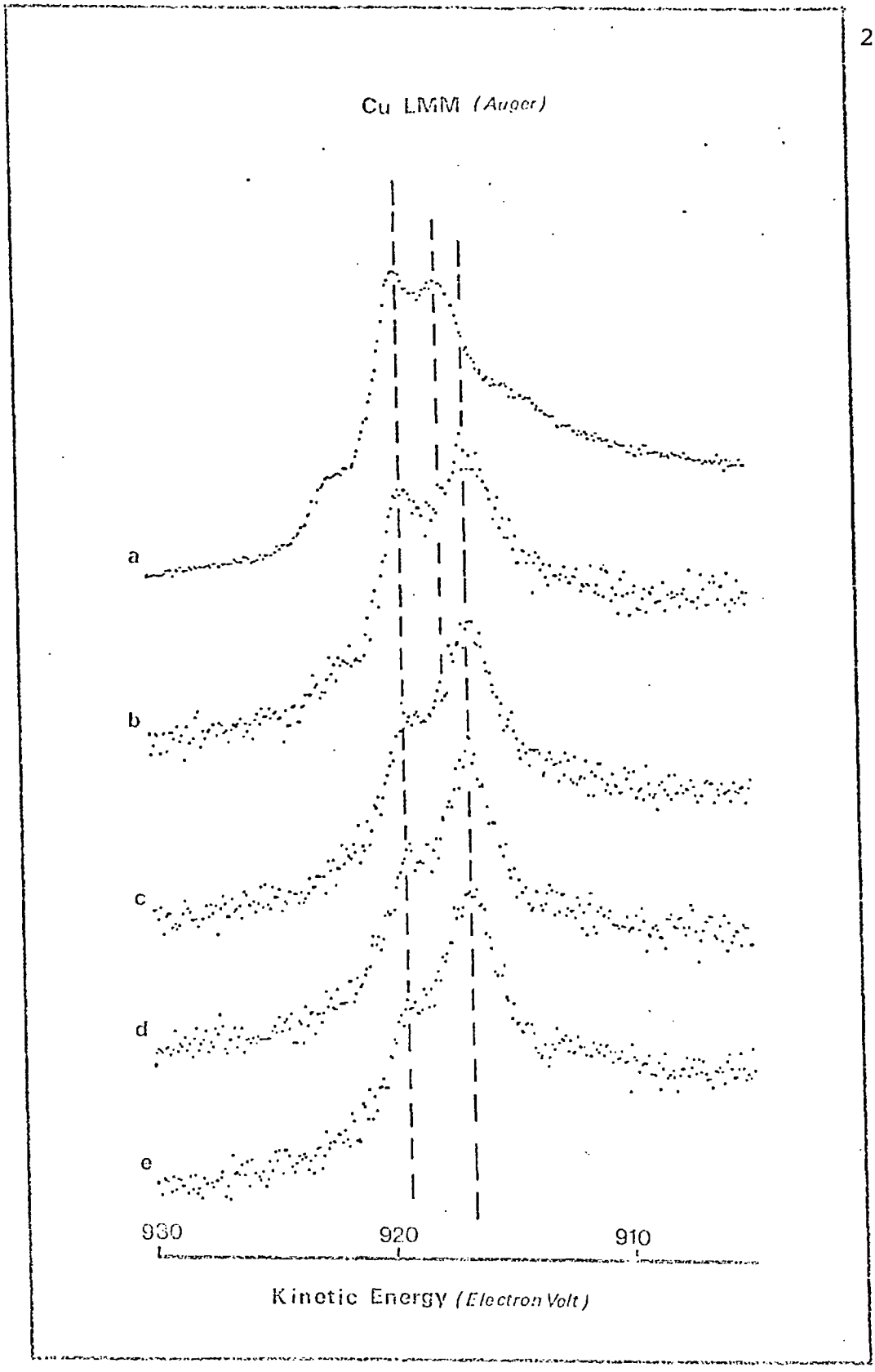


Figure 7.20: X-AES spectra of polished copper samples: (a) exposed to air for ½ hour. Exposure of similar samples to MBT solution (pH≈3) for : (b) 5 min.; (c) 10 min.; (d) 30 min.; (e) 40 min.

after 10 minutes treatment. At this stage, the formation of a complex film is evident by the appearance of a new peak at 916.7 eV k.e. The intensity of this peak increases with exposure time to MBT solution. Figure 7.16(d) and 7.16(e). It is quite clear now, thatthe model suggested for the Cu-BTA system is applicable to other Cu-inhibitor systems such as Cu-MBT.

7.3 Films formed on Copper-based Alloys

The interaction of a 2-mercapto-benzothiazole on copper-nickel and brass alloys was studied in order to compare the inhibitive properties of MBT with that of BTA.

Alloys with composition, 70Cu:30Ni, 30Cu:70Ni, and 70Cu:30Zn were chosen as in the case of BTA. Once again, it was assumed that the ratio of peak heights, in 2p region is a reasonable estimate of the relative surface concentrations of the alloy constituents. However, it is only the relative changes after treatment with inhibitors that are of interest.

Samples were treated with MBT solution at pH~7 in 0.5M NaCl. Copper-nickel alloys showed the same behaviour as for BTA. The XPS spectra of copper-nickel samples treated with MBT showed no peaks due to Ni 2p. This was the result of relatively short periods of treatment for 70Cu:30Ni (e.g. 5 minutes) and for 30Cu:70Ni about 16 hours.

In order to make sure that this was an effect of the inhibitor, samples were exposed to identical solutions in the absence of any inhibitor for comparable times.

The behaviour described above does not occur in inhibitor -free solution. Figure 21(a) shows an XPS spectrum of a 70Cu:30Ni alloy after Argon ion etching : (21(b)) a polished sample and (21(c)) the same sample exposed to MBT solution for 5 minutes. Figure 22(a) shows an XPS spectrum of a 30Cu:70Ni after being etched with Argon ions and (22(b)) shows the same sample polished before etching. Treatment of this sample MBT solution for 16 hours results in the disappearance of the Ni2p peaks. These results indicate the formation of a copper-MBT complex with little or no contribution from Ni. This also shows that the interaction of Cu/Ni alloys with MBT is identical to that of BTA. This is not the case for brass.

Figure 23(a) shows an XPS spectrum of a 70Cu:30Zn brass after being etched with Ar ions. Figure 23(b) shows the same sample before being etched, and the XPS spectrum of this sample exposed to MBT solution for 16 hours is shown in Figure 23(c). Apparently the $Zn2p_{3/2}$ peak has almost disappeared from the spectrum. This shows that, in contrast to BTA, in the treatment of brass with MBT, the only metal responsible for film formation is copper.

In all these studies, it has been shown that Cu-MBT complex films formed on the samples are sensitive to air oxidation, although the rate of oxidation is much slower than for Cu-BTA complexes. The binding energies of the various peaks are given in Binding Energies Table App.B.

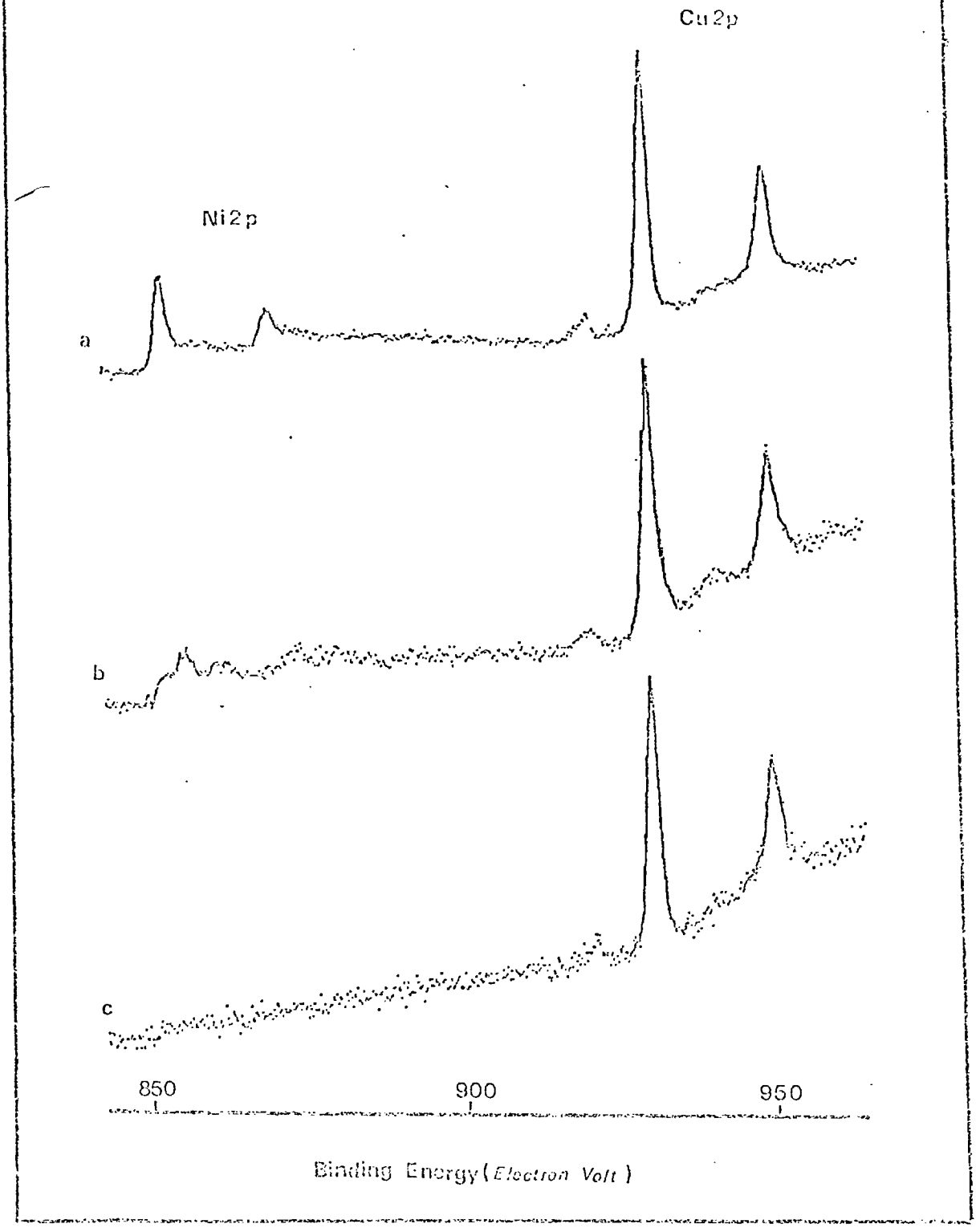


Figure 7.21: XPS spectra of 70Cu:30 Ni alloy (a) polished and argon etched ; (b) polished ; (c) exposed to MBT solution for 5 min.

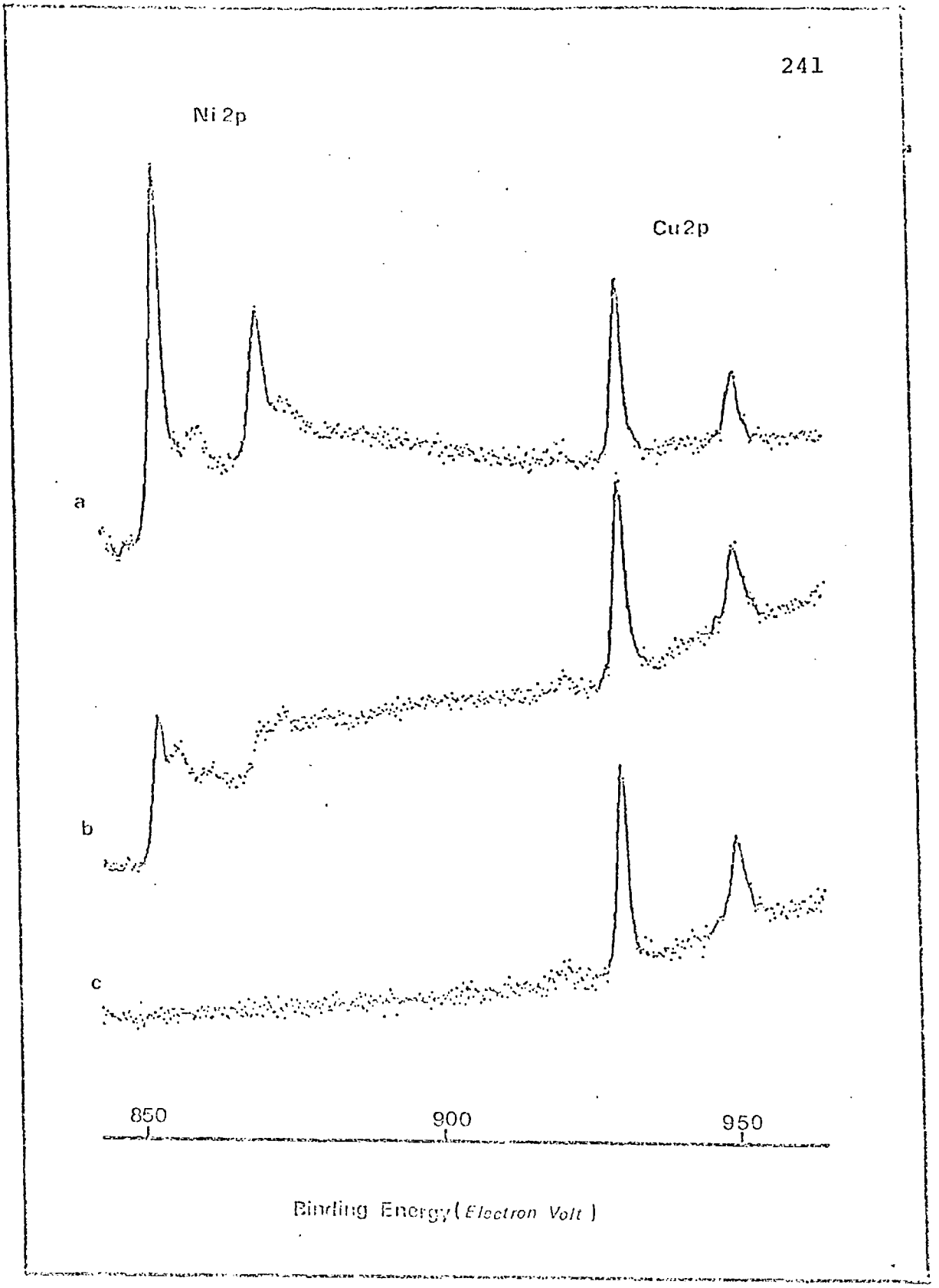


Figure 7.22: XPS spectra of 30Cu 70Ni alloy (a) polished and argon etched; (b) polished; (c) exposed to MBT solution for 16 hours.

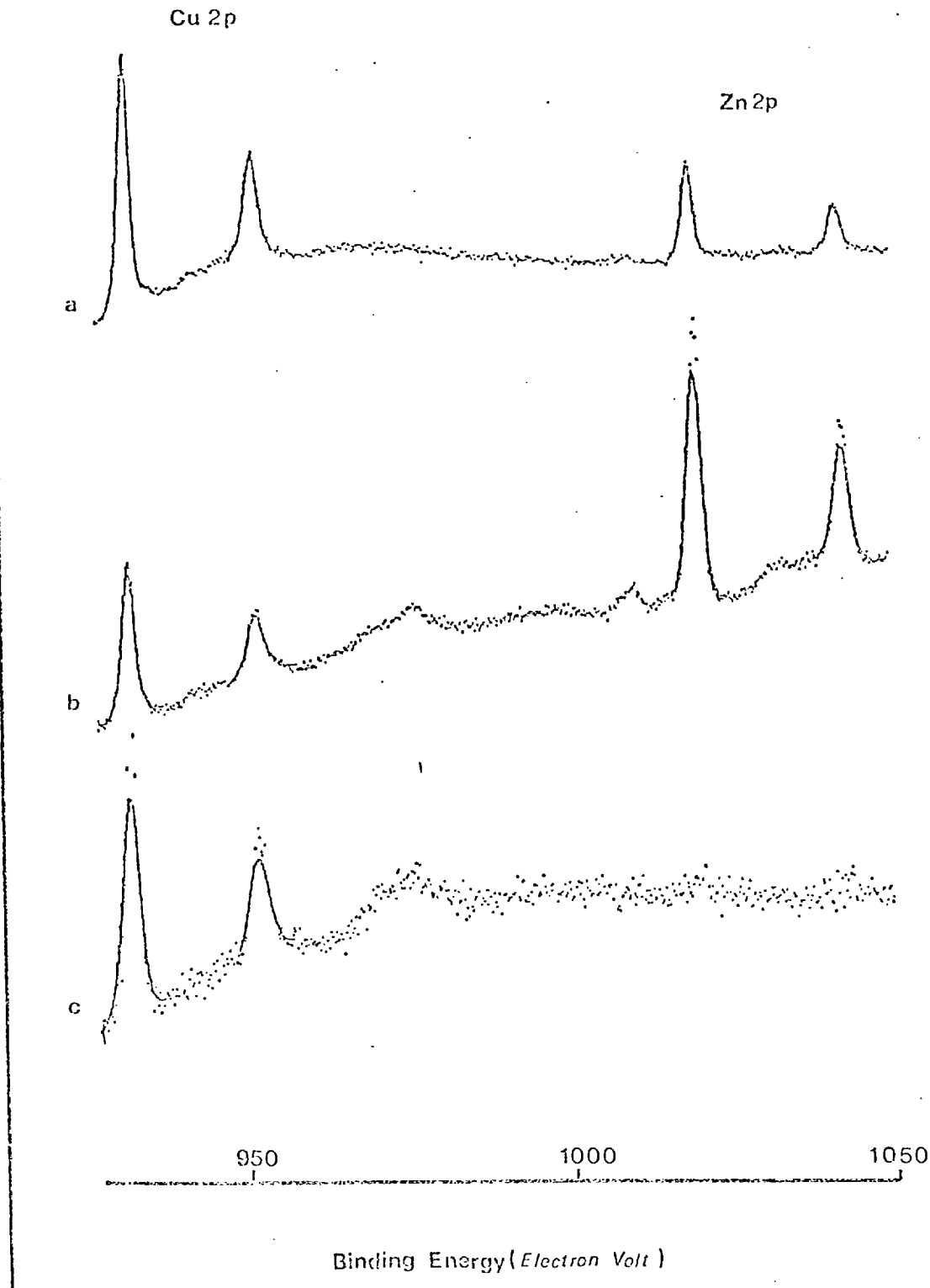


Figure 7.23: XPS spectra of 70Cu:30Zn brass (a) polished and argon etched; (b) polished; (c) exposed to MBT solution for 16 hours.

7.4 Films Formed From Non-Aqueous Media

Adsorption from non-aqueous media was carried out using suitable solvents such as dry benzene and toluene. These experiments showed that although complex films forms in non-aqueous solutions, the thickness of these films stays very low (probably a monolayer), regardless of prolonged exposure time. This is the case for copper-based alloys. Treatment of these alloys with a non-aqueous solution of MBT did not result in thick film formation.

7.5 Summary

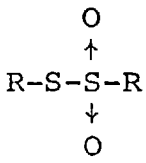
1. The present study showed that the mechanism of film formation by 2-mercaptobenzothiazole on copper is essentially similar to that of benzotriazole. That is to say, an adherent complex film is formed on the surface of the metal to be protected resulted from interaction of MBT with copper. This film is responsible for protection of metallic copper substrate.

2. Surface complexes proved to be identical to those prepared from the solution.

3. In the case of Cu-II-MBT complex, it is shown that because of an internal electron transfer, it is not possible to obtain this complex at ordinary conditions. This complex transforms to a Cu(I)-MBT complex, identical to Cu(I)-MBT complexes prepared from cuprous salts.

4. All Cu(I)-MBT complexes proved to be sensitive to atmospheric oxidation. This oxidation followed by dimerization reaction, results in decomposition

and degradation of the protective surface films. The resultant dimerized inhibitor and CuO have no longer good protective properties and could be wiped or washed away. Dimerization reaction takes place through -S-S- bond formation. The dimerized compound of R-S-S-R, in its turn, on exposure to air, undergoes oxidation, forming



5. Finally, the present work on both BTA, MBT and some other relative compounds, shows that the ESCA technique, i.e. XPS together with X-AES, is a very powerful method for the studying of corrosion inhibition. The technique has also been of great value in the interpretation of electrochemical polarization measurements.

CHAPTER EIGHT

ELECTROCHEMICAL POLARIZATION OF COPPER IN THE PRESENCE OF ORGANIC INHIBITORS.

ESCA and I.R. investigation of the effect of corrosion inhibitors on copper surfaces showed that these compounds exercise their effect through formation of a protective surface film, the nature of which properties and its mechanism of formation have been discussed. However, these techniques are unable to differentiate between the effectiveness of such films from the corrosion inhibition point of view. Thus, electrochemical measurements are important and have been used extensively by many workers (46, 51, 71). Unfortunately, it is not easy always to obtain meaningful and reproducible results in such measurements because of too many factors affecting the measurements. This is perhaps the reason for the Cu-H_2O-Cl system in the presence and absence of inhibitors being subjected to considerable investigations. In view of this, and also to compare inhibition properties of BTA, MBT and some other relevant compounds, a thorough investigation seemed necessary.

8.1 Cathodic and Anodic Polarization of Copper in Brine Solutions

Copper electrodes were prepared for this part of study using an epoxy resin (Araldite) to cover most of the electrode. Only one surface of the electrode was exposed to the solution. Electrodes, after being abraded on emery papers with different sizes, were polished with

diamond pastes, with the last one being 1μ. The electrode after being washed was introduced into a diluted nitric acid solution for a short period of time (say 30 seconds), followed by washing with distilled water. Treatment of the electrodes with nitric acid solution has been recommended by several workers (36, 67). A test was also made to see if treatment with HNO_3 solution leaves any residue on the surface. ESCA examination of the surface treated in this way, revealed no residue remained due to HNO_3 treatment. A platinum auxiliary electrode was used and the electrochemical cell was enclosed in a thermostatic bath. For details of the cell design see Chapter 5. A saturated calomel electrode was used as a reference electrode and triply distilled water was used to prepare electrolytes.

8.1.1 Cathodic Polarization of Copper Using Linear Potential Sweep

Copper electrodes prepared for this study were exposed to the solution prior to measurement for 15 hours. Thistime was fixed throughout these measurements. Potentials moved towards more noble potentials starting from extreme cathodic potential (i.e. -0.7V). Experimentation with the range of potentials used indicated that -0.7 to + 0.3 contains all the relevant data.

Figure (1) shows a typical polarization curve of copper in aerated, 0.1M NACl solution obtained with a scanning speed of 0.05 mV/sec. It is clear from Figure (1) that in the cathodic part for overpotential values smaller than 0.3V, the voltage is linearly related

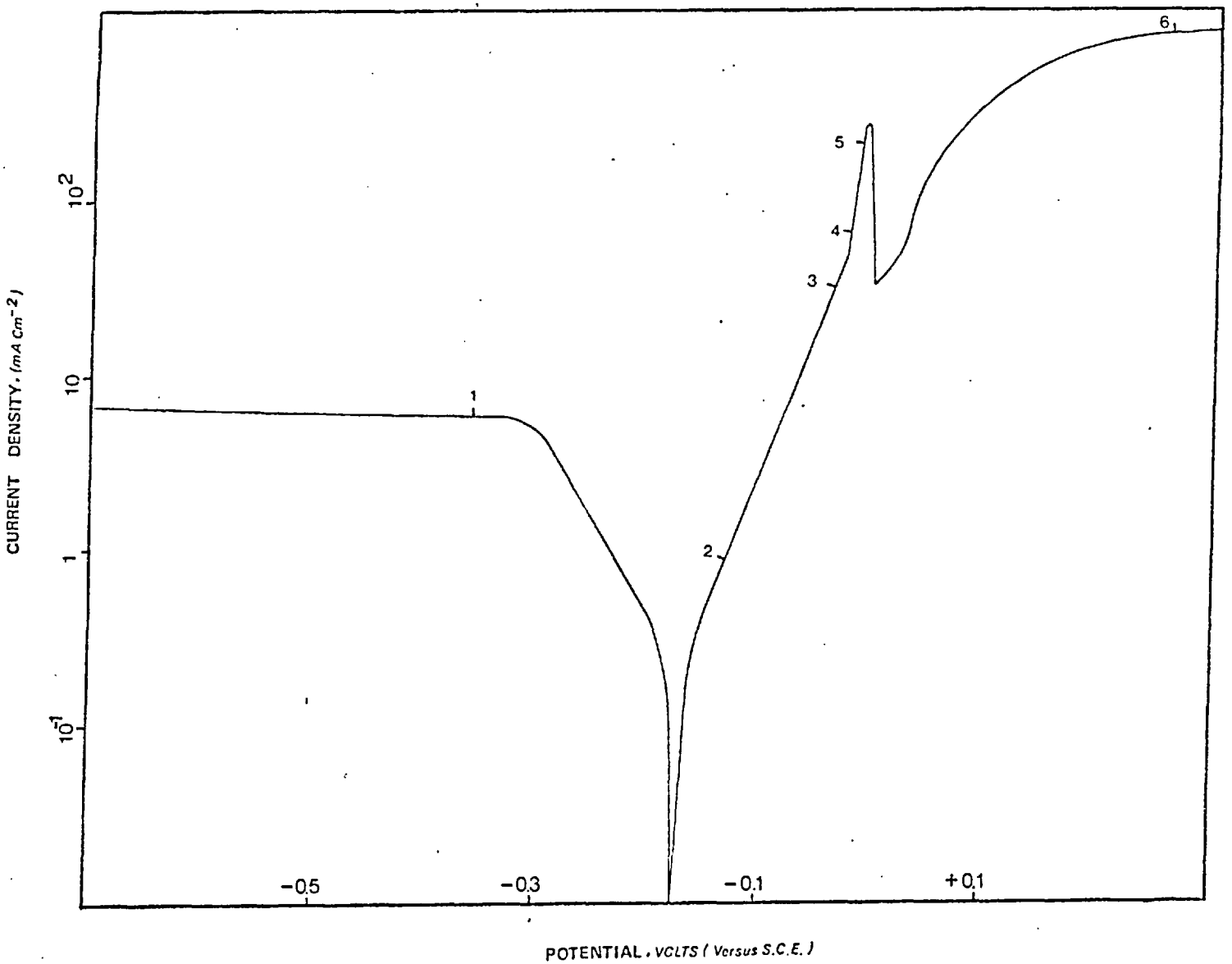


Fig. 8.1: Electrochemical cathodic and anodic polarization curves for copper electrode in 0.1M NaCl aerated solution at 30°C.

to the log of the current density (Tafel region). For overpotential greater than this diffusion control occurs as will be discussed later.

If there are two or more cathodic processes taking place simultaneously, normally no linear part in the cathodic polarization curve is to be found. The existence of a Tafel region in this part indicates that there is one pre-dominant cathodic process. This predominant cathodic process appeared to be oxygen reduction which has also been suggested by other workers (69, 71). If the oxygen is removed from the solutionthe Tafel line disappears and the corrosion potential moves towards more negative potentials by as much as 0.25V. The corresponding current density values for cathodic overpotentials in this case is substantially less than the case when oxygen is present. Fig. 8.2(a) shows polarization curve of copper in a 0.5M NaCl solution and Fig. 8.2(b) shows a polarization curve for a similar electrode in a similar but deaerated solution. The solution was deaerated by purging nitrogen at 95-98^{o}C for 15 minutes followed by continuous purging at room temperature for 15 hours. Bubbling air through the solution has a reverse effect, i.e. corrosion potential moves towards positive (noble) direction. The oxygen reduction reaction takes place via. the diffusion of oxygen molecules to the surface followed by oxygen adsorption. The O_2 reduction takes place according to Equation (8.1) in neutral or basic solutions.

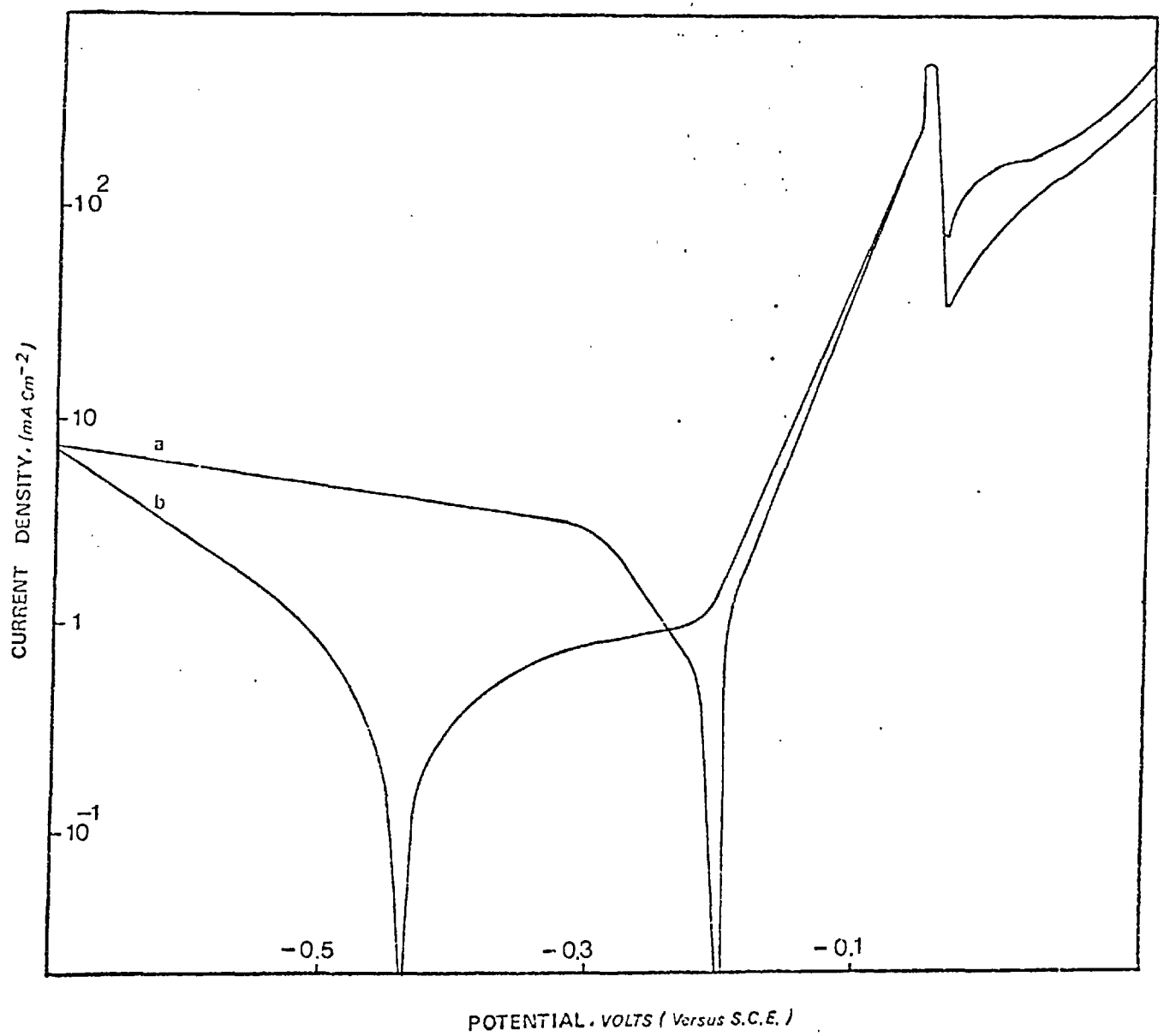


Figure 8.2: Polarization curves for Cu electrode in 0.5M NaCl solution : (a) aerated, (b) deaerated.

$$O_{2(ads)} + 2H_2O + 4e = 4OH^- \qquad (8.1)$$

For higher cathodic potentials, e.g. V in this case, oxygen reduction reaction takes place under diffusion control. If this reaction is not under diffusion control, stirring or flowing the electrolyte will have little or no effect upon cathodic reaction. This is certainly not the case in the present system. The effect of stirring on the cathodic process will be explained in section (8.4.5).

The solubility of oxygen in an electrolyte is an important factor in the cathodic reaction and as a result, the corrosion rate. The solubility of oxygen in water is about 8ppm at 25°C. It depends on temperature and also on the concentration of soluble salts. The change in solubility of oxygen with the change in concentration of sodium chloride has been discussed by Scully (103). He showed that the maximum oxygen solubility in water corresponds approximately to a 3% solution of NaCl, i.e. sea water. The oxygen solubility then falls with increasing the NaCl concentration.

Thus, the conclusion is; (a) the main cathodic reaction in this system is in fact oxygen reduction; (b) the rate of oxygen reduction for high overpotentials is controlled by the diffusion of oxygen to the metal surface.

8.1.2 Anodic Polarization of Copper

The behaviour of copper under anodic polarization is complex but very reproducible. The first anodic reaction which takes place in brine solution and is

responsible for a linear relationship between overpotential values and the log of the current density is the formation of cuprous oxide. Examination by ESCA of samples taken in this linear part (Points 2 and 3) indicated a progressive oxidation takes place when potential is scanned in a positive direction. Examination of the electrolyte by atomic absorption spectrophotometer showed that no dissolution of copper takes place in this part of polarization curve. The slope of this linear part which corresponds to Cu_2O formation is measured to be about 61 $mV/_{decade}$ which is in good agreement with reported figure of 60 $mV/_{decade}$ by Bacarella and Griess (69) and also by Boden (102).

The conclusion is that for the first linear section of the anodic curve, the corresponding anodic reaction is the formation of Cu_2O on the surface of the electrode according to Equation (8.2).

$$2Cu + H_2O \rightarrow Cu_2O + 2H^+ + 2e \qquad (8.2)$$

This anodic reaction has also been proposed by other workers (68).

At higher potentials, i.e. -0.07V vs. S.C.E. the second distinct region of the anodic curve can be observed (Points 3 and 4 in Figure 8.1). Clearly there is a vast difference between the slope of this region and the region representing Cu_2O formation. The slope of this region is about 19.1 $mV/_{decade}$, showing for a small increase in potential, a large increase in current

density takes place. Also a sudden visible change in the colour of the electrode occurs as soon as the potential reaches this region.

ESCA examination of the electrode surface in this region (Points 4 and 5) showed that the surface now is covered with CuCl, evident from a small shift of $Cu2p_{3/2}$ XPS peak to higher binding energies compared to Cu_2O, a small shift of CuLMM Auger peak tolower kinetic energy and appearance of a Cl2p peak. This is in accordance with the conclusion reached by Lal and Thirsk (67). $Cu2p_{3/2}$ XPS spectra showed no evidence for the formation of any Cu^{2+} species.

Examination of the solution by atomic absorption spectrophotometry showed a sudden increase in copper concentration in the solutions. U.V. absorption spectra of this solution showed no adsorption band, indicating that the dissolved copper is in fact Cu(I).

It is clear from these results that in this region copper dissolution takes place via. Cu^+ ionswhich in contact with the solution containing chloride ions, forms insoluble CuCl. This soon reaches its limit of solubility and, as a result, precipitates onto the surface. This mechanism is similar to that of Cu_2O disproportionation in acid solution in presence of chloride ions, explained in Chapter 7.

In the third region of the anodic polarization curve for an electrode in NaCl solution, there is a sudden drop in current densities for small changes in overpotentials. This is due to formation of a relatively thick adherent CuCl film on the surface. In general, a compact anodic

film can be formed if the solution contains anions which form insoluble compounds with the cations emerging from the metal lattice as a result of anodic current, and such a product is thermodynamically stable. This may block the anode and, instead of the metal, it is now solid anodic product that is in contact with the solution. The further course of the anodic process depends primarily on the properties of the film, on the nature of its charge carrier (ions, electrons or both), on its conductivity and on the strength with which it is adhered to the metal.

The last part of the anodic polarization curve for copper in NaCl solutions is a transpassive region. The transpassive region occurs at higher overpotentials. An ESCA examination of the electrode surface at this region (Point 6 in Figure 8.1) showed that the surface film contains Cu^{2+} species. This is in accordance with Pourbaix diagram (86) for copper in aqueous solutions.

XPS and X-AES spectra of samples corresponding to points (1-6) of Figure (8.1) are given in Figure (8.3). Figure (8.3(a)) shows the XPS and X-AES spectra of a copper electrode polarized cathodically (corresponds to Point 1). These spectra show that the surface in this region is metallic. Small amount of Cu_2O present in X-AES spectrum is because of transfer and drying time. Figure 8.3(b) shows spectra corresponding to Point 2 and 8.3(c) representing Point 3. A progressive oxidation is evident from X-AES spectra of Point 2 and 3. Points 4 and 5 are represented by Figure 8.4(c&d). Small shifts in both XPS and X-AES and also appearance of a Cl peak in XPS spectra (not shown here) indicates formation of

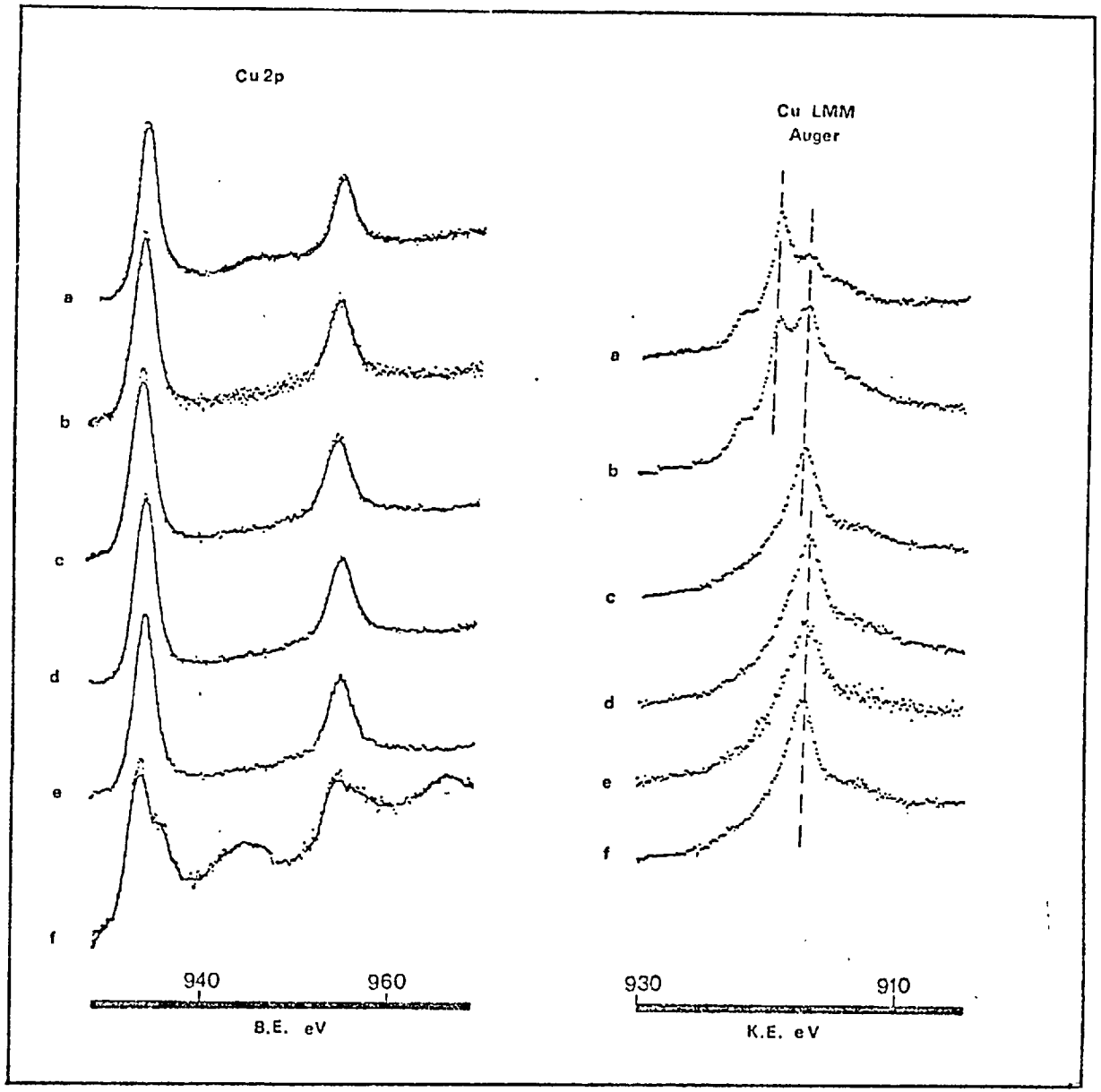


Figure 8.3: XPS and X-AES spectra of Cu electrodes surfaces at different points on polarization curves (Fig. 8.1 Points (1-6)).

of CuCl. Figure 8.3(e) represents Point 6 and as discussed earlier formation of some Cu(II) species is evident from XPS spectrum.

8.1.3 Time Dependence of the Cathodic and Anodic Processes

A very important parameter effecting the polarization curves of copper obtained in NaCl solutions proved to be the speed of scanning. It is extremely important to fix this speed for different measurements and moreover to find the correct speed (which in any case is not to be more than 0.05 mV/sec), to obtain curves with good reproducibility. Cathodic and especially anodic processes proved to be time dependent processes during the course of these experiments. A relatively fast change in potential, could easily eliminate one or more of the electrochemical processes. Figures 8.4(a) and (b) show polarization curves of copper in aerated, 0.5M NaCl solution obtained with a scanning speed of 0.05 mV/sec and 0.5 mV/sec. respectively. This shows that both the cathodic and anodic curves are completely different in Figure 8.4(b) (0.5 mV/sec) can be found. This curve does not show any passivation in the anodic part.

The results obtained from slow scanning have good reproducibility particularly in the anodic part. The speed of scanning throughout this study was fixed on 0.05 mV/sec and wherever it differs from this, it will be stated.

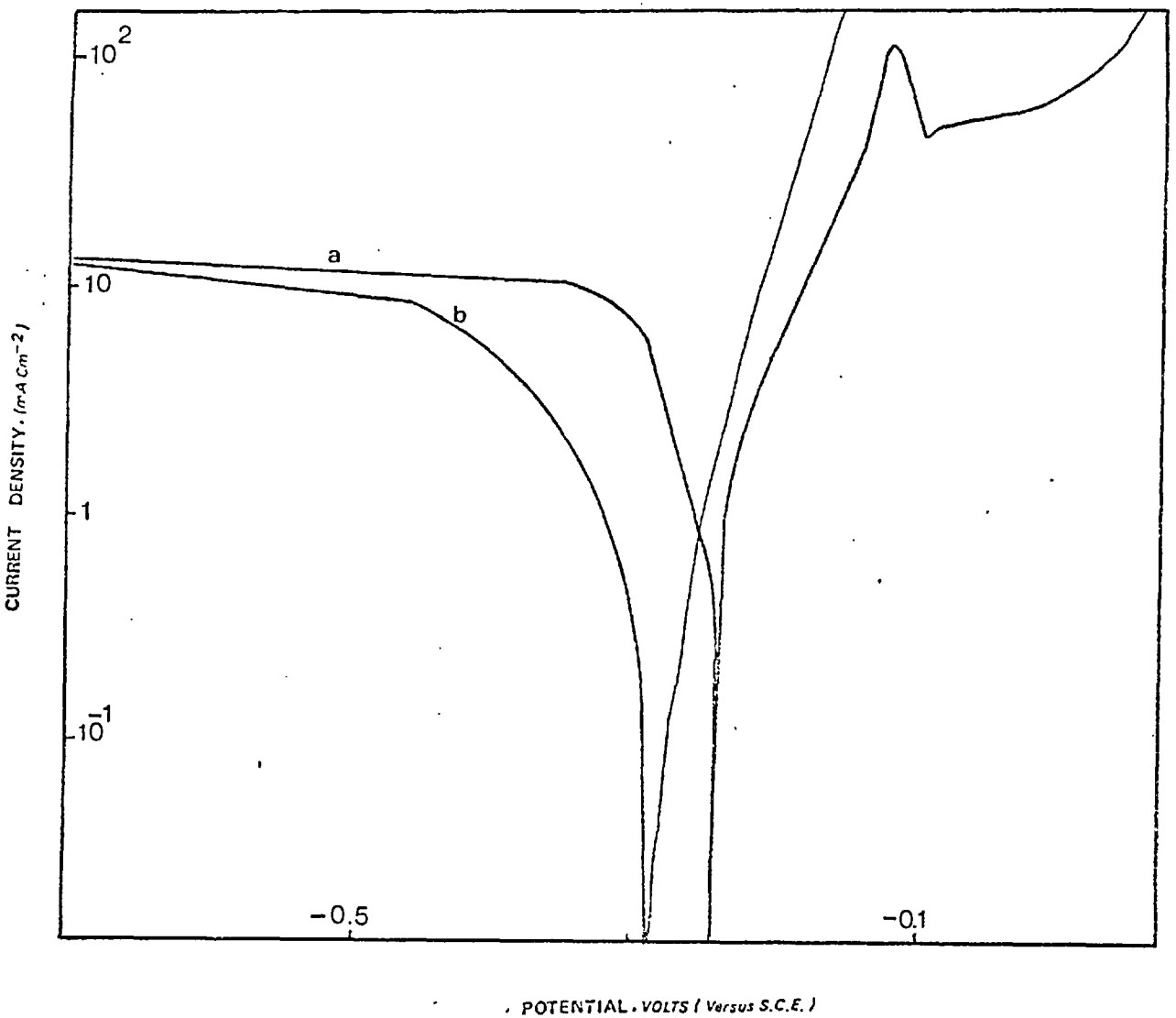


Figure 8.4: Polarization curves for Cu electrode in 0.5M NaCl solution obtained with a scanning speed of (a) 0.05mV/sec., (b) 0.5mV/sec.

8.1.4 Effect of Chloride Ion Concentration

Since the formation of CuCl depends upon the chloride ion concentration, this has a great effect on the anodic branch of the polarization curve. Moreover, as stated already, Scully (103) has shown the concentration of dissolved oxygen is related to the salt concentration and with increase in concentration, oxygen solubility decreases. So it is expected that changing the salt concentration results in change in cathodic polarization curve. Figure 8.5(a), (b) and (c) show the polarization curves at 0.01M, 0.1M, and 1M, sodium chloride unstirred solution. Tafel lines in cathodic region becoming smaller and more steep when NaCl concentration increases. Also, because the cathodic reaction in higher overpotentials is a diffusion limiting reaction, a high concentration of NaCl results in smaller current density for a given cathodic overpotential. The corrosion potential also shifts towards more negative values as a result of increase in NaCl concentration (Figure (8.5)).

The effect of Cl^- ion concentration on anodic branch of polarization curve is more significant. For a given anodic overpotential, unlike cathodic branch, values for current densities increase with increase in NaCl concentration. It is also obvious that for small Cl^- concentration the active/passive transition is negligible (Figure 8.5(c)) whereas for a concentration of 1M NaCl, passivation takes place more intensively. The potential and the current density at which passivation takes place

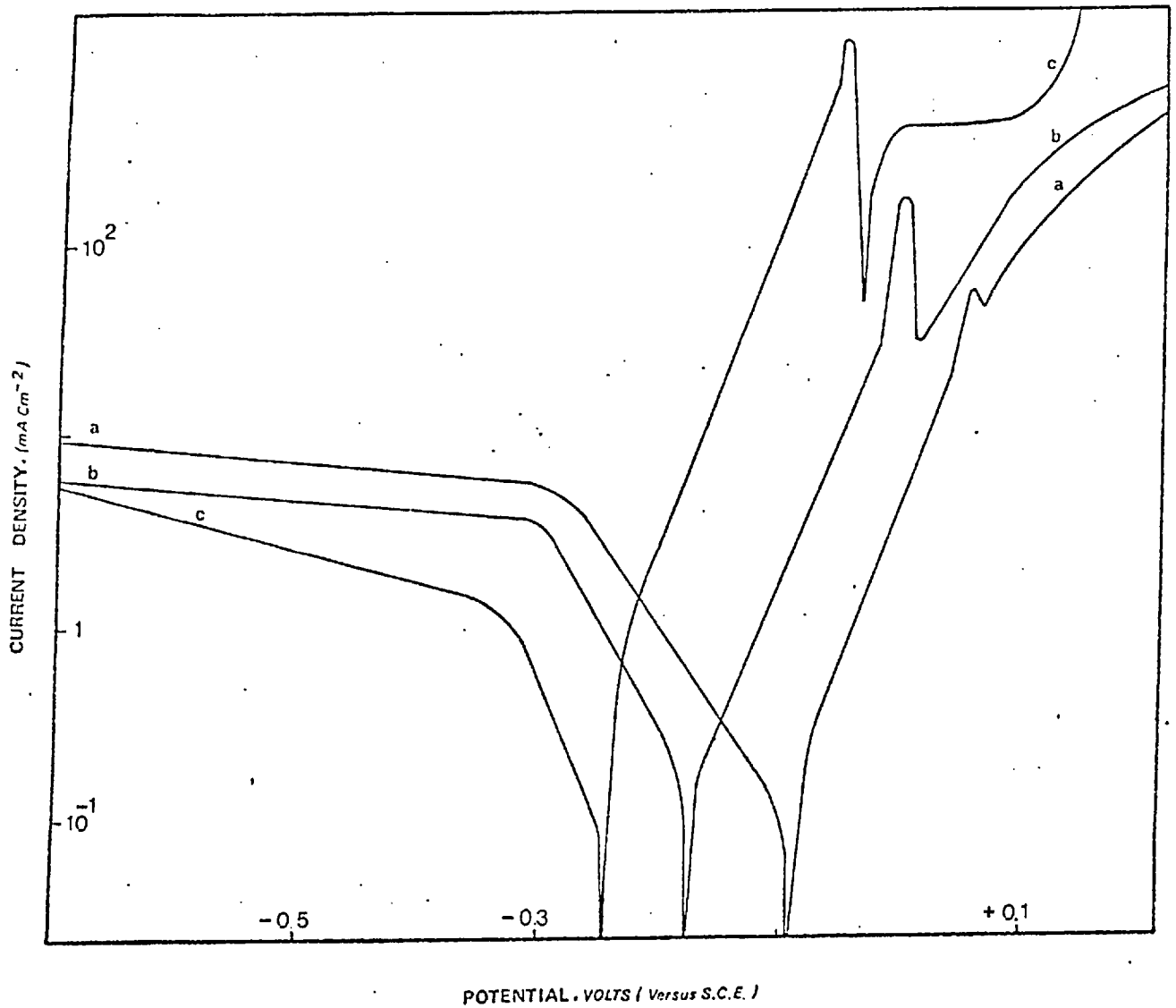


Figure 8.5: Polarization curves for Cu electrodes in (a) 0.01M,(b) 0.1M, (c)1.0M, NaCl solution

varies with different NaCl concentrations. Passivation takes place at higher current densities for higher NaCl concentrations.

8.1.5 Effect of Temperature

The temperature of the electrolyte affects the polarization behaviour of copper. The effect of temperature on passivation is quite significant as shown by Lekie for Cu in H_2SO_4 (65). In NaCl solution at higher temperatures, the CuCl formed is more soluble in solution than in solutions at lower temperatures.

In the cathodic part of the polarization curve, a higher current density was observed for a given over-potential when the temperature increases. This is presumably due to an alteration in diffusion reaction rate at cathodic part. Figure 8.6(a), (b) and (c) show the Cu polarization curve in a 0.5M NaCl aerated unstirred solution, at 30, 40 and 60^{o}C respectively.

To investigate a wide range of temperatures, a potential was chosen (in this case -0.5V vs. S.C.E.) and a curve of current densities versus different temperatures was constructed. Figure 8.7 shows this curve. The temperature starts from +3.5^{o}C and moves upwards to 90^{o}C. After about 50^{o}C, the curve does not show any increase in corrosion current density due to increase in temperature. This must be noted that the temperature of the solution was brought down to +3.5^{o}C and then by putting the reaction vessel in a thermostatic bath at 95^{o}C, the temperature allowed to vary freely. The increase in temperature values were measured in different periods of time. This is the reason why the scale of temperatures (i.e. x axis) is not

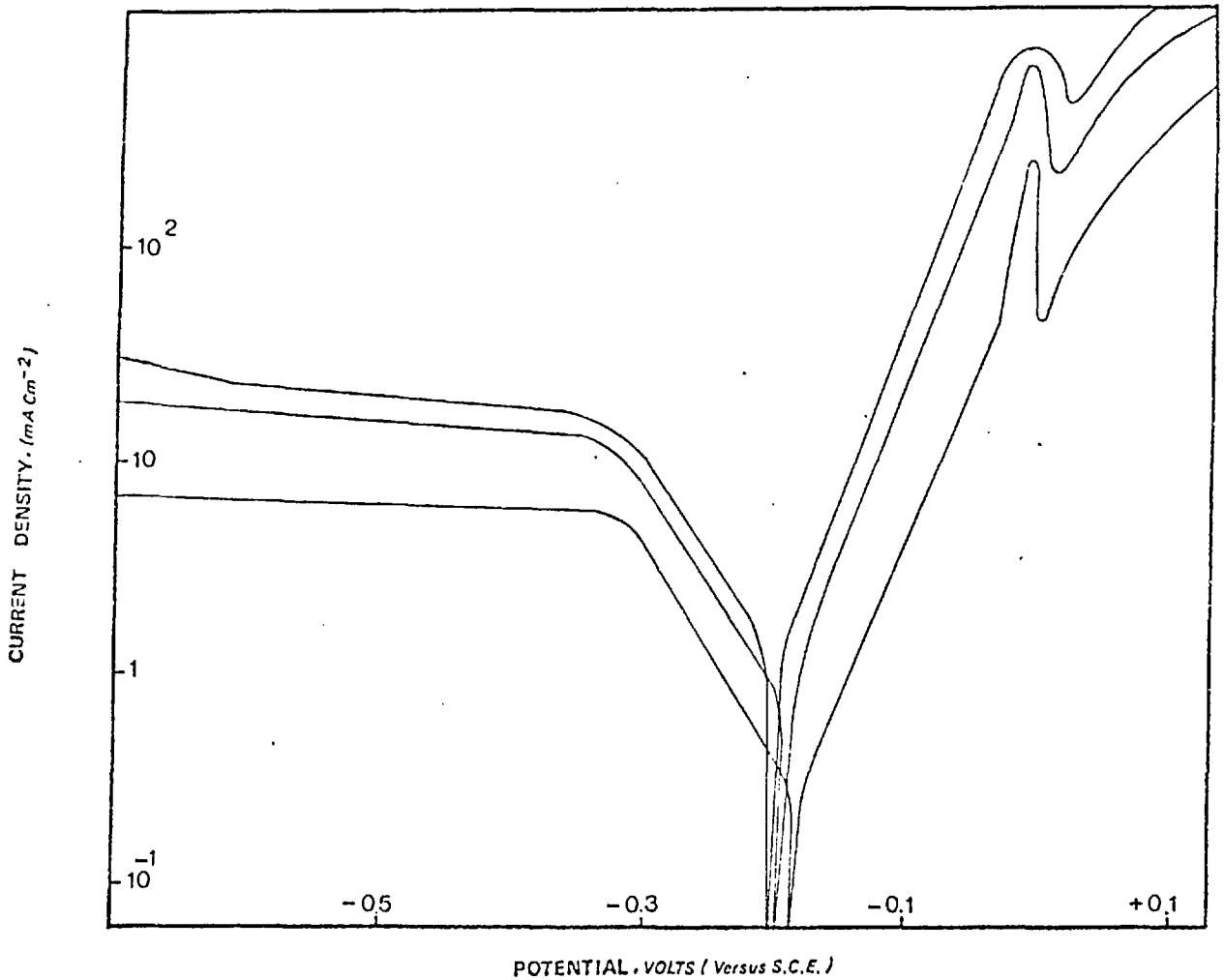


Figure 8.6: Polarization curves for Cu electrode in an aerated 0.1M NaCl solution at (a) 30°C; (b) 40°C; (c) 60°C.

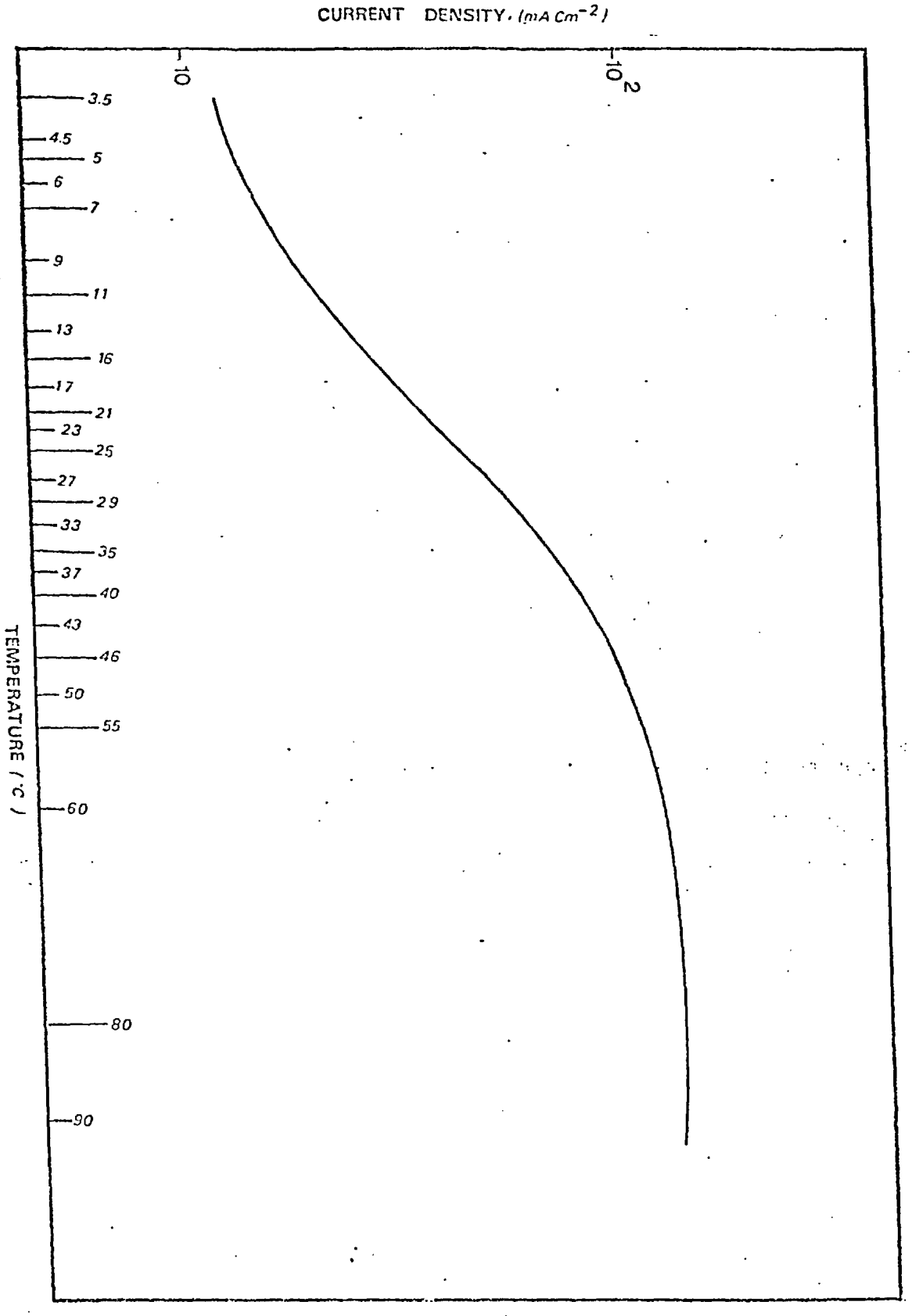


Figure 8.7: Variation of current density with temperature for a Cu electrode in an aerated 0.1M NaCl solution.

linear.

8.1.6 Effect of CuCl Concentration

Since the passivation was shown to be due to the formation of CuCl, if the solution is already saturated from CuCl, the passivation is expected to be stronger. Figure 8.8(a) and (b) show polarization curves for Cu electrode in 0.5M NaCl solutions (unstirred and aerated) and Cu electrode in an identical solution saturated with CuCl, respectively. Obviously the passivation is much more extensive in the case of CuCl addition. The reason for the high current density in the cathodic part and also for the disappearance of the Tafel region, is due to the addition of a new cathodic reaction, namely the reduction of Cu^+ to metallic copper. The corrosion potential shifts in the noble direction due to the addition of CuCl. Values for overvoltages as well as corrosion potentials are given in Appendix C .

8.1.7 Effect of Stirring

Stirring has little effect on the anodic branch of the polarization curve except for the passivation part. When the solution was stirred a less pronounced active/passive transition compared to the unstirred solution occurred. This is because stirring the solution prevents a localized high concentration of CuCl and disperses the CuCl molecules in the electrolyte. The more rigorous the stirring, the less extensive was the observed passivation. This phenomenon has been observed already by Lal and Thirsk (67).

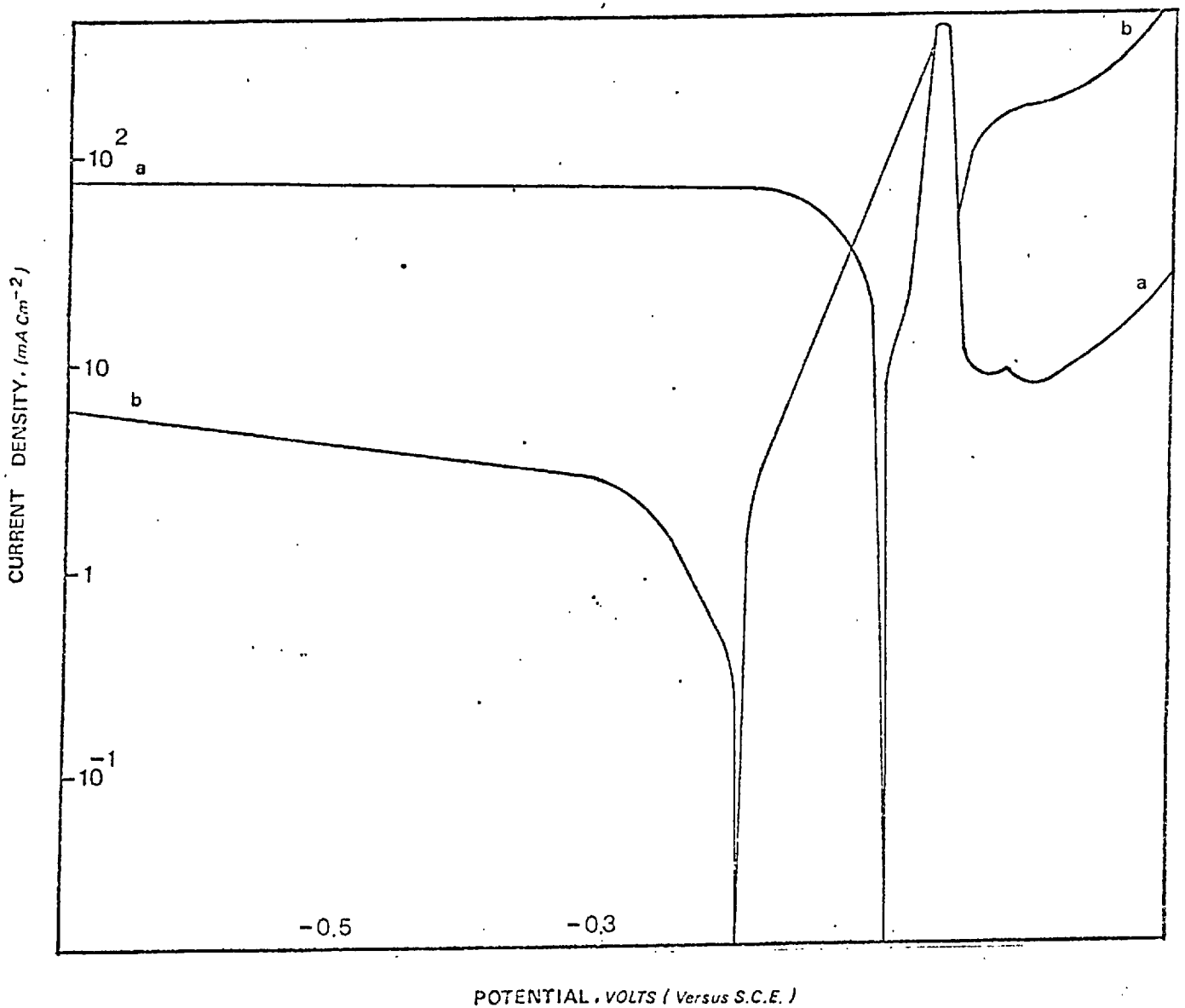


Figure 8.8: Polarization curves for Cu electrode in an aerated 0.5M NaCl solution (a) and with addition of CuCl (b).

The effect of stirring on the cathodic part is quite significant. This is because the reaction is a diffusion limited and obviously stirring the solution changes the limiting current density. Figure 8.9(a) shows the effect of stirring on current density at a given potential in the cathodic part. The solution was stirred with a magnetic stirrer and steps on this curve represents increasing the speed of stirring. Figure 8.9(b) shows the reverse process i.e. starting point represents the well stirred solution and then the solution was left unstirred.

8.2 Polarization Behaviour of Copper in the Presence of Inhibitors

The cathodic process (i.e. O_2 reduction) taking place in a Cu/NaCl system is a series of complex reactions including diffusion and adsorption of oxygen onto the surface. Since oxygen reduction takes place on the surface, it is reasonable to assume any modification of the surface may effect the oxygen adsorption and hence the cathodic processes. When a copper electrode is dipped in a solution containing inhibitors such as BTA, MBT, etc., it has been shown that the surface becomes covered with a complex of Cu/inhibitor and this may be expected to influence the cathodic reactions. Depending upon the nature and electrical properties of this film the cathodic reaction may be different from the one for the clean metallic surface.

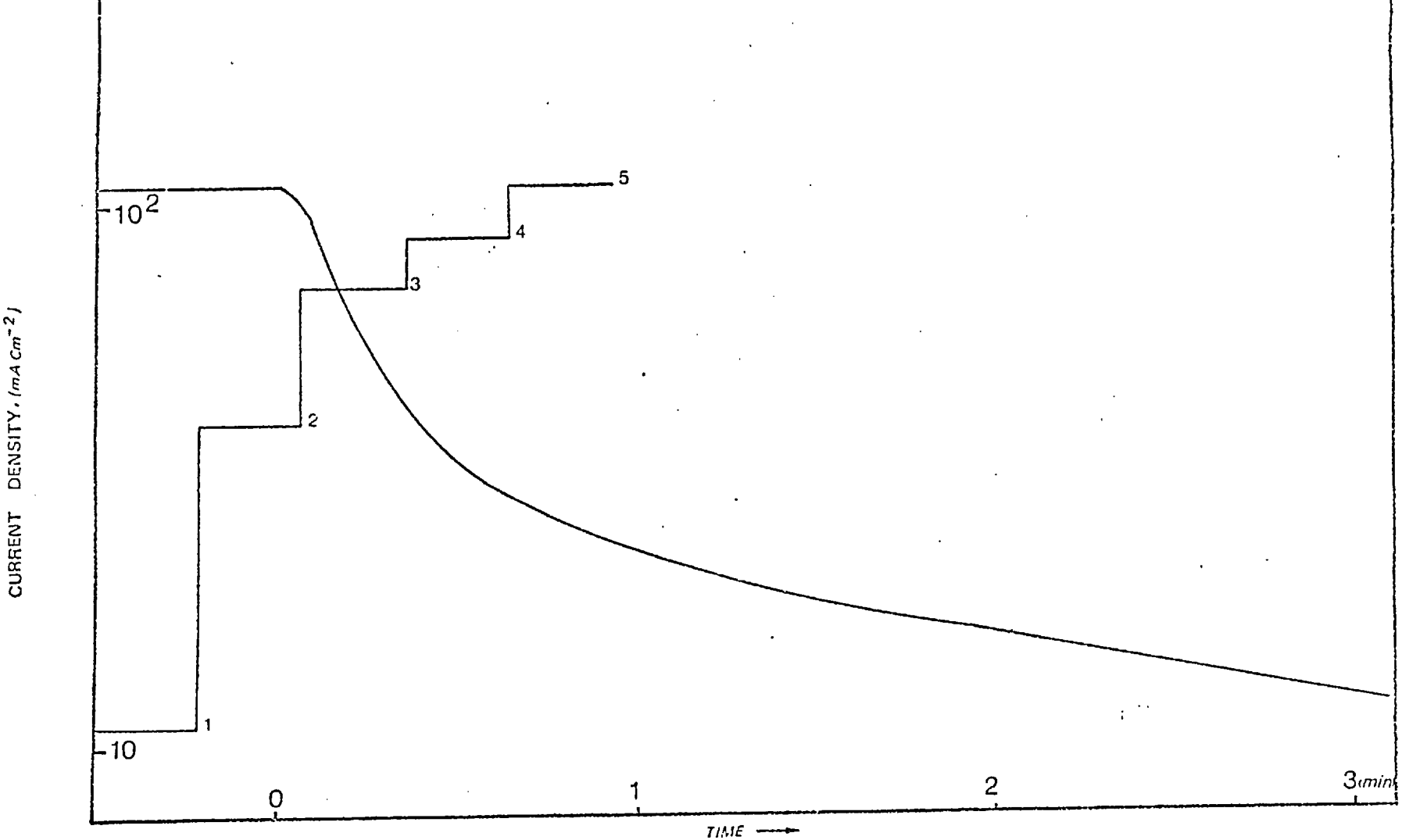


Figure 8.9: Stirring effect on current density for a Cu electrode in NaCl solution. Steps (1-5) shows different degrees of agitation. The curved line indicates a full speed of agitation (0 time). At this point stirrer was switched off and the rest of the curve shows variation of current density with agitation.

In the anodic part, the presence of inhibitor may interfere with anodic reactions. For instance the formation of the first anodic process i.e. Cu_2O may be affected. This is probably because of the interference by inhibitor with anodic nucleation which results in retardation of the process. The second anodic process i.e. CuCl formation, is of particular interest in presence of inhibitors. This is because of the ability of these inhibitors to form a complex with CuCl.

Six different inhibitors were used in this part of the experiments. These were benzotriazole, benzimiazole, benzothiazole, benzothiophene, 2-mercaptobenzothiazole and 2-mercaptobenzimiazole. Among these compounds only benzotriazole and benzimidazole are soluble in measurable amounts. For the rest of these inhibitors, which are only slightly soluble, saturated solutions were used. This represents a problem which makes direct comparison of these inhibitors impossible. Nevertheless, these results are still valid because they reveal the inhibition power of these compounds in saturated solutions. This is important because the possible industrial usage of these compounds as corrosion inhibitors involves saturated solutions (for details of structural formula of these compounds see Appendix A).

As stated already, it was noticed during this study that the most reproducible results were obtained when the concentration of NaCl was equal to or greater than 0.5M. For smaller NaCl concentrations e.g. 0.1M, it was shown that addition of inhibitor drastically changes the shape

of the polarization curves, but with a poor reproducibility.

8.2.1 Polarization of Copper in the Presence of Benzotriazole

Figure 8.10(a,b, and c) shows polarization curves of copper electrode in an aerated, unstirred 0.1M NaCl solution in presence of none ((8.10(a)), 2×10^{-5} (8.10(b)), and 2×10^{-4} (8.10(c)) BTA, respectively. In these concentrations, BTA affects the polarization behaviour of copper in both cathodic and anodic branches. A small active/passive transition has occurred in 2×10^{-5}M BTA concentration and as evident from Figure 8.10(b), is probably due to the reaction of BTA with Cu^{+} ions to form solid Cu-BTA. At higher concentrations, the anodic reaction is drastically modified with much lower currents (Figure 8.10(c)). Values of overpotentials are given in Appendix C.

Better results with very good reproducibility were obtained in 0.5M NaCl, stirred and aerated solutions. Figure 8.11(a) shows a polarization curve of copper in such a solution.Figure 8.11(b) and 8.11(c) show the result of the addition of 5×10^{-5}M and 5×10^{-4}M to identical solution, respectively.

The cathodic branch of the polarization curve in Figure 8.11(c) resembles Figure 8.2(b) in which oxygen was removed by nitrogen purging. Corrosion potentials are suppressed in both cases by almost the same amount. The only difference is when inhibitor is added to the electrolyte, because of the influence of "anionic specific adsorption" at the extreme cathodic overpotential, i.e. H_2 evolution, the effect of inhibitor is inverted. This

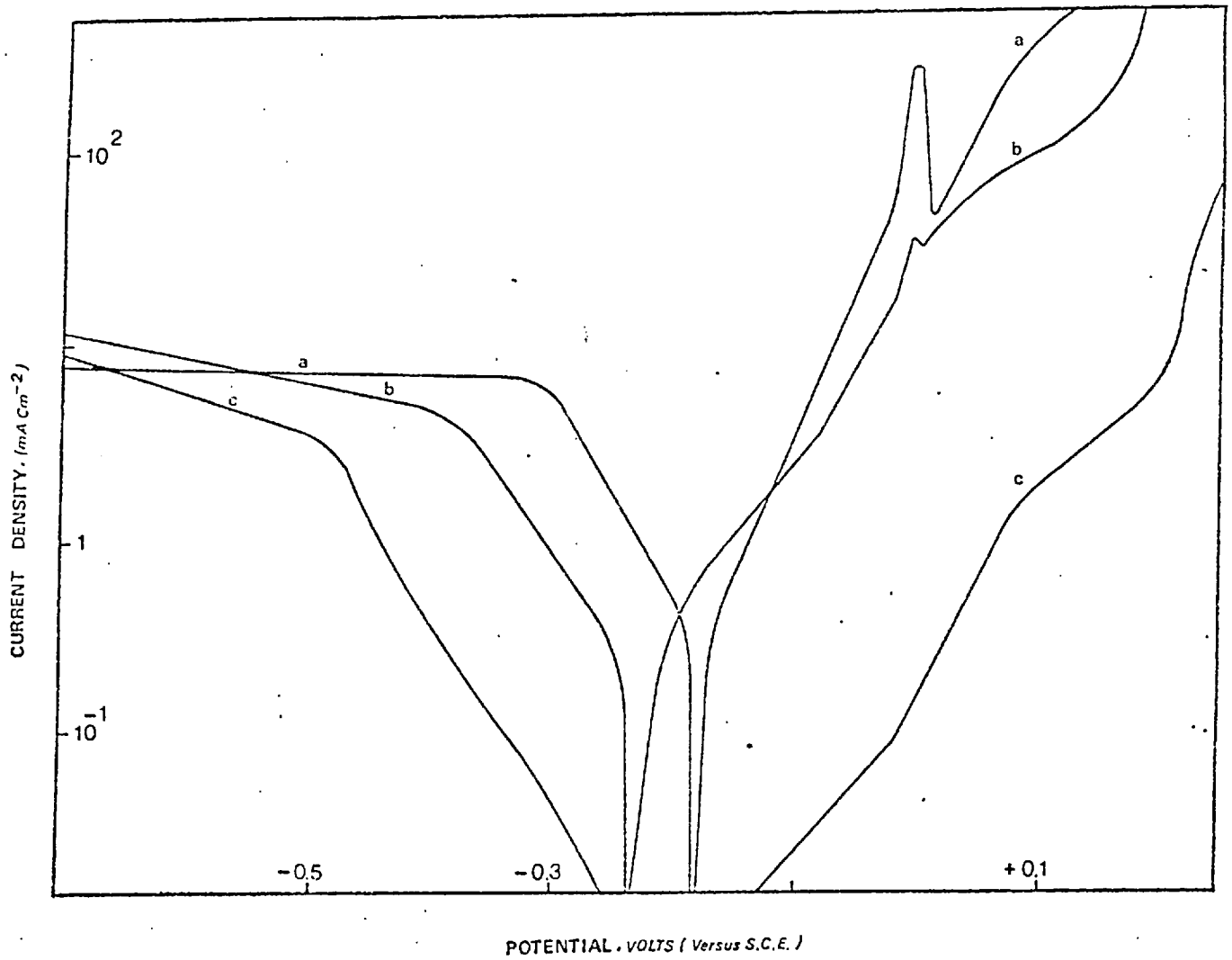


Figure 8.10: Effect of benzotriazole on Cu electrode polarization curves in 0.1 NaCl solution for BTA concentrations of (a) none; (b) 2×10^{-5}M; (c) 2×10^{-4}M.

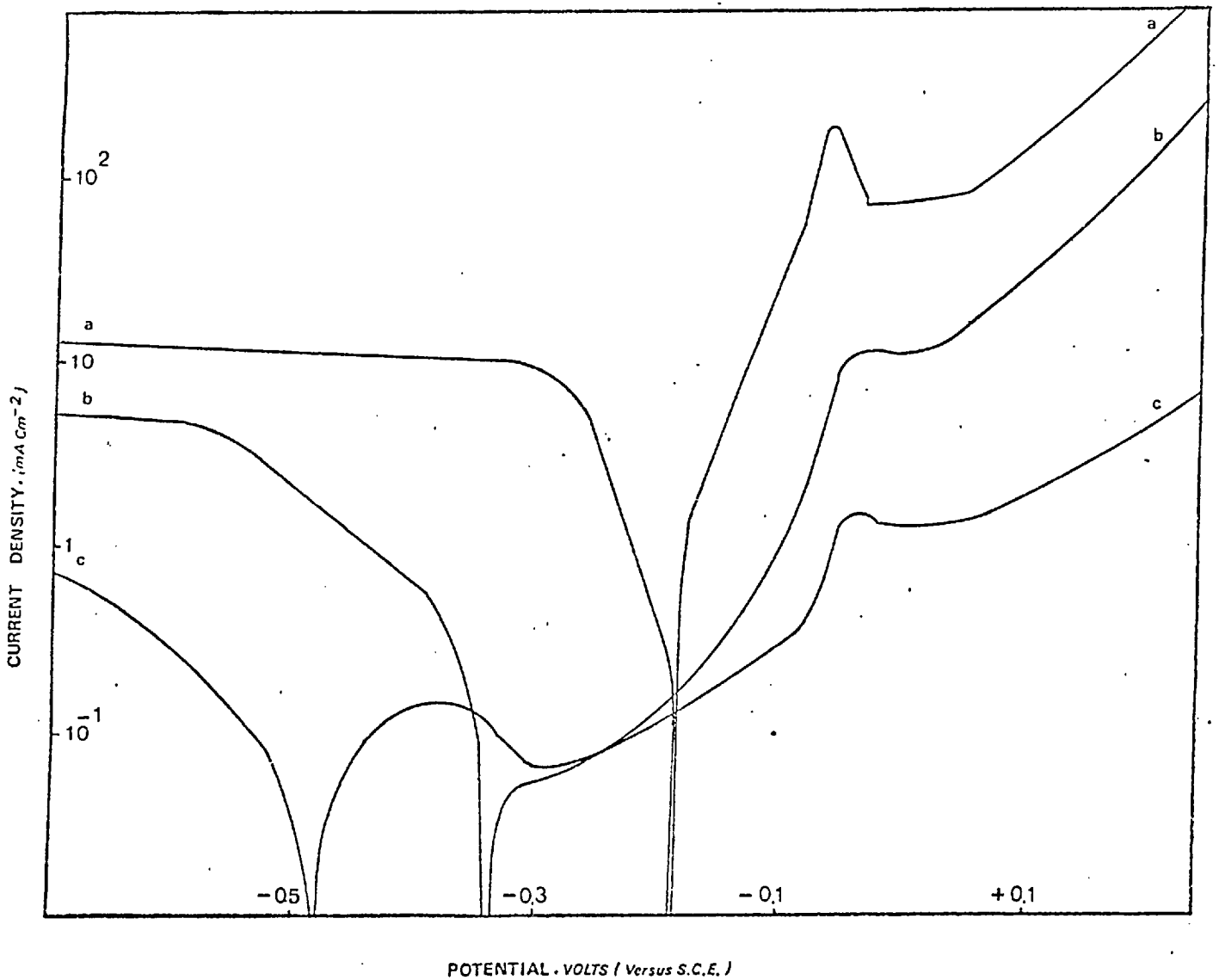


Figure 8.11: Polarization curves for Cu electrode in 0.5M NaCl solution in the presence of: (a) none; (b) 5 x10^{-5}M; (c) 5 x10^{-4}M BTA.

phenomenon has been noticed by Cotton (71) and Mansfield et al (72). For detail see Chapter 5. Cathodic polarization curves obtained for copper electrode in deaerated 0.5M NaCl solution showed that the addition of BTA into such solution has only a little effect on the cathodic cycle of the polarization curves. These results show that the effect of BTA on cathodic processes, is mainly upon the oxygen reduction, in contrast with the conclusion reached by Poling (51).

The anodic branch of the polarization curve shows no Tafel region in the presence of BTA, indicating the interference of the inhibitor with the anodic processes. An apparent change can be observed in the anodic curves as the potential reaches to CuCl formation. When the concentration of BTA is sufficiently large i.e. 10^{-5} (Figure 8.11(c)) for a certain increase in the overpotential, no increase in current density is observed. After this region, increasing the potentials, results in an increase in the current densities (corresponds to transpassive region in inhibitor free solutions). However the values of current density for any given potential in this region is significantly less when BTA is present. The suppression of current densities and corrosion potentials is related to amount of BTA present.

8.2.2 Polarization of Copper in the Presence of Benzimidazole

The same behaviour was observed for benzimidazole except this compound need to be almost ten times greater in concentration to induce similar effect of BTA on Cu/NaCl

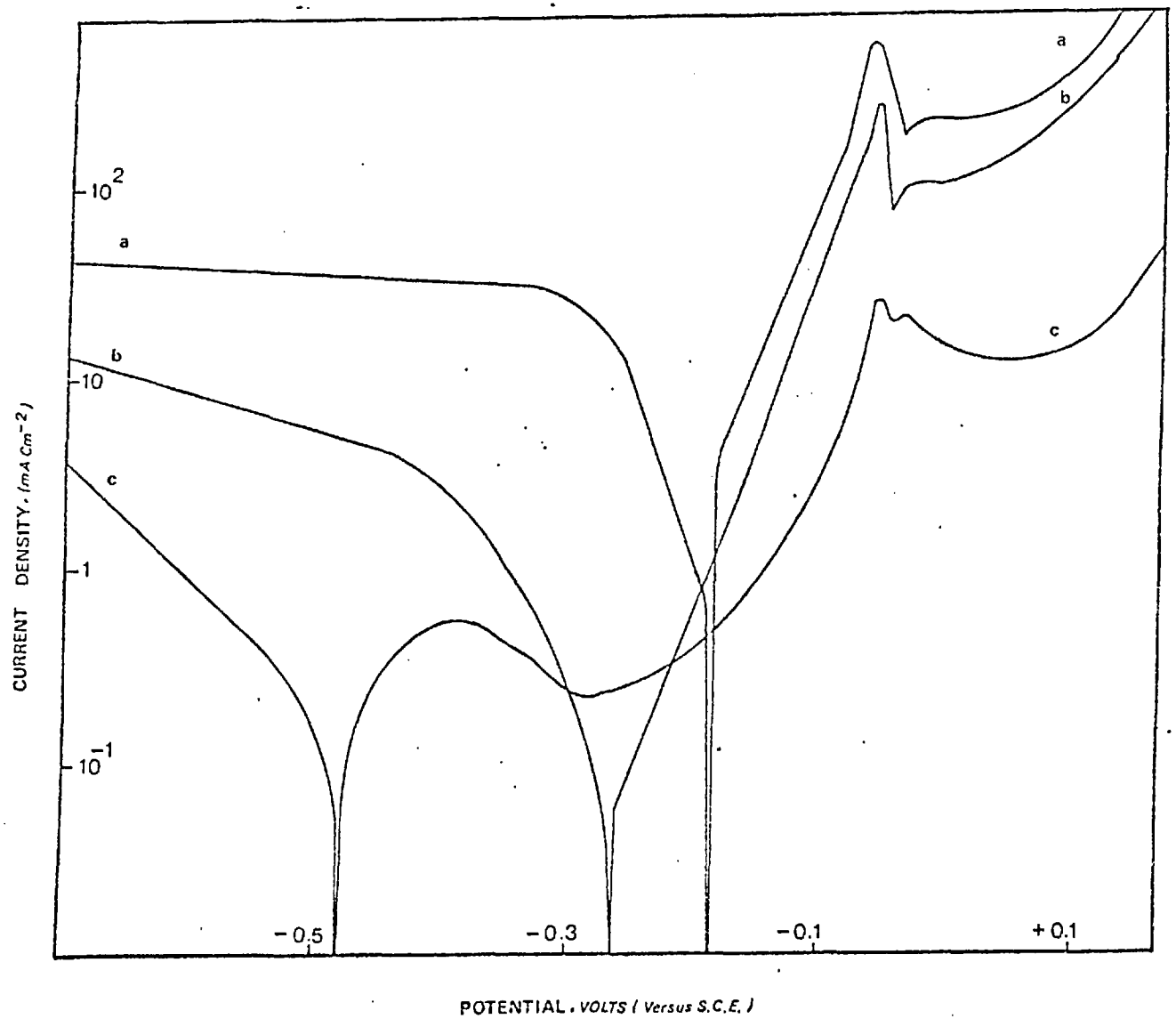


Figure 8.12: Polarization curves for Cu electrode in 0.5M NaCl solution in the presence of: (a) none; (b) 5 x 10^{-4} M; (c) 5 x 10^{-3} M benzimidazole.

solution system. This must be noted that even with ten times greater concentrations, benzimidazole showed higher current density for given anodic overpotential than BTA. Effect of this compound on cathodic polarization curves at higher concentrations (e.g. 5×10^{-3}) is the same as BTA. In anodic part even with this concentration, some formation of Cu^{+} probably as CuCl, can be observed. This indicates that benzimidazole is probably less reactive towards CuCl. Figure 8.12(a) shows a polarization curve for copper in an aerated stirred 0.5M NaCl solution and Figure 8.12(b) and (c) show the result for an identical system with addition of 5×10^{-4} and 5×10^{-3}M. benzimidazole to the solution.

Above results justifies the assumption that BTA is at least ten times stronger than benzimidazole in respect to effect on cathodic and anodic processes and hence on corrosion rate.

8.2.3 Polarization of Copper in the Presence of Other Inhibitors

As stated already, BTA and benzimidazole were the only two among the rest which are appreciably soluble. So direct comparison of the rest is not possible. However, in saturated solutions, benzothiazole, 2-mercaptobenzothiazole and 2-mercaptobenzimidazole exhibited the same effect on cathodic part of polarization curve. Figure 8.13(a) shows a polarization curve for copper in aerated, stirred, 0.5M NaCl solution and Figure 8.13(b), (c) and (d) show the results of addition of inhibitors in such a solution.

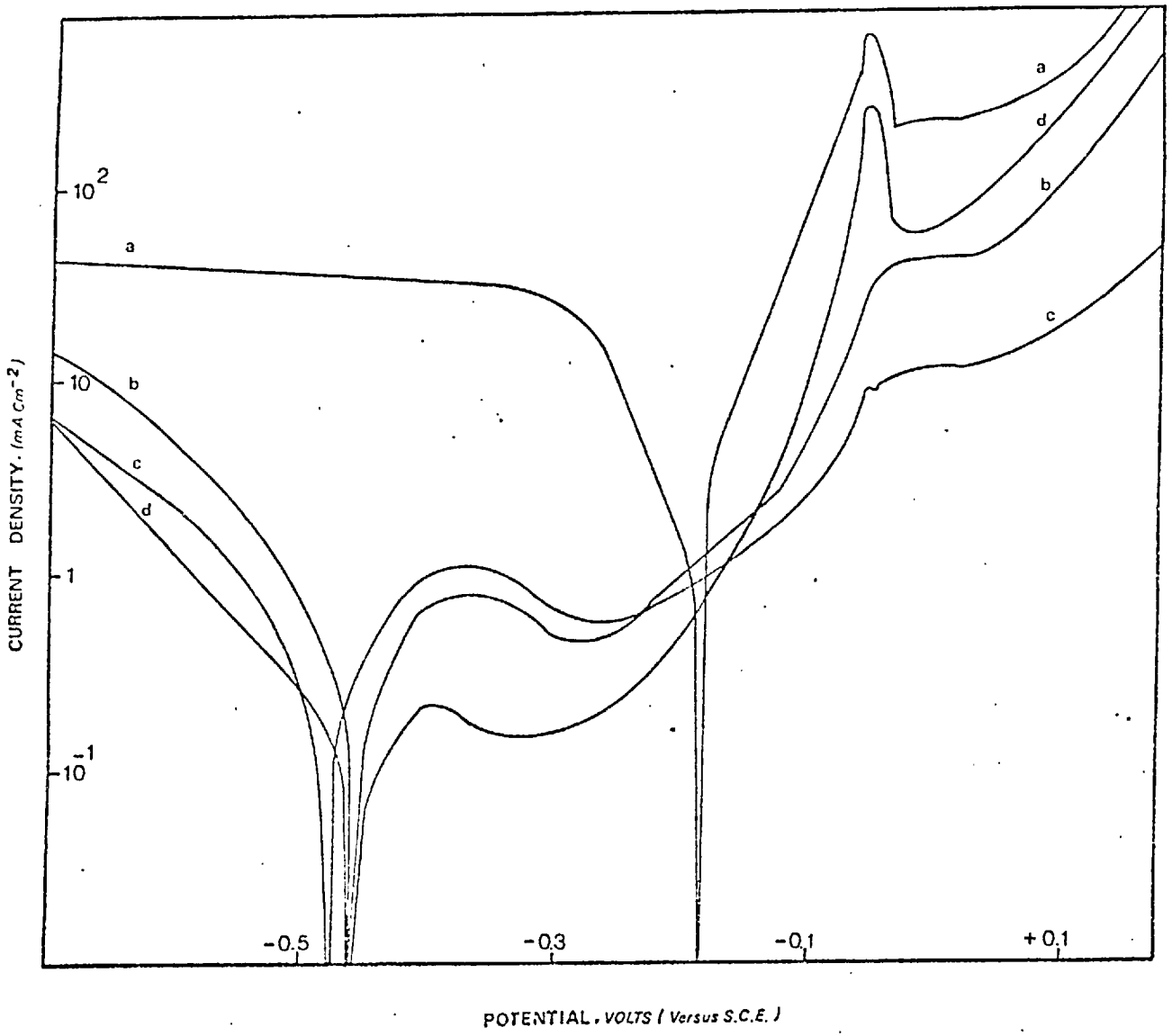


Figure 8.13: Polarization curves for Cu electrode in 0.5M NaCl solution in the presence of (a) none; (b) benzothiazole (sat.); (c) 2-mercaptobenzimidazole (sat.); (d) 2-mercaptobenzothiazole (sat.).

In the case of MBT (Figure 8.13(d)) the cathodic process of O_2 reduction is inhibited by addition of MBT. In anodic part, although for small overpotentials MBT gives the smallest values of current densities compared to the other inhibitors, for higher overpotentials the anodic branch of polarization curve sharply rises. Production of Cu^+ ions leading to formation of CuCl and subsequent passivation is almost similar to that of the uninhibited Cu electrode. This is probably due to very small concentration of MBT in solution such that it cannot react with all the Cu^+ produced. 2-mercaptobenzimidazole has the most effectiveness after BTA in saturated solutions. Benzothiazole in this respect falls somewhere between MBT and 2-mercaptobenzimidazole. In Table (8.1) inhibitors are listed according to their effectiveness. The strongest appears at the top. All values for overpotentials and corrosion potentials for different inhibitors are given in Appendix C.

Finally, it must be stated that benzothiophene showed no effect on polarization curves. Moreover this compound unlike the rest, failed to form a precipitate with copper salts in aqueous solutions.

The results, in Table (8.1) indicate, that according to these measurements, BTA appears to be the strongest inhibitor for both cathodic and anodic processes. A great advantage of BTA is that this compound is appreciably soluble (about 2 grams/litre), MBT which seemed to be a promising inhibitor (40) and shows good inhibition properties in the cathodic part, appeared to be worst (ignoring benzothiophene) in the anodic part.

	Cathodic	Anodic
1	benzotriazole ($5x10^{-4}$M)	benzotriazole ($5x10^{-4}$M)
2	benzimidazole ($5x10^{-3}$M)	2-mercaptobenzimidazole (sat.)
3	2-mercaptobenzothiazole (sat.)	benzimidazole ($5x10^{-3}$M)
4	2-mercaptobenzimidazole (sat.)	benzothiazole (sat.)
5	benzothiazole (sat.)	2-mercaptobenzothiazole (sat.)
6	benzothiophene (sat.)	benzothiophene (sat).

Table 8.1: Effectiveness of Inhibitors on Cathodic and Anodic Polarization of Copper (effectiveness decreases from top to bottom).

8.3 Summary

In the electrochemical polarization investigation of copper in NaCl solution in the presence and absence of inhibitors, it has been shown that the predominant cathodic process in an aerated solution is the oxygen reduction reaction. In the anodic part an active/passive region was found which is concluded to be due to formation of CuCl on the surface. At lower overpotentials, the anodic process was identified as Cu_2O formation. A transpassive region was observed at higher overpotentials. At extreme anodic overpotential values, the formation of Cu^{++} species was demonstrated.

A comparison of the inhibition power of six different inhibitors was carried out by observing their effectiveness on cathodic and anodic branches of polarization curves. In this respect BTA appeared to be the most powerful inhibitor in the series and benzothiophene the worst.

CONCLUSION

The final conclusions reached in the present study are:

1. Organic corrosion inhibitors for copper and copper-based alloys used in the present study exercise their action through the formation of a protective surface film.

2. The nature of these surface films is a complex between the organic molecule and ions which is identical to the solution prepared cuprous complexes. These cuprous complexes are responsible for protection even in the case of copper alloys.

3. Exposure of these protective films to the atmosphere oxidizes and degrades them to such an extent that they are no longer protective. Thus it is concluded that in any industrial treatment, provision must be made to ensure that there is always a sufficient reservoir of inhibitor present in the system.

4. Finally, ESCA (XPS and X-AES) is one of the most powerful techniques for investigating corrosion inhibition. This work shows ESCA can be used successfully in elucidation of the nature of the surface films, the mechanism of film formation, and the oxidation and degradation of such films.

APPENDIX A

MATERIALS AND EXPERIMENTAL

(a) Materials

Materials and their specifications used in the present study are given below:

1. Metals and Alloys

Copper samples for infrared reflectance spectroscopy, ESCA and electrodes were machined from pure electrolytic copper from I.N.C.O. (Mond) Ltd. The whole range of Cu/Ni alloys as well as pure copper and pure nickel, were donated by Dr W.H. Wilman. Pure copper, nickel and 55/45 copper/nickel alloy foils were obtained from Goodfellow Metals Ltd. Metallic zinc foil was obtained from Hopkin and Williams Ltd., with a purity better than 999%. Brass samples were machined from a 67/33 copper/zinc alloy with following composition

Fe	less	than	0.7%
Ni	"	"	0.2%
Pb	"	"	0.03%
Al	"	"	0.3%
S	"	"	0.05%
Sb	"	"	0.15%

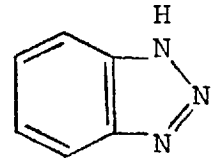
The maximum limits of impurities in electrolytic copper were as follows:

Acid-insoluble matter	0.01%
As	0.0001%
Bismuth and Pb	0.002%
Fe	0.005%
Mn	0.002%
Ni	0.0008%
Sn	0.001%

2. Chemicals

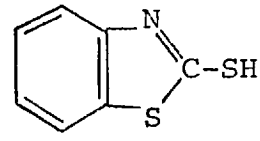
All chemicals and reagents used in this study were the purest available (Analar grade or equivalent). Organic compounds used, are listed below with their formula, the place they have obtained and their impurities.

(a) Benzotriazole

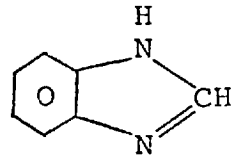


Obtained from BDH Chemicals Co.(99%).

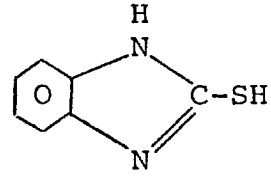
(b) 2-mercaptobenzothiazole



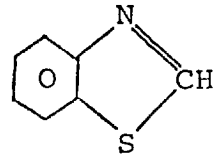
Obtained from BDH Chemical Co. and was not less than 99 per cent (ex sulphur) and sulphated ash not more than 0.1%.

(c) Benzimidazole 

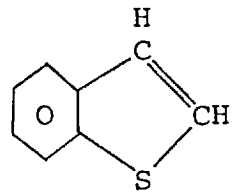
Obtained from Aldrich Chemical Co. (98%).

(d) 2-mercaptobenzimidazole 

Obtained from Aldrich Chemical Co. (98%).

(e) Benzothiazole 

Obtained from Aldrich Chemical Co. (99%).

(f) Benzothiophene 

Obtained from Aldrich Chemical Co. (97%).

(g) Cuprous oxide, cupric sulphate, sodium and potassium chloride and inorganic acids all were obtained from BDH Limited all in Analar grade.

(b) Experimental

(1) Electrochemical Polarization Experiment Techniques

Polarization of the copper samples were carried out using a Wenking Model PCA 72M Potential Control Amplifier Model VSC 72 Voltage Scan Generator. A Bryans X-Y recorder 26000 with a logarithmic amplifier unit

(Model 26238) for Y axis, was used to record polarization curves. A platinum electrode was used as an auxilliary electrode and the temperature was controlled using a water bath. Analar grade sodium chloride and triply distilled water were used for making electrolytes. Injection of inhibitors following by cathodic polarization of copper samples was carried out using the same potential amplifier. This was carried out by potentiostating the copper sample in a pure NaCl electrolyte at 0.90V vs. S.C.E. for sometime (say ½ hour) to make sure all oxides are reduced to metallic copper. The circuit was then broken followed by injection of inhibitor from a side arm. The samples were then exposed to this solution for a period of time. The samples afterwards were removed, washed and air dried. Films of Cu_2O on copper samples were grown electrochemically in 1M KOH solution. The polished samples were etched in diluted nitric acid solution first, then rinsed and potentiostated in KOH solution at -0.95V vs. S.C.E. in order to reduce the oxide to copper metal. The potential then was dropped to -0.45V vs. S.C.E. to form Cu_2O. The sample then rinsed with distilled water thoroughly.

Working electrodes were prepared from a cylindrical rod of pure electrolytic copper with known diameter. The electrodes were cut in 3 mm. thickness and then covered with an epoxy resin (Araldite) in order to have only one face exposed to solution. No contamination from epoxy resin was noticed.

(2) Electron Spectroscopy Experimental Technique

ESCA spectra of samples obtained with a V.G. ESCA-3 using an AL x-ray anode (for detail see Chapter4). Samples were cut and machined for a bulk of pure copper (7 mm. x 5 mm.), then abraded and polished in the way described earlier. Argon ion sputtering was used to clean at final stage inside the spectrometer. A typical rate of etching by argon ion bombardment was found to be ½ Å per minute per 1μA for Ni. Powder samples were mounted in double sided adhesive tapes. For the samples which were to be examined at very low temperature (e.g. BTA), the samples were mounted on a low temperature probe, into which liquid nitrogen was sucked by a pump. Temperatures as low as -150^{o}C could be obtained easily using this technique.

(3) I.R. Reflectance Spectroscopy Experimental Techniques

Reflectance spectra of samples were recorded on a Perkin-Elmer infrared spectrometer model 457, using a Specac Multi-reflectance unit with a maximum 25 reflections. An air gap of approximately 2 mm. was used between the two highly polished sample mirrors. The mirrors were cut from pure copper in approximate size of 52 mm. x 28 mm., then polished to obtain mirrors. Powder samples were pressed in a K Br disc with 15 torrs pressure.

(4) Complexes Preparation

Cu-inhibitor complexes for both ESCA and I.R. spectroscopy were prepared by addition of unimolar solutions of copper salts and inhibitor. In the case of inhibitors with very small solubility such as MBT, a

saturated solution of MBT was added to a dilute solution of copper salt. The precipitate then were collected and after several washes with triply distilled water were dried in air. To investigate the effect of Cl^- concentrations on precipitants, different amounts of NaCl (varying between O-2M.) was added to the original solution.

APPENDIX B

BINDING AND KINETIC ENERGIES

All binding and kinetic energies for different elements and compounds used in this study is listed in Table B1. All binding energies are relative to C 1s = 285.0 eV. Kinetic energies were corrected for charging effect where necessary.

TABLE B1:

Sample	$Cu2p_{3/2}$ B.E.(eV)	CuLMM K.E.(eV)	$Ni2p_{3/2}$ B.E.(eV)	NiLMM K.E.(eV)	$Zn2p_{3/2}$ B.E.(eV)	ZnLMM K.E.(eV)	N 1s B.E.(eV)	S 2p B.E.(EV)	Cl 2p B.E.(eV)	Br 3p B.E.(eV)
Copper (etched)[a]	932.9	919.7								
Cuprous Oxide[b]	933.1	917.1								
Cu(I)-BTA surface film	933.0	915.7					399.9			
Cu(I)-BTA surface film after oxidation	935.8	916.6					399.8			
Cu_2-BTA Cl surface film	933.0	915.6					399.9		198.7	
Cu_2-BTA Cl surface film after oxidation	935.9	916.4					400.0		198.6	
Cu(I)-BTA (prep. chemicallY)[c]	932.9	915.9					399.9			
Cu(I)-BTA complex after oxidation	935.8	916.5					399.9			
Cu(II)-BTA (prep. chemically)[c]	935.4	916.6					399.7			
70Cu:30Ni air exposed	932.8	919.4	852.9 856.1	846.9						

TABLE B1 (continued)

Sample	$Cu2p_{3/2}$	CuLMM	$Ni2p_{3/2}$	NiLMM	$Zn2p_{3/2}$	ZnLMM	N 1s	S 2p	Cl 2p	Br 3p
70Cu:Ni etched	932.7	919.3	853.0 -	846.8						
70Cu:30Ni + BTA	932.9	9[d]					399.8			
30Cu:70Ni (air exposed)	933.1	919.5	853.1 (856.2)	846.8						
30Cu:70Ni etched	933.0	919.6	853.1 -	846.9						
30Cu:70Ni + BTA (5 min.)	932.9	-	853.0 (856.0)	?			400.0			
30Cu:70Ni + BTA	932.9	?					400.0			
Ni Polished			853.0 (856.1)	846.9						
Ni (etched)			852.9	846.8						
Ni + BTA			853.0 (856.3)	846.9			~400.0			
70Cu:30Zn (air exposed)	932.9	919.6			1021.4	993.0 (988.4)				
70Cu:30Zn (etched)	932.9	919.4			1021.1	993.1 -				

TABLE B1 (continued)

Sample	$Cu2p_{3/2}$	CuLMM	$Ni2p_{3/2}$	NiLMM	$Zn2p_{3/2}$	ZnLMM	N 1s	S 2p	Cl 2p	Br 3p
70Cu:30Zn + BTA	932.8	916.0?			1021.9	987.0	399.9			
Zinc (polished)					1021.0	992.9 (988.4)				
Zinc (etched)					1021.8	993.0				
Zinc + BTA					1021.7	987.2	399.7			
Cu(I)-MBT surface film	932.9	916.7					400.1	164.1		
Cu(I)-MBT after oxidation	935.6	916.3					400.2	164.1 (168.2)		
Cu(i)-MBT complex [d]	933.1	916.4					399.8	163.9		
Cu(I)-MBT complex oxidized)	935.7	916.3					400.0	164.0 (168.3)		
70Cu:30Ni + MBT	933.0						399.7	163.9		
30Cu:70Ni + MBT	932.2						399.7	164.1		
70Cu:30Zn + MBT	932.9						399.9	163.9		
benzotriazole (BTA)							398.3			
2-mercaptobenzothiazole(MBT)							399.8	164.1		

TABLE B1 (continued)

Sample	$Cu2p_{3/2}$	CuLMM	$Ni2p_{3/2}$	NiLMM	$Zn2p_{3/2}$	ZnLMM	N 1s	S 2p	Cl 2p	Br 3p
benzimidazole							397.8			
2-mercaptobenzi-midazole (MBIA)							399.6	162.95		
Cu(I)-MBIA Complex before oxidation	933.0						399.5	163.2		
Cu(I)-MBIA Complex after oxidation	935.8						399.7	163.2 168.0		
Cu(I)- benzimidazole before oxidation	932.7						399.4			
Cu(I)-benzimidazole after oxidation	935.5						399.5			
Cuprous chloride	933.1	917.0							199.03	
Cuprous bromide	932.7									182.66
CuBr + BTA	933.1						399.5			181.9

a - Argon ion etched inside the spectrometer (see Appendix A)
b - Grown electrochemically (see Appendix A).
c - Prepared from precipitations in solution (see Appendix A).
d - Question marks show that the signal is too weak to allow measurements with reasonable accuracy.

APPENDIX C

Table C1: Values of Electrochemical Overpotentials and Corrosion Potentials for Copper Electrode in Brine Solution.

ELECTROLYTE	$E_{corr.}$ mV/SCE	η_c mV	η_a mV
0.01M NaCl	-100	-132	+72
0.1M NaCl	-170	-670	+70
1.0M NaCl	-247	-192	+34
0.5M NaCl (unstirred)	-229	-114	+47
0.5M NaCl (stirred)	-220	- 40	+22
0.5M NaCl (deaerated)	-436	- 99	+238
0.1M NaCl + 2×10^{-5}M BTA	-238	-150	+141
0.1M NaCl + 2×10^{-4}M BTA	-250	-229	+385
0.5M NaCl + 5×10^{-5}M BTA	-329	- 44	+274
0.5M NaCl + 5×10^{-4}M BTA	-471	-166	+404
0.5M NaCl + 5×10^{-4}M BIA	-248	-111	+ 85
0.5M NaCl + 5×10^{-3}M BIA	-470	-156	+359
0.5M NaCl + Sat. BA	-441	- 82	+315
0.5M NaCl + Sat. MBT	-446	-152	+307
0.5M NaCl + Sat. MBIA	-470	- 95	+344

All values of overpotentials are at $5\mu A/cm^2$.

APPENDIX D

I.R. spectra of benzimidazole, benzothiazole and 2M-benzimidazole and their copper(I) complexes.

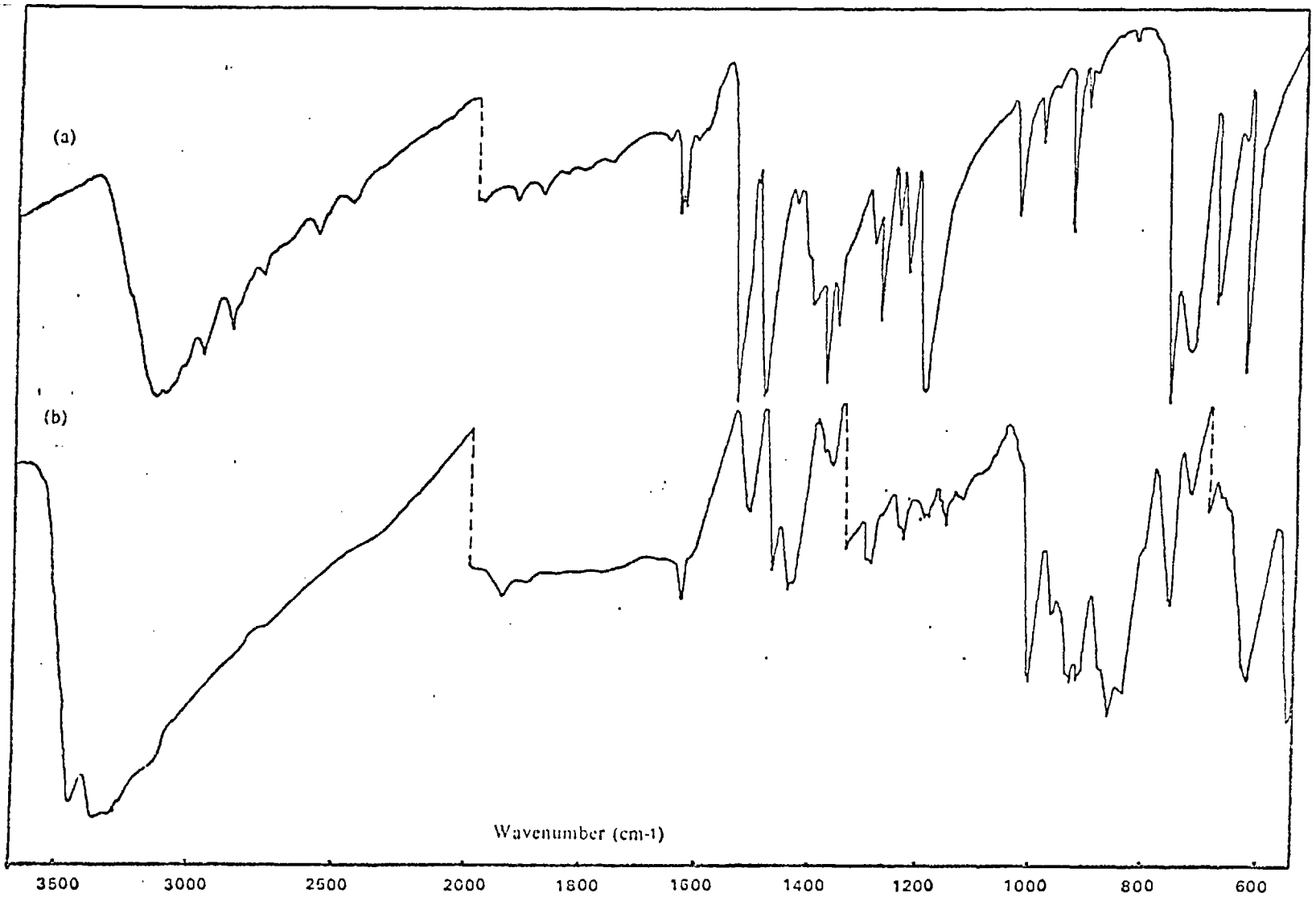


Figure D1: Infrared spectra of (a) 2-mercaptobenzimidazole in K Br pellet; (b) copper (I) complex of this compound in K Br.

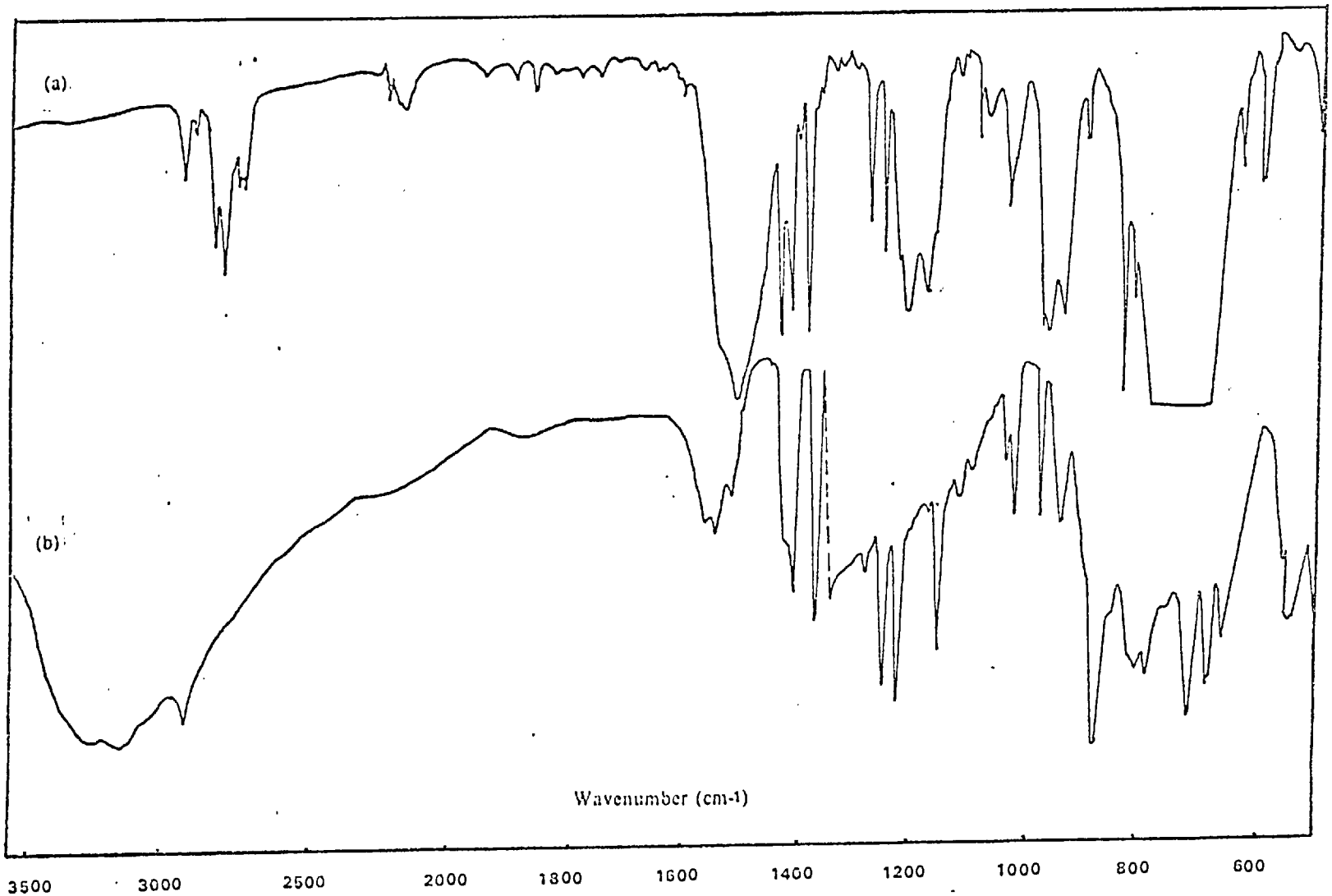


Figure D2: Infrared spectra of (a) benzothiazole in K Br pellet; (b)copper (I) complex of this compound in K Br.

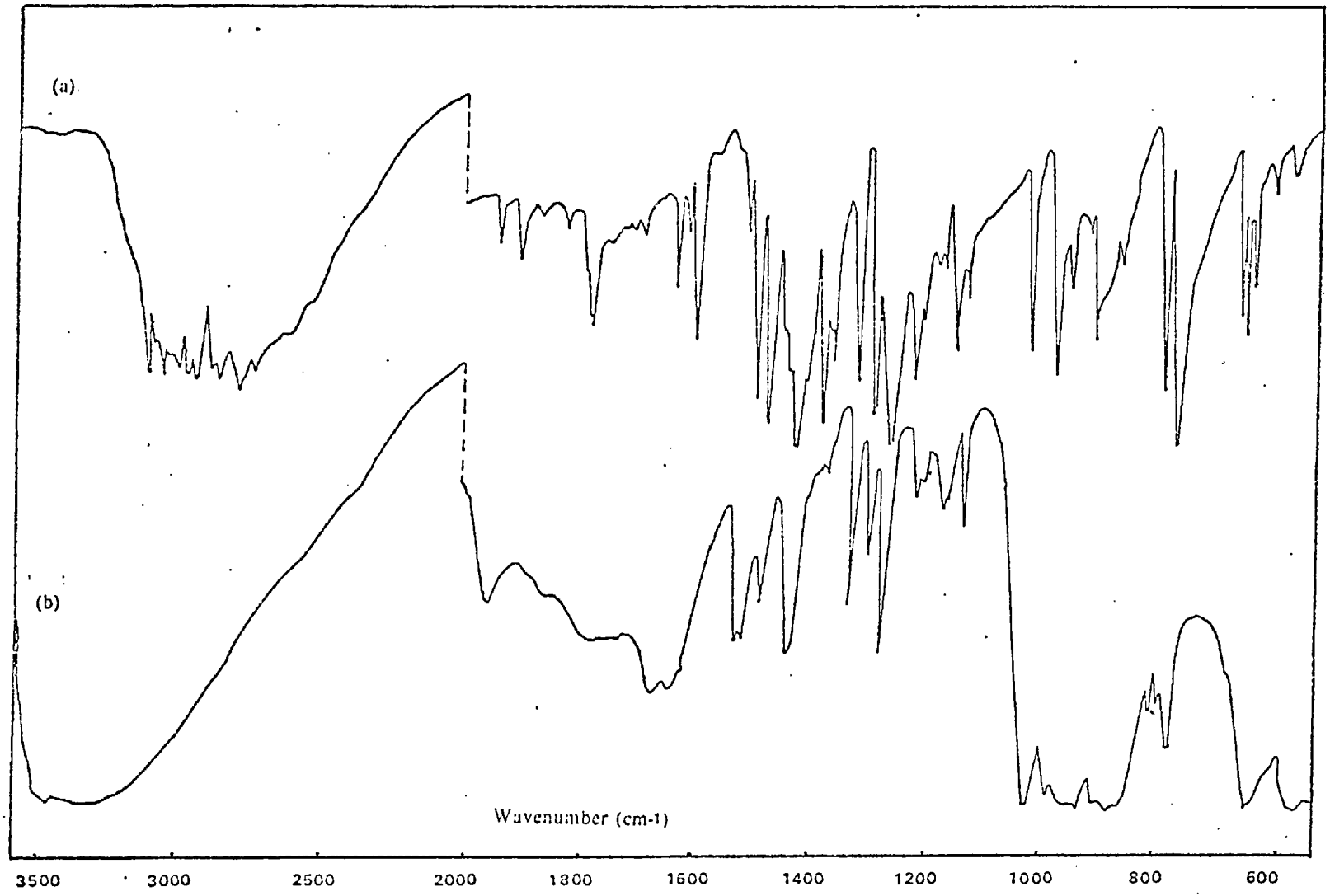


Figure D3: Infrared spectra of (a) benzimidazole in K Br pellet; (b) copper (I) complex of this compound in K Br.

REFERENCES

1. Report of the Committee on Corrosion and Protection, Department of Trade and Industry, London 1977.

2. Uhlig, H.H., Corrosion, 6, 29, (1950).

3. Liechtenstein, S., The Many Faces of Corrosion, Technical News STR-3454, National Bureau of Standards, NBS, Washington D.C., 1966.

4. Chadwick D. and Jamei, M., Presented at: "Chemical Process Hazards with Special Reference to Plant Design", symposium. The Institution of Chemical Engineers Symposium Series No. 49, 1977.

5. Tomashov, N.D., Theory of Corrosion and Protection metals, The McMillan Co., New York-London, 1966.

6. Speller, F.N., Corrosion Causes and Prevention, McGraw-Hill, New York, 1951.

7. Patterson, T.A., Carrer, J.C., Leyden, D.E. and Hercules, D.M., J. Phys. Chem., 80, 1700 (1976).

8. Castle, J.E., Surface Science, 68, 583, (1977).

9. Greene, N.D., Experimental Electrode Kinetics, Rensselaer, New York, 1965.

10. Eischen, R.P., and Pliskin, W.A., Advances in Catalysis, Vol. X., Academic Press Inc., New York, 1958.

11. Francis S.A. and Ellison, A.H., J. Opt. Soc. Am., 1959, 49, 131.

12. Leja, J., Little, L.H., and Poling, G.W., Bull. Inst. Mining Met., 676, 414, (1963).

13. Carlson, T.A., Photoelectron and Auger Spectroscopy, Plenum Press, New York, 1975.

14. Siegbahn, K., Nordling, C., Fahlman, A., Nordberg, R, Hamrin, K., Hedman, J., Johannson, G., Belgmark, T., Kartsson, S.E., Lindgren, I., and Linberg, B., ESCA: "Atomic, Molecular and Solid State Structure Studied by Means of Electron Spectroscopy".

15. Sevier, K.D., Low Energy Electron Spectrometry, Wiley-Interscience, New York, 1972.

16. Prutton, M., Surface Physics, Claredon Press, Oxford,(1975).

17. Frost, D.C., McDowell, C.A., and Tapping, R.L., J. Electron Spectrosc., 7, 297, (1975).

18. Brisk, M., and Baker, A.D., J. Electron Spectrosc., 7, 81, (1975).

19. Tolman, C.A., Riggs, W.M., Linn, W.J., King, C.M., and Wendt, R.C., Inorg. Chem., 12, 2770, (1973).

20. Rosencwaig, A., Wertheim, G.K., and Guggenheim, H.J., Phys. Rev. Lett., 27, 479, (1971).

21. Yin, L., Alder, I., Tsang, T., Matienzo, L.J, and Grim, S.O., Chem. Phys. Lett., 24, (1974), 81.

22. Kim, K.S., J. Electron Spectroscopy., 3, 217, (1974).

23. Pignataro, S., Foffani, A., and Distefano, G., Chem. Phys. Lett., 20, 350, (1973).

24. Hamer, A.D., Tisley, D.G., and Walton, R.H., J. Inorg. Nucl. Chem., 36, 1771, (1974).

25. Spears, D.P., Fischbeck, H.J., and Carlson, T.A., Phys. Rev. A., 9, 1603, (1974).

26. Pignataro, S., DiMarino, R., Distefano, G., and Mangini, A., Chem. Phys. Lett., 22, 352, (1973).

27. Johansson, G., Hedman, J., Berndtsson, A., Kasson, M., and Nilsson, R., J. Electron Spectroscopy., 2, 295, (1973).

28. Chadwick, D.C., Chem. Phys. Lett., 21, 291, (1973).

29. Krause, M.O., and Wuilleewmiev, F., Electron Spectroscopy (D.A. Shirley, editor), North Hollan Publ. Co. Amsterdam (1972).

30. Novakov, T, and Prins, R., Solid Communication, 9, 1975 (1971) and

Novakov, T., Phys. Rev. B., 2693, (1971).

31. Frost, D.C., Ishtani, A., and McDowell, C.A., Mol. Phys. 24, 861, (1972).

32. Larson, P.E., J. Electron Spectroscopy, 4, 213, (1974).

33. Rosencwaig, A., and Wertheim, G.K., J.Electron Spectrosc., 1, 495, (1973).

34. Wagern, C.D., Anal. Chem., 44, 1050, (1972).

35. Jørgensen, C.K., and Berthou, H., Faraday Discussion, 54, 269, (1972).

36. Roberts, R.F., J. Electron Spectrosc., 4, 273, (1974).

37. Evans, U.R., The Corrosion and Oxidation of Metals, Edwards Arnold Ltd., London (1960).

38. May, R., J. Inst. Met., 82, 65, (1953).

39. Cotton, J.B., Proceedings of Second International Congress on Metallic Corrosion, New York, 1963,

also with: I.R. Scholes, Brit. Corrosion J., 2, 1, (1967).

40. Bregman, J.I., Corrosion Inhibitors, The MacMillan Co., New York, 1963.

41. Desai, M.N., and Rana, S.S., Werkstoffe Korros., 18, 8, (1967).

42. Desai, M.N., Werkstoffe Korros., 17, 870, (1966).

43. Brasher, D.M., Comptes Rendus 2 ème Symposium European sur les Inhibiteurs de Corrosion, Annali Univ. Ferrara, N.S., Sez.V, Suppl. n.4. (1966) pp.559.

44. Neznamova, T.G., Dobrovol'skaya, V.P., and Barannik, U.P., Zh. Prikl. Khim., 38(10), 2388, (1965).

45. Neznamova, T.G., Dobrovol'skaya, V.P., and Barannik, U.P., Ukrain, Fiz. Zhur., 31, (12), 1337 (1965).

46. Trabanelli, G., Zucchi, F., Brunoro, G., and Carassiti, V., Werkstoffe und Korrosion, 24, 602, (1973).

47. Walker, R., Corrosion, 31, 97, (1975).

48. Dobrovol'skaya, V.P., Neznamova, T.G., and Barannik, U.P., Zh. Prikl. Khim., 40(8), 1841, (1967).

49. Hall, K.H, and Davies, I., J. Appl. Chem., 15(8), 389, (1965).

50. Prall, J.K., and Shrier, L.L., Trans. Inst. Metal. Finishing, 41, 29, (1964).

51. Poling, G.W., (1), Corrosion Science, 10, 359, (1970).

52. Mansfield, F., and Smith, T., Corrosion, 29, 105, (1973).

53. Ogle, I.C.G., and Poling,G.W., Can. Metal. Quart., 14, 37, (1975).

54. Noyota, T., and Poling, G.W., Corrosion, 32, 216, (1976).

55. Morito, N., and Suctaka, W., Nippon Kinkozo Grakkaishi, 35, 1165, (1971).

56. Thibault, S., Corrosion Science, 17, 701, (1977).

57. Jarvis, J.A.J., et al: Acta Cristallogr., 13, 1027 (1960).

58. Thibault,S., and Talbot, J., C.R. Acad. Sci. Ser. C ., 1974, 278(8), 503.

59. Bassoli, M., Bonora, P.L., Ponzano, G.P., Pagetti, A.L., and Lorenzelli, V., C.R. Acad. Sci. Ser. C., 1974, 272(14), 943.

60 Thibault, S., and Talbot, T., Met. Corros.Ind., 50(594), 51, (1975).

61. Patel, M.M., Patel, N.K., Shah, R.S., and Vora, J.C., J. Ind. Chem. Soc., 51(12), 1053, (1974).

62. Patel, N.K., Chem. Era, 11(2), 6, (1975).

63. Jeannin, S., Jeannin, Y., and Lavigne, G., Proc. Int. Conf. Coord. Chem., 16th. 1974, pp.3.

64. Hedges, E.S., J. Chem. Soc., 969, (1928), 561, (1930).

65. Hickling, A., and Taylor, D., Trans. Faraday. Soc., 44, 262, (1948).

66. Ives, D., and Rawson, A., J. Electro. Chem. Soc., 109, 447, (1962).

67. Lal, H., and Thirsk, H.R., J. Chem. Soc., 2638, (1953).

68. Leckie, H.P., J. Electrochem. Soc., 117, 1478, (1970).

69. Bacarella, A.L., and Griess, J.C.,J. Electrochem. Soc., 120, 459, (1973).

70. Taylor, A.H., J. Electrochem. Soc., 118, 854, (1971).

71. Dugdale, I., and Cotton, J.B., Corrosion Science, 3, 69, (1963).

72. Mansfield, F., Smith, T., and Parry, E.P., Corrosion, 27, 289, (1971).

73. Allen, J.A., Trans. Faraday. Soc., 48, 273, (1952).

74. Robert, T., and Offergeld, G., Phys. Status Solidi, (a), 14, (1972), 277.

75. O'Sullivan, D.G., J. Chem. Soc., 2343, (1960).

76. Morgan, K.J., J. Chem. Soc., 2343, (1961).

77. Harzel, L.W., and Benson, F.R., J. Amer. Chem. Soc., 76, 667, (1954).

78. Lieber, E., Levering, R.D., and Patterson, L.J., Anal. Chem., 23, 1594, (1951).

79. Khullar, I.P. , and Agarwala, U., Austr. J. Chem., 27, 1877, (1974).

80. Udupa, M.R., and Padmanabham, M., J. Inorg. Nucl. Chem., 1808, 37, (1975).

81. Hadzi, D., and Prevorsek, D., Spectrochim. Acta, 10, 38, (1957).

82. Bailar, J.C. Comprehensive Inorganic Chemistry, Vol. 3, Pergamon Press, Oxford (1973).

83. Brown, I.D., and Dunitz, J.D., Acta. Cryst., 14, (1961), 480.

84. H. Remy, Treatise on Inorganic Chemistry, Vol. II, Elsevier Publishing Co., (1956).

85. Clifton, J.R. and Yoke, J.T., Inorg. Chem., 5, 1630, (1966).

86. Pourbaix, M., Atlas of Electrochemical Equilibria in Aqueous Solution, Pergamon Press, London (1966).

87. Cotton, F.A., and Wilkinson, G., Advanced Inorganic Chemistry, Interscience Publishers, New York, 1966.

88. Hatfield, W.E., et al: Transition Metal Chem., 1969, 5, 47.

89. Moeller, T., Inorganic Chem., (546), p.1840: John Wiley and Sons Ltd., New York, 1952.

90. Castle, J.E., Nature Phys. Sci., 234, 93, (1971).

91. Castle, J.E., and Epler, D., Proc. Roy. Soc. London, A 339, 496, (1974).

92. Castle, J.E. and Nasserian-Riabi, M., Corrosion Sci., 15, 537, (1975).

93. Norton, P.R., and Tapping, R.L., Faraday Discussion, 60, 71, (1975)

and : Grim, S.O., Matienzo, L.J., and Swartz, W.E., J. Amer. Chem. Soc., 94, 5116, (1972).

94. Briggs, D., Faraday Discussion, 60, 81, (1975).

95. Siegbahn, K., 'Electron Spectroscopy' Upsala University, Institute of Physics, June 1976, U.U.I.P.-940.

96. Weiss, J., Tollin, G., and Yoke, J.T., Inorg. Chem., 3, 1344, (1964).

also: Inorg. Chem., 2, 1210, (1963).

97. Tamura, M., Hada, H., Noguchi, J., and Hayashi, S., J. Phys. Chem., 66, 559, (1962).

98. Little, L.H., and Ottewill, R.H., Can. J. Chem., 40, 2110, (1962).

99. Kauffmann, T., Beissnev, G., Köppelmann, E., Kuhlmann, D., Schott, A., and Schreeken, H., Angew Chem. Internat. Edit. 7, 131, 1968.

also: Angew Chem. Internat. Edit., 6, 633, (1967).

100. Ermakov, O.A., Davydova, G.F., Shtyrokov, V.N., and Grigoreva, N.V., Zh. Prikl. Khim., 50(2), 368, (1977).

101. Axelson, G., Hamrin, K., Fahlman, A., Nordling, C., and Lindberg, B.J., Spectrochim. Acta, 23A, 2015, (1967).

102. Boden, P.J., Corrosion Science, 11, 353, (1971).

103. Scully, I.C., The Fundamentals of Corrosion, Pergamon Press, Oxford 1966.

Journal of Electron Spectroscopy and Related Phenomena, 10 (1977) 79–83
© Elsevier Scientific Publishing Company, Amsterdam – Printed in The Netherlands

Short communication

Benzotriazole adsorption on copper studied by X-ray photoelectron spectroscopy

D. CHADWICK and T. HASHEMI

Department of Chemical Engineering and Chemical Technology, Imperial College, London SW7 2BY (Gt. Britain)

(Received 22 March 1976)

Benzotriazole, $C_6H_5N_3$, has been found to be an effective corrosion inhibitor for copper in a variety of environments[1–5]. Benzotriazole, BTA, is conveniently adsorbed onto copper from acidic aqueous solutions sometimes containing NaCl, and forms a surface film of variable thickness in the range 40–140 Å depending upon conditions[6]. It appears that this surface film can act as a barrier to cathodic reactions[1–7], thus imparting a degree of corrosion resistance to the copper substrate. In recent years there has been considerable research effort devoted to the identification of the nature of the surface film[1–8] formed on copper during exposure to BTA-containing solutions and various possible structures have been proposed[1, 2, 7, 8]. Two distinct alternatives may be identified: a cuprous surface complex, Cu(I)BTA, which is thought to consist of linear polymeric chains[1, 2], and a cupric surface complex, Cu(II)BTA, which is possibly a network structure[1, 2, 8], though the details are not clear. Infrared spectroscopy studies[7] and chemical analysis of film extracts[7] have produced evidence marginally in favour of a cuprous complex, but the results are not conclusive. Copper is usually covered[8, 9] with a thin layer of copper oxide and it has been recognised that this is probably the substrate for BTA adsorption[1–3, 6–8].

In a recent paper[8], X-ray photoelectron spectroscopy was used to study the surface films formed by adsorption of BTA on cuprous and cupric oxides. In the case of cuprous oxide it was concluded[8] that the surface film was a mixture of Cu(I)BTA and Cu(II)BTA, the relative amount of Cu(II)BTA increasing with increased exposure to aqueous BTA solutions at 60 °C. We have made an extensive study of adsorbed corrosion inhibitors on copper[10] and the above result runs contrary to our experience. In X-ray photoelectron spectroscopy studies of BTA adsorption on copper and cuprous oxide surfaces under a variety of conditions[10] we have found no correlation of the cuprous/cupric ratio with exposure time to the BTA solutions. However, in all cases the treated surfaces underwent fairly rapid oxidation on exposure to air after removal from the BTA solutions.

EXPERIMENTAL

X-ray photoelectron spectra were obtained with the Vacuum Generators ESCA-3 using an Al X-ray anode which was operated at the lowest possible power level to avoid any photoreduction in the sample[11]. Since the spectra were obtained by digital accumulation, it was possible to verify that no photoreduction took place during acquisition of the spectra. In fact, no evidence for photoreduction of Cu(II) to Cu(I) was obtained from any spectrum under the prevailing conditions in our spectrometer and the short times taken to collect data. The binding energy scale was chosen such that the C(1*s*) level arising from BTA or surface contamination was 285.0 eV[12].

Copper samples were machined from I.N.C.O. (Mond) Ltd. pure electrolytic copper and benzotriazole was obtained from B.D.H. Ltd. Surface films of Cu_2O were produced electrochemically in KOH solution[8]. A typical BTA treatment was immersion in a N_2-purged solution containing 0.02 M BTA and 0.5 M NaCl at pH 3 and 25°C, followed by washing with triply-distilled water and drying in air. Several methods of washing were tried, for example, agitated or static, but no visible differences in the spectra were produced.

RESULTS AND DISCUSSION

The X-ray photoelectron spectrum in the Cu(2*p*) region of an electrochemically grown Cu_2O surface is shown in Fig. 1(a). The appearance of the spectrum, the Cu(2*p*) binding energies, and the LMM Auger peaks are in agreement with Cu_2O spectra from numerous previous investigations of copper compounds[8, 11, 13]. In particular, the satellites associated with shake-up processes in Cu(II) are absent[11, 13–15]. In all Cu(II) compounds examined by X-ray photoelectron spectroscopy relatively strong satellites have been observed 6–10 eV on the high binding energy side of the main peaks[11, 14, 15]. The observation of these satellites is now considered to be indicative of the presence of Cu(II).

After immersion of a copper sample with an electrochemically grown Cu_2O surface in an aqueous solution containing 0.02 M BTA and 0.5 M NaCl at pH 3 and 25°C with N_2 purging for 10 min the spectrum shown in Fig. 1(b) was obtained. Immersion of a similar copper sample in an identical solution for an exposure time of 20 hrs produced the spectrum in Fig. 1(c). That the surface film contained BTA was established in all cases by the strong N(1*s*) peak and the enhanced intensity of the C(1*s*) peak over untreated surfaces. Clearly, the spectra in Fig. 1(b) and (c) are virtually identical. A small amount of Cu(II) is present in the surface film as evidenced by the high binding energy shoulders and the weak satellites. Identical spectra were obtained for many intermediate exposure times and these results indicate that the amount of Cu(II) present in the surface film is not significantly affected by the exposure time to BTA solutions under the above conditions.

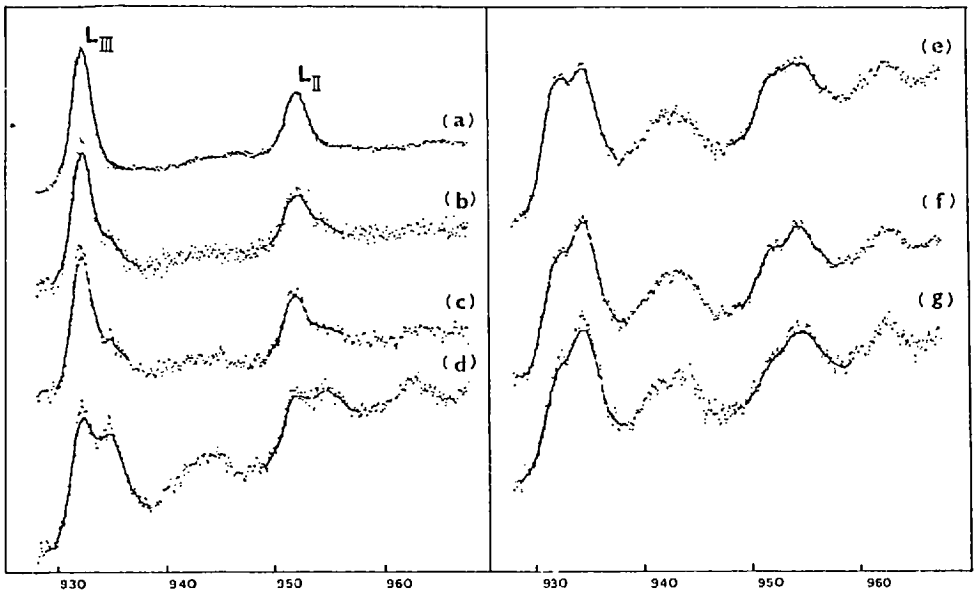


Figure 1. Photoelectron spectra of Cu (a) with an electrochemically grown Cu_2O surface; (b) after immersion in 0.02 M BTA solution containing 0.5 M NaCl at pH 3 and 25 °C for 10 min; (c) after immersion for 20 hrs. Exposure of sample (c) to air for: (d) 2 hrs; (e) 3 hrs; (f) 16 hrs; (g) 48 hrs.

Similar results were obtained with abraded surfaces or surfaces polished with diamond paste (1 micron), washed with acetone, methanol, triply distilled water and dried in air. The spectra of these samples before BTA treatment were identical to that in Fig. 1(a) and the LMM Auger peaks indicated that the surface was covered with a thin layer of Cu_2O[9, 13]. Thus, it is not surprising that these samples behaved in a similar manner with respect to BTA adsorption as those samples with electrochemically grown Cu_2O surfaces.

Following these results a variety of conditions for the BTA treatment were investigated. In each case a series of sample immersion times were examined and both polished copper samples and samples with electrochemically grown Cu_2O surfaces were used. The various conditions were: (i) 0.02 M BTA, 0.5 M NaCl at pH 1 and 25 °C; (ii) 0.02 M BTA, 0.5 M NaCl at pH 3 and 60 °C; (iii) variation of BTA concentration at pH 3 and 25 °C; (iv) variation of NaCl concentration at pH 3 and 25 °C; (v) variation of the degree of agitation; (vi) adsorption from $CHCl_3$ at 25 °C (one of the few organic solvents in which BTA is appreciably soluble). In all cases the spectra of the surface films produced were similar to Fig. 1(b) and (c) regardless of immersion time.

The above results differ from the conclusions of Roberts[8]. For this reason surface films produced by BTA adsorption from aqueous solutions (pH $\simeq$ 5.25) and 25–60 °C with N_2 purging for a wide range of BTA concentrations and immersion

times were studied. The resulting spectra were similar to Fig. 1(b) and (c) regardless of immersion time, in complete agreement with the results obtained for BTA solutions containing NaCl.

It is quite clear from our results that the amount of Cu(II) present in the surface is not correlated with immersion time in BTA solutions for a wide variety of conditions. Although in general N_2 purging was carried out throughout the treatments, it was found that even if air was blown through the BTA solutions no increase in the relative amount of Cu(II) resulted.

In all cases the BTA treated copper specimens proved very sensitive to exposure to air, during which oxidation of Cu(I) to Cu(II) took place. This is demonstrated in Fig. 1(d)–(g) for the sample which had been given originally a 20-hr immersion time in BTA solution and whose spectrum is shown in Fig. 1(c). The spectra were obtained after 2, 3, 16 and 48 hrs exposure to air and indicate progressive oxidation of Cu(I) in the surface film to Cu(II). This is evident from the increasing intensity of the high binding energy shoulders and the shake-up satellites. After 48 hrs the surface is almost completely oxidised to Cu(II). This sequence of spectra was typical of all the BTA treated copper samples studied.

The observation of Cu(II) in the spectra obtained shortly after removal from the BTA solutions is easily explained by oxidation during the finite time (5–15 min) needed to dry the samples in air before insertion into the spectrometer. Finally, a check was made to see if running the spectra at intermediate times during the oxidation process accelerated the process through radiation damage, but no effect was detected.

CONCLUSION

We conclude that the surface films produced on Cu_2O surfaces on copper by adsorption of BTA from aqueous solutions under the wide variety of conditions studied and probably from most polar organic solvents, consist of a Cu(I)BTA surface complex. In addition, Cu(II) is produced only on removal of the treated copper from the liquid phase when the Cu(I)BTA surface complex reacts with air. The structure produced by such an oxidation process would not be the Cu(II)BTA referred to earlier. Many simple Cu(I) compounds have been found to be easily oxidised to Cu(II) by exposure to air[11, 16]. Thus, we suggest that the corrosion inhibition properties of BTA are associated with the formation of a Cu(I)BTA surface film. The detailed structure of this surface compound remains to be determined. However, in the working environment it is possible that the Cu(I)BTA surface film produced by BTA treatment may be oxidised to Cu(II) by air exposure and that this latter compound imparts corrosion resistance.

REFERENCES

1 J. B. Cotton, *Proc. 2nd Int. Congr. Met. Corros., NACE*, New York, 1963, p. 590.
2 I. Dugdale and J. B. Cotton, *Corros. Sci.*, 3 (1963) 69.
3 J. B. Cotton and I. R. Scholes, *Br. Corros. J.*, 2 (1967) 1.
4 F. Mansfield, T. Smith and E. P. Parry, *Corrosion (Houston)*, 27 (1971) 289.
5 S. M. Mayanna and T. H. V. Setty, *Corros. Sci.*, 15 (1975) 625.
6 F. Mansfield and T. Smith, *Corrosion (Houston)* 29 (1973) 105.
7 G. W. Poling, *Corros. Sci.*, 10 (1970) 359.
8 R. F. Roberts, *J. Electron Spectrosc. Relat. Phenom.*, 4 (1974) 273.
9 J. A. Allen, *Trans. Faraday Soc.*, 48 (1952) 273.
10 D. Chadwick and T. Hashemi, to be published.
11 D. C. Frost, A. Ishitani and C. A. McDowell, *Mol. Phys.*, 24 (1972) 861.
12 G. Johansson, J. Hedman, A. Berndtsson, M. Klasson and R. Nilsson, *J. Electron Spectrosc. Relat. Phenom.*, 2 (1973) 295.
13 P. E. Larson, *J. Electron Spectrosc. Relat. Phenom.*, 4 (1974) 213.
14 M. A. Brisk and A. D. Baker, *J. Electron Spectrosc. Relat. Phenom.*, 7 (1975) 197.
15 D. C. Frost, C. A. McDowell and R. L. Tapping, *J. Electron Spectrosc. Relat. Phenom.*, 7 (1975) 295.
16 T. Robert and G. Offergeld, *Phys. Status Solidi A*, 14 (1972) 277.